博士論文

Study on Reinforcement and Oxo-biodegradability of Polypropylene Materials by Fibrous Cellulose and Quasi-enzyme System

2012 年

宮崎　健輔

Study on Reinforcement and Oxo-biodegradability of Polypropylene Materials by Fibrous Cellulose and quasi-enzyme system

Contents

Chapter 1: General Introduction

1-1 Introduction of Polypropylene (PP)

Propylene was first polymerized by Giulio Natta and his coworkers in March 1954 [1]. It is the most important commercial polyolefin. Ziegler-Natta catalysts can make highly isotactic polypropylene. The highly isotactic polypropylene is responsible for its high melting temperature and crystallinity, rigidity, toughness, and heat resistance [2]. Currently, isotactic polypropylene (iPP) is used in various field, such as film, battery cases, container, crates, automotive parts, electrical components, medical are and so on [3].

The world production of PP has grown from around 1.5 million tons in the 1970's to over 70.0 million tons in 2008[4]. It is expected that the production will exceed 89.8 million tons in 2014. Such drastic growth is due to cost performance, excellent properties, strong and continuous expansion of process versatility, and environmental friendly processes and materials, during manufacturing, use, and polymer recycling process [5, 6].

It has been known that PP is semi-crystalline that has an effect on morphology. The ability of crystallization of chain is a critical factor governing the morphology. The crystallinity of PP is governed primarily by the stereoregularity of the chain. According to stereoregularity, PP is classified into three types by the arrangement of the methyl group. It is defined meso or raceme units. In the case of iPP, the methyl groups always have the same configuration with respect to the main chain (Figure 1-1(a)). In the case of syndiotactic PP (sPP), the methyl groups have an alternating configuration with respect to the main chain (Figure 1-1(b)). In the case of atactic PP, the methyl groups

have random configuration (Figure 1-1(c)).

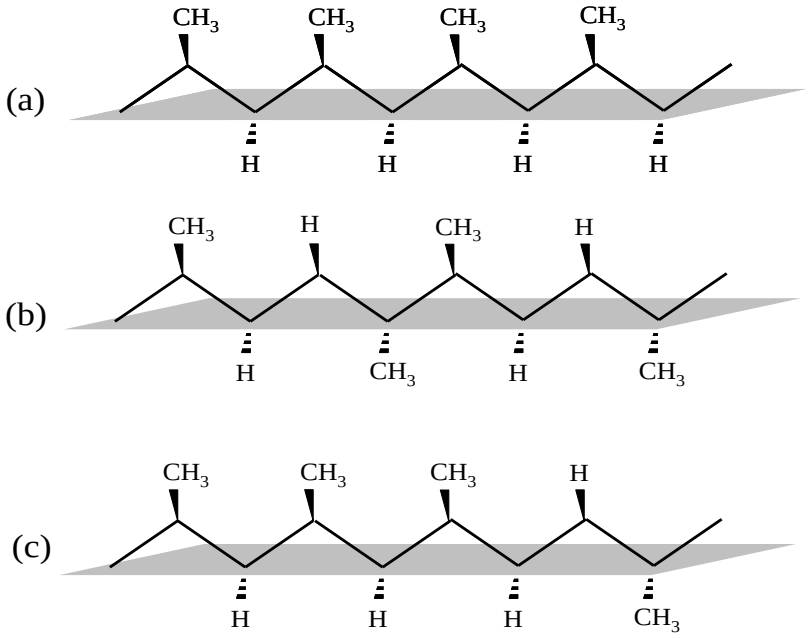

Fig1-1 Illustration of the stereo chemical configuration of PP.

(a): isotactic, (b): syndiotactic, (c): atactic

This stereoregularity affects not only crystal structure and physical properties but also oxidative degradation behavior. iPP is major commodity plastic material. However, it cannot be used without stabilizers because of susceptibility to air oxidation. In the case of industrial applications, serious problems have been raised by various molding processes. In the case of daily use, the product of iPP degrades over a period of week or months depending on the physical form, temperature, sun-light, available oxygen, atmospheric pollutants, and so on [7, 8].

PP is often used with talc, calcium carbonate, barium sulfate, calcium silicate and cellulose as composites, to improve the mechanical properties. Especially, PP/ cellulose composites are attracted attentions and are widely investigated from standpoint of environmental conservation.

1-2 Cellulose

Cellulose is the most abundant and widely used polymer in the world. As the major constituent of plant matter, billion of tons of it are created each year through photosynthesis. In the form of wood, paper, cotton textiles, rayon, film, coatings, and a myriad of other uses including fuel, we consume about 450,000,000 tons of cellulose per year [9].

The cellulose is polysaccharides only consisting of glucose which is made from carbon, hydrogen, oxygen, and glucose is produced by the photosynthesis of the plant. In cell wall of the plant, hemicellulose, lignin and cellulose exist. Therefore, relative content rate of cellulose is 40- 70 % in the plant.

The advantage of cellulose is low cost, low density, renewability, biodegradability, nontoxicity. The cellulose also has attracted much attention of many researchers as composite materials [10-20]. In particular, the attention has recently concentrated on its biodegradability and renewability from the viewpoint of environmental advantage. Composite based on cellulose has been considered a useful way to employ such features.

1-3. PP Composite

PP is a commodity polymer that has properties that can be extended into the applications of high performance polymers. PP has become a universal polymer, and it is applied in each of the areas where special properties are required: moldings, extrusions, sheets, films including cast and blow, thermoformed containers, foamed materials, and fibers. PP has higher strength than other polyolefins, low density, and acceptable thermal resistance and is available in many grades differing in molar mass and copolymer type and distribution. It has two main restrictions: PP is brittle at lower temperatures and it has only moderate strength and is subject to creep. The Properties of PP can be enhanced to make it competitive with typically higher performing polymers by increasing its strength and creep resistance with fillers and toughening with elastomer inclusion. Natural fibers of many varieties have been used to form ecocomposites, or green composites, with polyolefins [20].

Many types of filler are use in PP composites. Typical mineral fillers are talc, calcium carbonate, barium sulfate, calcium silicate (wollastoneite), and kaolin. Glass fiber is typically used for high performance. Natural fibers are increasingly gaining interest due to their Young's modulus, strength, wide availability, and suitability for the type of applications of PP composites, because the performances of nylon, polycarbonate, and polyester composites with glass and carbon fibers are not achievable. The Young's modulus and strength refer to the corresponding absolute value divided by the density, which reflects the modulus and strength relative to the mass of the structure. Natural fibers are almost entirely cellulose base. Some examples of cellulose fibers are wood flour, wood fiber, bast fibers such as flax, hemp, jute, ramie and kenaf, rice and wheat husks and straw, cotton, bagasse, sisal, waste paper, and many other fibrous

materials that are available as by-products form crops (see Table 1 for examples of properties). With the exception of wood, the fibers are obtained from fast-growing crops [20].

Table 1 Comparative Mechanical properties and cost of fibers [20]

Natural fiber	Tensile strength (MPs)	Tensile modulus (Gpa)	Cost ($/kg)
Cotton	287-597	5.5-12.6	3.5-4
Glass	2000-3500	70	7
Flax	345-1035	27.6	1-2
Ramie	400-938	61-128	0.7
Jure	393-773	26.5	0.6
Hemp	690	-	1-2
Kenaf	11,900	60	-
Bagasse	170-290	15-29	-
Sisal	511-635	9.4-22	0.9

The relative ease of preparation, formability, or recycling suitability and the performance to cost consideration make PP-natural fiber composites useful for many structural and cladding materials. The preparation techniques are diverse compared with typical thermoplastic composites because of the various kinds of fibers and the adaptability of PP. PP hydrophobic, while natural fibers are hydrophilic, so some compatibilization or modification of the interface is usually needed. The main requirement is mechanical properties, and these will be reviewed. Each individual application provides its own challenge for additional requirement. Therefore, the additives and properties will be considered for specific examples.

1-3-1 Application of PP Composite

PP is convenient thermoplastic with a balance between processing and performance. The melting temperature (Tm = 162 – 165 °C) is high enough to resist boiling water and is low enough to permit ease of thermoforming composeite sheets. PP is available in grades intended for extrusion into film, sheet and profiles, injection molding, and thermoforming. PP is hydrophobic and therefore lacks interaction with cellulose fibers. However, the interactions between PP and cellulose are improved by compatibilizer. Automotive lining panels are a significant volum application for natural fibers and wood flour PP composites. Similar composites can be used for building panels, acoustic materials, furniture, biodegradable containers, plant pots, and geotextiles. Water-resistant lumber is available for outdoors uses. Wood texture can be included to provide materials that appear like timber and can be sawn and nailed [20].

The use of bio fibers in automotive applications has been investigated. Composites mainly based on PP are used in interior and exterior components. Uses include door panels, seat backs, headliners, package trays, dashboards, and trunk liners. Typical fibers include jute, flax, hemp, kenaf, and wood. A concept car has been development called the Eco Car. The Eco Car is constructed from bio fiber composite panels.

1-3-2 Compatibilizer

Attention has been paid to improving the compatibility of the filler with the polymer matrix, by providing an interaction between the filler and the polymer. There are several types of “Compatibilizers”. First type, it can be chemically attached either to a filler (e.g. cellulose fibers), or to a polymer. Second type, it can form a covalent chemical bond between filler and polymer. Third type, it can help to form a sort of uniform “alloy” between two or several polymeric components ordinarily not very compatible with each other. Generally, compatibilizers can improve adhesion between fiber and plastic and markedly improve physical properties of the polymeric composite, its weatherability, and overall performance [21].

1-3-3 Mechanical Properties

The important mechanical properties of PP-cellulose fiber composites are tensile, flexural, and impact. The tensile properties are derived from the tensile properties of the fibers and the fiber-matrix adhesion. Long fibers will provide the best tensile modules and strength, with typically low break strain. The tensile strength of composites made from felted or woven mats is high because the fiber entanglements reduce dependence on adhesion to the matrix. Typical fiber volume theoretical approaches have been found to describe the tensile properties, including fiber orientation effect. In each of the mechanical properties, the cellulose fibers are superior to wood flour.

1-4. Biodegradable plastics

Since the first developments of polymeric materials, scientists and engineers have made intensive efforts to increase the stability of these materials with regard to their diverse environmental influences. As a result, very durable polymeric materials (plastics) are now used in our life. During the past decade, the intense use of modern plastics, combined with their enormous stability, has created serious problems with plastic waste. The main problems are caused by plastic packaging. As possible alternative waste management strategies to landfilling, incineration or plastics recycling are not optimal, and the problems remain the subject of much controversy and discussion among both scientists and the public. On the basis of these problems, an intensive activity has been undertaken since the early 1990's to develop novel plastics which have performance comparable with that of conventional polymers, but are also susceptible to microbial degradation. The intention was that these materials would reduce waste deposit volume while undergoing degradation in a landfill, or alternatively they could be treated in composting plants. These technologies offered a new approach to the management of plastics waste. Moreover, when this waste management system is combined with the use of renewable resources to produce the polymers initially, it is likely that biodegradable plastics may simply become part of a natural cycle. The biodegradability of plastics provides these materials with novel and additional properties which may also be beneficial during their use. For example, in agriculture, biodegradable mulch films would not need to be collected after use. They would be decomposed with time and could simply be plowed into the soil, where they would biodegrade. Hence, it is not surprising that this concept of using biodegradable plastics has become of major interest during recent years. Biodegradable plastics, as

novel materials, make claims to be environmentally friendly [22]. It is difficult that biodegradable plastics are used as substitute materials of synthetic polymeric materials because the cost performance and mechanical properties of biodegradable plastics are lower than that of synthetic polymeric materials.

PP, which is one of the synthetic polymeric materials, is non-biodegradable polymeric materials. Therefore, Cellulose /PP composites are only biodegraded in the part of cellulose. To give biodegradable PP materials such as PP and Cellulose /PP composites, Oxo-Biodegradation of PP is investigated.

1-4-1 Oxo-Biodegradable PP

As above, synthetic polymeric materials easily accumulate in environment because their biodegradability is considerably less, and PP is one of such materials and is known as a non-biodegradable polymer. Generally large molecule such as PP cannot easily enter into cells of microorganisms. Therefore, PP is hard to be metabolized in microorganisms. If PP is spontaneously degraded to low molecular weight compounds, the biodegradability must certainly appear. In fact, it has been known that polyethylene (PE), which is similar to PP chemical structure, is given biodegradability by pro-oxidant [23-27]. This method is called as “oxo-biodegradation”. The mechanism involves two stages which are abiotic oxidation and microbial oxidation. The rate of the biodegradation process strongly depends on the abiotic oxidative degradation stage.

1-5 Oxidative Degradation of PP

The abiotic degradative reaction of polyolefin has been widely recognized as a free radical mechanism called “autooxidation” [28-31]. There are four steps in the degradative reaction, and distinguish as radical initiation, propagation, Chain-branching and termination. The “autooxidation” has generally been believed to consist of the following steps [32].

Initiation

$$\text{Polymer} \rightarrow P\bullet + P\bullet \quad (1)$$

Propagation

$$P\bullet + O_2 \rightarrow POO\bullet \quad (2)$$

$$POO\bullet + PH \rightarrow POOH + P\bullet \quad (3)$$

Chain-branching

$$POOH \rightarrow PO\bullet + \bullet OH \quad (4)$$

$$PH + \bullet OH \rightarrow P\bullet + H_2O \quad (5)$$

$$PH + PO\bullet \rightarrow P\bullet + POH \quad (6)$$

$$PO\bullet \rightarrow \text{various chain-scission reactions} \quad (7)$$

Termination(leading to nonradical products)

$$POO\bullet + POO\bullet \rightarrow POOOOP(\rightarrow POOP + O_2) \quad (8)$$

$$POO\bullet + P\bullet \rightarrow POOP \quad (9)$$

$$P\bullet + P\bullet \rightarrow PP \quad (10)$$

In thermal oxidation, initiation [Eq. (1)] results from thermal dissociation of chemical bonds. In photodegradations, photophysical processes, such as the formation

of electronically excited species, energy-transfer processes, or direct photodissociation occur, and these processes lead to bond cleavage.

In the propagation sequences, it is the key reaction that polymer alkyl radicals (P•) react with oxygen to form polymer peroxy radicals [Eq. (2)]. This reaction is very fast, however, it can be diffusion-controlled. In the next propagation step, [Eq. (3)] polymer peroxy radicals react with hydrogen of polymer to form a polymer hydoroperoxide (POOH) and a new polymer alkyl radical (P•). In polypropylene, hydrogen abstraction occur preferentially from the tertiary carbon atoms which are the most reactive [Eq. (11)].

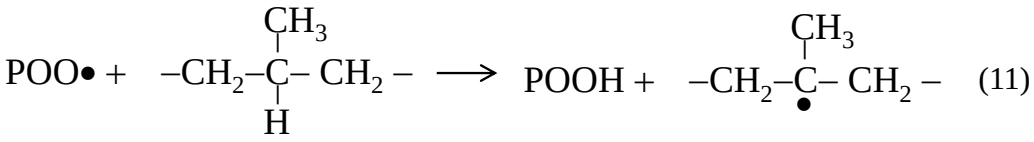

$$POO\bullet + -CH_2-\underset{\displaystyle H}{\overset{\displaystyle CH_3}{\overset{|}{\underset{|}{C}}}}-CH_2- \longrightarrow POOH + -CH_2-\underset{\displaystyle \bullet}{\overset{\displaystyle CH_3}{\overset{|}{C}}}-CH_2- \quad (11)$$

In the case of polyethylene, hydrogen abstraction occurs from secondary carbon atom [Eq. (12)], and may also occur in polypropylene, but with lower reaction rate.

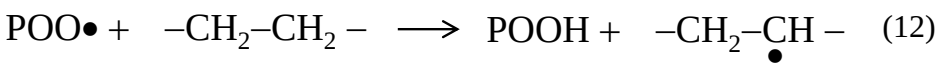

$$POO\bullet + -CH_2-CH_2- \longrightarrow POOH + -CH_2-\underset{\displaystyle \bullet}{CH}- \quad (12)$$

For polypropylene, intramolecular hydrogen abstraction in a six-ring favorable stereochemical arrangement can preferentially lead to the formation of blocks of hydroperoxides in close proximity [32-25]. Infrared studies of polypropylene hydroperoxides indicated that more than 90 % of these groups intramolecularly formed hydrogen-bond. From the result, the peroxide groups were present in sequences of two or more, which supported intramolecular hydrogen abstraction during the oxidation[33]. It was also indicated that the cleavage reaction accompanied the oxidation propagation,

rather than the termination reaction. Roginsky [37] also suggested that the reaction of solid polypropylene was dominated by the formation of rather compact blocks of hydroperoxide group.

Chain-Branching is shown in Eq. (4). Polymer hydroperoxides (POOH) produce very reactive polymer alkoxy radicals (PO•) and hydroxyl radicals (•OH). The highly mobile hydroxyl radical reaction and polymer alkoxy radical reaction is shown in Eq. (5) Eq. (6). Both radicals can abstract hydrogen atoms from the same or from a nearby polymer chain [38]. Polymer oxy radicals can react further to result in β-scission [see Eq. (13)] the formation of in-chain ketones [see Eq. (14)], or can be involved in termination reactions.

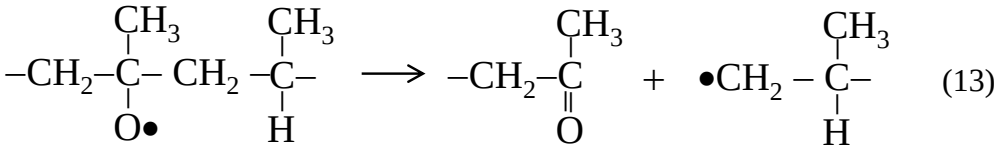

(13)

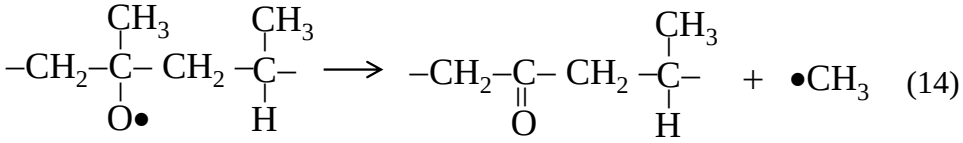

(14)

In the termination, polymer radicals react with each other, and various bimolecular recombinations occur. When the oxygen pressure is sufficient, the termination is almost exclusively via the reaction in Eq. (8). When the oxygen pressure is low, other terminations reactions may take place [38]. The recombination is influenced by cage effects, steric control, mutual diffusion, and the molecular dynamics of the polymer matrix [38-40]. In the case of solid polymers, the recombination of polymer peroxy radicals (POO•) is subject to the rate of their encounter with each other and is influenced by the intensity of molecular motion [41].

1-5-1 Secondary Reactions and Product Formation

1-5-1-1 Formation of Acids and Peracids

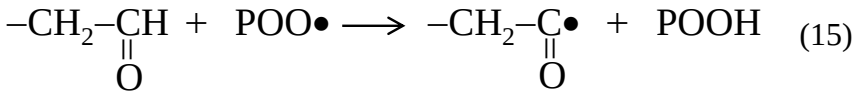

(15)

Hydorogen abstraction of end aldehyde group can form Polymer acyl radicals [Eq. (15)]. Polymer acyl radicals also can be produced by the Norrish type I reaction during photodegradation.

Polymer acyl radicals are easily further oxidized to polymer peracid radicals [Eq. (16)]. Polymer peracid radicals can abstract hydrogen to form peracides [Eq. (17)].

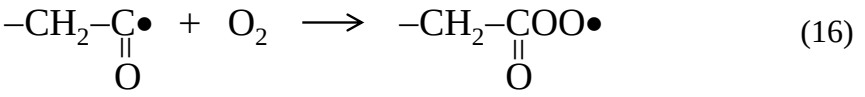

(16)

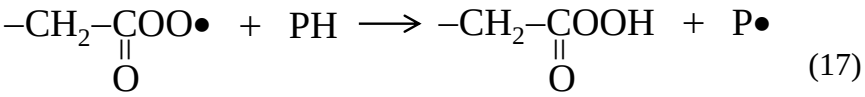

(17)

The cleavage of peracids can form polymer carboxy and hydroxyl radicals [Eq. (18)]. The carboxy radicals can abstract hydrogen to form carboxylic groups [Eq. (19)] [42].

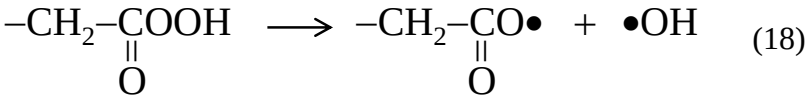

(18)

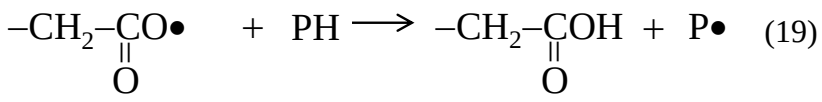

(19)

In another related mechanism, the primary alkyl radicals produced by β-scission [see Eq. (20)] to yield peroxy and carboxylic acids [Eq. (21)] [43].

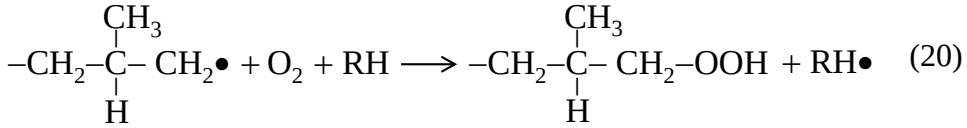

(20)

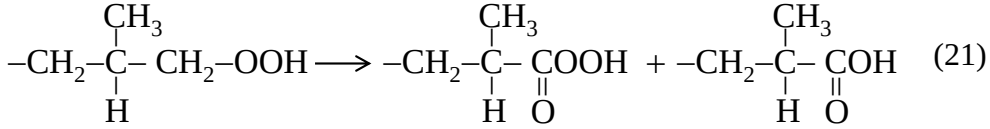

(21)

Studies of photooxidation of iPP revealed formation of peracids in quantities representing 15-20 % of overall peroxide level [44]. Solubility measurements indicated that the peracids were of macromolecular nature formed by the oxidation of macroaldegydes, presumably through radical attack on methyl hydrogens, subsequent peroxidantion., and disproportionation [44]. The analysis of peroxides formed during the oxidation of PP between 50 °C and 90 °C also suggested the presence of different types of peroxides, such as fast-decomposing and slow-decomposing ones. Chemical analysis of fast-decomposing species showed that these peroxides were peracids [43] formed by foregoing mechanisms.

1-5-1-2 Carbonyl Group Activity

Although the thermal oxidation primarily take place through the foregoing free radical reaction, some additional reactions can occur in the photodegradation of the polymer. Carbonyl groups, either present in the virgin polymer or foumed during the degradation, are sensitive to secondary phototransformations and can be photolyzed by the Norrish type I [Eq. (22)] or type II [Eq. (23)] reactions [41].

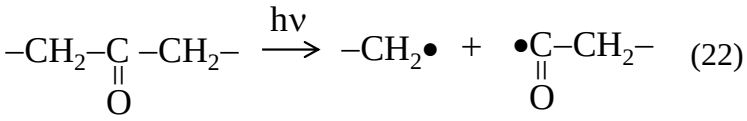

(22)

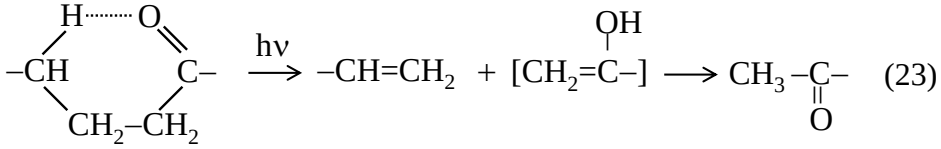

(23)

The Norrish type II is essentially a nonradical intra molecular process, dependent on the formation of a six-membered cyclic inter mediate, and it requires at least one γ-hydrogen relative to the carbonyl group.

1-5-1-3 Photodecomposition of Hydroperoxides

The light quanta in solar radiation are energetically sufficient to cleave PO–OH (176 kJ/mol) and P–OOH (293 kJ/mol), but hardly POO–H (377 kJ/mol) and bonds. The large difference in the bond dissociation energy between PO–OH and P–OOH means that the formation of PO• and •OH radicals will be the predominant reaction of photocleavage during irradiation [38]. Hydroperoxide groups have a very low molar absorptivity at a wavelength of 340 nm. The O-O bond has no low-lying, stable excited

state, and the potential energy surface of the first excited state are dissociative. The quantum yield in the near UV is close to 1.0 [38]. The average lifetime of an hydroperoxide group in a PP film under constant UV irradiation was quoted as approximately 25h, equivalent to roughly 4-5 days under solar irradiation [45]. Photodecomposition of hydroperoxides in polymers may also occur by energy-transfer processes from excited carbonyl or aromatic groups that have a higher molar absorptivity at the wavelengths of terrestrial sunlight [38, 41].

1-5-2 Prooxidant of PP

Prooxidant is added in Oxo-biodegradable polyolefin to accelerate abiotic degradation of polymer. Especially, transition metals (e.g. Co, Mn, Fe) salts possess a remarkable ability to decompose the hydroperoxides formed during the oxidation process of polymers[46]. The reaction of decomposing the hydroperoxides is the rate controlling reaction of "autooxidation" [47].

Titanium dioxide (TiO_2) is known as a semiconductor and a photocatalyst. TiO_2 has been widely investigated as a prooxidant of PP [48-50]. Photocatalytic reactions of TiO_2 are shown in the following:

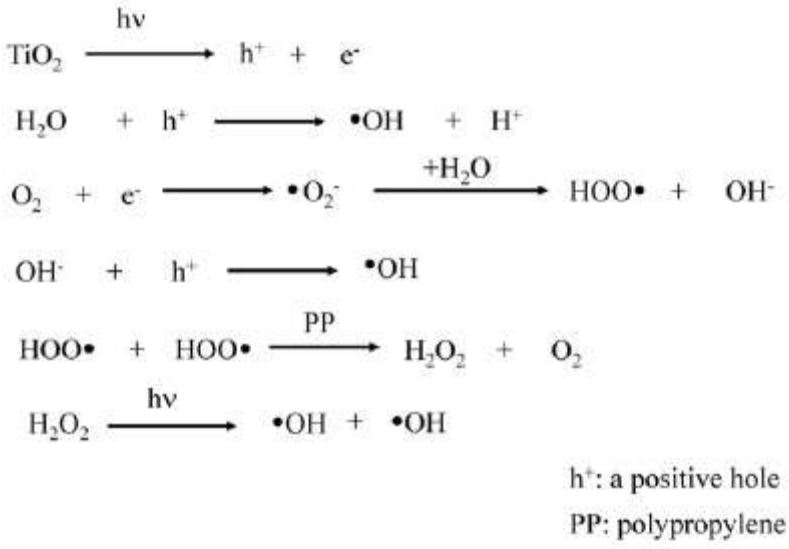

Figure 1-2 Mechanism of production of hydroxyl radical by TiO_2 [51]

TiO_2 reacts with H_2O in air under sunshine exposure, and OH• is produced by photocatalytic effect. Since the OH• has highly reactivity, PP degradation can be initiated by the OH• [51]. The degradation rate is, however, considerably slow because of nonexistence of H_2O in PP matrix. In general, the additive effect of TiO_2 on PP degradation is low.

Poly(ethylene oxide) (PEO) is a polyether compound with many applications from

industrial manufacturing to medicine. PEO can be degraded by the photocatalytic effect of $TiO_{2,}$ and then acid and aldehyde are produced[52, 53]. acid and aldehyde facilitate the PP degradation by the acceleration of the hydroperoxide decomposition[54, 55]. Hence, the combination of TiO_2 and PEO became the excellent prooxidant which has the effects of initiation and acceleration.

Lignin is covalently linked to hemicellulose and thereby crosslinks different plant polysaccharides. The structure confers mechanical strength to the cell wall and by extension the plant as a whole. Lignin is a biological polymer, but its reactivility is low. White-rot fungus can decompse a lignin. It is known that white-rot fungus have several enzymes (e.g. lignin peroxidase, Mn(II)-dependent peroxidase, lacase, phenol oxidase) [56,57].

The prooxidant of the combination of TiO_2 and PEO has a similar effect which can decompose the lignins. Wood flour decomposing by TiO_2 and PEO is shown as Figure 3. Therefore author named the prooxidant of the combination of TiO_2 and PEO "quasi-enzyme system"

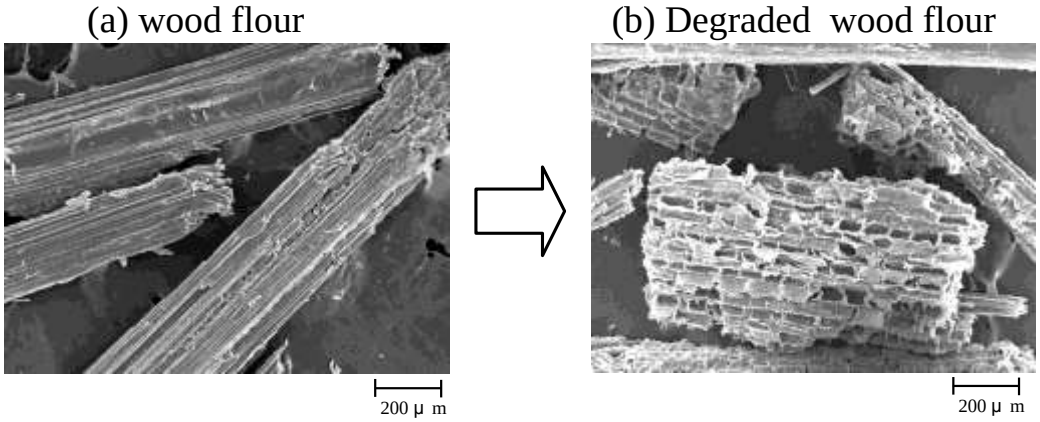

Figure 1-3 SEM photograph of wood flour. (a): wood flour

(b): wood flour degraded with TiO_2/ PEO

Degradation condition is 30 °C for 48 hour under the UV irradiation

1-6: Objective of this study

The composite with polypropylene (PP) has been widely studied. This is due to the commercial importance of PP as applicable materials for household appliance, medical ware, automotive and other industrial products. The most popular combination is PP and cellulose. The addition of cellulose stiffness has been expected. In fact, the composite obtained certainly improved the stiffness, but drastically became brittle. The cellulose is hydrophilic and tends to aggregate, causing poor processability and inherent incompatibility with hydrophobic PP. In this study, one of the purposes is improvement compatibility and toughening of PP cellulose composites.

In the Chapter 2, oxidatively degraded PP and maleated PP are added in PP/ cellulose composites as compatibilizers to improve interfacial adhesion. Effects of the molecular weight and concentration of oxidatively degraded and maleated PP Compatibilizers on tensile behavior of cellulose/ PP composites are studied.

In the Chapter 3, to improve toughness, Poly(ethylene oxide) (PEO) is added in cellulose/ PP composites. Effects of mechanical properties of PP and PP/ cellulose composites by the addition of PEO are studied.

Biodegradable plastics has become of major interest during recent years, as an environmentally friendly material. It is known that cellulose can be biodegraded. However, PP is known as a non-biodegradable polymer. Therefore, cellulose/ PP composites are only biodegraded the part of cellulose, and there is no biodegradability in the PP matrix.

Generally large molecule such as PP cannot easily enter into cells of microorganisms. If PP is degraded to low molecular weight compounds, the biodegradability must certainly appear. To accelerate PP degradation, a pro-oxidant is added in PP. This

method is called as “oxo-biodegradation”. The mechanism involves two stages which are abiotic oxidation and microbial oxidation. We use the PEO microcapsule containing TiO_2 (PEO/ TiO_2) as a novel pro-oxidant. To develop oxo-biodegradable cellulose/ PP composite, oxo-biodegradation of PP using a novel pro-oxidant is investigated, at first. Subsequently, oxo-biodegradation of PP/ cellulose composite is also studied.

In the chapter 4, abiotic oxidation of PP/ PEO/ TiO_2 is studied. In the Chapter 5, to control the abiotic oxidation, the PEO microcapsule containing TiO_2 modified by calcium phosphate (PEO/ modified TiO_2). abiotic oxidation of PP/ PEO/ modified TiO_2 is studied. In the Chapter 6, biotic oxidations of PP/ PEO/ TiO_2 and PP/ PEO/ modified TiO_2 are studied. In the Chapter 7, abiotic and biotic oxidations of PP/ cellulose/ PEO/ TiO_2

References

[1] Peter J. T. Morris, *Polymer Pioneers* 2005, 76.

[2] J.P. Soares L.C. simon, T. Meyer and T. F. Keurentijes Eds., WILEY-VCH Verlag GmbH & Co. KCaA, Germany, Weinheim, 2005, chapter 8, 365

[3] T. Meyer and, T. F. Keurentijes, T. Meyer and T. F. Keurentijes Eds., *Handobook of polymer Reaction Engineering*,., WILEY-VCH Verlag GmbH & Co. KCaA, Germany, Weinheim, 2005, 2

[4] "Future supply and demand trend of world petrochemical products", *report of Ministry of Economy, Trade and Industry of Japan*, 2010

[5] N. P. Cheremisinoff, *Guidbook to commercial polymers, properties and applications*, PTR Prentice Hall, New Jersey 1993, 62

[6] R.B. Saymour, C. Vasile, M. Rusu, *Handbook of polyolefins,* , Marcel Dekker, New York, 1993, 1007

[7] R. F. Becker, L. P. J. Burton, S. E. Amos, E.P. Moore Jr. Eds., *Polypropylene Handbook*, Carl Hanser Verlag, Munich Vienna New York 1996, 177

[8] T.Q. Nguyen, T. Meyer and T. F. Keurentjes Eds., *Handbook of Polymer Reaction Engineering*, WILEY-VCH Verlag GmbH & Co. KCaA, Germany, Weinheim, 2005, 757

[9] E. Ott, H. M. Spurlin, Eds. *Cellulose and Cellulose Derivatives*, Interscience Publishers, New York, 1954, 1

[10] S. Takase, N. Shiraishi, *J. Appl. Polym. Sci.*, 1989, 37, 645.

[11] D. Maldas, B. V. Kokta, C. Daneault, *J. Appl. Polym. Sci.*, 1989, 37, 751.

[12] R. G. Raj, B. V. Kokta, D. Maldas, C. Daneault, *J. Appl. Polym. Sci.*, 1989, 37,

1089.

[13] P. Hedenberg, P. Gatenholm, *J. App.l Polym. Sci.*, 1996, 60, 2377.

[14] F. Zhang, W. Qiu, L. Yang, T. Endo, *J. Mater. Chem.*, 2002, 12, 24

[15] W. Qiu, F. Zhang, T. Endo, T. Hirotsu, *J. Appl. Polym. Sc i.*, 2003, 87, 337.

[16] W. Qiu, F. Zhang, T. Endo, T. Hirotsu, *J. Appl. Polym. Sc i.*, 2004, 91, 1703.

[17] J. M. Felix, P. Gatenholm, *J. Appl. Polym. Sci.*, 1991, 42, 609.

[18] W. Qiu, F. Zhang, T. Endo, T. Hirotsu, *J. Appl. Polym. Sci.*, 2004, 94, 1326.

[19] V. N. Hristov, S. T. Vasileva, M. Krumova, R. Lach, G. H. Michler, *Polym. Compos.*, 2004, 25, 521.

[20] D. Nwabunma, T. Kyu, *Polyolefin composites*, John Wiley ans Sons. Hoboken, New Jersey, 2008, 33

[21] A. A. Klyosov, *Wood-Plastic Composetes*, John Wiley ans Sons. Hoboken, New Jersey, 2007, 86

[22] A. Steinbücheil, R. J. Müler, *Biopoymers vol. 10*, 2004, 365

[23] A. C. Albertsson, S. O. Andresson, S. Karlsson, *Polym. Degrad. Stab.*, 1987, 18(1), 73

[24] A. C. Albertsso, C. Barenstedt, S. Karlsson, *Polym. Degrad. Stab.*, 1992, 37(2), 163

[25] M. Weiland, A. Daro, C. Dacid, *Polym. Degrad. Stab.*, 1995, 48(2), 275

[26 I. Jakubowicz, *Polym. Degrad. Stab.*, 2003, 80(1), 39.

[27] M. M. Reddy, R. K. Gupta, R. K. Gupta, S. N. Bhattacharya, R. Parthasarathy *J. Polym. Environ.*, 2008, 16(1), 27

[28] Y. Kato, D. J. Carlsson, D. M. Wiles, *J. Appl .Polym. Sci*. 1969, 13, 1447

[29] D. J. Carlsson, D. M. Wiles, *Macromolecules*, 1969, 6, 597

[30] J. H. Adams, *J. Polym. Sci. A1*, 1970, 8, 1077

[31] N. C. Billingham, *Makromol. Chem. Macromol. Symp.*, 1989, 28, 145

[32] G. A. George, M. Celina S. Halim Hamid Eds., *Handbook of Polymer Degradation* Marcel Dekker, New York, 2000, 280

[33] J. Scheirs, D. J. Carlsson, S. W. Bigger, *Polym. Plast. Technol. Eng.* 1995, 34, 97

[34] J. C. W. Chien, E. J. Vandeberg, H. Jabloner, *J. Polym. Sci. A1*, 1968, 6, 381

[35] F. R. Mayo, *Macromolecules*, 1978 11, 942

[36] A. Garton, D. J. Carlsson, D. M. Wiles, *Makromol. Chem.*, 1980, 1811

[37] V. A. Roginski, N. Grassie, ed. *Developments in Polymer Degradation*, Applied Science, London, 1986, 193

[38] J. F. Rabek, *Photostabilization of Polymers- Principales and Applications*, Elsevier Applied Science, London, 1990, 33

[39] A. Garton, D. J. Carlsson, D. M. Wiles, *J. Polym. Sci. A1*, 1978, 16, 33

[40] A. Garton, D. J. Carlsson, D. M. Wiles, *Macromolecules*, 1979 12, 1071

[41] J.F. Rabek, *Mechanisms of Photophysical Processes and Photochemical reactions in Polymer.* Wiley, Chichester, p. 1987

[42] S. Commerce, D. Vaillant, J. L. Philippart, J. Lamaire, D. J. Carlsson, *Polym. Degrad. Stab.*, 1997, 57, 175

[43] P. Gijsman, J. Sedlar, D. Dastych, *Polym. Degrad. Stab.*, 1993, 42, 95

[44] A. Zahradmickova, J. Sedlar, D. Dastych, *Polym. Degrad. Stab.*, 1991, 32, 155

[45] D. J. Carlsson, A. Garton, D. M. Wiles, N. Grassie, Eds. *Development in Polymer Degradation*, Applied Science, London, 1979, 219

[46] Z. Osawa, N. Kurisu, K. Nagashima and K. Nankano, *J. Appl. Polym. Sci.*, 1979, 23, 3583

[47] P.K. Roya, P. Surekhaa, C. Rajagopala, S.N. Chatterjeeb and V. Choudhary, *Polym.*

Degrad. Stab., 2006, 91(8), 1791

[48] B. Ohtani, S. Adzuma, H. Miyadzu, S. Nishimoto, T. Kahiya, *Polym. Degrad. Stab.*, 1989, 23(3), 271.

[49] T. J. Turton, J. R. White, *Polym. Degrad. Stab.*, 2001, 74(3),559.

[50] M. F. Mina, S. Seema, R. Matin, M. J, Rahaman, R. B. Sarker, M. A. Gafur, et al. *Polym. Degrad. Stab.*, 2009, 94(2), 183.

[51] I. Blakey, G. A. George, *Polym. Degrad. Stab.*, 2000, 70(2), 269.

[52] S. P. Vijayalakshmi, G. Madras, *J. Appl. Polym. Sci.*, 2006, 100(5), 3997.

[53] T. Kagiya, N. Yokoyama, K. Takemoto, *Bull Inst Chem Res Kyoto Univ* 1976, 54(1), 15.

[54] R. Broska, J. Rychlý, K. Csomorová, *Polym. Degrad. Stab.*, 1999, 63(2), 231.

[55] P. Eriksson, T. Reiberger, B. Stanberg, *Polym. Degrad. Stab.*, 2002, 78(1), 183.

[56] M. Tien, K. Kirk, Methods in Enzymology, 1988, 161, 238

[57] M. Leena, N. Paavola, E. Karhunen, P. Salola, V. Raunio, Biochem, 1988, 254, 877

Chapter 2: Effect of the Molecular Weight and Concentration of Oxidatively Degraded and Maleated Polypropylene Compatibilizers on Tensile Behavior in Cellulose/Polypropylene Composites

2-1: Introduction

Cellulose is one of the most abundant natural resources and has been used for the manufacture of paper for a long time. The advantages of cellulose are low-cost, high-modulus, renewable, and biodegradable. Recently, cellulose has attracted much attention as a composite material [1–10] because it has great potential for the preparation of composite materials with high modulus and renewability.

As the most popular composite based on cellulose, the composite with polypropylene (PP) has been extensively prepared. This is due to the commercial importance of PP as a material applicable to household appliances, medical wares, and automotive and other industrial products. In the case of the composite, fibrous cellulose (FC) has been generally used as the cellulose source because it has been expected instead of glass or carbon fibers. FC, however, is hydrophilic and tends to aggregate; this causes poor processability and phase separation with hydrophobic PP.

The preparation of the applicable composite has been studied in the modification of FC surfaces with maleated polypropylene (MAPP)[1, 6, 8, 9, 11, 12] a surfactant,[12] isocyanate coupling,[13, 14] and corona discharge [15, 16].

We use oxidatively degraded polypropylene (DgPP) as a novel compatibilizer. Oxidative degradation reaction of PP easily occurs under the influence of elevated temperature and sunlight [17-21]. The oxidative degradation of PP has been widely

recognized as a free-radical mechanism called “autooxidation” [17, 18, 20, 21]. In this autooxidation, methyl ketone compound is produced via a reaction involving hydroperoxide group (ROOH) formation. Therefore, the most suitable method to evaluate the degree of PP degradation is the determination of the ketone concentration. The infrared (IR) measurement has been used as a brief method for measuring of such concentration. In addition, the IR peak intensity obtained is also proportional to the concentrations of γ-lactone, aldehyde and acid groups, which are produced onto the degraded PP chain [19]. The chemical structure and formation behavior of these function groups have already investigated by Adams et al. [19], and the concentrations of those groups can be briefly obtained from the IR peaks. Among of these function groups, the γ-lactone and the acid groups are seems to be interesting since some kinds of ester such as ε-caprolactone and lactide allow OH group of cellulose surface to be modified by esterification [22, 23].

These compatibilizers play an important role in converting the hydrophilic FC surface to a hydrophobic one. The mechanism is a similar binding reaction between the OH group on the FC surface and the reactive groups in the compatibilizers. These compatibilizers adhere to the FC surface by the reaction. The adhesion style, however, is considerably different because of the arrangements of the reactive groups in the compatibilizers. One style involves adherence at the compatibilizer chain end, and the other one occurs at the inner compatibilizer chain. This difference undoubtedly affects the mechanical properties of the added composite because the distribution of applied stress is dependent on the adhesion location. In the case of polymer-type compatibilizers such as MAPP and DgPP, the compatibilizer chain adhering to FC interacts with the matrix consisting of PP chains through the entanglement of the mutual chains and brings

about stronger interfacial adhesion between the PP matrix and FC [9]. The adhesion style must be of particular importance to polymer-type compatibilizers. However, little has been investigated about this. In addition, DgPP can be easily obtained from an oxidative degradation reaction of PP at an elevated temperature and in sunlight and could be an application for recycled PP. A comparison of the compatibilizer ability of DgPP and MAPP would provide useful information for the application of DgPP.

In this study, DgPP and MAPP compatibilizers have been used as models of polymer-type compatibilizers. These compatibilizers have similar ester bonds, which are produced between the OH group in FC and the reactive groups (-lactone, acid, and maleic anhydride) in their polymer chains. The adhesion styles using the ester bond, however, are considerably different, so DgPP has the reactive group at the chain end [24] and MAPP has one in the inner chain.[9, 25] These additive effects on the tensile behavior of FC/PP composites have been extensively studied, including the dependence of the molecular weight of DgPP and the reactive group content in MAPP.

2-2: Experimental

2-2-1: Materials

PP (meso pentad fraction = 98%) was supplied by Japan Polypropylene Co. (Yokkaichi, Japan). The number-average molecular weight (M_n) and polydispersity [weight-average molecular weight/number-average molecular weight (M_w/M_n)] of PP were 4.6×10^4 and 5.7, respectively. PP was reprecipitated from a boiling xylene solution into methanol and dried at 60°C for 8 h, and it was used as samples without an antioxidant. FC (W-100GK) was donated by Nippon Paper Chemicals Co., Ltd. It was dried in a desiccator for 7 days before preparation. Two kinds of MAPP were purchased

from Sigma–Aldrich (St. Louis, MO). The MAPPs with lower (ca. 0.6 wt %) and higher (ca. 8 wt %) maleic anhydride contents were denoted LMAPP and HMAPP, respectively. The melt index of LMAPP was 115 g/10 min (190°C/2.16 kg). The M_n *and* M_w/M_n values of HMAPP were 3.9×10^3 and 2.3, respectively.

2-2-2: Preparation of DgPP

PP was molded into a thin film (50 μm) by compression molding at 190°C under 50 MPa for 5 min. It was put into a vial and was allowed to stand in the heating block in air. Thermal oxidative degradation was carried out at 130°C for 10 or 18 h. The PPs obtained after 10 and 18 h were called LDgPP ($M_n = 1.0 \times 10^4$, $M_w/M_n = 2.0$) and HDgPP ($M_n = 5.0 \times 10^3$, $M_w/M_n = 2.3$), respectively. The total contents of the oxidation compounds (γ-lactone and acid compounds) were calculated from the peak area between 2.1 and 2.3 ppm in the ^{1}H-NMR spectra. In the case of LDgPP, the total content calculated from the area was about 0.9 mol %, whereas that of HDgPP was about 1.6 mol %.

2-2-3: Preparation of the composites

Composites were prepared with an Imoto Seisakusyo IMC-1884 melting mixer (Kyoto, Japan). After a small amount (ca. 0.5 wt %) of a phenolic antioxidant (AO-60, Adekastab) was added, mixing was performed at 180°C and 60 rpm for 5 min. The obtained composites were molded into films (100 μm) by compression molding at 190°C under 5 MPa for 5 min.

2-2-4: Gel permeation chromatography analysis

A sample in a small vial was dissolved in 5 mL of *o*-dichlorobenzene with 2,6-*di*-*t*-butyl-*p*-cresol added as an antioxidant, and the obtained sample solution was directly measured by gel permeation chromatography. The molecular weight was determined by gel permeation chromatography (SSC-7100, Senshu, Tokyo, Japan) with styrene–divinylbenzene gel columns (HT-806M, Shodex) at 140°C with *o*-dichlorobenzene as a solvent.

2-2-5: Nuclear magnetic resonance spectroscopy and Fourier transform infrared spectrometer measurements

The ^{1}H-NMR spectrum of degraded PP was measured with a Varian Gemini-300 spectrometer (Palo Alto, CA) at 120°C on a 10% (w/v) solution in hexachloro-1,3-butadiene. 1,1,2,2-Tetrachloroethane-d_2 was added as an internal lock and used as an internal chemical shift reference.

The Fourier transform infrared spectrum was measured with a PerkinElmer Spectrum One spectrometer (Waltham, MA) with a film sample.

2-2-6: Tensile testing

The stress–strain behavior was observed with a Shimadzu EZ-S (Kyoto, Japan) at a crosshead speed of 5 mm/min. The sample specimens were cut into dimensions of 30 × 2 × 0.1 mm^3, and the gauge length was 10 mm. All tensile testing was performed at 18°C. The values of Young's modulus were obtained from the slope of the stress–strain curve (until ca. 1% of the strain value). All obtained results were the average values of 10 measurements.

2-2-7: Scanning electron microscopy (SEM) measurement

The morphology of the composite was examined with a JEOL JSM-T200 (Tokyo, Japan) at 25 kV. The plate of the composite was fractured in liquid nitrogen, and then the fractured surface was sputter-coated with gold.

2-2-8: Differential scanning calorimetry (DSC) measurements

DSC measurements were made with a Mettler DSC 820 (Küsnacht, Switzerland). Samples of about 5 mg were sealed in aluminum pans. The measurement of the samples was carried out at a heating rate of 20°C/min under a nitrogen atmosphere.

2-2-9: Wide-angle X-ray diffraction measurement

Wide-angle X-ray diffraction diffractograms were recorded in reflection geometry at 2° (2θ/min) under Ni-filtered Cu Kα radiation with a Rigaku Rint 1200 diffractometer (Tokyo, Japan).

2-2-10: Polarized Optical Microscope (POM) Observation

Spherulite observations were carried out with a Nikon ECLIPSE 50/POL optical microscope (Nikon Corp. Tokyo, Japan) under nitrogen atmosphere. The isothermal crystallization temperature was controlled by a hot-stage system (Microscopy Hot-Stage, Imoto Seisakusyo, Kyoto, Japan). All samples were heated in the hot-stage and kept at 200 °C for 5 min. They were quickly cooled to 130 °C and were observed isothermally.

2-3: Results and Discussion

2-3-1: Effect of Degraded Polypropylene (DgPP) Compatibilizer

2-3-1-1: Characterization of DgPP

Figure 2-1 shows the buildup of methyl ketone peak around 1,715 cm^{-1} during thermal oxidative degradation at 130 °C. The concentration increased up to about 18 h and then was almost constant.

γ-lactone compound is a main product of the secondary reaction of autooxidation [19]. The corresponded IR peak appears around 1,775 cm^{-1} and has an average molar absorptivity of 600 mol L^{-1} cm^{-1} [19].

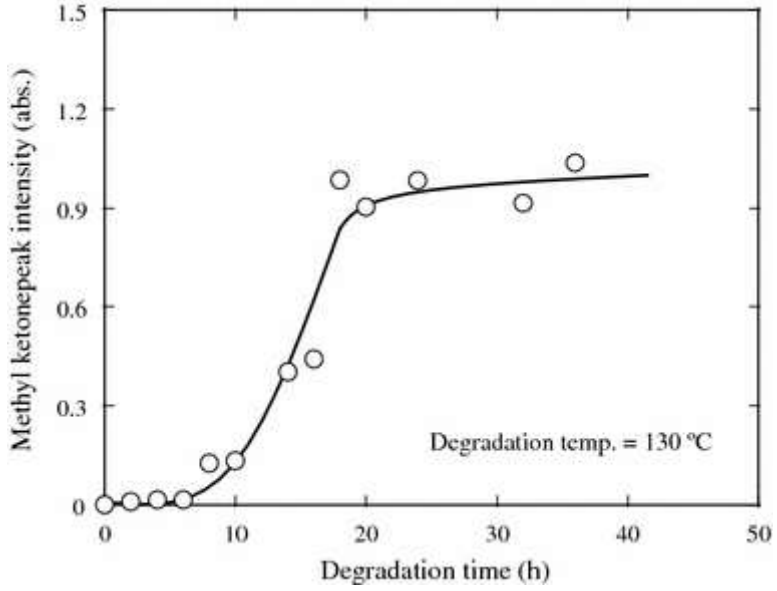

Figure 2-1 Buildup of methyl ketone peak in HDgPP film during thermal oxidative degradation

Figure 2-2 shows the IR spectra of degradation time of 10, 18 and 36 h. The buildup of γ-lactone as well as that of the methyl ketone apparently reached the maximum in 18 h. This behavior suggests that a volatilization of highly oxidized PP part occurs simultaneously after 18 h. The degradation time of 18 h is considered to be the optimal

preparation time from the viewpoint of the oxidized compound contents. In addition, acid compound is also a main product of the secondary reaction of autooxidation. However, the corresponded IR peak (ca. 1,710 cm^{-1}) overlaps with that of the methyl ketone [19] and is indistinguishable.

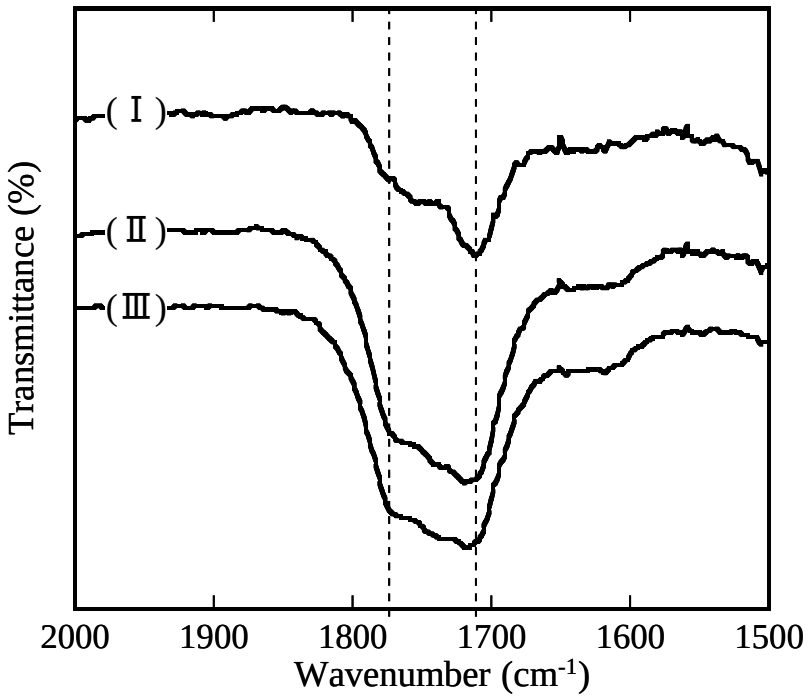

Figure 2-2 γ-lactone and methyl ketone peaks (FT-IR spectra). (Ⅰ): degradation time 10 hour. (Ⅱ): degradation time 18 hour. (Ⅲ): degradation time 36 hour

The γ-lactone content in the 18 h is 0.98 mol%, of which value was calculated by Lambert-Beer law using the average molar absorptivity and the PP density (0.9 g/mL). Figure 2-3 shows the ^{1}H-NMR spectrum. The peak assignment referred to that of γ-lactone monomer. The methylene hydrogen (denoted as "a" in the figure) can be assigned to the peak of ca. 2.15 ppm (γ-lactone monomer: 2.1 ppm), and the methine one (denoted as "b") can be done to ca. 2.18 ppm (2.3 ppm). Whereas, the methylene and the methine hydrogen peaks (denoted as "c" and "d") of the acid compound are

almost the same as the location of the γ-lactone peaks. Thus, the total content of γ-lactone and acid compounds calculated from the area is ca. 1.6 mol%. The acid compound content would be the subtraction (ca. 0.62 mol%) between the values obtained from the ^{1}H-NMR and the IR measurements.

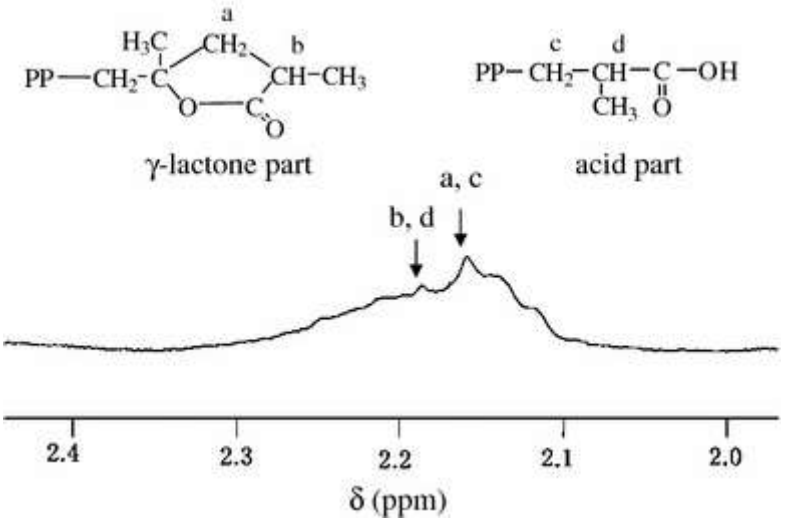

Figure 2-3 ^{1}H-NMR spectrum of HDgPP. Degradation time = 18 h. Degradation temperature = 130 °C

The molecular weight ($M_n = 5.2 \times 10^3$, $M_w/M_n = 5.7$) of the HDgPP decreased to about 10% of that of the virgin PP. Figure 2-4 shows the optical micrographs of the PP and the HDgPP. It appears that the spherulite shape of HDgPP is considerably coarser than that of PP. In particular, the openness of crystal texture is remarkable. Interestingly this behavior is well similar to that of isotactic and atactic PP blend [26]. This would be due to a retardation of crystallization of an undegraded PP part by dilution of a degraded PP part. In other words, the phenomenon, in which the degraded part acts as the diluent, suggests that PP and HDgPP are miscible.

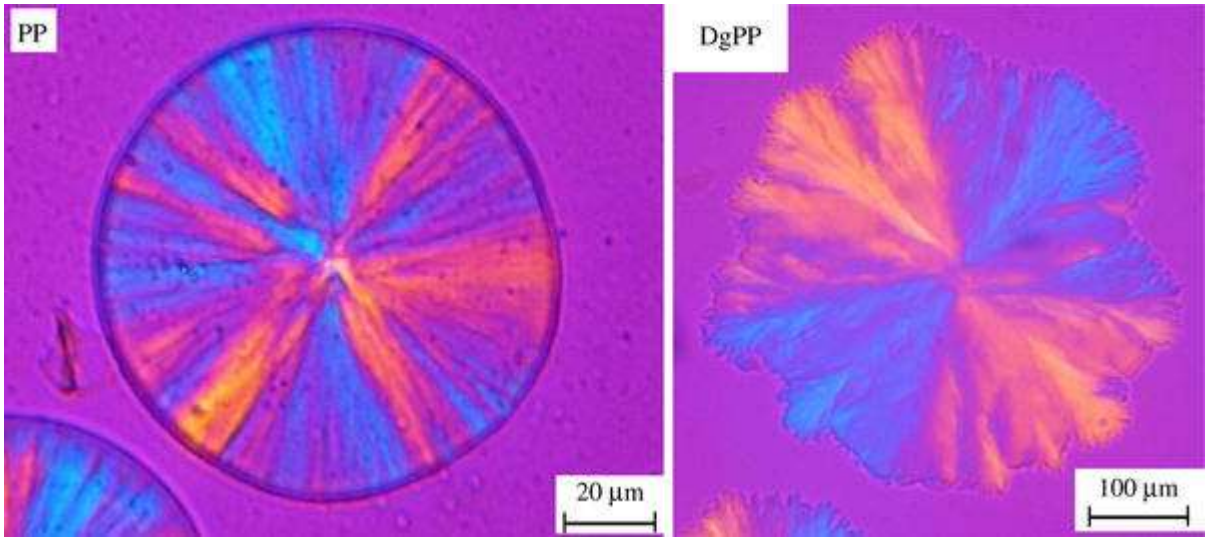

Figure 2-4 Optical micrographs of PP and HDgPP. Isothermal crystallization at 130 °C under nitrogen

2-3-1-2: Evaluation of Dispersity of Fibrous Cellulose (FC)/Polypropylene (PP)/Degraded Polypropylene (HDgPP) Composites

Figure 2-5 shows the particle size distribution of FC. Most of the particles were the sizes from 10 to 100 µm. Preparation of composites was carried out with this FC.

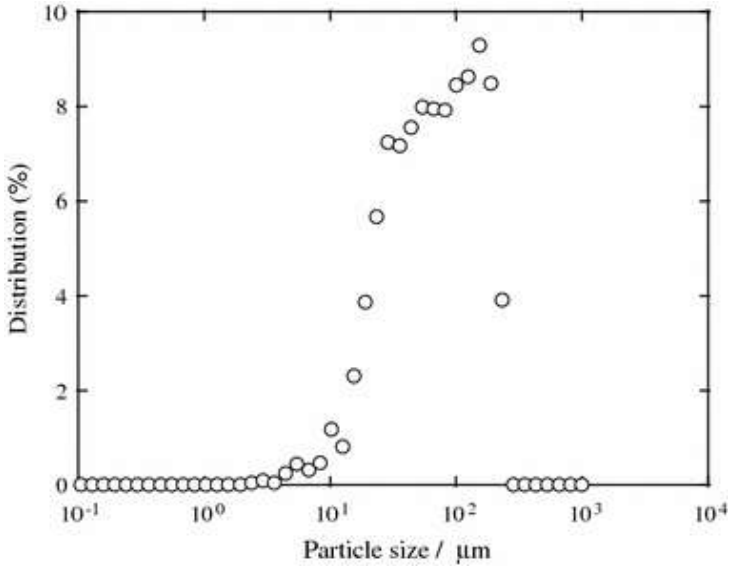

Figure 2-5 Particle size distribution of FC

The transparency of the composites was evaluated by the average transmittance in the range of visible light (380–780 nm). These results were summarized in Table 2-1.

Table 2-1 Average transmittance in the range of visible light (380–780 nm) of composites

Sample	**Average transmittance[a] from 380 to 780 nm (%)**
PP	62
PP(90 wt%)/DgPP(10 wt%)	63
FC(7 wt%)/PP(93 wt%)	40
FC(7 wt%)/PP(92.5 wt%)/DgPP(0.5 wt%)	48
FC(7 wt%)/PP(92 wt%)/DgPP(1 wt%)	48
FC(7 wt%)/PP(91 wt%)/DgPP(2 wt%)	53
FC(7 wt%)/PP(89 wt%)/DgPP(4 wt%)	50
FC(7 wt%)/PP(87 wt%)/DgPP(6 wt%)	52
FC(7 wt%)/PP(85 wt%)/DgPP(8 wt%)	53
FC(7 wt%)/PP(83 wt%)/DgPP(10 wt%)	46

[a]From UV–VIS spectrometer

The average transmittance of PP/HDgPP is the same of PP, indicating that the PP and the HDgPP are miscible as mentioned above. In contrast, the transmittance of FC/PP is considerably lower due to the aggregation of FC as shown in Figure 2-6. This is typical behavior on composite of hydrophilic and hydrophobic materials. It is noticed here that

the existence of HDgPP brings about improvement in the dispersity of FC. Apparently the transmittances of FC/PP/HDgPP composites were up around 20% and 30% compared with the transmittance of FC/PP. The improvement in transparency suggests that a modification of the FC surface occurs by the addition of HDgPP.

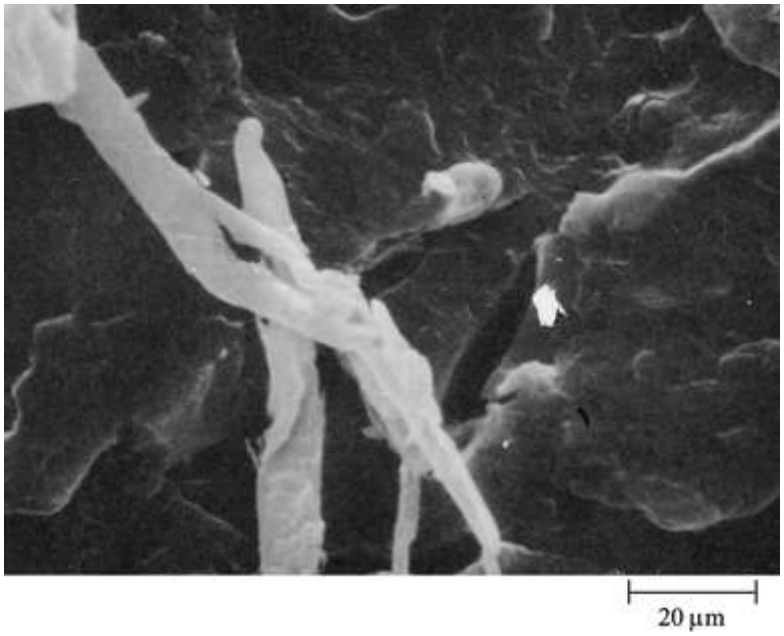

Figure 2-6 SEM micrograph of fracture surfaces of FC(7 wt%)/PP(93 wt%)

Figure 2-7 shows FT-IR spectra of the composites. A new peak appeared around 1,745 cm^{-1} in only the FC/PP/HDgPP composite. This peak would be assigned to ester group [19]. In case of cellulose and maleated PP (MAPP), it is known that an esterification between cellulose and MAPP occurs by melt mixing [6] and heat treatment in a hot toluene solution [8]. According to the literature, a new peak at 1,730 cm^{-1} [6] or at 1,746 cm^{-1} [8] arose from ester bond, which was caused by the reaction between OH group of cellulose surface and maleic anhydride group grafted onto the PP chain. This grafted MAPP brought about hydrophobic surface on the cellulose and improved dispersity of the cellulose in PP matrix. The HDgPP contains the

γ-lactone and the acid compounds. As shown in Figure 2-8, it seems that the formation of ester bond occurs by the reaction between the OH group of FC surface and the γ-lactone and acid parts in HDgPP.

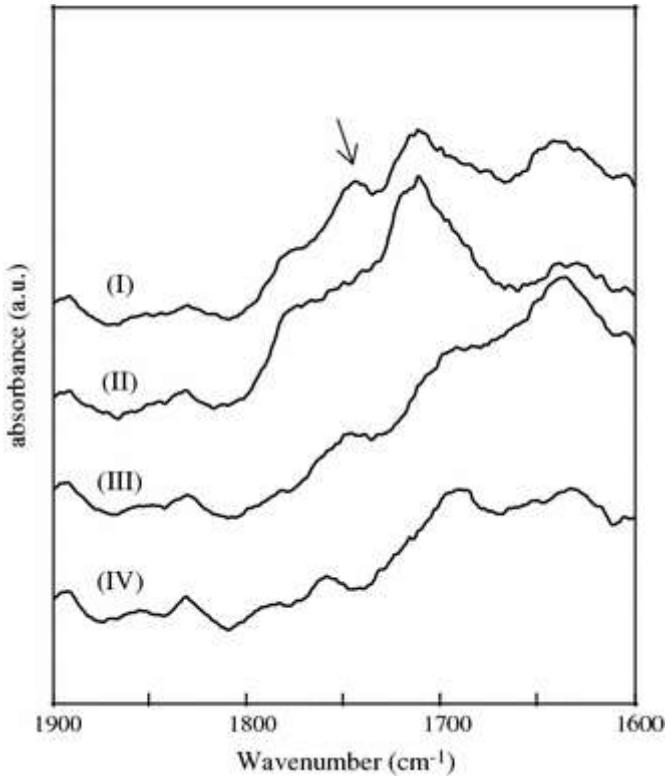

Figure 2-7 FT-IR spectra of PP and composites.

(I): FC(7 wt%)/PP(91 wt%)/HDgPP(2 wt%). (II): PP(90 wt%)/HDgPP(10 wt%).

(III): FC(7 wt%)/PP(93 wt%). (IV): PP. The arrow indicates a new peak

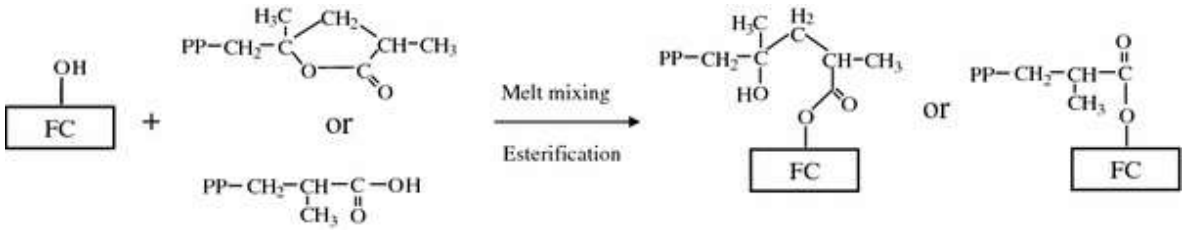

Figure 2-8 Plausible formation mechanism of ester compound between FC and HDgPP

The additive effect of HDgPP on crystallization behavior of FC/PP composites was studied by POM observation. In general, cellulose/PP composite exhibits transcrystalline morphology under an isothermal crystallization condition as shown in Figure 2-9(a-c). The transcrystallization is ascribed to an interaction between cellulose and PP at a molecular level [28]. The existence of HDgPP apparently disturbs the interaction as shown in Figure 2-9(d–f and g–i). The FC surface seems to be extensively covered with the grafted HDgPP chain. In addition, with only 2 wt% of HDgPP, the effect sufficiently appeared because the transcrystalline morphology was unseen. It appears that the esterification reaction proceeds smoothly and efficiently

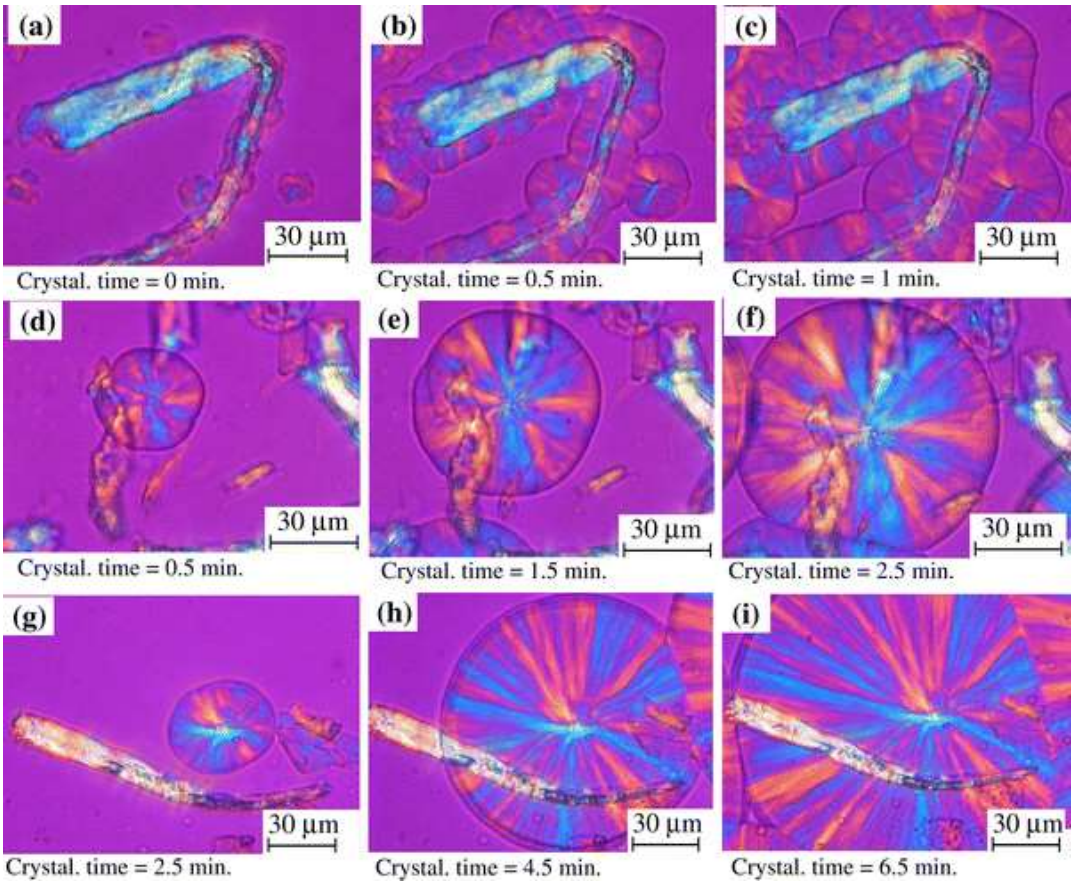

Figure 2-9 Optical micrographs of composites at 130 °C under nitrogen. a–c FC(1 wt%)/PP(99 wt%). d–f FC(7 wt%)/PP(91 wt%)/HDgPP(2 wt%). g–i FC(7 wt%)/PP(83 wt%)/HDgPP(10 wt%)

SEM micrographs of fractured surfaces of the composites PP/HDgPP and FC/PP/HDgPP are shown in Figure 2-10. There was no observation of an aggregated part in the PP/HDgPP micrograph. This indicates that the PP and the HDgPP are miscible. In the micrograph of FC/PP/HDgPP, several rod-like celluloses were clearly seen. The celluloses of all size were about 30 μm and were in good agreement with the FC particle size measured by the laser diffraction particle size analyzer (see Figure 2-5). This result strongly supports that the addition of HDgPP disturbs the aggregation of the FC particle.

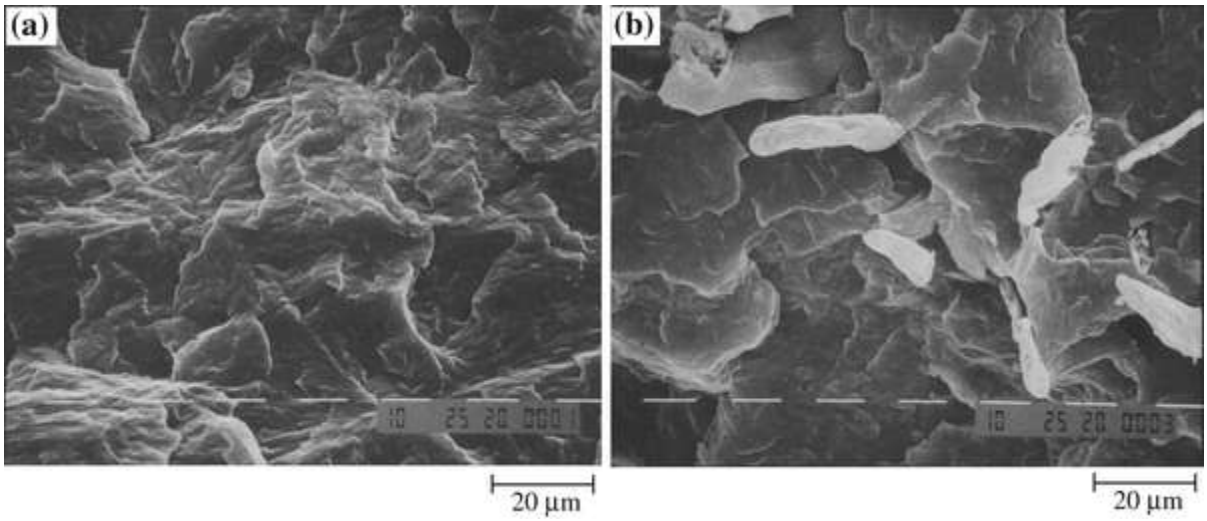

Figure 2-10 SEM micrographs of fracture surfaces of composites. a PP(90 wt%)/HDgPP(10 wt%). b FC(7 wt%)/PP(83 wt%)/HDgPP(10 wt%)

Figures 2-11 and 2-12 show the magnified SEM micrographs of the FC/PP/HDgPP and of the untreated FC. As shown in both figures, the FC surface in the FC/PP/HDgPP is different from the scale-like one of the untreated FC. The FC is coated with a polymer (probably HDgPP) layer. It appears that the nature of the FC surface is changed into hydrophobicity by coating with the HDgPP.

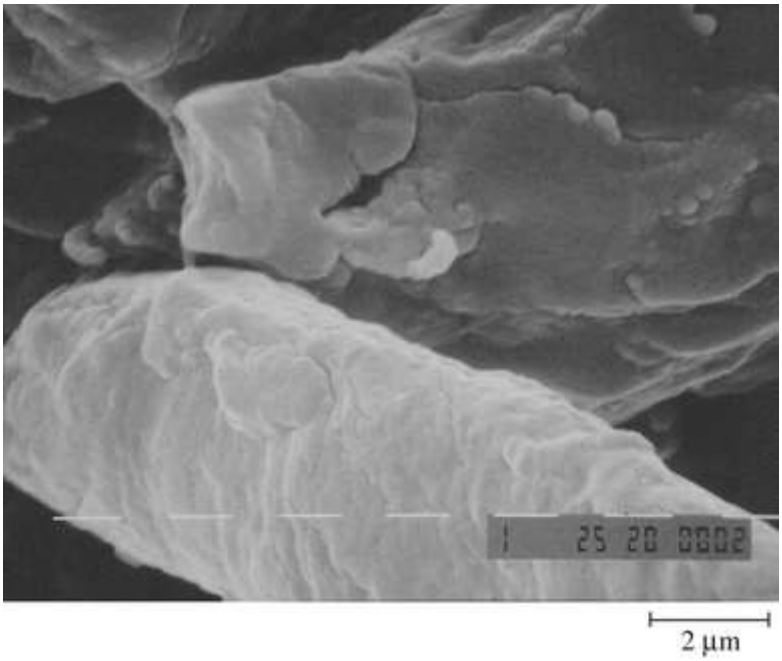

Figure 2-11 Magnified SEM micrograph of fracture surface of FC(7 wt%)/PP(83 wt%)/HDgPP(10 wt%)

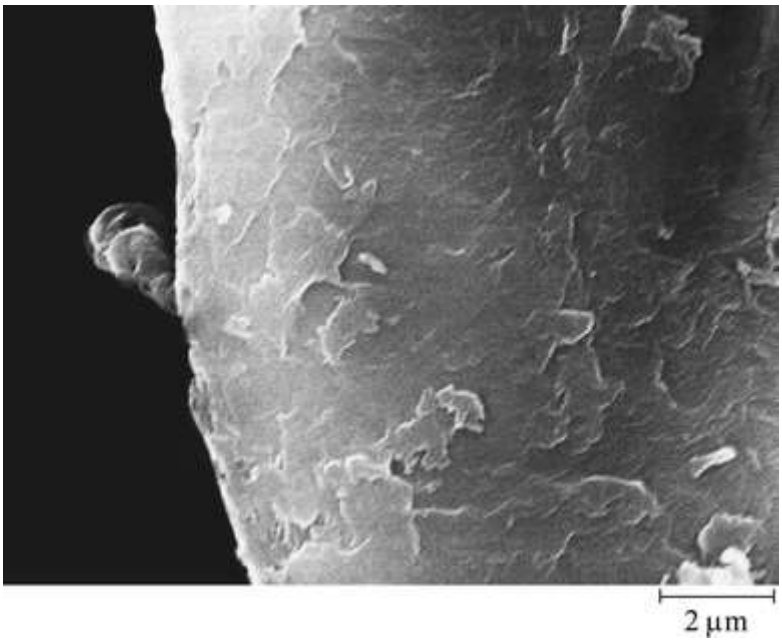

Figure 2-12 Magnified SEM micrograph of untreated FC surface

2-3-1-3: Evaluation of Mechanical Properties of Fibrous Cellulose (FC)/Polypropylene (PP)/Degraded Polypropylene (HDgPP) Composites

Figure 2-13 shows the stress–strain curves of the FC(7 wt%)/PP and the composites with various HDgPP content. The tensile behavior evidently depends on the HDgPP content. The composite containing 1 wt% of the HDgPP exhibits the higher tensile strength than that of the composite without the HDgPP. However, the composites containing over 2 wt% of the HDgPP reduce the tensile strength. These behavior suggest that some parts of the HDgPP act as the coupling agent for the FC/PP composite and the remainder parts do as a mechanical defect due to its considerably lower molecular weight (see experimental section) compared to the original PP. As shown in Figure 2-9(d–f), the FC surface can be extensively covered with a small amount of the grafted HDgPP chain. The HDgPP required as the coupling agent would be a small amount.

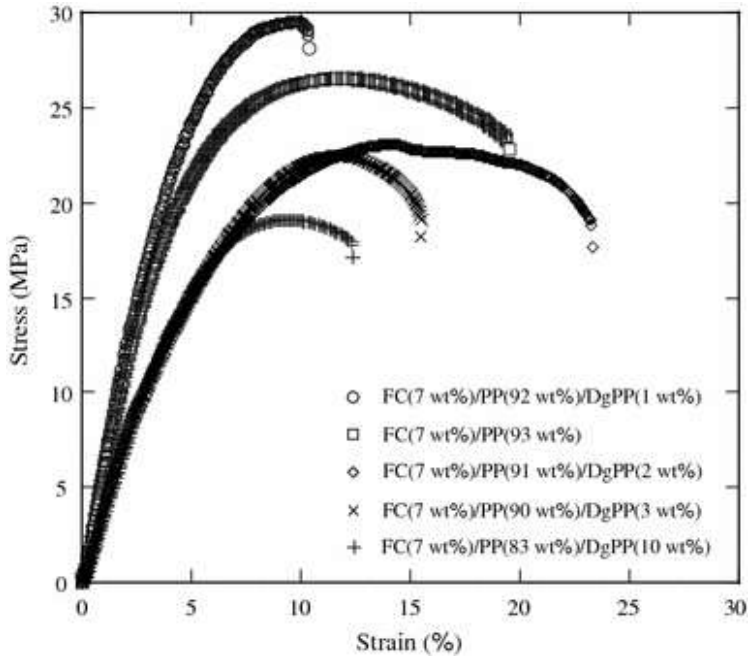

Figure 2-13 Stress–strain curves of FC(7 wt%)/PP and FC(7 wt%)/PP/HDgPP composites

The DSC curves of FC(7 wt%)/PP and FC(7 wt%)/PP/HDgPP composites are shown in Figures 2-14 and 2-15. Although the glass transition temperatures (T_g) are not so clear, they are slightly observable from −1 °C to 0 °C and seem to hardly change against the amount of the HDgPP. Whereas, the melting points (T_m) are gradually decreasing with the HDgPP. This behavior supports that the retardation of crystallization of an undegraded PP occurs by the dilution effect of the HDgPP mentioned above.

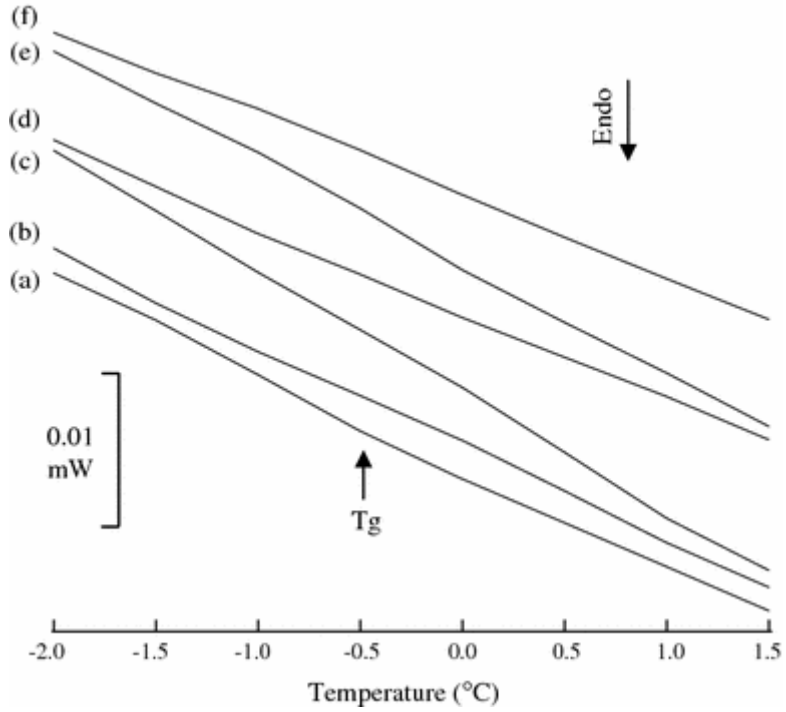

Figure 2-14 DSC curves of FC(7 wt%)/PP and FC(7 wt%)/PP/HDgPP composites around a glass transition temperature (T_g).

(a): FC(7 wt%)/PP(93 wt%). (b): FC(7 wt%)/PP(91 wt%)/HDgPP(2 wt%).

(c): FC(7 wt%)/PP(89 wt%)/HDgPP(4 wt%).

(d): FC(7 wt%)/PP(87 wt%)/HDgPP(6 wt%).

(e): FC(7 wt%)/PP(85 wt%)/HDgPP(8 wt%).

(f): FC(7 wt%)/PP(83 wt%)/HDgPP(10 wt%)

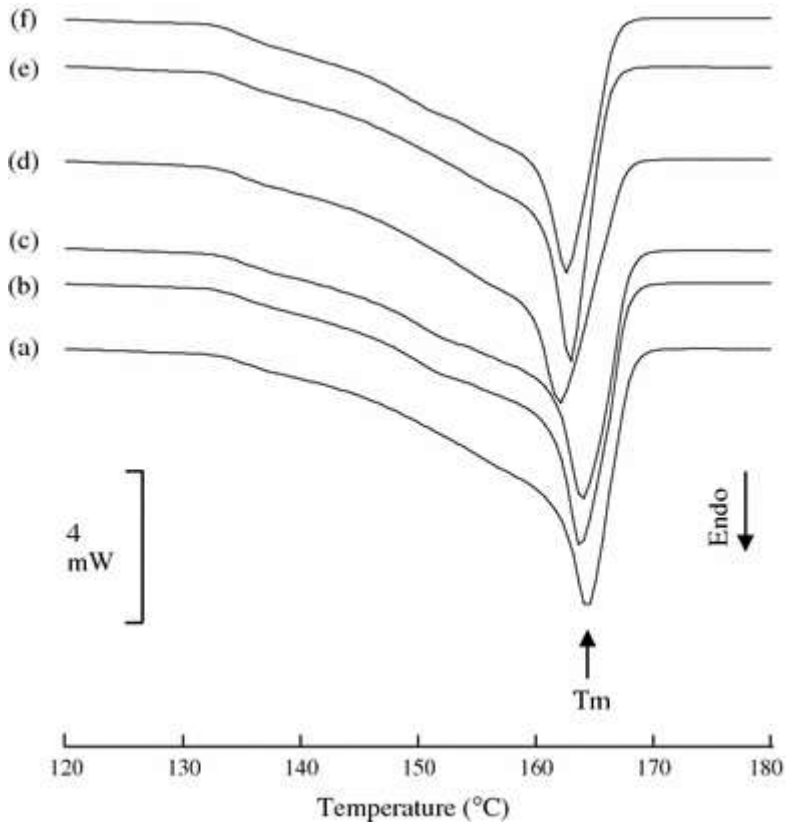

Figure 2-15 DSC curves of FC(7 wt%)/PP and FC(7 wt%)/PP/HDgPP composites around a melting point (T m).

(a): FC(7 wt%)/PP(93 wt%). (b): FC(7 wt%)/PP(91 wt%)/HDgPP(2 wt%).

(c): FC(7 wt%)/PP(89 wt%)/HDgPP(4 wt%).

(d): FC(7 wt%)/PP(87 wt%)/HDgPP(6 wt%).

(e): FC(7 wt%)/PP(85 wt%)/HDgPP(8 wt%).

(f): FC(7 wt%)/PP(83 wt%)/HDgPP(10 wt%)

2-3-2: Effect of the Molecular Weight and Concentration of DgPP and MAPP

SEM micrographs of fractured surfaces of the FC/PP composites are shown in Figure 2-16. In Figure 2-16(a), the micrograph of the FC (30 wt %)/PP (70 wt %) composite clearly shows that there are many ellipse-like holes in the PP matrix. As shown in Figure 2-16(b), the holes are the imprints of aggregated FCs. In addition, the edges of the holes are quite smooth, and the FCs are not fractured. These results suggest that the interfacial adhesion between FC and PP is poor and requires improvement.

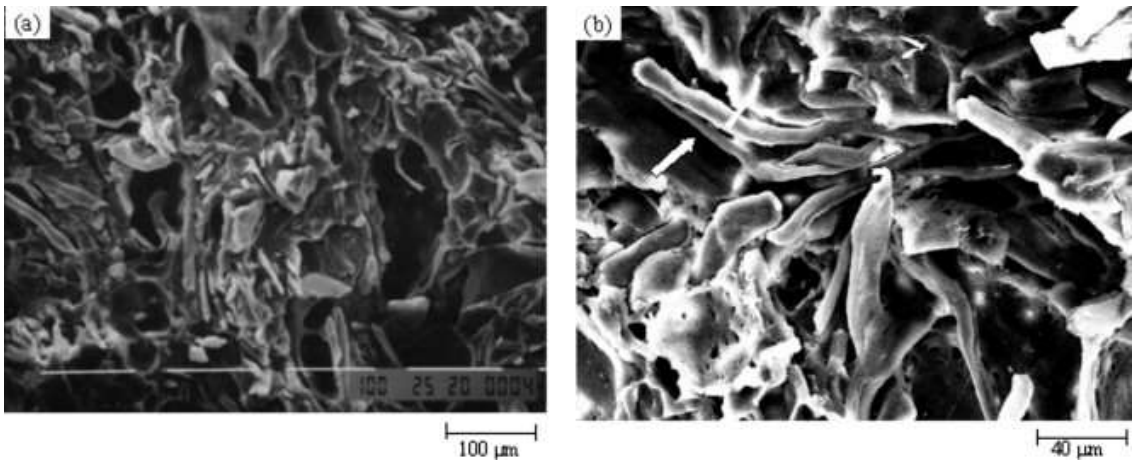

Figure 2-16 SEM micrographs of fracture surfaces of an FC (30 wt %)/PP (70 wt %) composite: (a) low magnification and (b) high magnification. The arrow indicates aggregated FCs.

As shown in Figure 2-17 a peak appears at 1745 cm^{-1} for the FC/PP composite with DgPP as well as MAPP added. This peak does not appear for PP (see Figure 2-17) and is assigned to the ester group [8]; this suggests that esterification occurs between OH groups in FC and reactive (γ-lactone and acid) groups in DgPP as well as maleic anhydride groups in MAPP. These grafted FCs will certainly bring about an improvement in the interface.

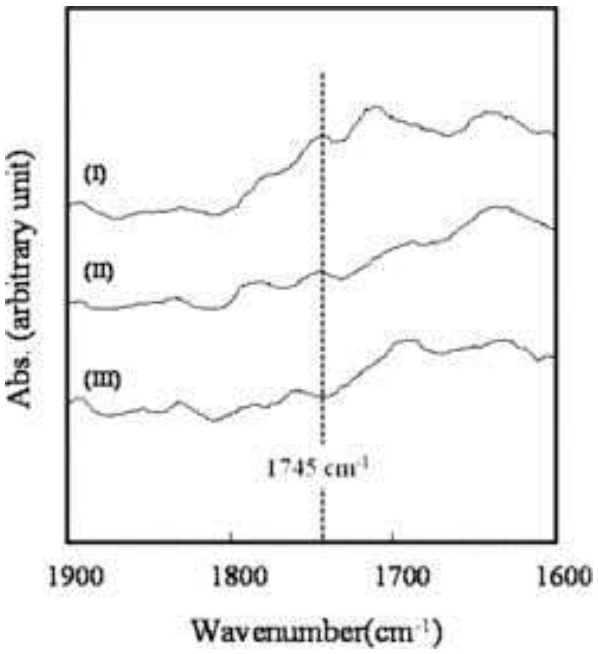

Figure 2-17 Fourier transform infrared spectra of PP and its composites: (I) FC (7 wt %)/PP (91 wt %)/HDgPP (2 wt %) (the content of the reactive groups was ca. 0.0003 wt %), (II) FC (7 wt %)/PP (83 wt %)/LMAPP (10 wt %) (the content of the reactive group was ca. 0.0006 wt %), and (III) PP (100%).

Figure 2-18 shows the stress–strain curves of FC (30 wt %)/PP (70 wt %), FC (30 wt %)/PP (69.5 wt %)/HDgPP (0.5 wt %), and FC (30 wt %)/PP (69.5 wt %)/HMAPP (0.5 wt %) composites. The additive effects on the tensile behavior of the FC/PP composite are obviously different between the HDgPP and HMAPP compatibilizers. The curve of the composite with HDgPP added exhibits a tensile strength almost equal to that of the FC/PP composite and a broader yield region under constant stress. In contrast, although the composite with HMAPP added exhibits higher tensile strength than that of the FC/PP composite, the mechanical behavior is quite brittle (without a defined yield region). The difference in the tensile behavior is based on the chemical

structures in the compatibilizer polymers. In the case of DgPP, the γ-lactone and acid groups have a greater tendency to be produced at the PP chain end [19]. In the case of MAPP, there mainly exist maleic anhydride groups in the inner PP chain [9, 25].

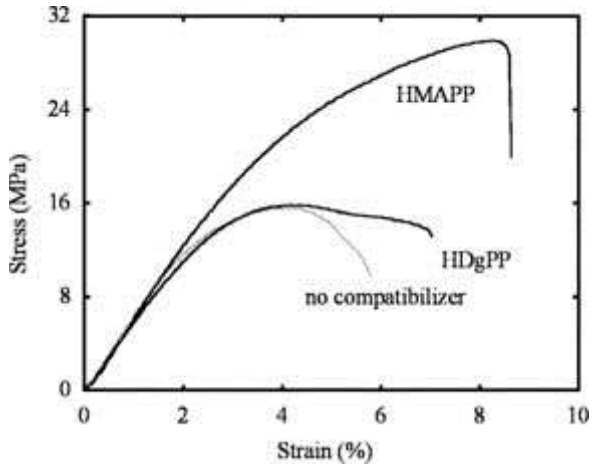

Figure 2-18 Stress–strain curves of an FC (30 wt %)/PP (70 wt %) composite and FC (30 wt %)/PP (69.5 wt %) composites with the addition of compatibilizers (0.5 wt %).

The style of adhesion is considerably different because of the arrangements of the reactive groups, as shown in Figure 2-19. In the case of adhesion at the chain end, such as DgPP, stress is intensively applied in one direction along the attached polymer chain, and the chain is unidirectionally stretched from FC (see Figure 2-19). If there are few chain entanglements between the chain and the PP matrix chain, FC is easily pulled out from the PP matrix without bending and fracturing. The broader yield region under constant stress likely originates from the pulling-out process because the stress should be constant during the process. However, MAPP has adhesion points in the inner chain. The adhesion location implies that the applied stress is distributed within one chain, as illustrated in Figure 2-19. This means that the MAPP chain is bidirectionally stretched from FC, and the dissolution of entanglements becomes hard. In this case, it seems that

FC is tightly linked to the PP matrix, and the fracture of the composite accompanies FC deformations such as bending and fracturing. The brittle behavior of the composite is likely due to these FC-destructive deformations, by which the formation of a void in the PP matrix is simultaneously caused.

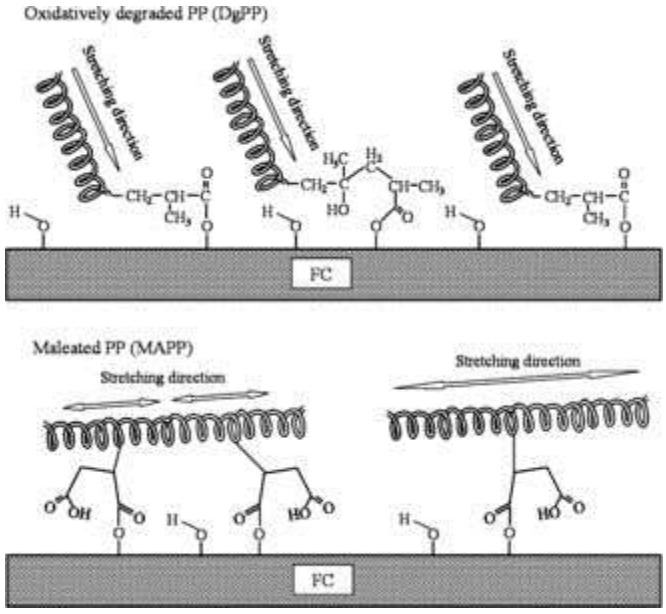

Figure 2-19 Model of DgPP and MAPP chains bound to an FC particle in composites.

These explanations can be substantiated by consideration of the SEM micrographs in Figure 2-20, which shows the fractured surfaces of the FC/PP composite with the HDgPP and HMAPP compatibilizers added. Figure 2-20(a) reveals that FC coated with a polymer layer is pulled out from the PP matrix (see the arrows). This FC is unbending and unfracturing. This indicates that the linkage between HDgPP and the PP chains is very weak. In contrast, as shown in Figure 2-20(b), the fracturing of FC can be observed in the composite with HMAPP added (see arrow). This means that the stress is directly applied to FC without pullout. These results support the idea that the stress–strain curves exactly reflect the kind of adhesion style

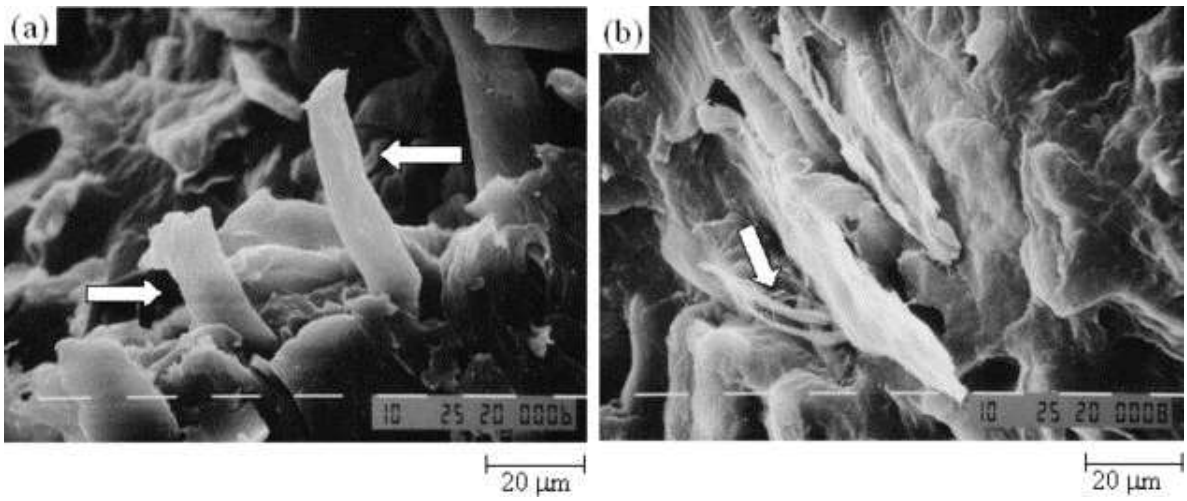

Figure 2-20 SEM micrographs of fracture surfaces of composites: (a) FC (30 wt %)/PP (67.5 wt %)/HDgPP (2.5 wt %) and (b) FC (30 wt %)/PP (69 wt %)/HMAPP (1 wt %). The contents of the reactive groups were similar (0.0004 and 0.0008 wt %, respectively). The arrows indicate pulled and fractured FCs, respectively.

The molecular weight of LDgPP is 2 times higher than that of HDgPP. The addition of LDgPP implies that the entanglement point between the PP chain increases, and the adhesion strength of the interface between the FC and PP matrix becomes stronger. As expected, the maximum stress (21 ± 0.2 MPa, the average of 10 measurements) of the FC/PP/LDgPP composite is about 30% higher than that (16 ± 0.9 MPa, the average of 10 measurements) of the FC/PP/HDgPP composite (see Figure 2-21), demonstrating that the interface adhesion strength becomes stronger because of the increase in the entanglement point. It can be observed here that the yield region is considerably smaller than that of the composite with HDgPP added. This behavior implies that interface exfoliation occurs when FC is being pulled out from the PP matrix. Figure 2-22 shows an SEM micrograph of the fractured surfaces of an FC/PP composite with the addition of LDgPP with the same reactive group content (ca. 0.0004 wt %) as that of HDgPP.

The pullout of FC is incomplete, and the fractured surface is partially turned up. The applied stress is likely over the maximum elastic modulus of FC. This indicates an increase in the interface adhesion strength. In addition, the adhesion strength seems not to be as strong as that of the composite with HMAPP added because fracturing of FC is not seen.

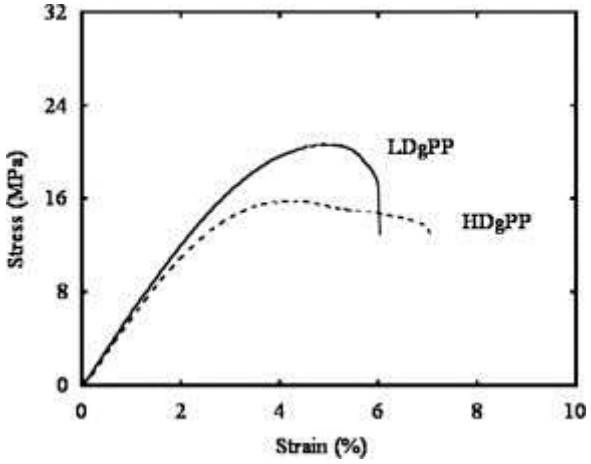

Figure 2-21 Stress–strain curves of FC (30 wt %)/PP (69.5 wt %)/DgPP (0.5 wt %) composites.

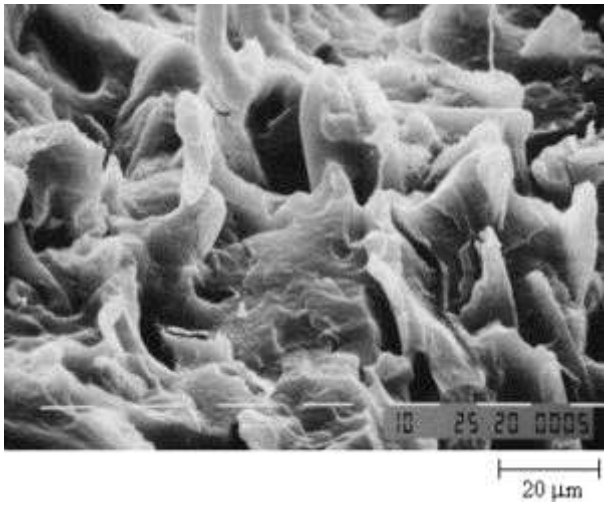

Figure 2-22 SEM micrograph of fracture surfaces of an FC (30 wt %)/PP (66 wt %)/LDgPP (4 wt %) composite. The content of the reactive groups was about 0.0004 wt %.

Interestingly, the composite with LMAPP added has a considerably higher Young's modulus than the other composites (see Figure 2-23 and Table 2-2). This suggests that the interface adhesion strength is independent of the value of Young's modulus. To clarify the additive effect of LMAPP on the PP matrix, a PP (90 wt %)/LMAPP (10 wt %) polymer blend, with the amount of LMAPP increased, was prepared, and its thermal properties were investigated with DSC measurements.

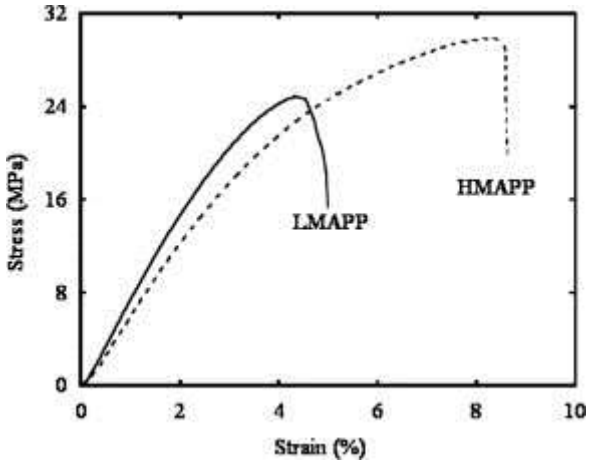

Figure 2-23 Stress–strain curves of FC (30 wt %)/PP (69.5 wt %)/MAPP (0.5 wt %) composites.

Table 2-2 Young's Modulus of FC (30 wt %)/PP (69.5 wt %) Composites Containing Compatibilizers (0.5 wt %)

Compatibilizer	HDgPP	LDgPP	HMAPP	LMAPP
Young's modulus (MPa)	592 ± 36	634 ± 49	636 ± 54	782 ± 15

Figure 2-24 shows the DSC curve of PP (90 wt %)/LMAPP (10 wt %). Only one melting point can be observed, and another melting point, such as the melting point corresponding to the maleic anhydride side chain group, is unseen.

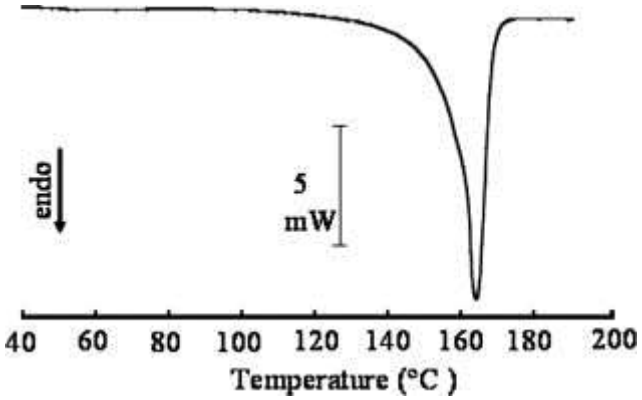

Figure 2-24 DSC curve of a PP (90 wt %)/LMAPP (10 wt %) polymer blend.

In the case of the FC (30 wt %)/PP (67 wt %)/LMAPP (3 wt %) composite, however, another new melting point appears in a higher temperature region (see Figure 2-25). This implies that the existence of FC affects PP/LMAPP. As shown in Figure 2-26, however, the crystal form of PP in the FC/PP/LMAPP composite is the α form (monoclinic), the same as that of common PP, and it exhibits no change in the crystalline morphology. The higher new melting point originates not from another crystal structure but from a thicker lamella with the same crystal structure. FC likely acts as a nucleating agent, leading to an increase in the crystallization rate of the PP/LMAPP part, although the nucleating mechanism is unclear. The higher melting point would be due to the nucleation effect. The produced lamella turns out to be considerably thick from the higher melting point around 170°C. The higher Young's modulus of the FC/PP/LMAPP composite is derived from such thick lamellae. FC seems to have no ability of nucleation against the PP/HMAPP composite. HMAPP is

believed to cover the entire surface of FC because of the higher maleic anhydride content. Therefore, the nucleation effect seems to not occur in the FC/PP/HMAPP composite.

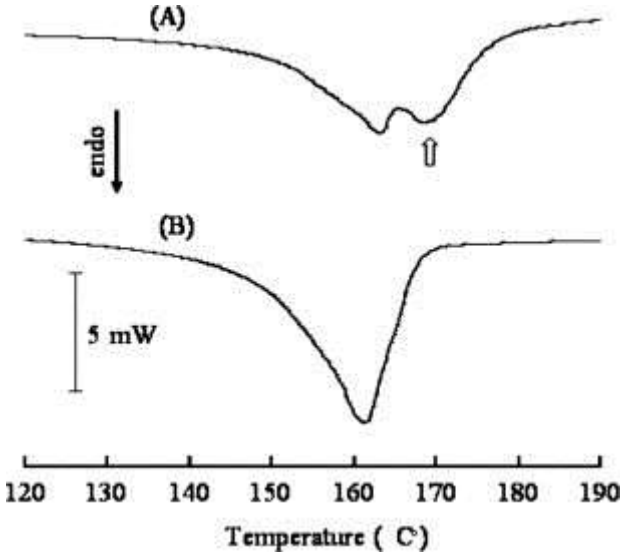

Figure 2-25 DSC curves of composites: (A) FC (30 wt %)/PP (67 wt %)/LMAPP (3 wt %) and (B) FC (30 wt %)/PP (67 wt %)/HMAPP (3 wt %).

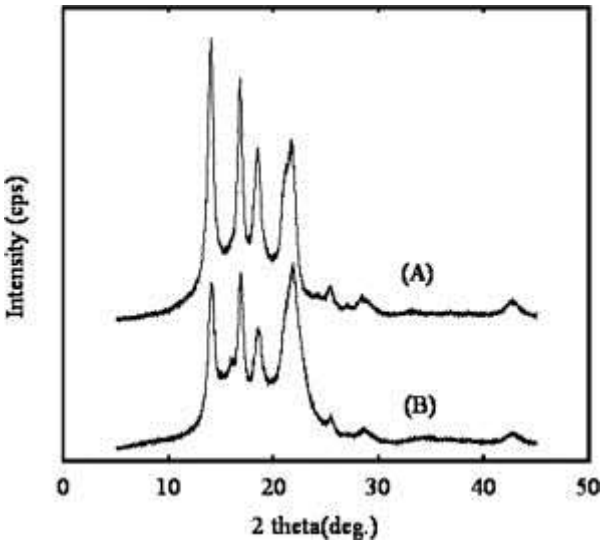

Figure 2-26 Wide-angle X-ray diffraction profiles: (A) PP and (B) FC (30 wt %)/PP (67 wt %)/LMAPP (3 wt %).

2-4: Conclusion

In order to develop a novel type of coupling agent for FC/PP composite, DgPP was studied. The adequate preparation time of thermal oxidative degradation for DgPP was 18 h at 130 °C. The DgPP contained γ-lactone and acid compounds, and its spherulite shape was considerably coarser than that of PP. The addition of the DgPP presented the transparency improvement of FC/PP composite. This behavior was originated from the grafted DgPP, which was produced by the esterification reaction between the OH group of FC surface and the oxidized (γ-lactone/acid) groups of DgPP. It was found from the SEM observation that the FC surface was covered with the grafted DgPP and the tensile strength of the FC/PP composite increased by an appropriate amount of the DgPP addition. These results demonstrated that the DgPP acted as the coupling agent.

The MAPP compatibilizer was studied. Both DgPP and MAPP compatibilizers had the same improvement mechanism using esterification between the OH group in FC and the reactive (γ-lactone, acid, and maleic anhydride) groups in the polymer chains. However, the adhesion style using the ester bond was considerably different because of the arrangements of the reactive groups. The DgPP compatibilizer had the reactive groups at the polymer chain end. In the case of the adhesion of the chain at this position, stress was intensively applied in one direction along the chain, and the chain unidirectionally stretched from FC. The MAPP compatibilizer had adhesion points in the inner chain, so the applied stress was distributed within one chain.

The stress–strain curve of the FC/PP/HDgPP composite exhibited lower tensile strength and a broader yield region, and this indicated that the composite was typically a ductile material. In contrast, although the FC/PP/HMAPP composite had higher tensile strength, the tensile behavior was quite brittle. In the SEM micrograph of the fractured

surface of the FC/PP/HDgPP composite, FC was shown to be pulled out from the PP matrix without bending or fracturing. This supported the idea that the broader yield region observed originated from the FC pullout process. However, in the micrograph of the FC/PP/HMAPP composite, the fracturing of FC was observed, indicating that the stress was directly applied to FC without pullout. This suggested that the characteristics of the tensile behavior, such as the higher tensile strength and brittleness, were based on the mechanism in which the applied stress was directly transmitted to FC. These results implied that arrangements of the reactive groups in the compatibilizers directly affected the tensile behavior of the FC/PP composite.

In the DgPP compatibilizer, the adhesion strength of the interface between the FC and PP matrix was found to become considerably stronger with an increase in the molecular weight of the compatibilizer. However, in the MAPP compatibilizer, a certain content of maleic anhydride groups was found to be directly linked to the tensile strength of the composite by a comparison of HMAPP with LMAPP having a considerably lower content of maleic anhydride groups. In addition, in the case of the FC/PP/LMAPP composite, a thicker lamella was produced and was found to give a higher Young's modulus to the composite.

References

[1] S. Takase, N. Shiraishi, *J. Appl. Polym. Sci.* 1989, 37, 645.

[2] D. Maldas, B. V. Kokta, C. Daneault, *J. Appl. Polym. Sci.* 1989, 37, 751.

[3] R. G. Raj, B. V. Kokta, D. Maldas, C. Daneault, *J. Appl. Polym. Sci.* 1989, 37, 1089.

[4] P. Hedenberg, P. Gatenholm, *J. Appl. Polym. Sci.* 1996, 60, 2377.

[5] F. Zhang, W. Qiu, L. Yang, T. Endo, *J. Mater. Chem.* 2002, 12, 24

[6] W. Qiu, F. Zhang, T. Endo, T. Hirotsu, *J. Appl. Polym. Sci.* 2003, 87, 337.

[7] W. Qiu, F. Zhang, T. Endo, T. Hirotsu, *J. Appl. Polym. Sci*.2004, 91, 1703.

[8] J. M. Felix, P. Gatenholm, *J. Appl. Polym. Sci.* 1991, 42, 609.

[9] W. Qiu, F. Zhang, T. Endo, T. Hirotsu, *J. Appl. Polym. Sci.* 2004, 94, 1326.

[10] V. N. Hristov, S. T. Vasileva, M. Krumova, R. Lach, G. H. Michler, *Polym. Compos.* 2004, 25, 521.

[11] N. Ljungberg, C. Bonini, F. Bortolussi, C. Boisson, L. Heux, J. Y. Cavaillé, *Biomacromolecules* 2005, 6, 2732.

[12] M. Baiardo, G. Frisoni, M. Scandola, A. Licciardello, *J. Appl. Polym. Sci.* 2002, 83, 38.

[13] C. Joy, R. Gauthier, M. Escoubes, *J. Appl. Polym. Sci.* 1996, 61, 57.

[14] V. R. Botaro, A. Gandini, *Cellulose* 1998, 5, 65.

[15] M. N. Belgacem, P. Bataille, S. Sapieha, *J. Appl. Polym. Sci.* 1994, 53, 1447.

[16] F. Massines, G. Gouda, *J. Phys. D* 1998. 31, 3411.

[17] Y. Kato, D. J. Carlsson, D. M. Wiles, (1969) *J. Appl. Polym. Sci.* 1969, 13, 1447

[18] D. J. Carlsson, D. M. Wiles, *Macromolecules*, 1969, 6, 597

[19] J. H. Adams, *J. Polym. Sci. A1* 1970, 8, 1077

[20] N. C. Billingham, *Makromol. Chem. Macromol. Symp.* 1989, 28, 145

[21] L. Audouin, V. Gueguen, A. Tcharkhtchi, J. Verdu, *J. Polym. Sci. A1* 1995, 33, 921

[22] H. Nakatani, S. Suzuki, T. Tanaka, M. Terano, *Polymer* 2005, 46, 12366

[23] Y. Teramoto, Y. Nishio, *Polymer* 2003, 44, 2701

[24] A. Mayumi, T. Kitaoka, H. Wariishi, *J. Appl. Polym. Sci.* 2006, 102, 4358

[25] W. Heinen, C. H. Rosenmöller, C. B. Wnzel, H. J. M. de Groot, J. Lugtenburg, *Macromolecules* 1996, 29, 1151.

[26] H. D. Keith Jr, F. J. Padden, *J. Appl. Phys.* 1964, 35, 1270

[27] J. M. Felix, P. Gatenholm, *J. Mater. Sci.* 1994, 29, 3043

Chapter 3: Effect of Mechanical properties of Polypropylene and Polypropylene/ Fibrous Cellulose Composites by the Addition of Poly(ethylene oxide)

3-1: Introduction

Cellulose is the most abundant polymer material in the world and has been used as a raw material for building materials and paper for a long time. Its advantages are its low cost, high modulus, renewability, and biodegradability. Cellulose also has attracted much attention from many researchers for use in composite materials [1–7]. In particular, their attention has recently been concentrated on its high modulus and renewability from the viewpoints of both mechanical and environmental advantages. A composite based on cellulose has been considered a useful way of taking advantage of the existing features. In general, milled wood materials have been used as composite cellulose materials. Such wood materials are commonly called wood flour or fibrous cellulose (FC).

The most popular example of such composites is a combination with polypropylene (PP) [1, 4–7]. This is due to the commercial importance of PP as an applicable material for household appliances, medical wares, and automotive and other industrial products. Moreover, in the PP composite, FC has been explored as an alternative to glass and carbon fibers and as a biodegradable material. The PP/FC composite is, however, quite brittle. Improvement of the mechanical properties is required.

It is well known that the addition of an elastomer is effective in improving the toughness of a brittle polymer [8–12]. The improvement method can be similarly applied for PP [13, 14]. In the case of PP, an incompatible polymer, such as a

styrene–ethylene–butadiene–styrene triblock copolymer, has been used as the additive elastomer [14]. If there exists an appropriate elastomer, the improvement method would be applicable for the PP/FC composite. Poly(ethylene oxide) (PEO) is regarded as one applicable elastomer because it is typically incompatible with PP [15, 16] and has high flexibility. In addition, both PEO and cellulose are hydrophilic, and the formation of hydrogen bonds is feasible between them [17]. A nanocomposite [18] and a thermoplastic composite [19] of cellulose and PEO can be prepared with the hydrogen bonds. The existence of the hydrogen bonds will bring about distinctly different properties for the PP/FC composite.

The purpose of this study was to clarify the effects of the addition of PEO on the morphology and tensile properties of PP and the PP/FC composite. For the PP/PEO polymer blend, the dependence of the PEO content and its molecular weight were studied. For the PP/FC composite, the effects of the difference in the PEO addition method and the amount of PEO contents on the morphology and tensile behavior were studied.

3-2: Experimental

3-2-1: Materials

PP (mesopentad fraction = 98%) was supplied by Japan Polypropylene Co. (Yokkaichi, Japan). The number-average molecular weight and polydispersity (weight-average molecular weight/number-average molecular weight) of PP were 4.6×10^4 and 5.7, respectively.

Two kinds of PEOs were purchased from Wako Pure Chemical Industries, Ltd. (Osaka, Japan). The PEOs with lower (20,000) and higher (500,000) average molecular

weights were denoted LPEO and HPEO, respectively.

FC (W-100GK) was donated by Nippon Paper Chemicals Co., Ltd. (Tokyo, Japan). The moisture of the FC was below 0.7 wt %. The dimensions were over 90% through a 100-mesh screen, and the average length was about 37 μm. The FC was dried in a desiccator for 7 days before preparation.

Maleated polypropylene (MAPP; maleic anhydride content ≈ 8 wt %), used as a compatibilizer, was purchased from Sigma–Aldrich (St. Louis, MO). The number-average molecular weight and polydispersity (weight-average molecular weight/number-average molecular weight) of MAPP were 3.9×10^3 and 2.3, respectively. MAPP is a very popular compatibilizer for PP composites. In the PP/FC composite, the availability of MAPP is well known [1,4,6]. Therefore, MAPP was used as the compatibilizer in this study.

3-2-2: Preparation of the PP/PEO polymer blend

The polymer blend was prepared with an Imoto Seisakusyo (Kyoto, Japan) IMC-1884 melting mixer. After a small amount of a phenolic antioxidant (AO-60, Adekastab; ~ 0.5 wt %) was added, the mixing was performed. The mixing conditions were 180°C at 60 rpm for 5 min in the LPEO addition, whereas they were 210°C at 60 rpm for 5 min in the HPEO addition. These samples were molded into a film (100 μm) by compression molding at 190°C under 5 MPa for 5 min and were quenched at 20°C. The obtained samples were dried in a desiccator over 1 day before the measurement and testing.

3-2-3: Tensile testing

Stress–strain behavior was observed with a Shimadzu (Tokyo, Japan) EZ-S at a crosshead speed of 5 mm/min. The sample specimens were cut with dimensions of 30 × 2 × 0.1 mm[3], and the gauge length was 10 mm. We chose the specialized specimen (like the ISO reed shape) to adapt to the size of our tensile testing machine. All tensile testing was performed at 20°C. All results were the average values of five measurements.

3-2-4: Single-edge-notch (SEN) tensile test

The fracture behavior was studied with an SEN test. The method of van der Wal and Gaymans [20] was used as the reference. The SEN test was carried out on a Shimadzu EZ-S at a crosshead speed of 5 mm/min with a strip specimen (30 × 2 × 0.1 mm^3) having a single-edge, 45°, V-shaped notch (tip radius = 0.3 mm). Although the SEN test of van der Wal and Gaymans was carried out with a standard dumbbell-shaped sample (ISO R27-1: 10 × 3 × 115 mm^3) with a V-shaped notch (tip radius = 0.25 mm), we chose the specialized specimen because of the smaller size of our tensile testing machine. All results were the average values of five measurements.

3-2-5: Wide-angle X-ray diffraction (WAXD) measurement and procedure for the crystallinity calculation

WAXD diffractograms were recorded in reflection geometry at 2° (2χ/min) under Ni-filtered Cu Kα radiation with a Rigaku Corp. (Tokyo, Japan). XG-Rint 1200 diffractometer. The crystallinity was estimated from the WAXD peak area, whose calculation was performed with software (Integral Analysis for Windows, version 5.0,

Rigaku).

3-2-6: Scanning electron microscopy (SEM) measurement

The morphology of the composite was examined with a JEOL (Tokyo, Japan) JSM-5800 at 30 kV. The plate of the composite was fractured in liquid nitrogen, and then the fractured surface was sputter-coated with gold.

3-2-7: DSC measurement

DSC measurements were made with a SHIMADZU DSC-60. The samples of about 5 mg weight were sealed in aluminum pans. The measurement of the samples was carried out from 40 to 200°C at a heating rate of 10°C/min under a nitrogen atmosphere.

3-3: Results and Discussion

3-3-1: Effect of Mechanical properties of Polypropylene by the Addition of Poly(ethylene oxide)

Figure 3-1 shows the stress–strain curve of the PP (92.5 wt %)/LPEO (7.5 wt %) blend. The tensile strength of the PP/LPEO blend is approximately 20% lower than that of the PP; however, the blend exhibits necking behavior and is not broken under the experimental conditions, just like the PP (see Table3-1). The tensile behavior reveals that the addition of PEO hardly impairs the ductility of PP.

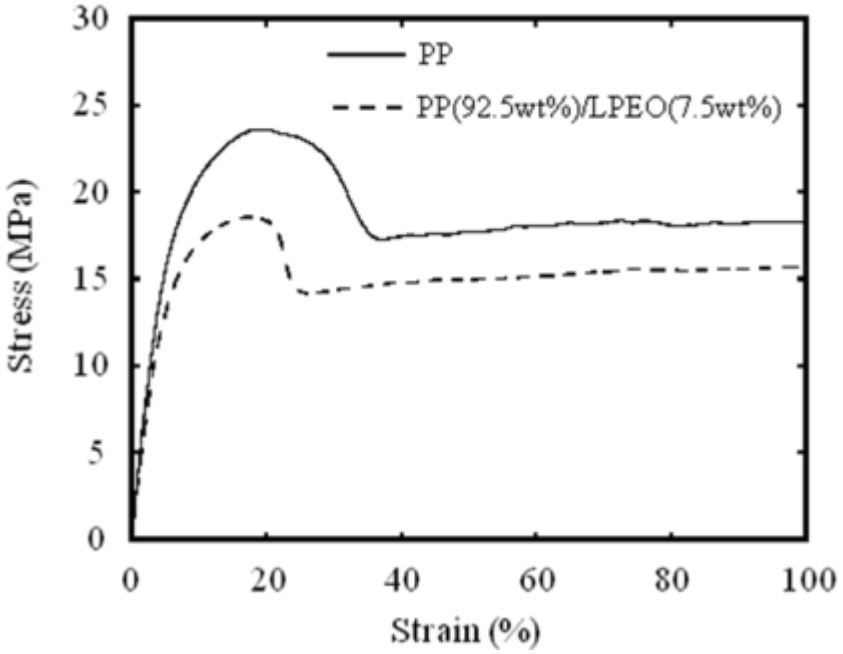

Figure 3-1 Stress-strain curves of PP and PP/LPEO

Figure 3-2 shows the WAXD profiles of PP/LPEO, PP, and LPEO. The crystal form of the PP in the PP (92.5 wt %)/LPEO (7.5 wt %) blend is the α-form (monoclinic), just like the PP. The WAXD peak corresponding to LPEO is unseen, and the degrees of crystallinity of the PP and PP (92.5 wt %)/LPEO (7.5 wt %) blend are 54 and 50 wt %, respectively. When we consider the existence of LPEO, the crystallinity (50 wt %) is in good agreement with the weight ratio of the PP, that is, 50/54 ≈ 0.925 (92.5 wt %), in the blend. These results suggest that the addition of LPEO brings about no changes in the crystalline morphology or in the crystallization rate of PP under the blend preparation conditions.

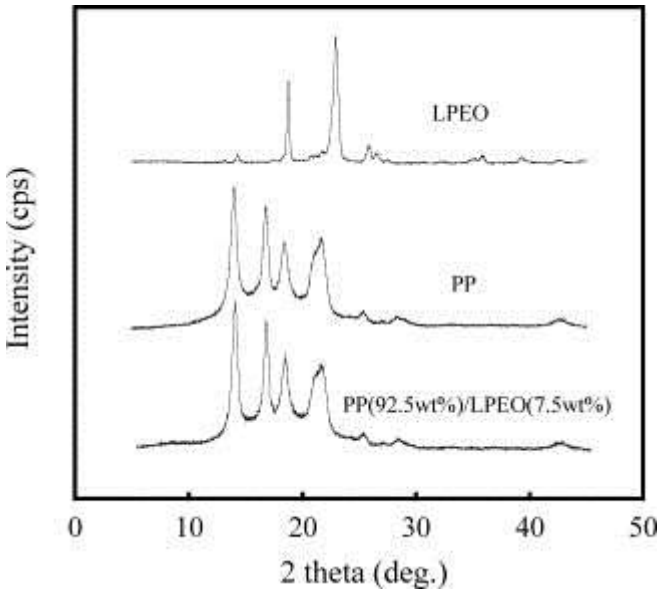

Figure 3-2 WAXD profiles of PP/LPEO, PP, and LPEO.

Figure 3-3 shows the stress–strain curves of blends with various LPEO contents. Although an increase in the LPEO content seems to cause a slight decrease in the tensile strength and a slight broadness of the yield region, major changes in the mechanical parameters do not appear up to a 10% concentration of LPEO, as summarized in Table 3-1.

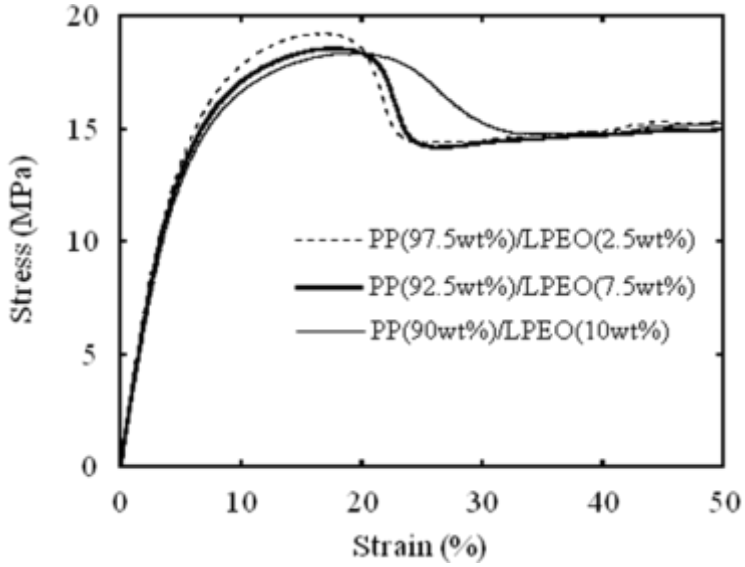

Figure 3-3 Stress-strain curves of PP/LPEO

Table 3-1 Mechanical properties of various PP blend samples

Sample	Young's modulus (MPa)	Tensile strength (MPa)	Elongation at break (%)
PP	370±10	23.6±0.4	over 200*
PP(97.5wt%)/LPEO(2.5wt%)	319±24	19.3±0.4	over 200*
PP(92.5wt%)/LPEO(7.5wt%)	318±23	18.8±0.3	over 200*
PP(90wt%)/LPEO(10wt%)	291±9	18.6±0.5	over 200*
PP(92.5wt%)/HPEO(7.5wt%)	328±11	18.8±0.6	over 200*

*All samples did not break in the tensile testing condition (till the elongation of 200 %).

The effect of the molecular weight of PEO on the tensile behavior of the PP/PEO blend is shown in Figure 3-4. The stress–strain curves of PP/LPEO and PP/HPEO are in good agreement with each other, and this indicates that the molecular weight is an independent factor in the tensile behavior of the PP/PEO blend. This implies that there are no other interactions (e.g., chain entanglement) except for the van der Waals force between PP and PEO chains.

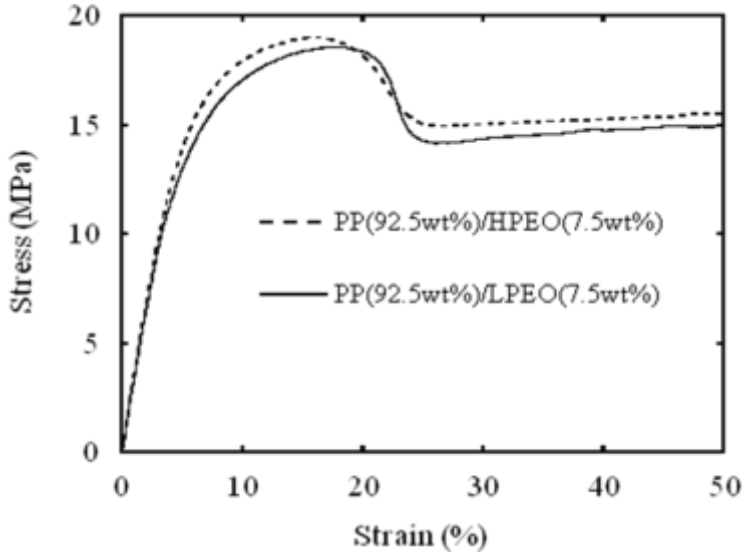

Figure 3-4 Stress-strain curves of PP/LPEO and PP/HPEO

SEM micrographs of fractured surfaces of the PP/LPEO blends are shown in Figure 3-5. The fracture surfaces are quite smooth, having many hemispherical holes, which correspond to the LPEO phase. The size of the holes obviously depends on the LPEO content. These phase-separated (sea-island) morphologies indicate that PP and PEO are typically an incompatible blend [15, 16].

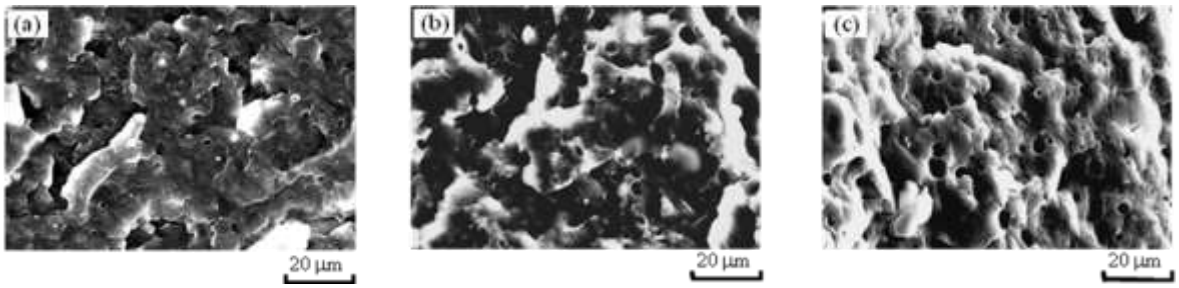

Figure 3-5 SEM micrographs of fracture surfaces of PP/LPEO.
(a): PP(97.5 wt%)/LPEO(2.5 wt%). (b): PP(92.5 wt%)/LPEO(7.5 wt%).
(c): PP(90 wt%)/LPEO(10 wt%).

Many investigators have reported that employing an incompatible elastomer/polymer blend is effective in improving the toughness of polymer materials [8-14]. The enhanced toughness is believed to be due to a strain constraint relaxation resulting from void formation in the dispersed elastomer phase [9]. In this relaxation mechanism, the elastomer, having lower mechanical strength, is desirable from the structural viewpoint of preferential void formation [10]. It is noted here that the PP/PEO blend sufficiently fulfills such toughening criteria because PEO is a flexible polymer and its mechanical strength is considerably less than that of PP. In addition, although PEO is a crystalline polymer, the elasticity is considerably lower than that of PP. PEO

acts as an elastomer in the PP matrix because of its lower elasticity. When tensile stress is applied, the weaker PEO phase is deformed. Many voids are preferentially generated in the PEO phase, leading to the relaxation of the strain constraint. The PEO phase is more highly deformed by the additionally applied stress and finally ends up as a slit-like shape, as shown in Figure 3-6. The decrease in the PP/LPEO tensile strength is ascribed to the reduced cross-section area of the PP matrix. The decrease is, however, not proportional to the LPEO content. The cross-section area of the PP matrix slowly decreases against the LPEO content because of the slit-like LPEO deformation. Therefore, the dependence of the tensile strength on the LPEO content would be ambiguous.

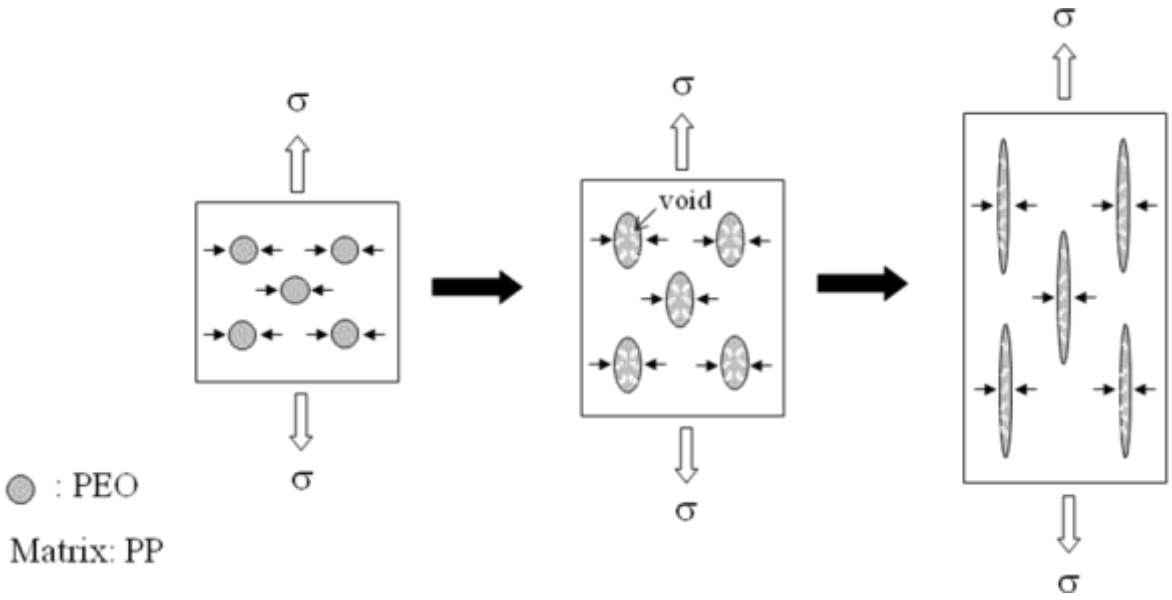

Figure 3-6 A schematic diagram illustrating the tensile deformation mechanism of PP/PEO blend.

Figure 3-7 shows the stress–strain curve of a PP (69.5 wt %)/FC (30 wt %) composite with MAPP (0.5 wt %) as a compatibilizer. Although the tensile strength is considerably higher than that of PP, the tensile behavior is typically brittle. It should be noted here that an increase in strain can be observed with the addition of LPEO to the PP/FC composite. As summarized in Table 3-2, the PP (62 wt %)/MAPP (0.5 wt %)/FC (30 wt %)+LPEO (7.5 wt %) composite has a considerably higher Young's modulus and a higher tensile strength versus PP. Additionally, the composite has about 30% higher elongation at break than that of the composite without LPEO added. This tensile behavior suggests that the toughening is capable of performing with the high stiffness maintained.

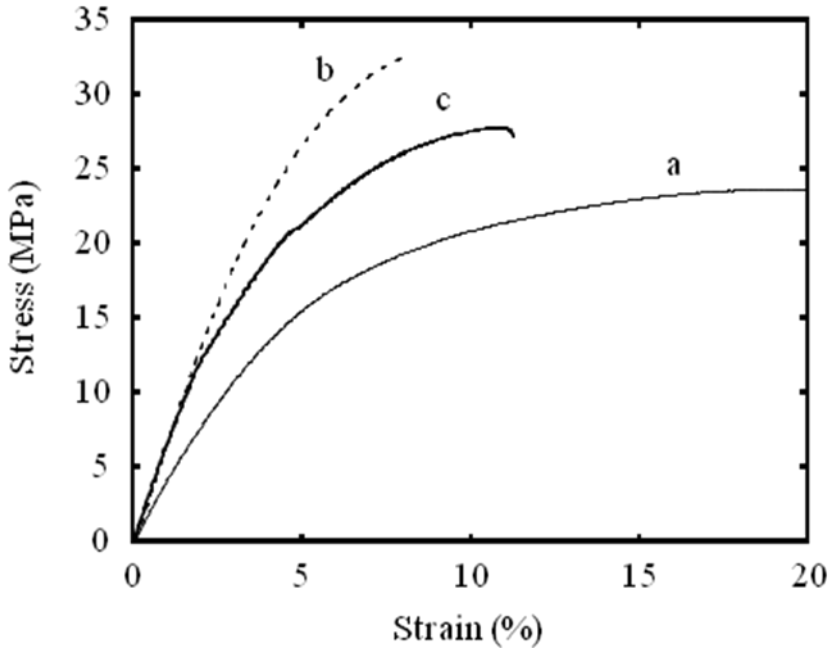

Figure 3-7 Stress-strain curves of PP, PP/MAPP/FC and PP/MAPP/FC+LPEO

a: PP. b: PP(69.5 wt%)/MAPP(0.5 wt%)/FC(30 wt%). c: PP(62 wt%)/MAPP(0.5 wt%)/FC(30 wt%)+LPEO(7.5 wt%).

The toughening effect can be interpreted if we consider the SEM micrographs in Figure 3-8, which shows the fractured surfaces of the PP (62 wt %)/MAPP (0.5 wt %)/FC (30 wt %)+LPEO (7.5 wt %) composite. Figure 3-8 reveals that the FC is tightly coated with the PP/MAPP layer. There are many fine holes in the matrix. These holes are assigned to the LPEO phase and play the role of void points, at which the relaxation of the strain constraint preferentially occurs, as mentioned previously. It has been found that the addition of PEO is an effective method for the improvement of the toughness of PP/cellulose composites.

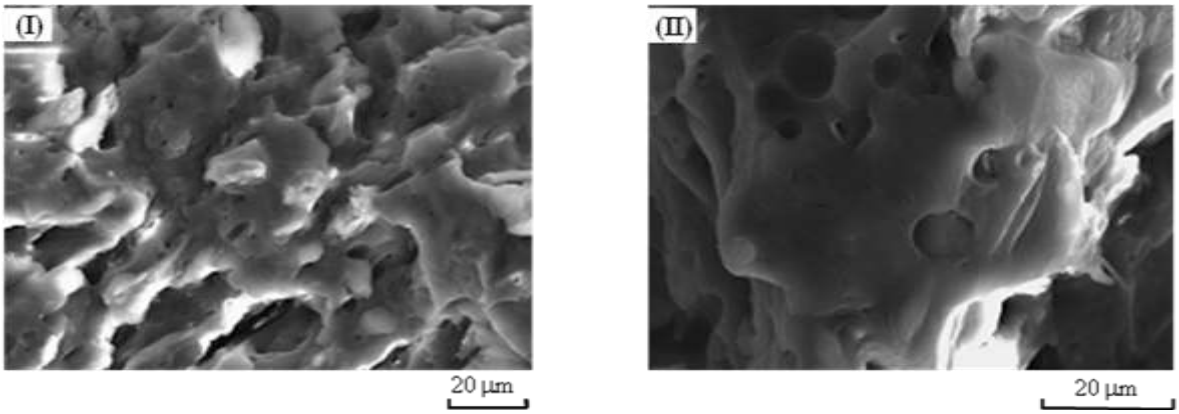

Figure 3-8 SEM micrograph of fracture surface of PP(62 wt%)/MAPP(0.5 wt%)/ FC(30 wt%)+LPEO(7.5 wt%). (I): ×1000. (II) ×1700.

FC and PEO are hydrophilic, and a hydrogen bond is formed between them [17]. The composite can be prepared with this hydrogen bond[18, 19]. In this work, the FC/LPEO composite was first prepared and was then mixed with PP and MAPP as a compatibilizer. The obtained composite was denoted LPEO/FC+PP/MAPP. The stress–strain curve of FC (30 wt %)/LPEO (7.5 wt %)+PP (62 wt %)/MAPP (0.5 wt %) is shown in Figure 3-9. Although the values of the Young's modulus and the tensile strength are approximately half of those of PP (69.5 wt %)/MAPP (0.5 wt %)/FC (30

wt %), the value of the elongation at break is approximately 4 times greater (see Table 3-2). In addition, the stress–strain curve is in good agreement with that of PP up to the strain value of 2–3%.

Table 3-2 Mechanical properties of various PP composite samples

Sample	Young's modulus (MPa)	Tensile strength (MPa)	Elongation at break (%)
PP	370±10	23.6±0.4	over 200 *
PP(69.5wt%)/MAPP(0.5 wt%) /FC(30 wt%)	628±51	30.8±2.7	8.4±0.3
PP(62 wt%)/MAPP(0.5 wt%) /FC(30 wt%)+LPEO(7.5 wt%)	533±22	26.8±0.9	11.1±0.8
FC(30 wt%)/LPEO(7.5 wt%) +PP(62 wt%)/MAPP(0.5 wt%)	355±22	12.3±1.1	30.1±8.1

* Sample did not break in the tensile testing condition (till the elongation of 200 %).

Esterification [1] occurs between the OH group in FC and the maleic anhydride group in MAPP, which is compatible with PP. The existence of the grafted MAPP/FC brings about a higher Young's modulus. The PP/MAPP/FC+LPEO composite exhibits a higher Young's modulus because of the formation of the grafted MAPP/FC component. In the case of the FC/LPEO+PP/MAPP composite, the formation of the grafted MAPP/FC would be blocked by LPEO. Therefore, the Young's modulus is low. The higher value of the elongation at break supports the existence of the FC blocked by the LPEO.

Figure 3-10 shows an SEM micrograph of the fracture surface of FC (30 wt %)/LPEO (7.5 wt %)+PP (62 wt %)/MAPP (0.5 wt %). The coated fibers and the

fibrous gaps can be observed. These are the FC/LPEO composite and its imprinted PP matrix. In addition, as shown in Figure 3-11, the interfacial bond between FC and LPEO can be observed. This suggests that a hydrogen bond is formed between FC and LPEO [17-19]. When tensile stress is applied, the FC/LPEO composite phase is deformed, as shown in Figure 3-12. Many voids are initially generated in the FC/LPEO phase as well as the PEO phase, leading to the relaxation of the strain constraint. The deformation is, however, restricted by the existence of FC. After the deformation becomes impossible, the applied stress is stored in the form of constrained plasticity in FC and finally overcomes the fibril strength of the PP/MAPP matrix (crack occurrence). There is no interaction between the FC and PP/MAPP matrix because of the covering with the LPEO layer. Therefore, the initial tensile behavior is similar to that of PP (see Table 3-2). In this preparation method, the obtained composite has less tensile strength and higher strain because of the isolated FC. This suggests that a stiff material at a high concentration (ca. 30 wt %) can be dispersed in the PP matrix without its ductility

The fracture behavior of the PP/MAPP/FC, PP/MAPP/FC+LPEO, and FC/LPEO+PP/MAPP composites was estimated by SEN testing [20]. As shown in Figure 3-13, the fracture process can be divided into crack initiation and crack propagation stages [20]. In the crack initiation stage, the stress builds up at the notch tip, but it is too low to enable crack propagation. Here it should be noticed that the crack propagation stage is linked to ductility behavior. The crack propagation stage begins at or past the maximum in the stress–displacement curve, and the energy supplied during the crack propagation is a measure of the ductility [20].

Figure 3-14 shows the force–displacement curves obtained by SEN testing for these

composites. The curve of the FC/LPEO+PP/MAPP composite exhibits the crack propagation region, suggesting that the composition is quite ductile. The fracture energy (surface area of the force–displacement curve) is considerably higher than those of the other compositions (see Table 3-3). This composition has plastic deformation even in the notch. This plastic deformation occurs so that the PP matrix has no interaction with FC. The fracture behavior supports the assumption that there is no interaction between the FC and PP/MAPP matrix because of the covering with the LPEO layer, as mentioned previously. However, the curves of the PP/MAPP/FC and PP/MAPP/FC+LPEO compositions contain no crack propagation regions. Both compositions typically exhibit brittle behavior. However, as shown in Table 3-3, the fracture energy of PP/MAPP/FC+LPEO is slightly higher than that of PP/MAPP/FC, and this indicates that the existence of LPEO brings about an improvement in the fracture toughness of the PP/MAPP/FC composite. Uotila et al [21]. reported that ethylene–propylene elastomer particles hindered crack propagation in a PP/silica composite [21]. The LPEO particles may play the role as well as the elastomer particles, although the ability to hinder crack propagation is quite low.

3-3-2: Effects of Additive Amount of Poly(ethylene oxide) on Young's Modulus and Morphology

Figure 3-15 shows the plot of Young's modulus versus LPEO content for the PP/MAPP/FC + LPEO and the LPEO/FC + PP/MAPP composites. In both cases, the Young's moduli are decreasing with increase in the LPEO. The behavior implies that the existence of LPEO disturbs the stress transference from the matrix to the FC. The decreasing tendencies are, however, different in each other. It should be noted here that the moduli of the LPEO/FC + PP/MAPP composites rapidly drop at around 7 wt % content of LPEO. This behavior implies that a change of the composite structure, for example, FC arrangement, occurs at the LPEO content.

Effect of composite structure on Young's modulus can be studied by the Kerner–Nielsen equation [22, 23].

$$M = M1\left(\frac{1+AB\phi}{1-B\psi\phi}\right) \qquad (1)$$

in which

$$A = k_E - 1 \qquad (2)$$

$$B\frac{\left(M2/M1\right)-1}{\left(M2/M1\right)+A} \qquad (3)$$

Where M, M_1, and M_2 are moduli of the composite, matrix, and additional component, respectively; ϕ is the volume fraction (vol %) of component; k_E is the Einstein coefficient; A is the transference efficiency from the matrix to the fiber; and ψ is a fitting factor that depends on the maximum packing fraction of additional

component. The Kerner–Nielsen equation can be applied to ternary composite [24]. The PP/MAPP/FC + LPEO and the LPEO/FC + PP/MAPP composites can also be regarded as ternary composite due to the low (0.5 wt %) content of MAPP. In the composites, we assume that the matrix and additional component are corresponding to the PP/MAPP/FC and the LPEO, respectively. The M_1 (636.8 MPa) and the M_2 (44.1 MPa) were directly obtained from PP (79.5 vol %)/MAPP (0.6 vol %)/FC (19.9 vol %) and from the LPEO, respectively. To obtain the k_E, the Poisson's ratio ν is required. The ν value of composite is approximately given by a mixture rule [25]:

$$\nu = \nu_m \phi_m + \nu_f \phi_f \qquad (4)$$

where ν_m and ν_f are the Poisson's ratios of matrix (PP) and filler (FC), respectively; ϕ_m and ϕ_f are the volume fractions of matrix and filler, respectively. The Poisson's ratios used in this approach having the following values: $\nu_m = 0.38$ [26] and $\nu_f = 0.30$ [25]. The ν obtained is 0.36. According to the data of Nielsen [23], in a rigid matrix having near ν value (0.35), the Einstein coefficient k_E was 3.81. Therefore, in this approach, the ν and the k_E have been regarded as 0.35 and 3.81, respectively, and the values of A and B have been estimated form eqs. (2)and (3)

The Kerner–Nielsen equations obtained are plotted in Figures 2-16 and 2-17, respectively. In the case of the PP/MAPP/FC + LPEO composite, the values of the Young's modulus are in good agreement with those of the Kerner–Nielsen equation. This behavior suggests that the structure of PP/MAPP/FC matrix is maintained. Whereas in the case of the LPEO/FC + PP/MAPP composite, the modulus values follow the Kerner–Nielsen equation about 6 vol % of the LPEO content and then suddenly

deviate from the equation. This behavior means that the matrix structure is critically changed at around the 6 vol % of LPEO content.

Figure 3-18 shows the WAXD profiles of PP, FC, and LPEO. The profile of the PP shows α-form (monoclinic) [27], and that of the FC exhibits crystalline cellulose I pattern [28]. The profile of the LPEO also shows two strong reflections at 2θ = 19.0° and 23.5° [29], indicating that the LPEO is a crystalline polymer. All the components of the composites used have crystalline parts.

Figure 3-19(a,b) shows the WAXD profiles of the PP/MAPP/FC + LPEO and LPEO/FC + PP/MAPP composites with various LPEO contents. These profiles are generally similar to that of the PP (α-form). It should be, however, noted that the peak around 2θ = 21.5° has a higher intensity and becomes broader with the increase of LPEO content. As the peak locations of FC (2θ = 22.5°) and the LPEO (2θ = 23.5°) are considerably close, the broader behavior is due to the overlapping peaks of the FC and the LPEO. There are no new peaks in the region, and the position of all peaks is in good agreement with that of PP. These results suggest that there are no changes of crystalline forms of each component in both composites

Figure 3-20(a,b) shows the DSC curves of the PP/MAPP/FC + LPEO and LPEO/FC + PP/MAPP composites with various LPEO contents. The profiles of both composites are well similar to each other. The T_m corresponding to the α-form of PP can be observed at about 165°C [30], and the other T_m corresponding to the LPEO obviously appears at around 60°C with the increase of the LPEO content. Other T_m is unable to observe. These results support that the changes of the crystalline forms of the PP and LPEO components do not occur in both the composites.

In the analysis of the Kerner–Nielsen equation, the deviation is not due to the

change of crystalline form but to the change of the PP/MAPP/FC matrix structure. To investigate the structure in both compositions, SEM observation has been carried out. The SEM micrographs of fractured surfaces of the PP/MAPP/FC + LPEO composites are shown in Figure 3-21(a–c). There are many hemispherical holes on the fracture surfaces. These holes are assigned to the LPEO phase. The size of the holes obviously depends on the LPEO content. The hole exists in the PP phase like an island and does not directly contact the FC part. This phase-separated (sea-island) morphology has been unchanged against the increase of the LPEO content. The interface between the PP and the FC has maintained certain unclarity, indicating that the PP/MAPP/FC matrix is maintained. This result is in good agreement with that of the evaluation using the Kerner–Nielsen equation.

Figure 3-21(d–f) shows the SEM micrographs of fractured surfaces of the LPEO/FC + PP/MAPP composites. With the increase of the LPEO content, it appears that the interface between the FC and the PP becomes worse (see arrows in the figures). The PP and LPEO are typically incompatible blend [31, 32], and hydrogen bond is formed between OH groups in the FC and the LPEO [33]. Thus, the defined interface is assigned to the LPEO component. In the case of existence of the MAPP component, if the LPEO content is too small to cover the FC, the esterification [1] occurs between OH group in the FC and maleic anhydride group in the MAPP, which is compatible with PP. Thus, as shown in Figure 3-21(d), the boundary becomes blurred between the FC and the PP.

As illustrated in Figure 3-22, in the case of small amount of PEO, the esterification between the free OH group and the MAPP, and/or an exchange reaction between the PEO and the MAPP will be allowed on the FC surface. With the increase of the PEO

amount, the PEO gradually covers the whole FC surface. The PP/MAPP/FC matrix is unable to be formed above certain PEO content because the ester bond formation between the MAPP and the FC is blocked by the excess PEO. The deviation of the Young's modulus from the Kerner–Nielsen equation is believed to be due to the disappearance of the ester bond.

Figure 3-23 shows the Young's modulus dependence of the LPEO (7.0 vol %)/FC (20.3 vol %) + PP/MAPP composite on the MAPP content. The value of the modulus increases about 2 vol % of the MAPP content and then is almost saturated. As shown in Figure 3-24, with the increase of the MAPP content, the interface boundary becomes blurred. This suggests that the esterification between the OH group in the FC and the MAPP occurs. The esterification is likely caused by the exchange reaction between the LPEO and the excess MAPP. As mentioned earlier, the existence of the grafted MAPP/FC brings about a higher Young's modulus. As the increase of the Young's modulus is saturated around 2 vol % of the MAPP content, the MAPP amount in which the graft reaction is feasible would be about 2 vol % in this composite.

The excess MAPP would react with the LPEO having OH group on the end chain and then would yield a copolymer (PEO-MAPP) part (see Figure 3-25). Figure 3-26 shows the elongation at break versus the MAPP content for the LPEO (7.0 vol %)/FC (20.3 vol %) + PP/MAPP composite. The elongation at break has the minimum value at about 2 vol % of the MAPP and then increases with the increase of the MAPP content. This behavior seems to be due to the existence of the PEO-MAPP part, which leads to the improvement of the interface between PP and PEO. It is noted here that the value of the elongation at break is increasing with its higher Young's modulus maintained (see Figures. 3-23 and 3-25). Figure 3-27 shows the value of toughness versus the MAPP

content for the LPEO (7.0 vol %)/FC (20.3 vol %) + PP/MAPP composite. Here, the toughness was defined as the area under the stress-strain curve. The toughness reaches a minimum value at around 2 vol % of MAPP content and then increases with the increase of the content as well as the value of the elongation at break. These results indicate that the adequate combination of the LPEO and the MAPP can provide both of the high Young's modulus and the high elongation at break (i.e., toughness) to the PP/FC composite.

3-4: Conclusion

With the aim of tensile modification of the PP/FC composite, the effects of the addition of PEO on the morphology and tensile properties of PP and PP/FC composites were studied. PEO was incompatible with PP, and its polymer blend exhibited a sea-island morphology. However, the existence of PEO hardly impaired the ductility of PP. The ductility was due to a strain constraint relaxation resulting from void formation in the dispersed PEO phase. The tensile behavior of the PP/PEO blend was little affected by the content (until 10 wt %) or molecular weight of PEO, and this suggested that the PEO phase was deformed into a slit-like shape and had no interaction with the PP matrix.

The effects of PEO on the morphology and tensile and fracture behavior of the PP/FC composite critically depended on the preparation method. In the case of the addition of PEO to the PP/FC composite, increases in the strain and fracture energy were observed in comparison with the PP/FC composite. The increment mechanism was due to the strain constraint relaxation and the hindrance of crack propagation by the separated PEO phase. In the case of the addition of the FC/PEO composite to the PP matrix, although the obtained composite showed a lower Young's modulus and tensile strength versus the PP/FC composites, the strain and fracture energy were considerably increased by the existence of the PEO layer coating the FC.

The effects of the PEO content on the Young's moduli of the two kinds of PP/FC composite were studied using the Kerner–Nielsen equation. In the case of the PP/MAPP/FC + PEO composite, all the values of the moduli with the various PEO contents were in good agreement with the theoretical values obtained from the Kerner–Nielsen equation. Whereas the moduli of the PEO/FC + PP/MAPP composite

followed the Kerner–Nielsen equation about 6 vol % of the PEO content and then unexpectedly deviated. In the SEM observation, the PP/MAPP/FC + PEO composite was found to have a sea-island morphology corresponding to the PP/MAPP/FC matrix and the PEO phase. This morphology had been unchanged against the increase of the PEO content. Whereas in the case of the PEO/FC + PP/MAPP composite, the SEM micrographs showed that the interface between the FC and the PP becomes worse with the increase of the PEO content, indicating that the formation of the PP/MAPP/FC matrix was blocked by the excess PEO. The deviation of the Young's moduli from the Kerner–Nielsen equation was due to the blocking of the PEO. It was found that the adequate combination of the PEO and the MAPP was able to supply the increase of the toughness of the PP/FC composite by investigating the dependence of the PEO/FC + PP/MAPP composite on the MAPP content.

References

[1] J. M. Felix, P. Gatenholm, *J. Appl. Polym. Sci.* 1991, 42, 609.

[2] P. Hedenberg, P. Gatenholm, *J. Appl. Polym. Sci.* 1996, 60, 2377.

[3] F. Zhang, W. Qiu, L. Yang, T. Endo, *J. Mater. Chem.* 2002, 12, 24.

[4] W. Qiu, F. Zhang, T. Endo T.; Hirotsu, *J. Appl. Polym. Sci.* 2003, 87, 337.

[5] W. Qiu, F. Zhang, T. Endo T.; Hirotsu, *J. Appl. Polym. Sci.*2004, 91, 1703.

[6] W. Qiu, F. Zhang, T. Endo T.; Hirotsu, *J. Appl. Polym. Sci.*2004, 94, 1326.

[7] Hristov, V. N.; Vasileva, S. T.; Krumova, M.; Lach, R.; Michler, G. H. *Polym. Compos.* 2004, 25, 521.

[8] S. Wu, *J. Appl. Polym. Sci.* 1983, 21, 699.

[9] Wu, S. *Polymer* 1985, 26, 1855.

[10] M. Ishikawa, I. Chiba, *Polymer* 1990, 31, 1232.

[11] A. Yanagase, M. Ito, N. Yamamoto, M. Ishikawa, *J. Appl. Polym. Sci.* 1996, 60, 87.

[12] A. Yanagase, M. Ito, N. Yamamoto, M. Ishikawa, *J. Appl. Polym. Sci.* 1996, 62, 1387.

[13] Y. Matsuda, M. Hara, T. Mano, K. Okamoto, M. Ishikawa, *Polym. Eng. Sci.* 2005, 45, 1630.

[14] Y. Matsuda, M. Hara, T. Mano, K. Okamoto, M. Ishikawa, *Polym. Eng. Sci*.2006, 46, 29.

[15] T. Tang, B. Huang, *J. Polym. Part B: Polym. Phys.* 1994, 32, 1991.

[16] T. Kowalewski, G. Ragosta, E. Martuscelli, A. Galeski, *J. Appl. Polym. Sci.* 1997, 66, 2047.

[17] Kondo, T.; Sawatari, C.; Manley, R. S. J.; Gray, D. G. *Macromolecules* 1994, 27, 210.

[18] E. E. Brown, M. P. G. Laborie, *Biomacromolecules* 2007, 8, 3074.

[19] T. Endo, R. Kitagawa, F. Zhang, T. Hirotsu, J. Hosokawa, *Chem. Lett.* 1999, 28, 1155.

[20] A. van der Wal, R. J. Gaymans, *Polymer* 1999, 40, 6045.

[21] R. Uotila, U. Hippi, S. Paavola, J. Seppälä, *Polymer* 2005, ***46***, 7923.

[22] Lewis, T. B.; Nielsen, L. E. *J. Appl. Polym. Sci.* 1970, **14**, 1449.

[23] Nielsen, L. E. *J. Appl. Phys.* 1970, **41**, 4626.

[24] Y. Long, R. A. Shanks, *J. Appl. Polym. Sci.* 1996, **61**, 1877.

[25] W. Helbert, J. Y. Cavaillé, A. Dufresne, *Polym. Compos.* 1996, **17**, 604.

[26] L. E. Asp, B. A. Sjögren, L. A. Berglund, *Polym. Compos.* 1997, **18**, 9.

[27] W. J. O'Kane,R. J. Young, A. J. Ryan, W. Bras, G. E. Derbyshire, G. R. Mant, *Polymer* 1994, **35**, 1352

[28] T. Endo, R. Kitagawa, F. Zhang, T. Hirotsu, J. Hosokawa, *Chem. Lett.* 1999, **10**, 1155

[29] N. Vasanthan, I. D. Shin, A. E. Tonelli, *Macromolecules* 1996, **29**, 263.

[30] K. Miyazaki, K. Moriya, N. Okazaki, M. Terano, H. Nakatani, *J. Appl. Polym. Sci*. 2009, 111, 1835.

[31] T. Tang, B. Huang, *J. Polym. Part B: Polym. Phys.* 1994, 32, 1991.

[32] T. Kowalewski, G. Ragosta, E. Martuscelli, A. Galeski, *J. Appl. Polym. Sci.* 1997, 66, 2047.

[33] T. Kondo, C. Sawatari, R. S. J. Manley, D. G. Gray, *Macromolecules* 1994, 27, 210.

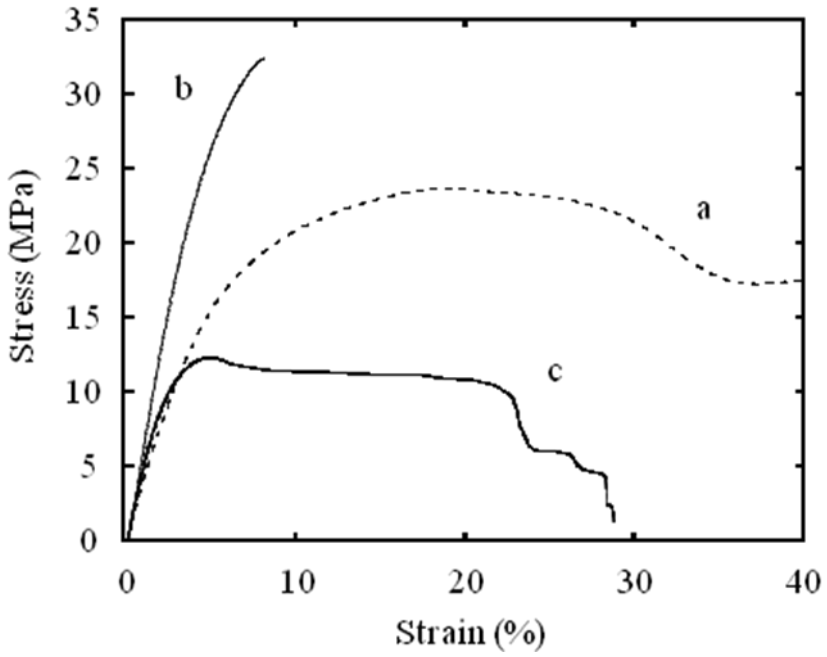

Figure 3-9 Stress-strain curves of PP, PP/MAPP/FC and FC/LPEO+ PP/MAPP

a: PP. b: PP(69.5 wt%)/MAPP(0.5 wt%)/FC(30 wt%). c: FC(30 wt%)/LPEO(7.5 wt%)+PP(62 wt%)/MAPP(0.5 wt%).

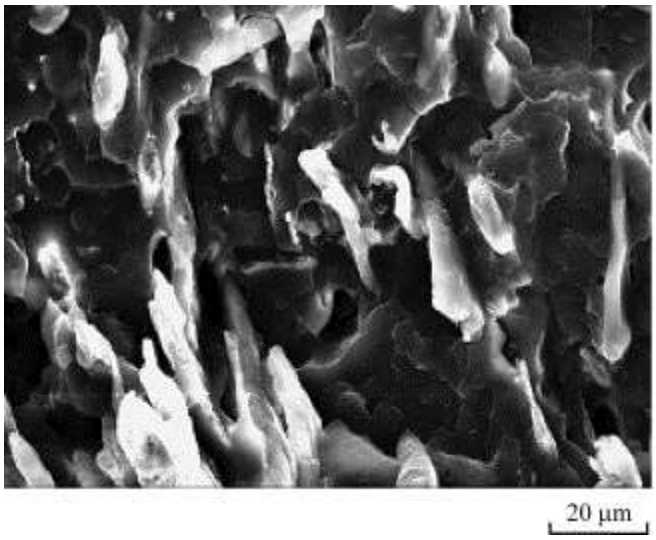

Figure 3-10 SEM micrograph of the fracture surface of FC (30 wt %)/LPEO (7.5 wt %)+PP (62 wt %)/MAPP (0.5 wt %).

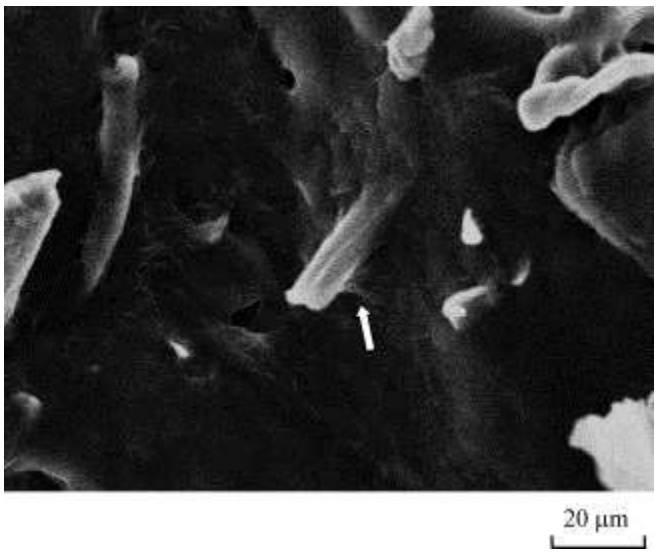

Figure 3-11 SEM micrograph of the fracture surface of FC (10 wt %)/LPEO (90 wt %). The arrow indicates the interfacial bond between FC and LPEO.

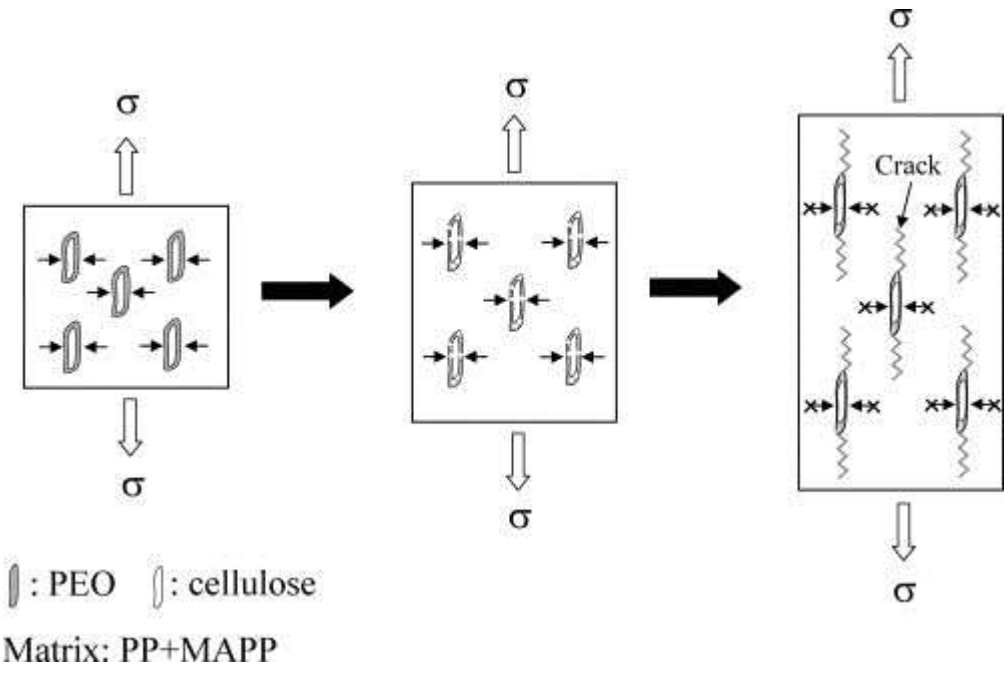

Figure 3-12 Schematic diagram illustrating the tensile deformation mechanism of the FC/LPEO+PP/MAPP composite.

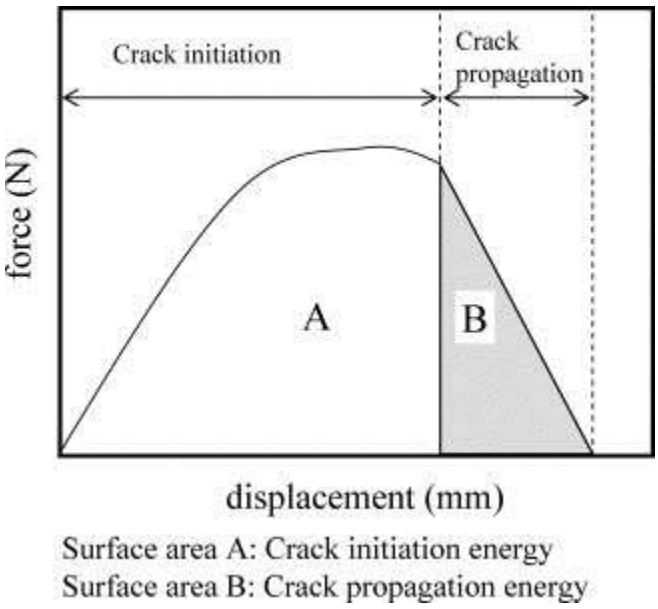

Figure 3-13 Schematic force–displacement graph obtained with the SEN tensile test.

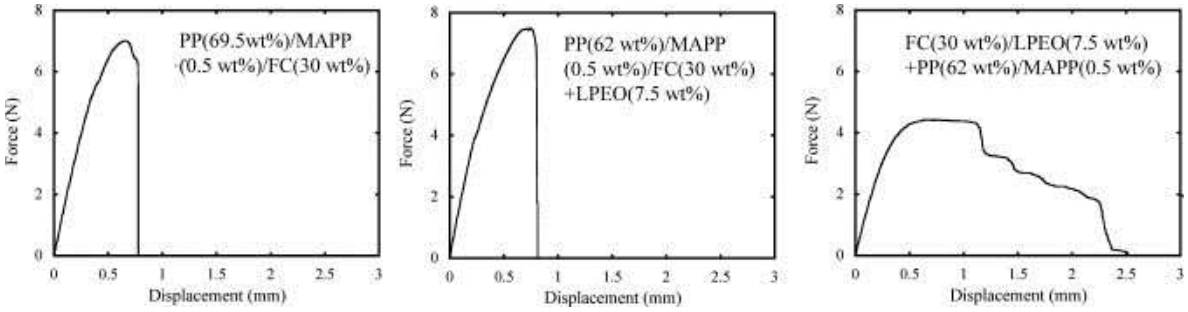

Figure 3-14 Force–displacement curves obtained with the SEN tensile test for various composites.

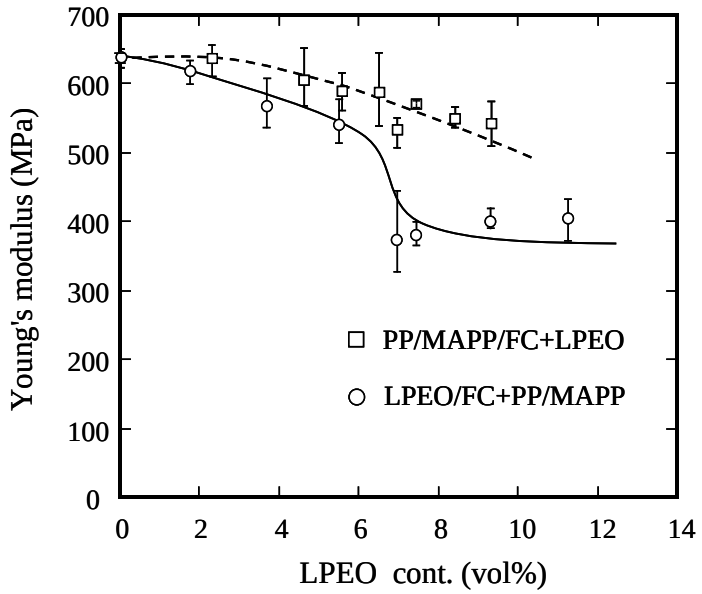

Figure 3-15 Young's modulus versus LPEO content (vol %).

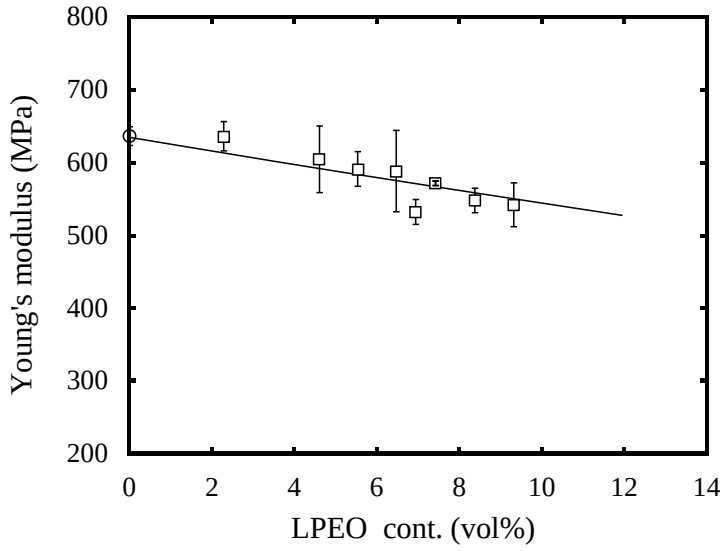

Figure 3-16 Young's modulus versus LPEO content (vol %) for PP/MAPP/FC + LPEO: The solid line is a fit, obtained using Kerner–Nielsen equation and the $\psi(=2)$ is a factor depending on the maximum packing fraction of component.

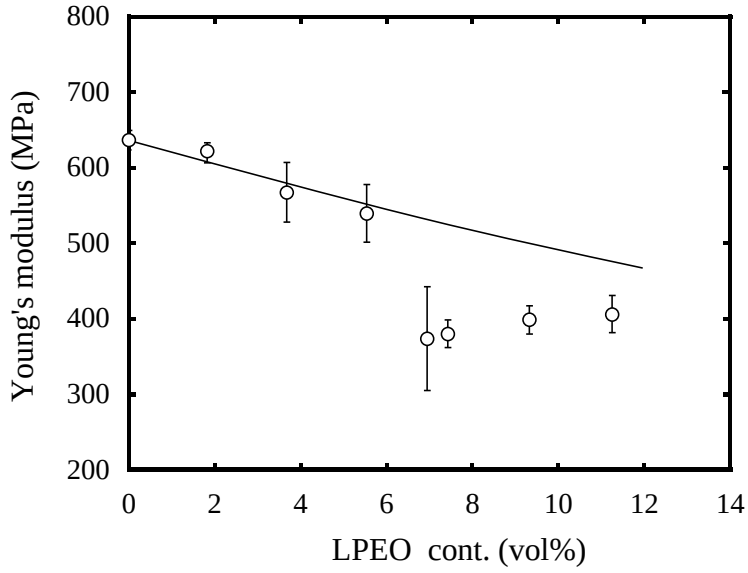

Figure 3-17 Young's modulus versus LPEO content (vol %) for LPEO/FC + PP/MAPP: The solid line is a fit, obtained using Kerner–Nielsen equation and the ψ(=6) is a factor depending on the maximum packing fraction of component.

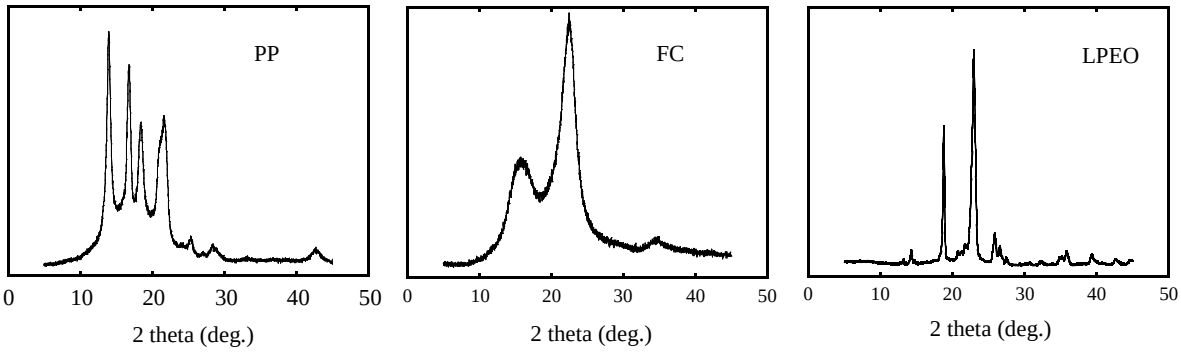

Figure 3-18 WAXD profiles of PP, FC, and LPEO.

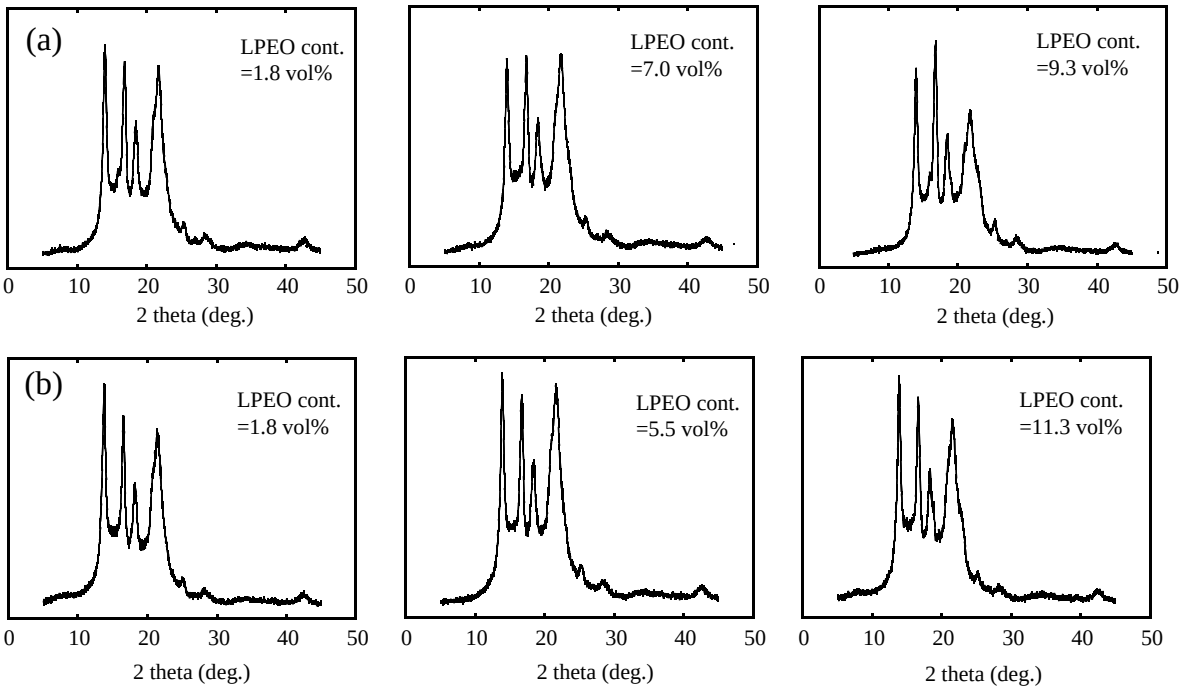

Figure 3-19 (a) WAXD profiles of PP/MAPP/FC + LPEO composites with different LPEO contents and (b) WAXD profiles of LPEO/FC + PP/MAPP composites with different LPEO contents.

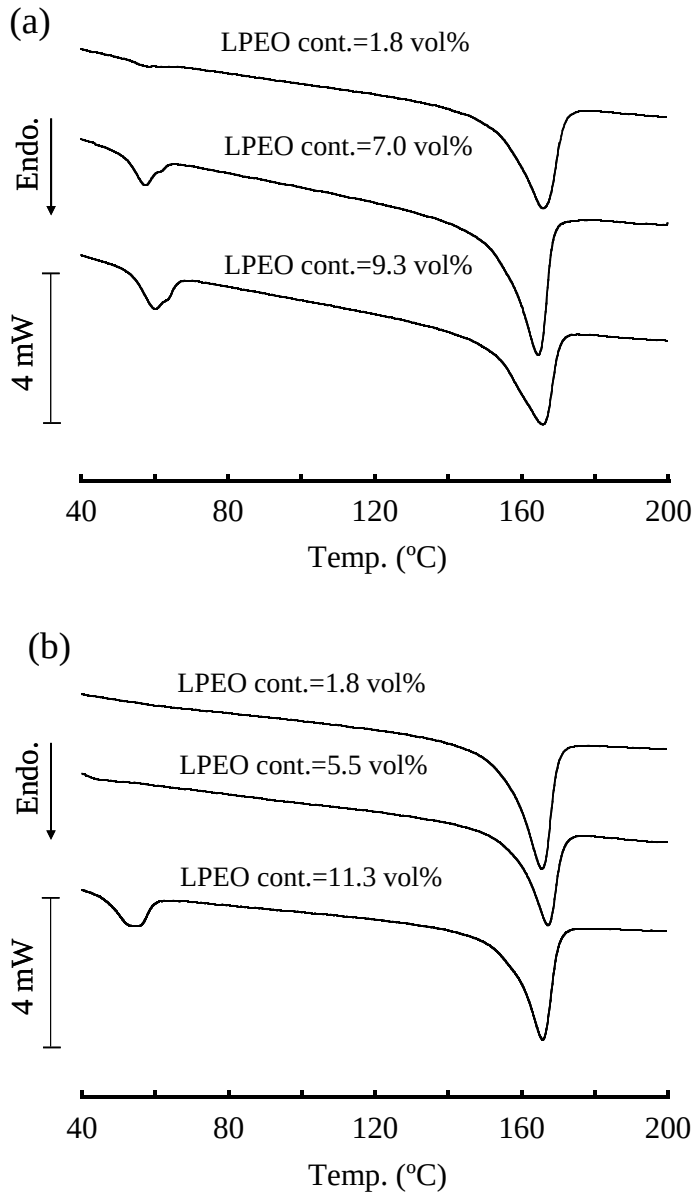

Figure 3-20 (a) DSC curves of PP/MAPP/FC + LPEO composites with different LPEO contents and (b) DSC curves of LPEO/FC + PP/MAPP composites with different LPEO contents.

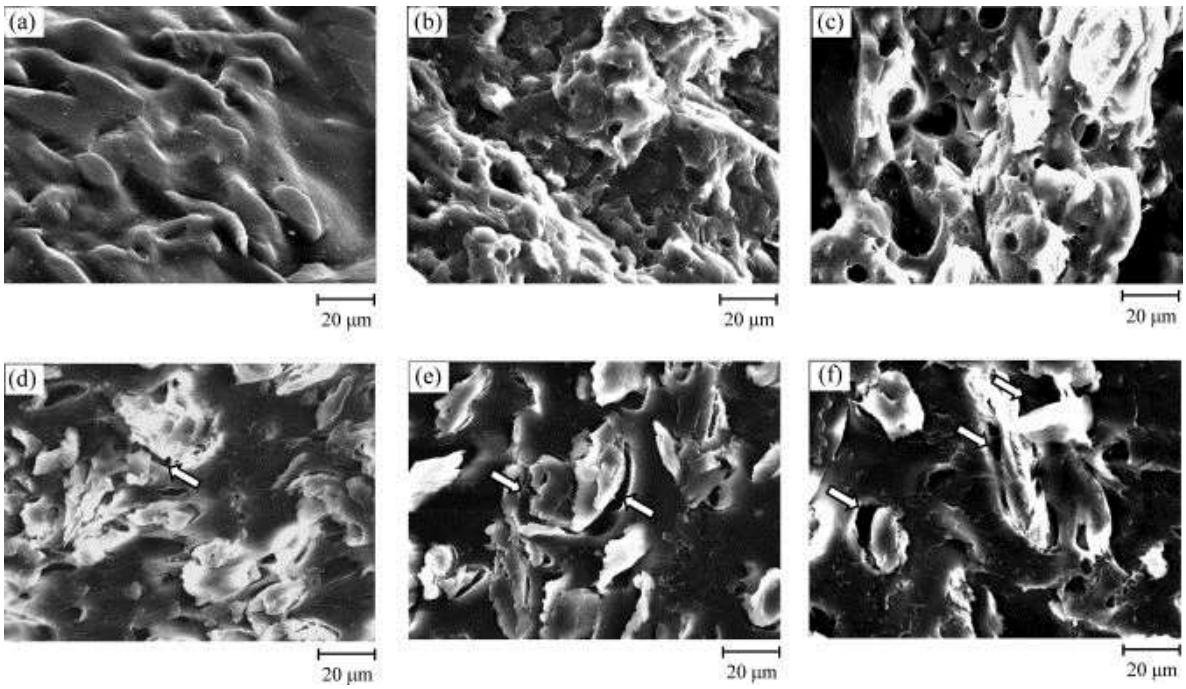

Figure 3-21 SEM micrographs of fracture surfaces of PP/MAPP/FC + LPEO and surfaces of LPEO/FC + PP/MAPP. The arrows indicate the LPEO interface.

a: PP (77.1 vol %)/MAPP (0.6 vol %)/FC (20.0 vol %) + LPEO (2.3 vol %);

b: PP (72.2 vol %)/MAPP (0.6 vol %)/FC (20.3 vol %) + LPEO (6.9 vol %);

c: PP (69.7 vol %)/MAPP (0.6 vol %)/FC (20.4 vol %) + LPEO (9.3 vol %);

d: LPEO (1.8 vol %)/FC (20.0 vol %) + PP (77.6 vol %)/MAPP (0.6 vol %);

e: LPEO (5.5 vol %)/FC (20.2 vol %) + PP (73.7 vol %)/MAPP (0.6 vol %);

f: LPEO (11.2 vol %)/FC (20.5 vol %) + PP (67.7 vol %)/MAPP (0.6 vol %).

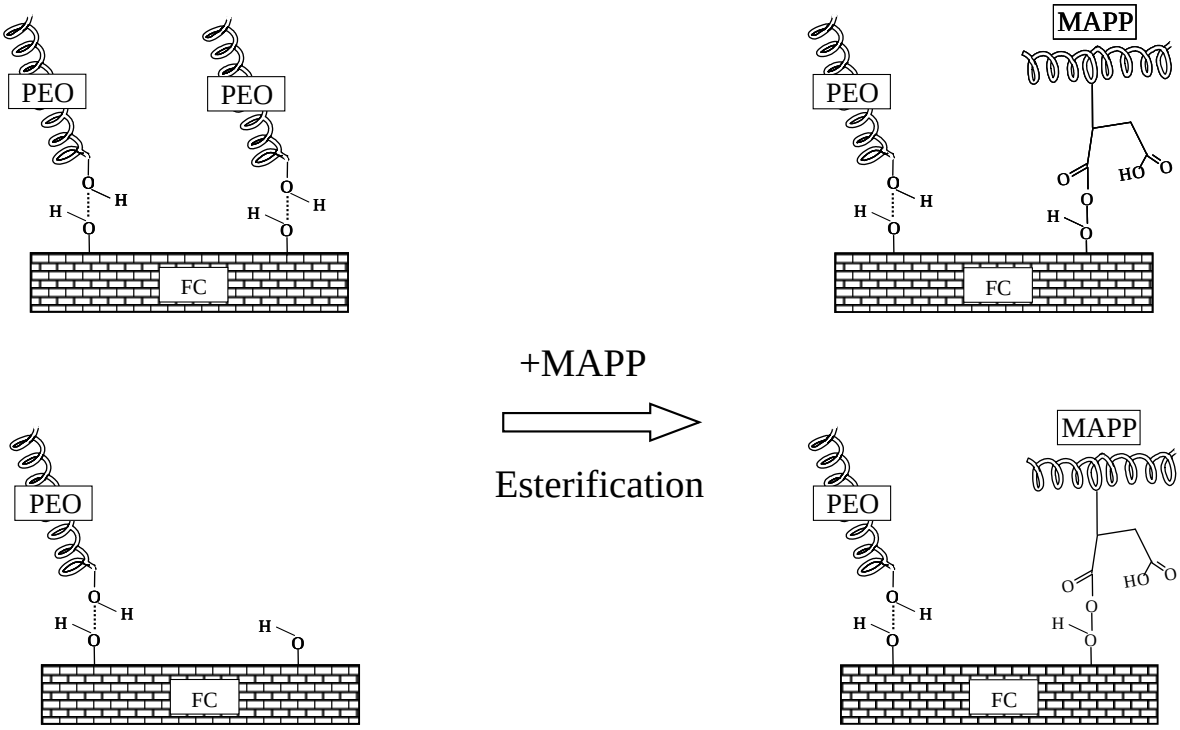

Figure 3-22 Plausible schematic formation model of the hydrogen and the ester bonds for the FC in the LPEO/FC + PP/MAPP composite.

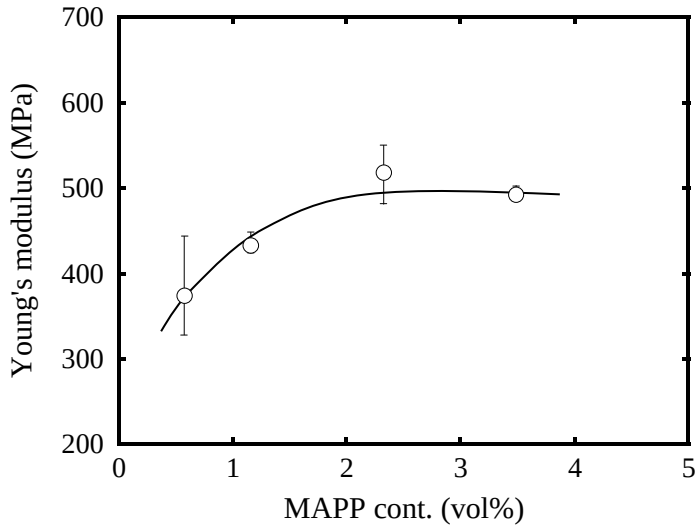

Figure 3-23 Young's modulus versus MAPP content (vol %) for LPEO (7.0 vol %)/FC (20.3 vol %) + PP/MAPP.

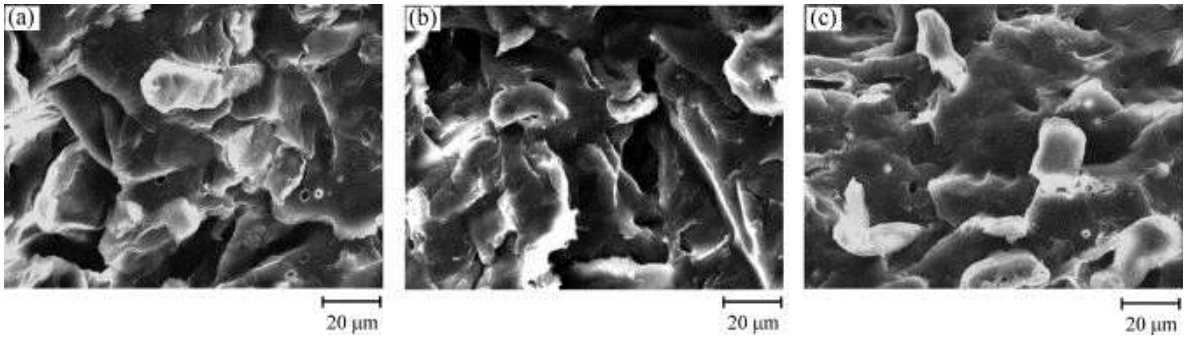

Figure 3-24 SEM micrographs of fracture surfaces of LPEO/FC + PP/MAPP: a: LPEO (6.9 vol %)/FC (20.3 vol %) + PP (71.6 vol %)/MAPP (1.2 vol %); b: LPEO (6.9 vol %)/FC (20.3 vol %) + PP (70.5 vol %)/MAPP (2.3 vol %); c: LPEO (6.9 vol %)/FC (20.3 vol %) + PP (69.3 vol %)/MAPP (3.5 vol %).

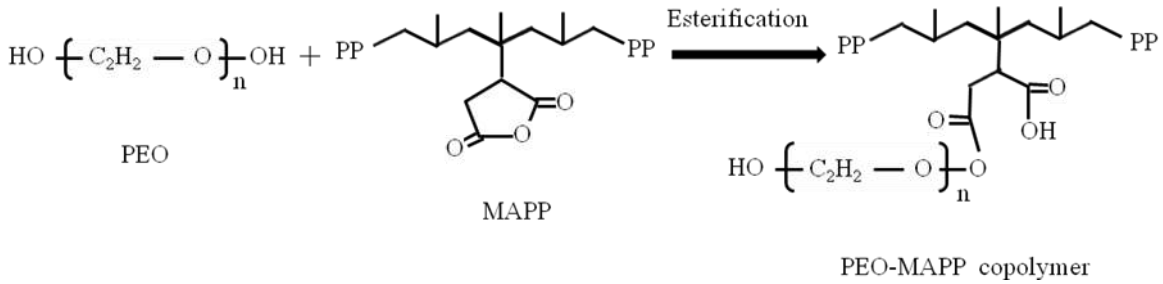

Figure 3-25 Plausible schematic formation model of LPEO-MAPP copolymer in the LPEO/FC + PP/MAPP composite.

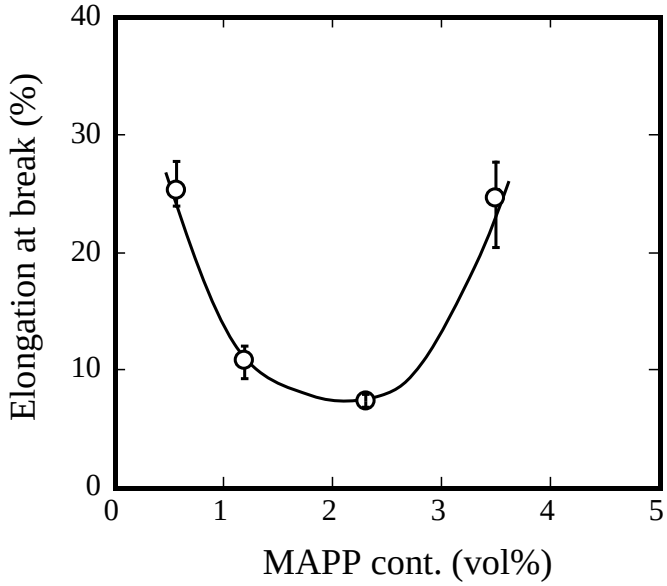

Figure 3-26 Elongation at break versus MAPP content (vol %) for LPEO (7.0 vol %)/FC (20.3 vol %) + PP/MAPP.

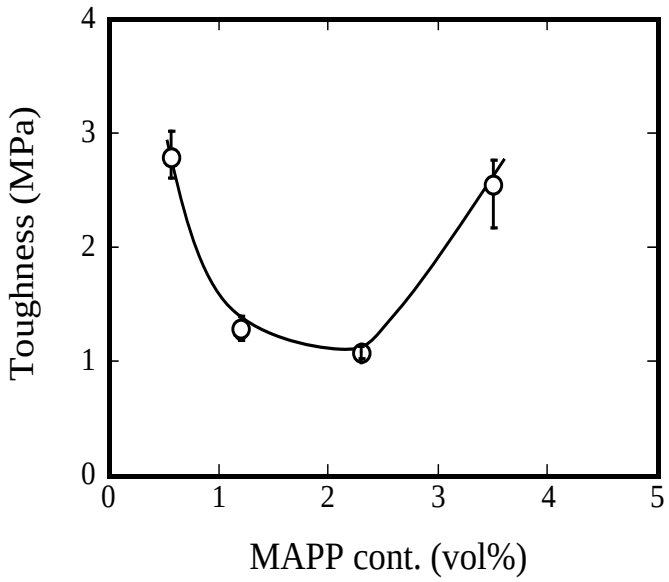

Figure 3-27 Toughness versus MAPP content (vol %) for LPEO (7.0 vol %)/FC (20.3 vol %) + PP/MAPP.

Table 3-3 Fracture Energies of Various PP Composite Samples

Sample	Fracture energy (kJ/m^2)*
PP (69.5 wt %)/MAPP (0.5 wt %)/ FC (30 wt %)	10.6 ± 0.9
PP (62 wt %)/MAPP (0.5 wt %)/ FC (30 wt %)+LPEO (7.5 wt %)	12.1 ± 0.7
FC (30 wt %)/LPEO (7.5 wt %) +PP (62 wt %)/MAPP (0.5 wt %)	18.8 ± 2.8

*Surface area of the force–displacement curves obtained by the SEN tensile test

Chapter 4: Development of degradable polypropylene by an addition of poly(ethylene oxide)microcapsule containing TiO_2

4-1: Introduction

Since polymeric materials have been developed, intensive efforts have been expended on the stabilization of these materials by scientists and engineers. As a result, polymeric materials are given an enormous stability and are widely used in our life. However, the intense use of the polymeric materials, which are combined with enormous stability, has created serious problems of plastic waste and has given rise to an intensive interest in new polymer systems such as biodegradable materials [1, 2] and [3]. The biodegradable materials have attracted much attention from the viewpoints of environmental compatibilities.

PP is one of the most useful polyolefins and is known as a non-biodegradable polymer. Generally large molecule such as PP cannot easily enter into the cells of micro organisms. Therefore, PP is hard to be metabolized in micro organisms. If PP is spontaneously degraded to low molecular weight products, the biodegradability will appear. In fact, it has been known that polyethylene (PE), which is similar to PP chemical structure, is given biodegradability by pro-oxidant [4, 5, 6, 7] and [8]. The mechanism of the PE biodegradation involves two stages which are abiotic oxidation and microbial oxidation. In addition, the rate of the biodegradation process depends on the abiotic oxidation stage initiated by pro-oxidant.

Study on PP degradation has been generally performed [9, 10, 11, 12] and [13]. The degradation mechanism is called as “autooxidation”. There is no difference in the

autooxidation between PE and PP. However the PE degradation frequently yields cross-linked productions, and the PP one mainly does low molecular productions originated from the polymer chain scission. The difference is due to the chemical structure in their polymer chains. Considering from the difference between these degradation productions, it seems that the abiotic oxidation rate of PP is much higher than that of PE. In order to acquire practical biodegradability, the abiotic oxidation must promptly advance under a mild condition such as sunshine and lower temperature exposures. In this point, PP is believed to have a higher potential to acquire biodegradability by pro-oxidant.

PP photo-degradation using TiO_2 photocatalysis has been studied [14, 15] and [16]. TiO_2 photocatalytically reacts with H_2O in air under sunshine exposure, and OH• is produced. Since the OH• has highly reactivity, PP degradation can be initiated by the OH under a mild condition [14] and [17]. The degradation rate is, however, considerably slow because of nonexistence of H_2O in PP matrix. In general, the additive effect of TiO_2 on PP degradation is low.

There is much literature on mechanisms of autooxidation of PP [9, 10, 11, 12] and [13]. Many researchers agree fundamentally with the following mechanistic scheme:

Initiation: $RH \rightarrow R\bullet$ (I)

Propagation: $R\bullet + O_2 \rightarrow ROO\bullet$ (II)

$ROO\bullet + RH + O_2 \rightarrow R\bullet + ROOH$ (III)

Chain branching (including chain scission)

$ROOH \rightarrow$ carbonyls$+ R\bullet$ (IV)

Among these reaction steps, the hydroperoxide decomposition (IV) is the rate-determining step. Thus, the facilitation of the hydroperoxide decomposition leads to the facilitation of the PP degradation. Some investigators reported that acid and aldehyde compounds have the potential to facilitate the hydroperoxide decomposition [18] and [19]. If a mechanism to produce acid and aldehyde compounds is built by TiO_2 photocatalysis, PP degradation can be considerably facilitated by the compounds.

As shown in the Chapter 4, we reported mechanical properties of PP/PEO blend. The PEO acted as an elastomer in the PP matrix because of its lower elasticity [20]. The existence of the PEO phase hardly impaired ductility of the PP. In addition, PEO is photocatalytically degraded by TiO_2, and then acid and aldehyde compounds are produced [21] and [22]. It appears that a combination of TiO_2 and PEO becomes an excellent pro-oxidant for PP photo-degradation.

In this study, we prepared a novel photo-degradable PP by an addition of PEO microcapsule containing TiO_2 (PP/PEO/TiO_2). The additive effect of the microcapsule on the PP degradation rate was evaluated by a Fourier transform infrared (FT-IR) measurement, a tensile testing and an optical microscope observation. In addition, a control of the degradation rate was investigated by a HALS and a phenolic antioxidant.

4-2: Experimental

4-2-1: Materials

PP (meso pentad fraction = 98%) was supplied by Japan Polypropylene Co. The number-average molecular weight (M_n) and the polydispersity (M_w/M_n) of the PP were 4.6×10^4 and 5.7, respectively. PEO was purchased from Wako Pure Chemical Industries, Ltd. The average molecular weight was 5.0×10^5. TiO_2 was purchased from Wako Pure Chemical Industries, Ltd. The crystal structure was anatase (over 98.5%), and the surface area was about 6 m^2/g. The TiO_2 was used without pretreatment. Phosphite antioxidant (ADK STAB PEP-36), HALS (tetra N-methylated hindered amine type light stabilizer: ADK STAB LA-52) and phenolic antioxidant (ADK STAB AO-60) were supplied by ADEKA Co., respectively.

4-2-2: Prepared PEO/TiO_2 blends

PEO/TiO_2 blend was prepared by an Imoto Seisakusyo IMC-1884 melting mixer. The mixing was performed with and without the HALS and the phenolic antioxidant at 180 °C at 60 rpm for 5 min.

4-2-3: Prepared PP/PEO/TiO_2 composites

PP/PEO/TiO_2 composite was prepared by the Imoto Seisakusyo IMC-1884 melting mixer. After a small amount of the phosphite antioxidant (ADK STAB PEP-36, ca. 0.1 wt%) was added, the mixing was performed at 180 °C at 60 rpm for 5 min. PP/TiO_2 composite was prepared in the same method.

4-2-4: Photo-degradation test

The samples were molded into a thin film (50 μm) by compression molding at 190°C under 50 MPa for 5 min. The Film was cut into the 2×2 cm, and put into a vial. A high-pressure mercury vapor lamp of 400 W (Toshiba H-400P, luminance value = 200 cd/cm^2) was used as a UV light source. The distance between specimens and the lamp was 50 cm. The photo-degradation tests were carried out at 30 °C.

4-2-5: Scanning electron microscope (SEM) and SEM/Energy dispersive X-ray spectrometer (EDS) analyses

SEM and SEM/EDS analyses were carried out with a JEOL JSM-5800 at 20 kV. The plate of sample was fractured in liquid nitrogen, and then the fractured surface was cut by a microtome to obtain the flat surface. The sample obtained was sputter-coated with gold. Ti atoms were measured with an EDS (Oxford Instruments INCA Microanalysis).

4-2-6: Wide-angle X-ray diffraction (WAXD) measurement

WAXD diffractograms were recorded in reflection geometry at 2 ° (2θ/min) under Ni-filtered Cu Ka radiation with a Rigaku Rint-1200 diffractometer.

4-2-7: Differential scanning calorimetry (DSC) measurement

DSC measurements were made with a SHIMADZU DSC-60. The samples of about 5 mg weight were sealed in aluminum pans. The measurement of the samples was carried out at a heating rate of 10 °C /min under a nitrogen atmosphere.

4-2-8: Fourier Transform Infrared (FT-IR) analysis

The FT-IR spectra were obtained by a spectrometer (Perkin-Elmer Spectrum One).

4-2-9: Nuclear Magnetic Resonance (NMR) Spectroscopy Measurement

The NMR spectrum of degraded PP was measured using a JEOL EX-400 spectrometer at 120 °C on 10% (w/v) solution in hexachloro-1,3-butadiene. 1,1,2,2-tetrachloroethane-d2 was added as an internal lock and used as an internal chemical shift reference.

4-2-10: Optical microscope observation

Optical microscope observations of sample were carried out with a Nikon ECLIPSE 50/POL polarized optical microscope.

4-2-11: Tensile testing

Stress-strain behavior was observed using a SHIMADZU EZ-S at a cross-head speed of 5 mm/min. The sample specimens were cut with dimensions 30×2×0.1 mm shape in which the gauge length was 10 mm. All of tensile testing was performed at 20 °C. All results obtained are the average values of ten measurements.

4-3: Results and Discussion

4-3-1: Morphology and crystal structure

Figure 4-1 shows the SEM microphotographs and the EDS analyses of the PP/TiO_2, the PP/PEO/TiO_2 and the PP/PEO/TiO_2 etched by THF for 6 hour, respectively. In the case of the PP/TiO_2, the TiO_2 particles are wholly distributed. Whereas, in the case of PP/PEO/TiO_2, some aggregated TiO_2 particles can be observed. As shown in Figure 4-1(c), the SEM photograph of the etched PP/PEO/TiO_2 shows many holes corresponding to the PEO phase [20], and the TiO_2 particles are hardly observed by the EDS analysis. The disappearances of the TiO_2 particles and the PEO phases indicate that the TiO_2 particles exist in the PEO phases.

Figure 4-2 shows the WAXD profiles of the PP/TiO_2, the PP/PEO/TiO_2 and the PP. The profile of the PP/PEO/TiO_2 is similar to that of the PP except the peak (at $2\theta = 25.2$ deg) assigned to anatase TiO_2. The crystal forms of the PP and the PP part in the PP/PEO/ TiO_2 are assigned to α-form (monoclinic). Whereas, the profile of the PP/TiO_2 shows the coexistence of α- and β-form (hexagonal) [23].

Figure 4-3 shows the DSC curves of the PP/TiO_2 and the PP/PEO/TiO_2. In the DSC curve of the PP/TiO_2, the peak assigned to the melting of the β-form part [24] is considerably small, suggesting that the content of the β-form is considerably less. It seems that the TiO_2 contains a small amount of impurities, which act as a nucleating agent of the β-form. In the case of the PP/PEO/TiO_2, as shown in Figure 4-2 and 4-3, the β-form is not observed. This behavior supports that the TiO_2 exists in only the PEO phase.

4-3-2: Photo-degradation

In the case of PP photo-degradation with TiO_2 under UV irradiation, the TiO_2 is photoexcited and produces an electron and a positive hole. The electron and the positive hole react with H_2O and O_2 and form OH• (Figure 4-4) [17, 21]. The OH• has a high reactive ability and initiates the PP autooxidation [17].

Figure 4-5 shows the FT-IR spectra of the PP/PEO/TiO_2 and the PP/TiO_2. These samples have been degraded for 21 hour. In the spectrum of the PP/TiO_2 sample, the peak assigned to carbonyl group appears at 1713 cm^{-1}. In the case of the PP/PEO/TiO_2, the corresponding peak shifts to 1722 cm^{-1}. The peak shift would be due to the peak superposition with the peaks of an ester, an acid and an aldehyde compounds, which are produced by the PEO degradation.

PEO degradation mechanism with TiO_2 is shown in Figure 4-6 [21, 25]. The degradation of PEO is initiated by OH•. Ester, formate, acid and aldehyde compounds are produced by the degradation. It is possible to determine these productions by ^{1}H-NMR measurement. Figure 4-7 shows the ^{1}H-NMR spectrum of the degraded PEO/TiO_2 by UV light irradiation for 21 hours. The peaks assigned to ester, formate, acid and aldehyde compounds appear at 4.3 ppm, 4.7 ppm and 4.9 ppm, respectively.

Figure 4-8 shows the buildups of the peaks of the carbonyl groups of the PP/PEO/TiO_2 and the PP/TiO_2 against the UV irradiation time. The carbonyl group peak in the PP/TiO_2 exhibits an induction time until about 9 h and then increases. Whereas, the carbonyl group peak in the PP/PEO/TiO_2 increases up to about 21 h and then becomes almost constant. The difference of the absorbance value between the PP/TiO_2 and the PP/PEO/TiO_2 is considerably large.

The elongation at break of PP reflects the degree of PP chain scission during

degradation of PP [26]. Figures 4-9 (a) and (b) show the stress-strain curves of the PP/PEO/TiO_2 and the PP/TiO_2 before and after the photo-degradation. The values of elongation at break of the PP/PEO/TiO_2 and the PP/TiO_2 are summarized in Table 4-1. It is noted here that the value of elongation at break of the degraded PP/PEO/TiO_2 rapidly decreases as compared with that of the PP/TiO_2. This behavior suggests that the degradation rate of the PP/PEO/TiO_2 is considerably faster than that of the PP/TiO_2. Figure 4-10 shows the optical micrographs of the degraded PP/PEO/TiO_2 and the degraded PP/TiO_2, respectively. In the case of the degraded PP/PEO/TiO_2, the cracks appear in the PP matrix, whereas there were no cracks in the degraded PP/TiO_2. This difference suggests that the existence of PEO phase facilitates the degradation of the PP matrix.

H_2O is hardly adsorbed to PP possessing hydrophobicity. In the case of the PP/TiO_2, the photocatalyzed reaction between TiO_2 and H_2O is confined to the surface contacting the atmosphere containing moisture. Therefore, as shown in Figure 4-11(a), the photocatalyzed reaction hardly occurs at the inner PP part, and the PP degradation is considerably slow. Whereas, PEO is hydrophilic and can adsorb moisture in the atmosphere. In the case of the PP/PEO/TiO_2, as shown in Figure 4-11(b), the TiO_2 can react with the adsorbed H_2O in the PEO phase, resulting that the OH• is produced and can initiate the PP degradation. In addition, the reaction of the PEO and the OH• produces acid and aldehyde compounds, which bring about the facilitation of the PP degradation [18, 19]. The higher degradation rate of the PP/PEO/TiO_2 is due to the existence of PEO.

HALS disturbs a photo degradation of plastics by trapping radical species [27]. In addition, Allen et. al. [28] reported that HALS and phenolic antioxidant have a

synergistic effect in photo-stabilization. It seems that an appropriate addition of these stabilizers brings about a control of the degradation rate of the PP/PEO/TiO_2. Therefore, the control of the degradation rate has been carried out with an addition of a HALS (LA-52) and a phenolic antioxidant (AO-60). Figure 4-12 shows the buildups of carbonyl group peak in the PP/PEO/TiO_2 containing the stabilizers under the UV irradiation. In the case of the samples containing only the HALS, the peak intensities of carbonyl group are decreased with the increase of the HALS content. As compared with the PP/PEO/TiO_2 without HALS, the peak intensities of the samples containing the HALS of 0.06 wt% and 0.6 wt% are decreased up to approximately 80 % and 60 %, respectively. These results suggest that the degradation of the PP/PEO/TiO_2 can be controlled by the HALS content. In the case of the PP/PEO/TiO_2 containing both the HALS and the phenolic antioxidant, the peak intensities of the carbonyl group are suppressed by the synergistic effect until 3 h and then become considerably higher as compared with the samples containing only the same amount (0.6 wt%) of the HALS. The suppression effect is rising by the simultaneous addition of the phenolic antioxidant in the early phase of the PP degradation. However, the simultaneous addition shows an antagonism after 4 h degradation. Since the HALS is a kind of base, it should also work as a neutralizer against the acid produced by the photocatalysis. In the case of the PP/PEO/TiO_2 containing the HALS, the facilitation of the PP degradation would be controlled by this neutralization as well as by the ordinary stabilization of radical species. Whereas, the phenolic antioxidant is a kind of acid [29], and the existence must disturb the neutralization between the HALS and the acid produced by the photocatalysis. In the case of the PP/PEO/TiO_2, the addition of the phenolic antioxidant is found to bring about the synergism with the HALS in the early phase of the PP degradation and the antagonism in the phase of the acid production, respectively.

4-4: Conclusion

In this study, the addition of PEO microcapsule containing TiO_2 to PP was performed to prepare the novel photo-degradable PP. The adsorbed H_2O in the PEO phase and the TiO_2 photo-catalytically reacted, and the hydroxyl radical (OH•), which initiated the PEO degradation, was produced. The degraded PEO produced the acid and the aldehyde, which were able to facilitate PP degradation. The addition of the PEO/TiO_2 microcapsule brought about the facilitative effect of the PP degradation. In addition, the addition of the HALS had the potential to suppress the PP degradation initiated by the microcapsule. The suppression effect was rising by the simultaneous addition of the phenolic antioxidant in the early phase of the PP degradation. However, the simultaneous addition showed the antagonism after 4 h degradation. In the case of the PP/PEO/TiO_2, the addition of the phenolic antioxidant is found to bring about the synergism with the HALS in the early phase of the PP degradation and the antagonism in the phase of the acid production, respectively.

References

[1] A. Steinbüchel and R.J. Müller, *Biopolymers* vol. 10, Wiley, New York, 2004, 365.

[2] R.A. Gross and B. Kalra, *Science* 2002,297, 803

[3] D. Briassoulis, *Polym. Degrad. Stab.* 2006, 91(6), 1256

[4] A.C. Albertsson, S.O. Andresson and S. Karlsson, *Polym. Degrad. Stab.* 1987, 18(1), 73

[5] A.C. Albertsson, C. Barenstedt and S. Karlsson, *Polym. Degrad. Stab*. 1992, 37(2), 163

[6] M. Weiland, A. Daro and C. Dacid, *Polym. Degrad. Stab.* 1995, 48(2), 275

[7] I. Jakubowicz, *Polym. Degrad. Stab.* 2003, 80(1), 39

[8] M.M. Reddy, R.K. Gupta, R.K. Gupta, S.N. Bhattacharya and R. Parthasarathy, *J Polym. Environ.* 2008, 16(1), 27

[9] Y. Kato, D.J. Carlsson and D.M. Wiles, *J. Appl. Polym. Sci.* 1969, 13(7), 1447

[10] D.J. Carlsson and D.M. Wiles, *Macromolecules* 1969, 6(2), 597

[11] J.H. Adams, *J. Polym. Sci. A* 1970, 8(5), 1077

[12] L. Audouin, V. Gueguen, A. Tcharkhtchi and J. Verdu, *J. Polym. Sci. A* 1995, 33(6), 921

[13] H. Nakatani, S. Suzuki, T. Tanaka and M. Terano, *Polymer* 2005, 46(26), 12366

[14] B. Ohtani, S. Adzuma, H. Miyadzu, S. Nishimoto and T. Kahiya, *Polym. Degrad. Stab*. 1989, 23(3), 271

[15] T.J. Turton and J.R. White, *Polym. Degrad. Stab.* 2001, 74(3), 559

[16] M.F. Mina, S. Seema, R. Matin, M.J. Rahaman, R.B. Sarker and M.A. Gafur et al., *Polym. Degrad. Stab.* 2009, 94(2), 183

[17] I. Blakey and G.A. George, *Polym. Degrad. Stab.* 2000, 70(2), 269

[18] R. Broska, J. Rychlý and K. Csomorová, *Polym. Degrad. Stab.* 1999, 63(2), 231

[19] P. Eriksson, T. Reiberger and B. Stanberg, *Polym. Degrad. Stab.* 2002, 78(1), 183.

[20] H. Nakatani and K. Miyazaki, *J. Appl. Polym. Sci.* 2009, 112(6), 3362

[21] S.P. Vijayalakshmi and G. Madras, *J. Appl. Polym. Sci.* 2006, 100(5), 3997

[22] T. Kagiya, N. Yokoyama and K. Takemoto, *Bull. Inst. Chem. Res. Kyoto Univ.* 1976, 54(1), 15

[23] Y. Shangguan, Y. Song, M. Peng, B. Li, Q. Zheng, *Eur. Polym. J.* 2005, 41(8), 1766

[24] J. Brandrup, E. H. Immergut, *Polymer Handbook 3rd ed.* New York, Wiley, 1999. 6, 159.

[25] G. Gallet, S. Carrocio, P. Rizzarelli, S. Karlsson, *Polymer* 2002, 43(4), 1081

[26] W. Feng, L. H. Yuan, S. Y. Zheng, G. L. Huang, J. L. Qiao, Y. Zhou, *Rad. Phys. Chem.* 2000; 57(3-6): 425-429.

[27] J. Karger-Kocsis, *POLYPROPYLENE,* Dordrecht: Kluwer Academic Publishers, 1999, 587.

[28] N. S. Allen, M. Edge, T. Corrales, F. Catalina, *Polym. Degrad. Stab.* 1998, 61(1), 139

[29] H. Yamashita, Y. Ohkatsu, *Polym. Degrad. Stab.* 2003, 80(3), 421

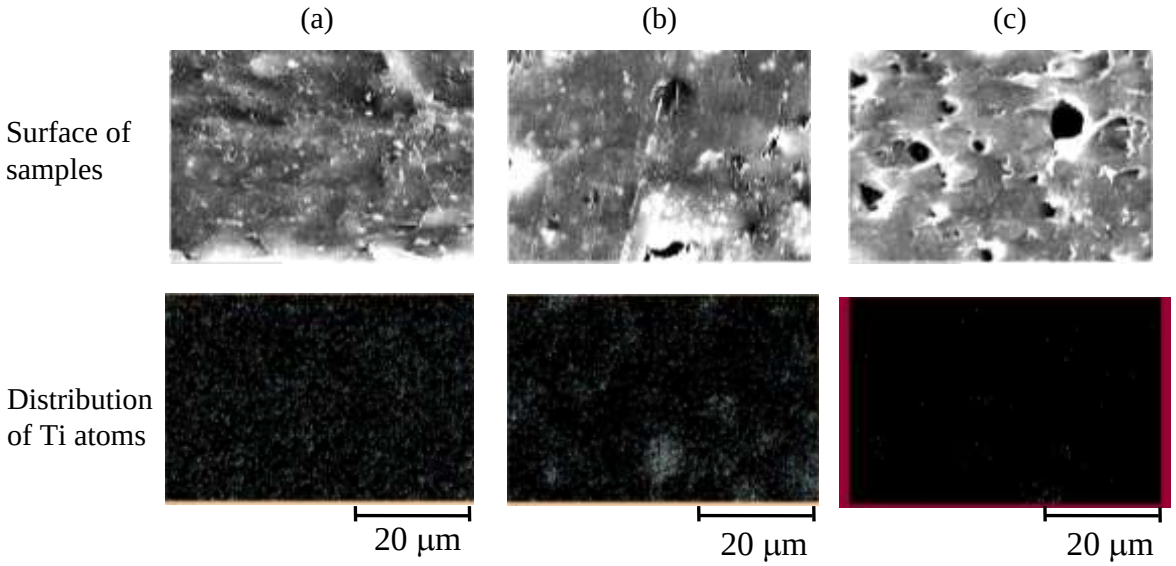

Figure 4-1 SEM microphotographs of the surface of the samples and SEM/EDS analysis of the surface the each sample.

(a): PP(97.3 wt%)/TiO_2(2.7 wt%)

(b): PP(89.8 wt%)/PEO(7.5 wt%)/TiO_2(2.7 wt%)

(c): PP(89.8 wt%)/PEO(7.5 wt%)/TiO_2(2.7 wt%) etched by THF for 6 hour.

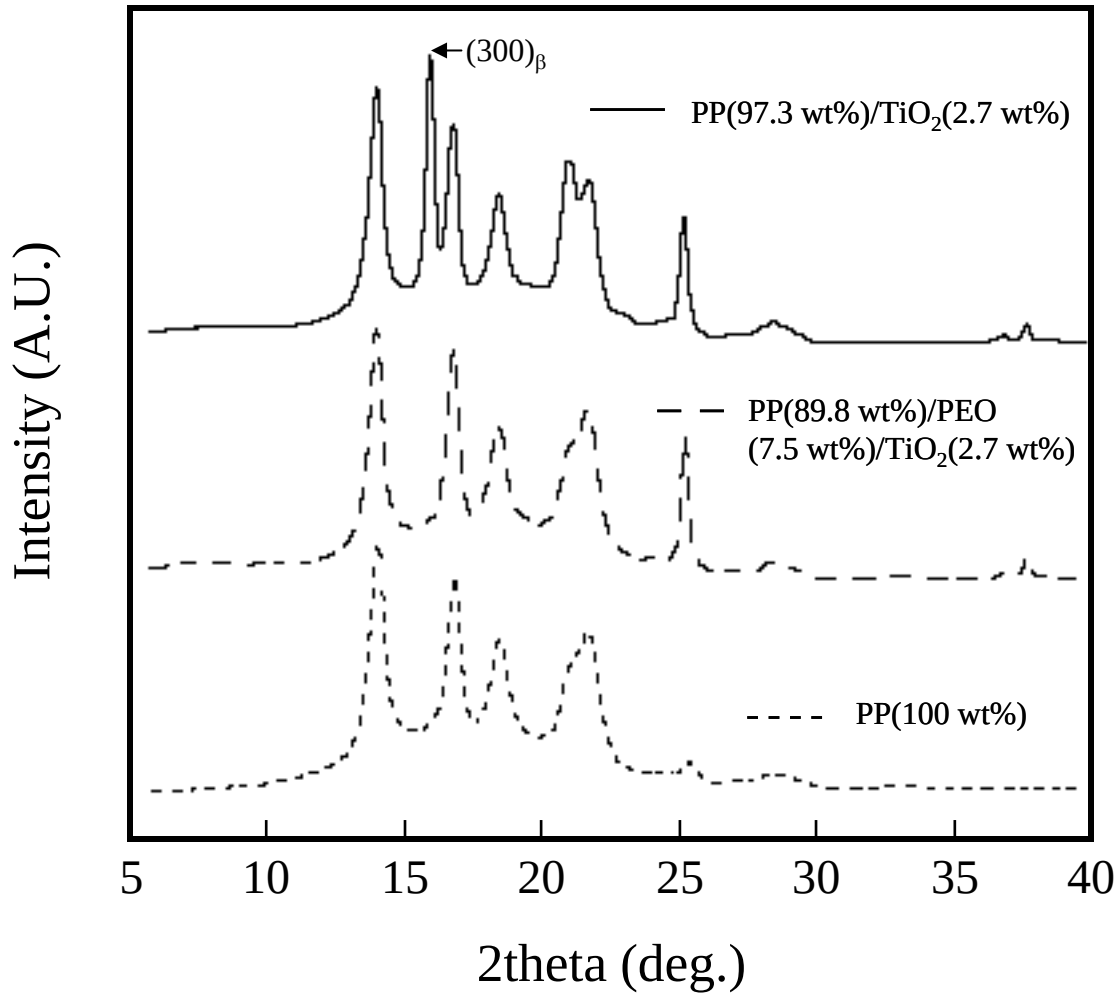

Figure 4-2 WAXD profiles of PP/TiO_2, PP/PEO/TiO_2 and PP.

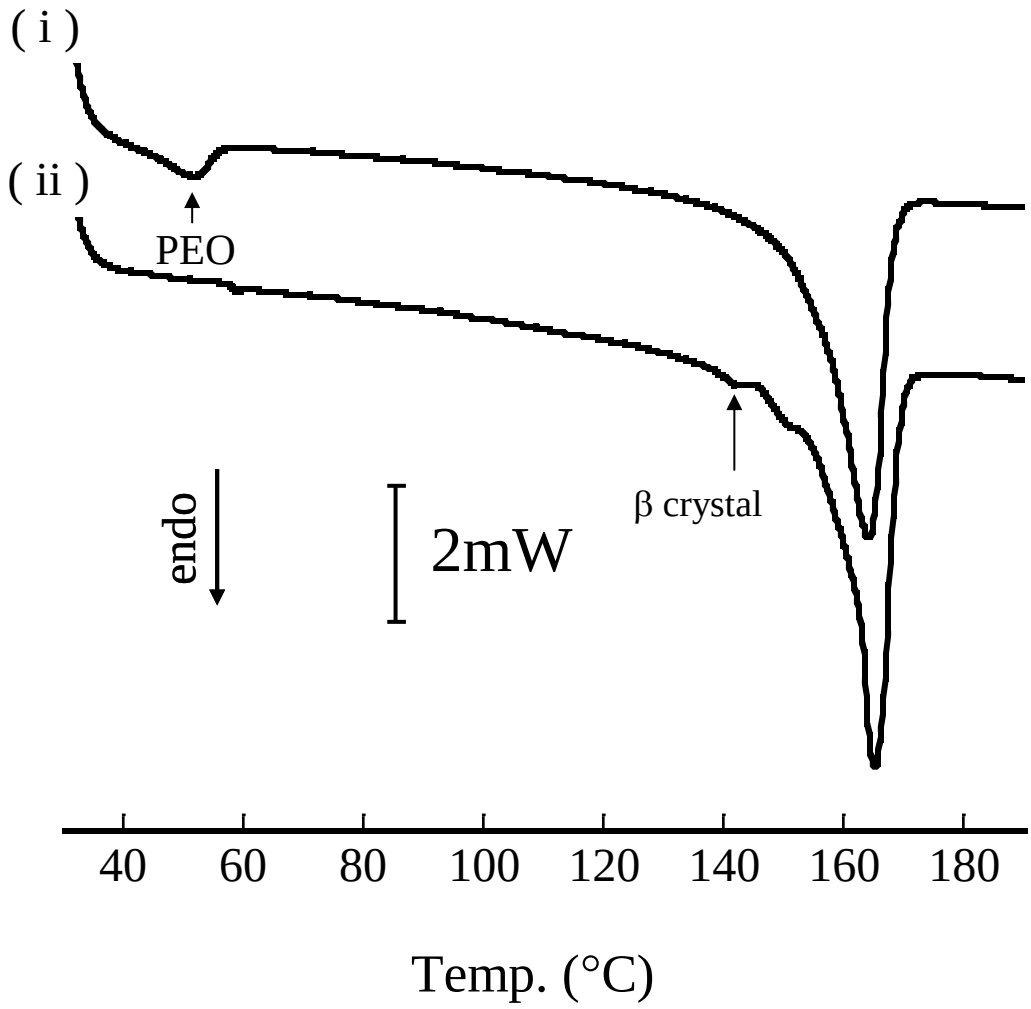

Figure 4-3 DSC curves of PP/TiO_2 and PP/PEO/TiO_2.

(i): PP(89.3 wt%)/PEO(7.5 wt%)/TiO_2(2.7 wt%)

(ii): PP(97.3 wt%)/TiO_2(2.7 wt%)

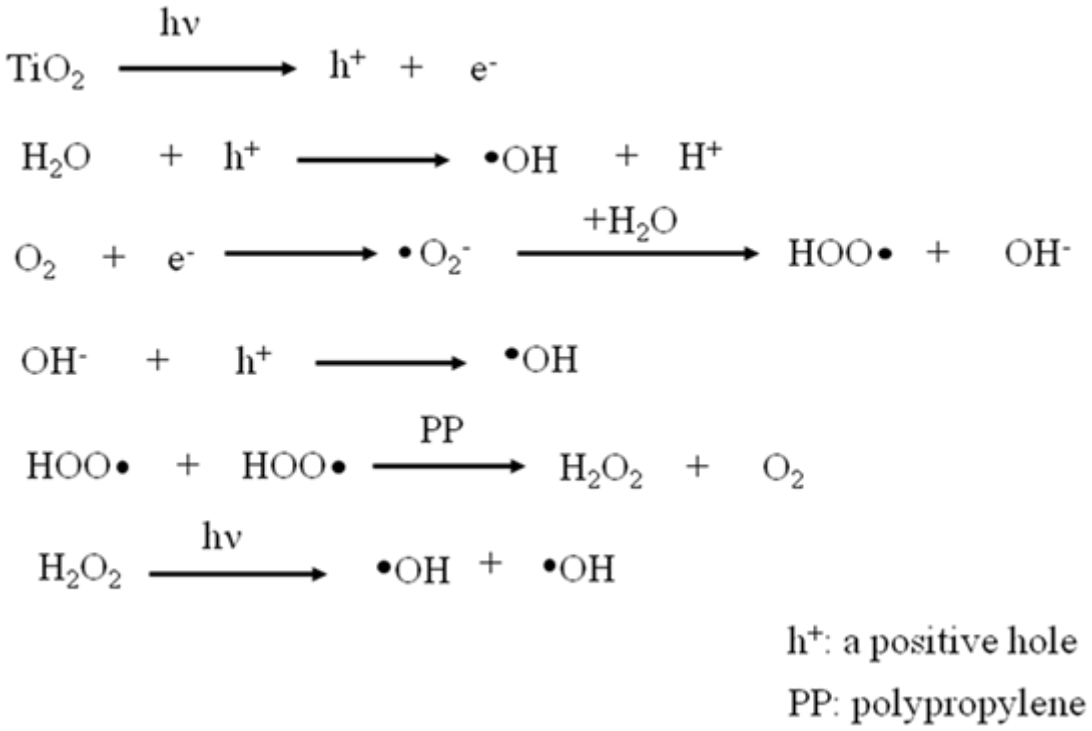

Figure 4-4 Mechanism of production of hydroxyl radical by TiO_2

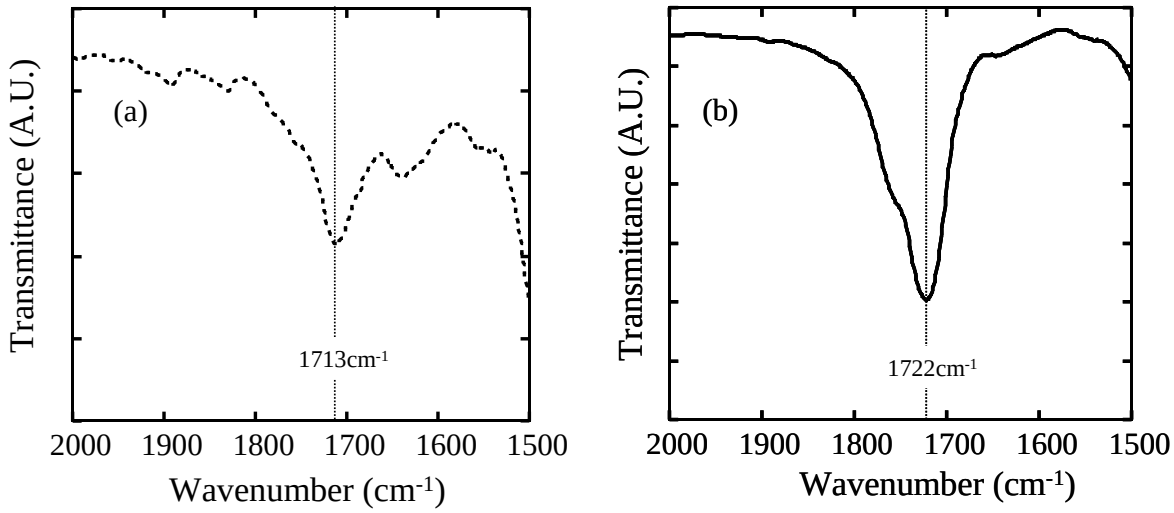

Figure 4-5 FT-IR spectra of degraded samples for 21h.

(a): PP(97.3 wt%)/TiO_2(2.7 wt%)

(b): PP(89.8 wt%)/PEO(7.5 wt%)/TiO_2(2.7 wt%)

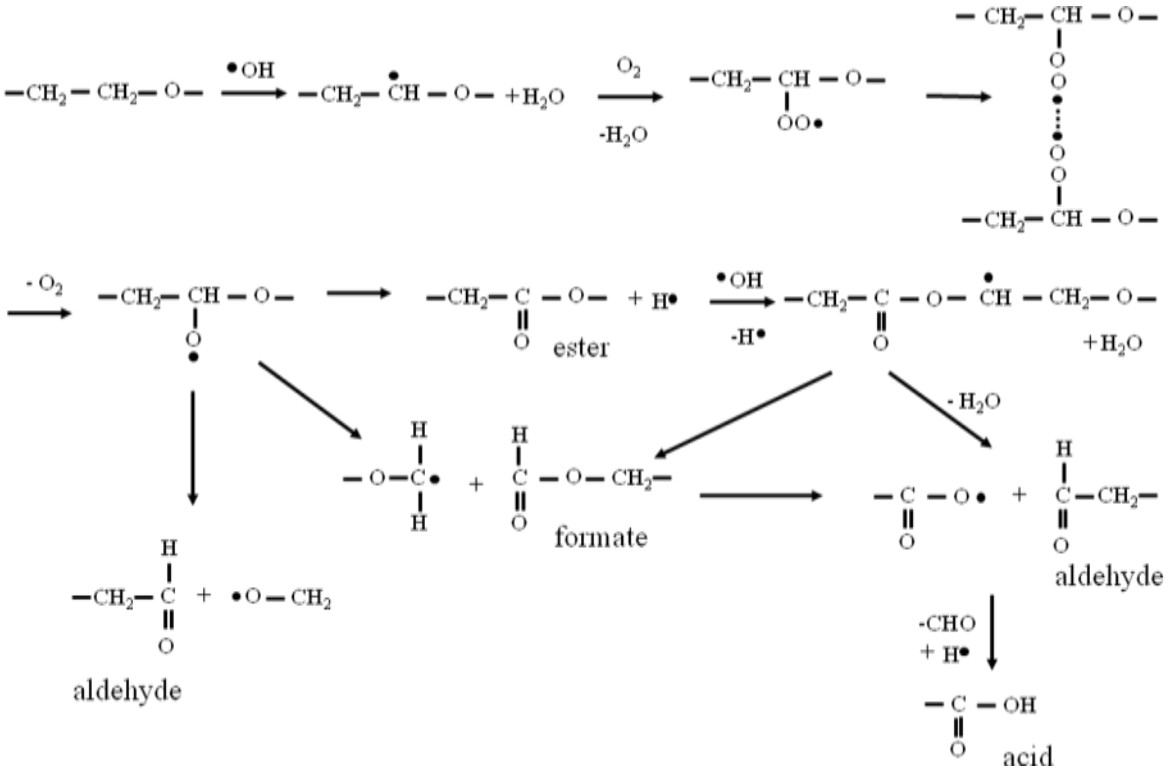

Figure 4-6 Degradation mechanism for PEO/TiO_2 under UV irradiation.

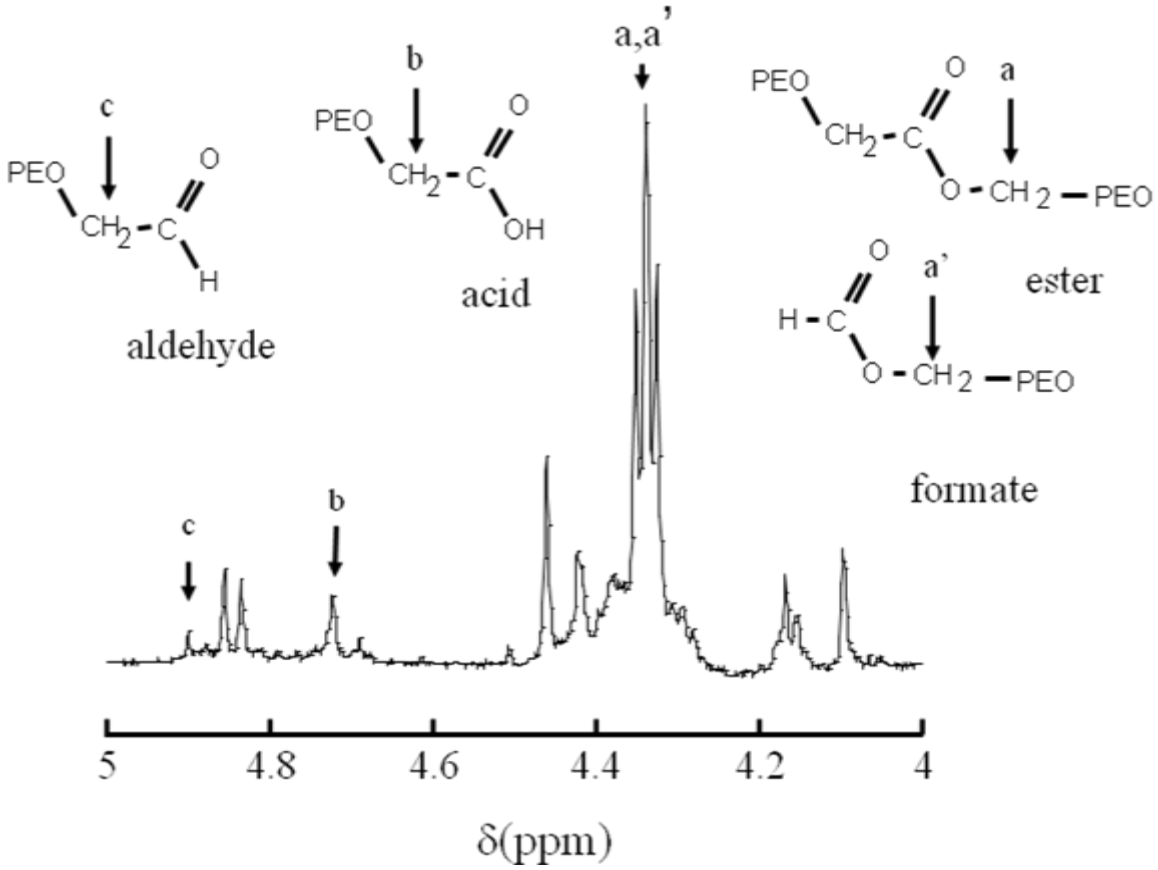

Figure 4-7 ^{1}H-NMR spectrum of PEO/TiO_2 degraded by UV light.

The degradation time is 21 hour.

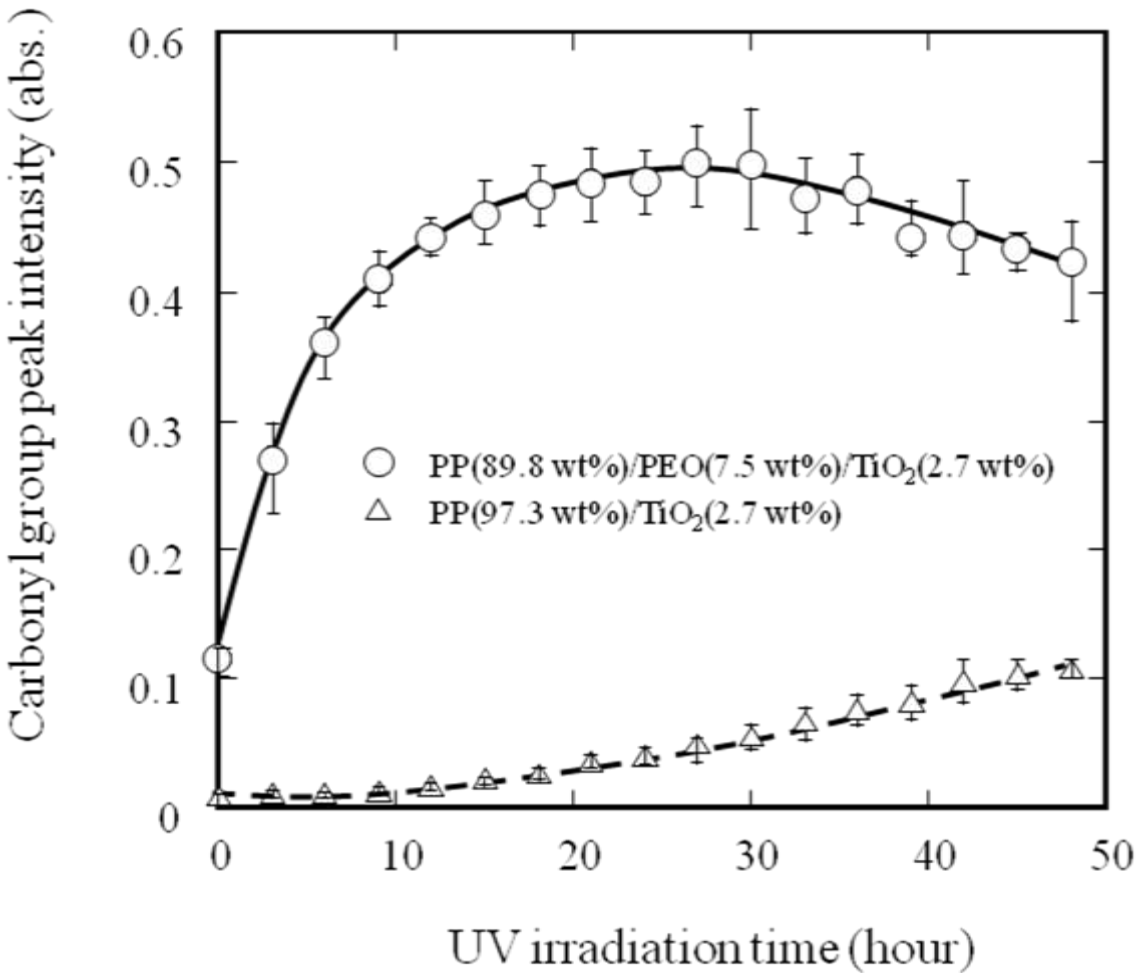

Figure 4-8 Buildup of carbonyl group peak in PP(89.8 wt%)/PEO(7.5 wt%)/TiO_2(2.7 wt%) and PP(97.3 wt%)/TiO_2 (2.7 wt%) film during oxidative photo degradation

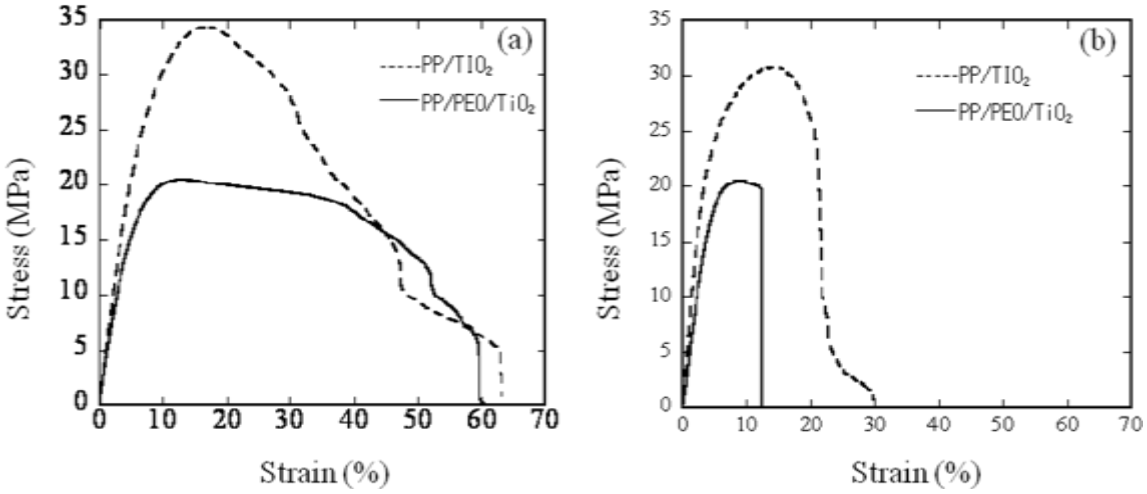

Figure 4-9 Stress-Strain curves of PP(89.8 wt%)/PEO(7.5 wt%)/TiO_2(2.7 wt%) and PP(97.3 wt%)/TiO_2 (2.7 wt%) . (a): raw samples (b): samples degraded for 6 hour

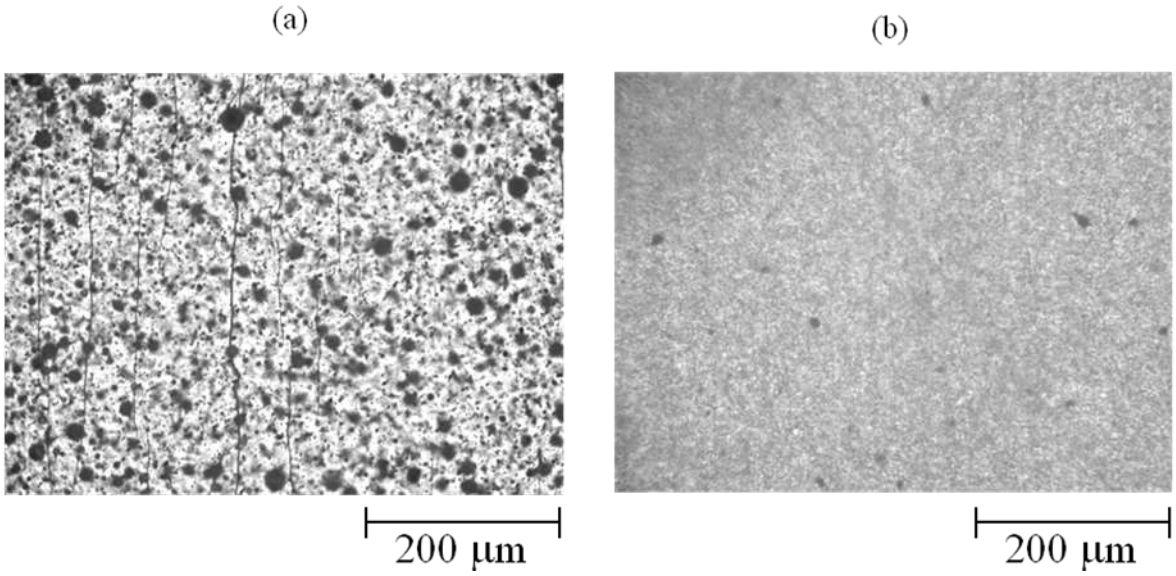

Figure 4-10 Optical micrographs of samples degraded for 48 hour.

(a): PP(89.3 wt%)/PEO(7.5 wt%)/TiO_2(2.7 wt%)

(b): PP(97.3 wt%)/TiO_2(2.7 wt%)

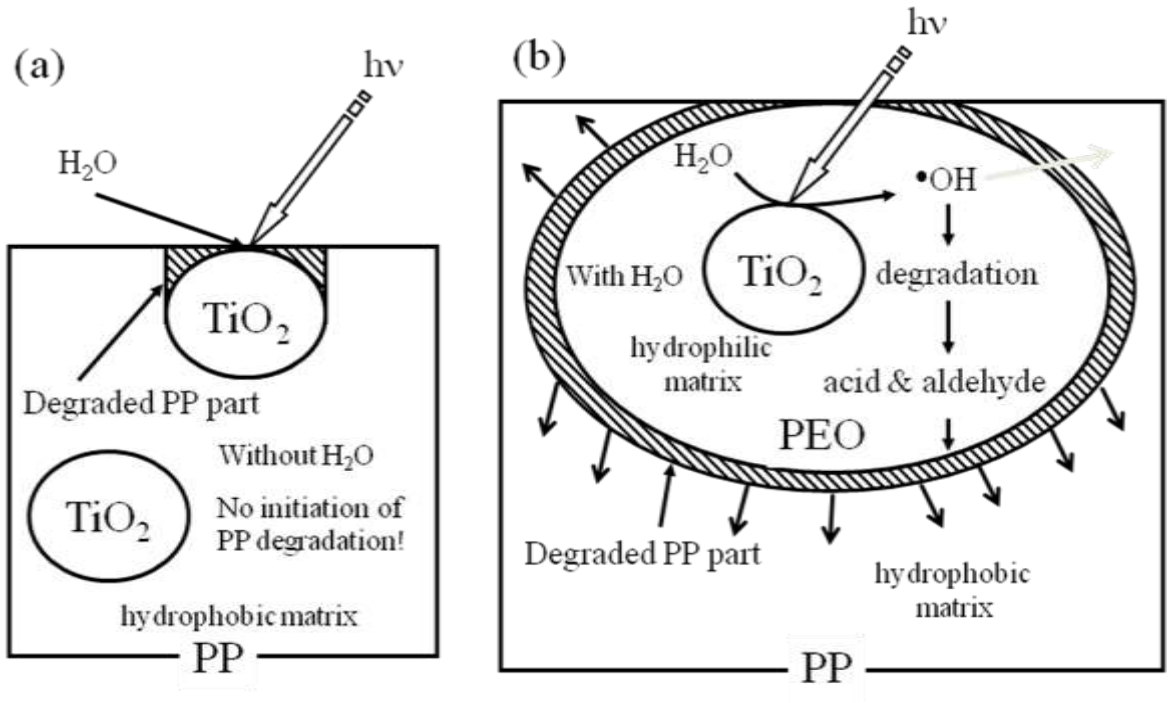

Figure 4-11 The degradation mechanisms for the PP/TiO_2 and the PP/PEO/TiO_2 under UV irradiation.

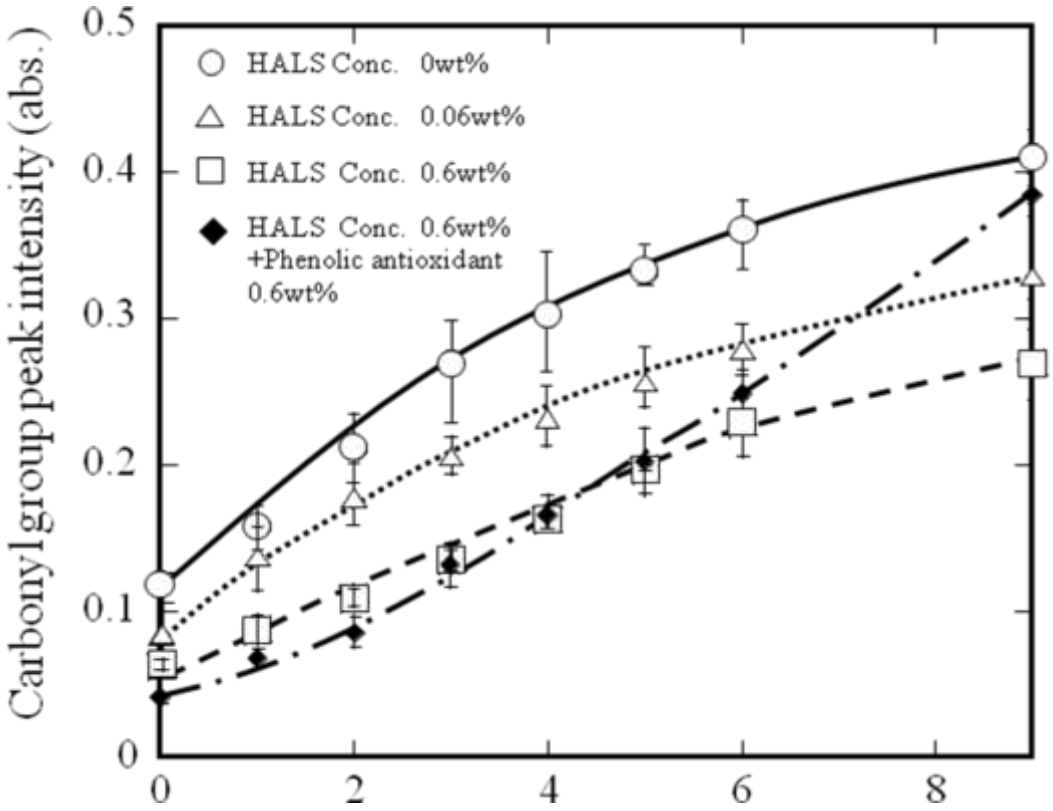

Figure 4-12 Buildup of carbonyl group peak in PP/PEO/TiO_2/HALS film and PP/PEO/TiO_2/HALS/phenolic antioxidant during photo degradation.

Table 4-1 Elongation at break values of PP(97.3 wt%)/TiO_2(2.7 wt%) and PP(89.3 wt%)/PEO(7.5 wt%)/TiO_2(2.7 wt%).

Sample	0 h degradation	6 h degradation
PP(97.3 wt%)/TiO_2(2.7 wt%)	63.5 ± 3.4%	31.1 ± 1.0%
PP(89.3 wt%)/PEO(7.5 wt%)/TiO_2(2.7 wt%)	60.6 ± 2.1%	12.9 ± 2.1%

Chapter 5: Development of degradable polypropylene by an addition of poly(ethylene oxide) microcapsule containing TiO_2 part II. Modification of calcium phosphate on the TiO_2 surface and its effect

5-1: Introduction

PP is one of the most useful polymeric materials and is known as a non-biodegradable polymer. Generally large molecule such as PP cannot easily enter into the cells of micro organisms. Therefore, PP is hard to be metabolized in micro organisms. If PP is spontaneously degraded to low molecular weight products, the biodegradability will appear. In fact, it has been known that polyethylene (PE), which is similar to PP chemical structure, is given biodegradability by pro-oxidant [1-5]. The mechanism of the PE biodegradation involves two stages which are abiotic oxidation and microbial oxidation. In addition, the rate of the biodegradation process depends on the abiotic oxidation stage initiated by pro-oxidant.

As shown in the Chapter 4, an addition of PEO microcapsule containing TiO_2 to PP (PP/PEO/TiO_2) was performed [6]. The PEO was photo-catalytically degraded by the TiO_2, and then acid and aldehyde compounds were produced. Since these products had an ability to facilitate PP degradation [7, 8], the addition of the microcapsule caused the PP photo-degradation rate to increase dramatically. In addition, an addition of a hindered amine light stabilizer (HALS) with basicity had a potential to suppress the PP degradation initiated by the microcapsule. The suppression effect was rising by the simultaneous addition of a phenolic antioxidant with acidity in the early phase of the PP degradation. However, the simultaneous addition showed an antagonism in the late

phase. This behavior suggested that the HALS with basicity also worked as a neutralizer of the produced acid. It appears that the PP degradation rate depends on the amount of the produced acid. When a new mechanism to produce more amount of acid is incorporated in this composite system, the PP degradation rate is believed to become much higher.

Octacalcium phosphate (OCP: $Ca_8(HPO_4)_2(PO_4)_4 \cdot 5H_2O$) is a kind of calcium phosphate compounds and consists of apatite and hydrate layers. The layered structure brings about some interesting characteristics to OCP [9]. The hydrate layer contains of HPO_4^{2-} ion, which acts as a pillar between the layers [9]. OCP covering TiO_2 surface brings about an improvement of biocompatibility of the surface [10] and certainly disturbs the photo-catalytic activity. However, it is noted here that OCP dissolves easily in low pH circumstances. OCP is more unstable for an acidic circumstance. When OCP is employed as the covering material on TiO_2 surface in the PP/PEO/TiO_2 composite system, it must be easily removed during the photo-degradation process. The OCP is dissolved by the acid, which is produced by the PEO degradation, and then additional H_2O and another acid (phosphoric acid ion) species are released in the composite system. The characteristics of OCP will be applied to a new mechanism to produce more amount of acid in the composite system. In addition, the HPO_4^{2-} ion can be substituted with various dicarboxylate ions. OCP intercalated with dicarboxylate ions is named as OCPC [9, 11]. OCPC have a possibility to bring about the further facilitation of the PP degradation as compared with OCP since various kinds of acid (dicarboxylate ion) species can be contained as the pillar.

In this study, with the aim of preparing a novel photo-degradable PP, the modification of the TiO_2 was performed by the synthesis of OCPC under various Ca/P

molar ratio conditions, and the modified TiO_2 samples obtained were analyzed by XRD, X-ray fluorescence spectrometry (XRF) and scanning electron microscope (SEM)/energy dispersive X-ray spectrometer (EDS) measurements, respectively. We prepared the photo-degradable PP by an addition of PEO microcapsule containing the modified TiO_2 (PP/PEO/modified TiO_2). The PP degradation rate in the composite was evaluated by a Fourier transform infrared (FT-IR) measurement and a tensile testing.

5-2: Experimental

5-2-1: Materials

PP (meso pentad fraction=98%) was supplied by Japan Polypropylene Co. The number-average molecular weight (M_n) and the polydispersity (M_w/M_n) of the PP were 4.6×10^4 and 5.7, respectively.

PEO was purchased from Wako Pure Chemical Industries, Ltd. The average molecular weight was 5.0×10^5.

TiO_2 was purchased from Wako Pure Chemical Industries, Ltd. The crystal structure was anatase (over 98.5 %), and the surface area was about 6 m^2/g. The TiO_2 was used without pretreatment.

Phosphoric acid (H_3PO_4, 85%), succinic acid and calcium carbonate ($CaCO_3$) were purchased from Kanto Chemical Co., Inc., respectively.

5-2-2: Synthesis of OCPC on TiO_2 surface and its characterization.

On the basis of Kamitakahara's report [12], the synthesis of OCP intercalated with carbonyl (succinic acid) ion (OCPC) was performed. In this work, a TiO_2 surface has to be saturated with precursor ions of the nucleating crystal before the OCPC crystallization on the surface starts [10]. In particular, a more excess amount of the calcium ion must be required as the counter ion against the phosphate and the carbonyl (succinic acid) ions to smoothly form the crystal nucleus on the TiO_2 surface. In order to prepare a solution containing a more amount of the dissolved calcium ion, the solubility enhancement was provided by adding 10 times amount of an acid compound (succinic acid) as compared with that of the reference's report. The synthesis condition was as follows: H_3PO_4 (0.01 mol) and 0.02 mol of succinic acid were added to 100 cm^3 of pure water, and then the mixture was vigorously stirred. The solution obtained was kept at 60 °C, and then 0.01 mol of TiO_2 and a predetermined amount (0.016, 0.03, 0.035 0.036, 0.04 and 0.06 mol) of $CaCO_3$ were under stirring for a determined time to adjust a

degree of OCPC modification for the TiO_2. The pH was monitored by a pH meter (D-51S, HORIBA. Ltd.) with a combined glass electrode. The suspension obtained was filtrated by suction filtration and washed with pure water and then dried at 60°C. The production was pounded in a mortar, and the powder sample obtained was employed in this study.

The crystal structure was investigated by XRD in a RIGAKUXG-RINT 1200 diffractometer. The XRD diffractogram was recorded in reflection geometry at 2° (2theta/min) under Ni-filtered $Cu_{K\alpha}$ radiation (λ=0.154nm).

The Ca/P molar ratio was measured by X-ray fluorescence spectrometry (XRF: HORIBA MESA-500).

5-2-3: Preparation of PEO/modified TiO_2 blend

PEO/modified TiO_2 blend was prepared by an Imoto Seisakusyo IMC-1884 melting mixer. The mixing was performed with and without the HALS and the phenolic antioxidant at 180 °C at 60 rpm for 5 min.

5-2-4: Preparation of PP/PEO/modified TiO_2 composite

Addition of PEO microcapsule containing TiO_2 (PEO/TiO_2) or modified TiO_2 (PEO/modified TiO_2) to PP was prepared by the Imoto Seisakusyo IMC-1884 melting mixer. After a small amount of the phosphite antioxidant (ADK STAB PEP-36, ca. 0.1 wt%) was added, the mixing was performed at 180 °C at 60 rpm for 5 min. The two kinds of photo-degradable composite obtained were denoted as "PP/PEO/TiO_2" and "PP/PEO/ modified TiO_2", respectively The PP/TiO_2 was prepared by the similar method.

5-2-5: Photo-degradation test

The samples were molded into a thin film (50 μm) by compression molding at

190°C under 5 MPa for 5 min. The Film was cut into the 2×2 cm, and put into a vial (Pyrex reactor). The photo-degradation test was performed with a Riko rotary photochemical reactor (RH400-10W, Riko-Kagaku Sangyo Co., Ltd.) equipped with a high-pressure mercury vapor lamp of 400 W (UVL-400HA ultrahigh-pressure mercury lamp with an intensity of 5 mW/cm^2; Riko-Kagaku Sangyo Co., Ltd.,). The test was carried out at 30 °C in air.

5-2-6: Scanning electron microscope (SEM) and SEM/Energy dispersive X-ray spectrometer (EDS) analyses

SEM and SEM/EDS analyses were carried out with a JEOL JSM-5800 at 20 kV. The sample obtained was sputter-coated with gold. The P, Ca and Ti atoms were measured with an EDS (Oxford Instruments INCA Microanalysis).

5-2-7: Fourier Transform Infrared (FT-IR) analysis

The IR spectra of 16 scans were measured with an FT-IR spectrometer (Perkin-Elmer Spectrum One) at a resolution of 2 cm^{-1} over the full mid-IR range (400-4000 cm^{-1}).

5-2-8: Tensile testing

Stress-strain behavior was observed using a SHIMADZU EZ-S at a cross-head speed of 5 mm/min. The sample specimens were cut with dimensions 30×2×0.1 mm shape in which the gauge length was 10 mm. All of tensile testing was performed at 20 °C. All results obtained are the average values of ten measurements.

5-2-9: Differential scanning calorimetry (DSC) measurement

DSC measurements were made with a Shimadzu DSC-60. The samples of about 5 mg weight were sealed in aluminum pans. The measurement of the samples was carried

out at a heating rate of 10 °C /min under a nitrogen atmosphere.

5-3: Results and Discussion

5-3-1: Synthesis behavior of OCPC on TiO_2 surface

Figure 5-1 and 5-2 show the pH dependence on stirring time in the H_3PO_4 /succinic acid/H_2O/$CaCO_3$/TiO_2 suspension at 60 ºC and the XRD patterns of the products for the 6h (360 min) of the synthesis time, respectively. OCPC (including OCP) crystal is metastable [9-12], and the formation is strongly dependent on pH and temperature during the hydrolysis. The stable phases at 60 ºC are dicalcium phosphate dihydrate (DCPD) for pH≤4.8, OCP (OCPC) for 4.8≤ pH≤6.0, and hydroxyapatite (HAp) for pH≥6 [11, 12]. As shown in Figure 5-1, in the case of the synthesis condition of the Ca/P=1.6 ratio, the pH overall shows the DCPD stable region, whereas, in the case of the Ca/P=3 ratio, the pH is within the OCPC stable region up to 180 min and then lowers to the DCPD stable one. In fact, the peak assigned to DCPD crystal is distinctly observed in their XRD patterns. In addition, in the case of the Ca/P=3 ratio, the peaks of OCPC (including OCP) and tricalcium phosphate (TCP) can be also observed. There exists in a side reaction in this synthesis, and the reaction would produce the TCP instead of the DCP. Since the formation of OCPC can be also obtained through TCP [9], the formation of the OCPC (including OCP) is believed to proceed through the two kinds of reaction step of the DCPD and the TCP in this synthetic condition, simultaneously. In the cases of the synthesis conditions of the Ca/P=3.5 and 3.6, the stable pH values of the OCPC are wholly kept. As shown in Figure 5-2, their XRD patterns exhibit the only OCPC crystal structure. Whereas, in the cases of the synthesis conditions of the Ca/P=4 and 6, these pH values are within the OCPC stable region up to 180 min and then rise to the HAp stable one. In their XRD patterns, the CaO, which is raw materials, can be observed, indicating that the amount of CaO is in excess. The Ca/P molar ratios of stoichiometric DCPD ($CaHPO_4•2H_2O$), pure OCP ($Ca_8(HPO_4)_2(PO_4)_4•5H_2O$) and OCPC ($Ca_8(HPO_4)_2$(OOC-R-COO)$(PO_4)_4•mH_2O$) are 1.0, 1.3 and 1.6, respectively. It is also possible to determine the composition of the

production from its Ca/P molar ratio by XRF measurement. In the cases of the synthesis conditions of the Ca/P=3.5 and 3.6 ratios for various synthesis time, Table 1 shows that all the samples obtained are from 1.43 to 1.61 Ca/P ratios. The XRF results also indicate that the main production obtained is the OCPC. It is found that that the synthesis conditions of the Ca/P=3.5 and 3.6 are suitable to synthesize the OCPC.

According to Combes *et. al.*[13], a crystallization process of DCPD on titanium powder progressed as follows: superficial oxide layer hydrolysis, hydrogenophosphate ions adsorption, calcium ions adsorption, and DCPD nucleation and growth. In the case of our synthesis process, the initial stage is unnecessary due to using the TiO_2 and, the transformation stage from the DCPD to the OCPC (including OCP) is added (see Figure 5-3). Figure 5-4 shows the change in the specified yield (the calcium compound (g) per the TiO_2 of 1g: calcium compound-g/TiO_2-g) against the synthesis time. The specified yield behavior between the Ca/P=3.5 and the Ca/P=3.6 synthesis conditions is considerably different although the amounts of the produced calcium compound are not so affected by the Ca/P value and the synthesis time. Formation of OCPC (OCP) is sensitive to concentrations of [H^+] and [PO_4^{3-}] [9]. The behavior is explained by the difference between the pH values at these Ca/P values. As shown in Figure 5-5 and Table 5-1, the calcium compound obtained is mainly the OCPC regardless of the Ca/P synthesis condition and the synthesis time. However, the microscopic composition must be different among these samples. As shown in Figure 5-4, the specified yields are approximately three (calcium compound-g/TiO_2-g), suggesting that the calcium phosphate compounds exist also in places besides the TiO_2 surface. In addition, formation of OCP on a Ti compound is very sensitive to pH [10]. Therefore, there is a possibility that the composition of the surface phase on the modified TiO_2 is

heterogeneous for the synthesis condition and the synthesis time. Since a photo-catalyst reaction occurs on the TiO_2 surface, the difference in the composition of the surface phase certainly affects the reaction. The composition obtained from the XRD and XRF measurements is not the one of the surface phase but the average one of the produced calcium phosphate compounds. The information about the composition of the surface phase is required to clarify the photo-catalyst behavior on the modified TiO_2.

The composition of the surface phase can be directly estimated by the Ca/P molar ratio obtained from the EDS analysis. Figures 5-6, 5-7, 5-8 and 5-9 show the SEM microphotographs of the surface of the modified TiO_2 (Ca/P=3.5 and 3.6) with various synthesis conditions (for 4, 6, 8 and 24 h at 60 ºC, respectively). The composition of each sampling spots has been measured by the EDS analysis in these figures. In the case of the synthesis condition of the Ca/P=3.5, as shown in Figure 5-6, the sampling spots showing much lower Ca/P (< 1) ratios are observed on the sample of the 4 h synthesis time, and these lower ratios indicate that there considerably exist the hydrogenophosphate and the calcium compound (see Figure 5-3 (I)) in the covering material. In the cases of the synthesis condition of the Ca/P=3.5 for the 6 and the 8 h synthesis time, the Ca/P ratios of the sampling spots are considerably close to 1, indicating that their covering materials are mainly composed of the DCPD. Whereas, in the case of the synthesis condition of the Ca/P=3.5 for the 24 h synthesis time, the Ca/P ratios increase up to the ratios of OCPC, indicating that the covering material is transformed from the DCP to the OCPC. These results suggest that the DCPD crystallization process and its transformation on the TiO_2 surface are considerably slower than those in other places. The nucleation and the crystallization rates in heterogeneous nucleation process are affected by many parameters such the size and the concentration of foreign particle [10]. In the case of the synthesis condition of the Ca/P=3.5, the transformation rate on the TiO_2 surface must be considerably slower since

the formation of the OCPC is sensitive to the pH value as mentioned above. In the early stage, it is difficult for the pH value around the TiO_2 surface to increase because of the existence of the adsorbed hydrogenophosphate ions (see Figure 5-3 (I)). Whereas, in the case of the synthesis condition of the Ca/P=3.6, the formation rate of the OCPC is much higher than that of the Ca/P=3.5 synthesis condition. As shown in Figure 5-6, the spot (No 3) shows the Ca/P =1.42 even for the 4 h synthesis time, indicating that there already exists the OCPC on the TiO_2 surface. It would be easy to raise the pH value on the TiO_2 surface because of the more amount of calcium ion as compared with that of the Ca/P=3.5 synthesis condition. In the cases of the synthesis condition of the Ca/P=3.6 for the 6 and the 8 h synthesis time, the Ca/P ratios of the sampling spots mainly show over 1 (see Figure 5-7 and 5-8), suggesting that the content of the OCPC (including OCP) is increasing in the covering materials. As shown in Figure 5-9, in the cases of the synthesis condition of the Ca/P=3.6, the sample of the 24 h synthesis time shows the much higher Ca/P ratios, and the covering material obtained is mainly composed of the OCPC as well as that of the 24 h modified TiO_2 at the Ca/P=3.5 synthesis condition.

5-3-2: Photo-degradation behavior of PP composites

Figure 5-10 shows the DSC curves of the PP and the PP/PEO/modified TiO_2 composite. The melting point (T_m) corresponding to the PP crystalline part can be observed at the same temperature (ca. 165 °C) in both of them, and the other T_m corresponding to the PEO one can be done at around 55 °C in the composite. In addition, the PP part crystallinities in both of them are also the same (43 %). These results suggest that the PP crystalline part is unaffected by the existence of PEO/modified TiO_2 microcapsule.

Figure 5-11 shows the FT-IR spectra in various samples during the photo-degradation. In the case of the PP/TiO_2, the peak (at ca. 1713 cm^{-1}) assigned to carbonyl group can be not observed, suggesting that the photo-degradation does not

occur under this photo-degradation condition. Whereas, in the cases of the PP/PEO/TiO_2 and the PP/PEO/modified TiO_2, the corresponding peaks can be observed at 1722 cm^{-1}, resulting that the photo-degradation advances. It is noted here that the peak shift (from 1713 cm^{-1} to 1722 cm^{-1}) is due to the peak superposition with the peaks of an ester, an acid and an aldehyde compounds, which are produced by the PEO degradation [6].

Figure 5-12 and 5-13 show the increments of carbonyl group peak intensity of the PP/TiO_2, the PP/PEO/TiO_2, the PP/PEO/modified TiO_2 composites against the UV irradiation time, respectively. The increment of carbonyl group peak intensity of the PP/TiO_2 has been not observed up to the 4h since the photo-degradation does not occur under this photo-degradation condition as mentioned above. Whereas, the peak intensity of the PP/PEO/TiO_2 increases with increase in the irradiation time, indicating that the PP photo-degradation advances. The difference between these degradation behavior is due to the existence of the PEO containing TiO_2 (PEO/TiO_2). The adsorbed H_2O in the PEO/TiO_2 photo-catalytically reacts, and the hydroxyl radical (OH•), which initiated the PEO degradation, is produced. And then the degraded PEO produces the acid and the aldehyde, which are able to facilitate PP degradation. The existence of the PEO/TiO_2 brings about the facilitative effect of the PP degradation [6]. In addition, it is noted here that the coexistences of the calcium phosphate compounds such as the DCPD and the OCPC have a possibility to bring about the further facilitation of the PP degradation since additional acids and H_2O are produced from these dissolutions initiated by the photo-catalytic reaction. The yield and the dominant chemical structure of the calcium phosphate compounds in the modified TiO_2 series are almost the same regardless of the Ca/P synthesis ratio and the synthesis time. It is expected that all of the PP/PEO/modified TiO_2 composites would show a similar degradation rate. However, the PP degradation rate considerably differs among these PP/PEO/modified TiO_2 composites. It seems that the PP degradation depends considerably on the kind of the calcium phosphate compound (covering material) of the surface phase. In the cases of

the synthesis conditions of the Ca/P=3.5 for the 4 h and the 6 h synthesis time, the PP/PEO/modified TiO_2 composites show almost the same carbonyl peak intensity as compared with that of the PP/PEO/TiO_2. As mentioned above, the covering material obtained from the 4 h synthesis time is mainly composed of the hydrogenophosphate and the calcium compound, whereas it obtained from the 6 h is mainly done of the DCPD. Since the difference of the PP degradation rate between these modified and unmodified composites is not observed, these coverages on the TiO_2 surface are believed to be considerably low. Whereas, in the case of the synthesis condition of the Ca/P=3.5 for the 8 h synthesis time, the degradation behavior of the PP/PEO/modified TiO_2 shows an induction period up to about 1 h. The covering material is mainly composed of the DCPD as well as that of the 6h synthesis time. However, this degradation behavior is considerably different. The induction period likely originates from the higher DCPD coverage. Initially the DCPD covering material blocks the UV irradiation. However, the adsorbed H_2O in the PEO/TiO_2 photo-catalytically reacts on the unblocked TiO_2 surface region, and the PEO degradation gradually occurs. The generated acid gradually dissolves the DCPD on the surface, and then the severe PP degradation starts. In the modified TiO_2 obtained from the 24 h synthesis time, interestingly, the degradation of the PP/PEO/modified TiO_2 does not show such induction period. The buildup of the carbonyl peak intensity is much higher than that of the PP/PEO/TiO_2, indicating that the PP degradation is considerably facilitated. The covering material is mainly composed not of the DCPD but of the OCPC (including OCP). As mentioned above, the transformation of the covering material occurs between the 8h and the 24h. Therefore, the coverage must be also changed by the transformation process and must be considerably low. In addition, the OCPC likely has an ability to facilitate the PP degradation. In fact, as shown in Figure 5-13, the PP/PEO/modified TiO_2 composites (synthesis conditions of the Ca/P=3.6 for 4h, 6h and 8h synthesis time) show that the degradation rates are considerably higher than the PP/PEO/TiO_2,

suggesting that the existence of the OCPC brings about the facilitation of the degradation. Whereas, the degradation rate of the 24 h composite is close to that of the PP/PEO/TiO_2. It seems that the degradation rate depends on the degree of the OCPC coverage as well as that of the DCPD one.

The tensile properties of composites before and after the PP degradation are summarized in Tables 5-2 and 5-3, respectively. As the remarkable changes of the tensile properties after the degradation, the increases of the Young's moduli and the decreases in the elongation at break are observed. Changes of tensile properties during photo-degradation are essentially caused by chain scission reaction [14]. In this work, these changes of the tensile properties are also explainable on the basis of the advance of the PP chain scission reaction. The PP chain scission releases the molecule segments from the entanglements and assists the recrystallization [15]. The degraded composites develop the Young's moduli by the recrystallization. However, the tensile residual stress caused by the recrystallization is simultaneously developed [15], resulting that the embrittlement occurs. Figure 5-14 shows the comparison of the elongation at break ratio (e/e_0) of the composites before and after the degradation. It is noted here that a lower value of the e/e_0 means a higher degree of the degradation. In fact, the behavior of the e/e_0 is in good agreement with the degradation behavior evaluated by the increment of the carbonyl peak intensity. For instance, the e/e_0 of the PP/TiO_2 is 0.93, suggesting that the degradation hardly advances as well as the result obtained from the increment of the carbonyl peak intensity. In the PP/PEO/modified TiO_2 at the Ca/P=3.5 synthesis condition, the e/e_0 values of the composites for the 4, 6 and 8 h synthesis time are almost the same as that of the PP/PEO/TiO_2. As mentioned above, the covering materials on these TiO_2 surface are the mixture of the hydrogenophosphate, the calcium compounds and/or the DCPD. Since the difference of the e/e_0 value between the PP/PEO/TiO_2 and these PP/PEO/modified TiO_2 is not observed, these covering materials would be dissolved in a short time during the photo-catalytic reaction.

Whereas, the e/e_0 of the composite with the 24 h synthesis time becomes lower and is almost the same as those of the ones with the 4 h, the 6 h and the 8 h synthesis time at the Ca/P=3.6 synthesis condition. The degradation behavior is in excellent agreement with that shown by the increment of the carbonyl peak intensity, suggesting that the OCPC (including OCP) covering material plays an important role in the control of the PP degradation.

The degradation process can be directly observed by SEM measurement. Figure 5-15 shows the SEM microphotographs of the surfaces of the PP/PEO/modified TiO_2 before and after the photo-degradation. The void space around the modified TiO_2 can be definitely observed in the degraded sample, indicating that the photolysis of the PP matrix starts from the modified TiO_2. The TiO_2 modification certainly affects the PP photo-degradation behavior since it leads to inhibition of the degradation reaction. The SEM results confirm the assumption in which the TiO_2 modification has the ability to control the PP degradation rate.

Figure 5-16 shows the photo-catalytic dissolution process of the covering materials in the PP/PEO/modified TiO_2 under the UV irradiation. In this composite system, acids are produced by the catalytic photolysis of the PEO component with the TiO_2 [6], and the covering materials such as the DCPD and the OCPC would be dissolved by them. However, the dissolution rate certainly depends on the kinds because of the difference in stability against acid. As mentioned above, the OCPC (including OCP) is more unstable for an acidic circumstance and is likely removed on the TiO_2 surface in a short time. Subsequently, the dissolution of the OCPC (including OCP) releases the H_2O and the acids (dicarboxylate and phosphoric acid ions) facilitating PP degradation [16]. The severer degradation behavior of the composites with the TiO_2 covered with the OCPC (including OCP) is due to the releasing of the acids. In the cases of the composites with the TiO_2 covered with the DCPD, the hydrogenophosphate and the calcium compounds, the facilitative effect of the degradation has been not observed. It seems that the H_2O

and the phosphoric acid ion released from the DCPD hardly affect the degradation rate. In addition, the coverage on the TiO_2 surface must be an important fact to bring about a change of the degradation rate. As shown in the increments of carbonyl group peak intensity of the PP/PEO/modified TiO_2 with the 8 h and the 24 h synthesis time at the Ca/P=3.5 and =3.6 synthesis conditions, the higher coverages of the DCPD and the OCPC bring about an induction period for the degradation. The light blocking structure certainly disturbs the photo-catalytic activity on the TiO_2. In particular, the OCPC is the effective covering material to control the PP degradation rate since it has the abilities to readily dissolve and to release the acid species (dicarboxylate ion).

5-4: Conclusion

In this study, the addition of PEO microcapsule containing the modified TiO_2 to PP was performed to prepare the novel photo-degradable PP. The synthesis conditions of Ca/P=3.5 and 3.6 molar ratios were suitable to prepare the OCPC. However, the microscopic composition on the TiO_2 surface was different between these Ca/P synthesis conditions. In the cases of the Ca/P=3.5 synthesis condition, the TiO_2 surface for the 4 h synthesis time covered with the hydrogenophosphate and the calcium compound, and those for the 6 h and at the 8h mainly did with the DCPD. Whereas, the synthesis time of the 24h at the Ca/P=3.5 and the all synthesis time of at the Ca/P=3.6 gave the OCPC on the TiO_2 surface. The PP photo-degradation behavior in these PP/PEO/modified TiO_2 was evaluated by the IR, the tensile testing and SEM/EDX measurements. There was no difference between the degradation rates of the PP/PEO/TiO_2 and of the PP/PEO/modified TiO_2 with the hydrogenophosphate, the calcium compound and the DCPD covering materials. Whereas, the OCPC covering material brought about the higher PP degradation rate. Since the severer degradation behavior of the PP/PEO/modified TiO_2 with the OCPC covering material was observed, it was confirmed that the dissolution of the OCPC released the acid species (dicarboxylate ion) facilitating PP degradation. In addition, it was found that the higher coverage of the OCPC brought about an induction period for the degradation.

Reference

[1] A. C. Albertsson, S.O. Andresson, S. Karlsson, *Polym. Degrad. Stab.* 1987, 18(1), 73

[2] A. C. Albertsson, C. Barenstedt, S. Karlsson, *Polym. Degrad. Stab.* 1992, 37(2), 163

[3] M. Weiland, A. Daro, C. Dacid, *Polym. Degrad. Stab.* 1995, 48(2), 275

[4] I. Jakubowicz, *Polym. Degrad. Stab.* 2003, 80(1), 39

[5] M.M. Reddy, R. K. Gupta, R. K. Gupta, S. N. Bhattacharya, R. Parthasarathy *J. Polym. Environ.* 2008, 16(1), 27

[6] K. Miyazaki, H. Nakatani, *Polym. Degrad. Stab.* 2009, 94, 2114

[7] S. P. Vijayalakshmi, G. Madras, *J. Appl. Polym. Sci.* 2006, 100(5), 3997

[8] T. Kagiya, N. Yokoyama, K. Takemoto, *Bull. Inst. Chem. Res. Kyoto Univ.* 1976, 54(1), 15

[9] A. Nakahara, S. Aoki, K. Sakamoto, S. Yamaguchi, *J. Mater. Sci. Mater. Med.* 2001, 12, 793

[10] M. Szekeres, G. Fodor, A. Fazekas, M. Radnai, K. Turzó, I. Dékány, *Colloid. Polym. Sci.* 2005, 283, 587

[11] H. Monma, M. Goto. *J. Inclusion. Phenomena.* 1984, 2, 127.

[12] M. Kamitakahara, H. Okano, M. Tanihara, C. Ohtsuki, *J. Ceram. Soc. Japan.* 2008, 116(3), 481-485.

[13] C. Combes, C. Rey, M. Freche, *Colloids. Surf. B* 1998, 11, 15.

[14] A. Tidjani, *J. Appl. Polym. Sci.* 1997, 64(13), 2497

[15] J. R. White, Weathering., Karger-Kocsis J, editor. Polypropylene: an A-Z reference. Dordrecht, Kluwer Publishers, 1999. 866.

[16] R. Broska, J. Rychlý, K. Csomorová, *Polym. Degrad. Stab.* 1999, 63(2), 231

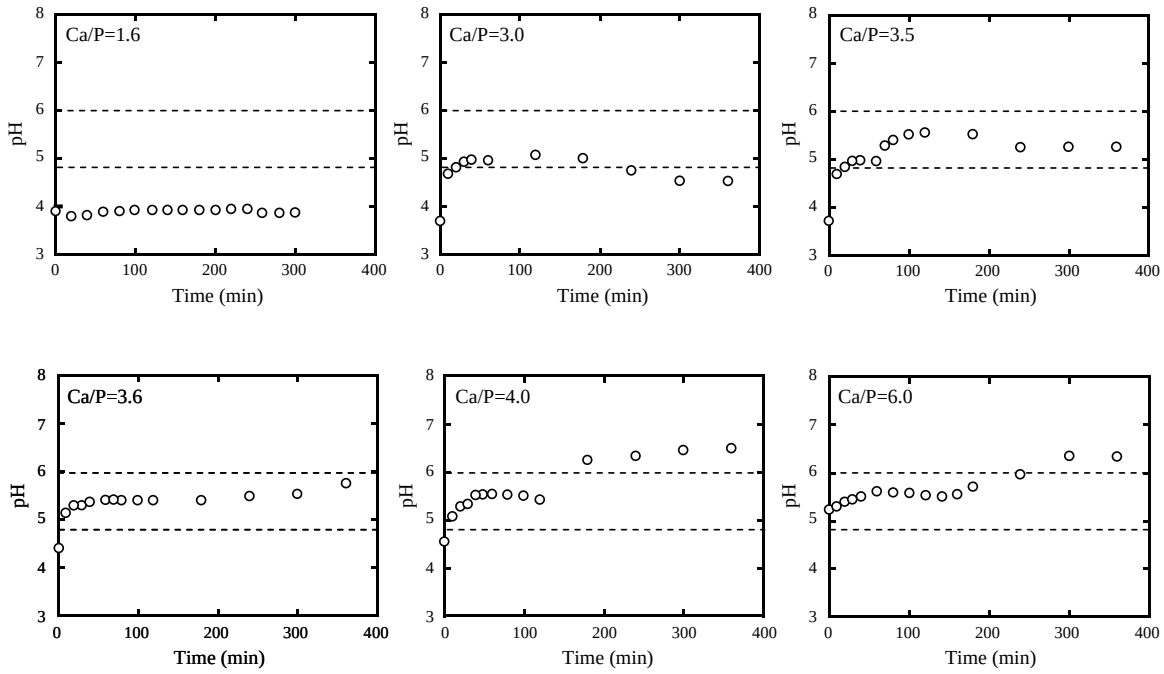

Figure 5-1 pH dependence on stirring time in the H_3PO_4 /succinic acid/H_2O/$CaCO_3$/TiO_2 suspension at 60 ºC: The area between the dot lines (pH=4.8 and 6) shows the pH range at which OCP is formed preferentially [11].

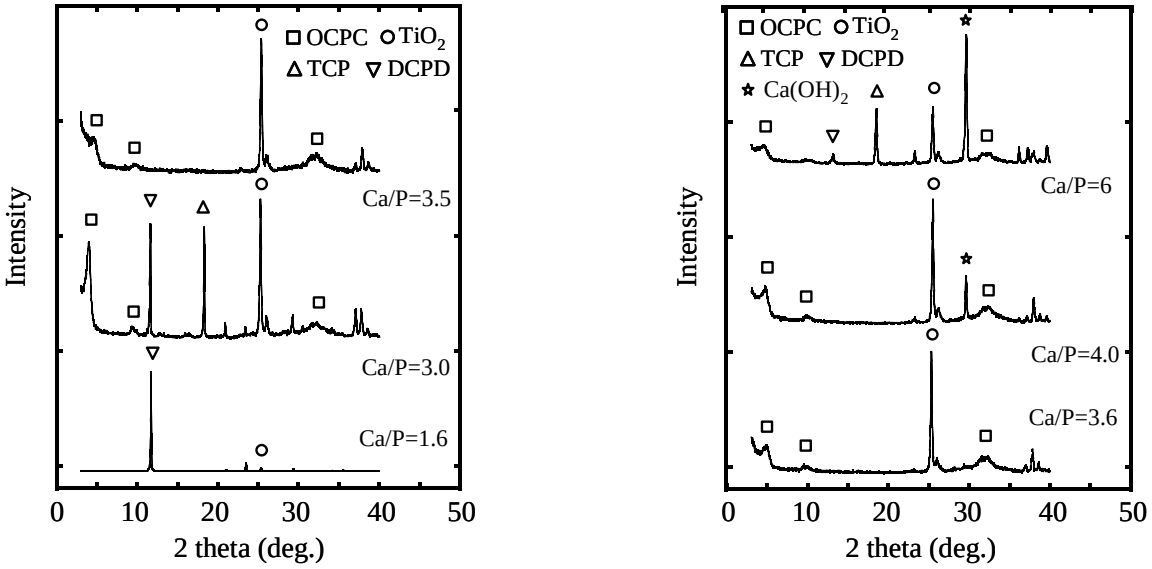

Figure 5-2 Survey XRD patterns of the products at 6h of the synthesis time: OCPC= octacalcium phosphate intercalated with carbonyl (succinic acid) ion. TCP= tricalcium phosphate. DCPD= dicalcium phosphate dihydrate.

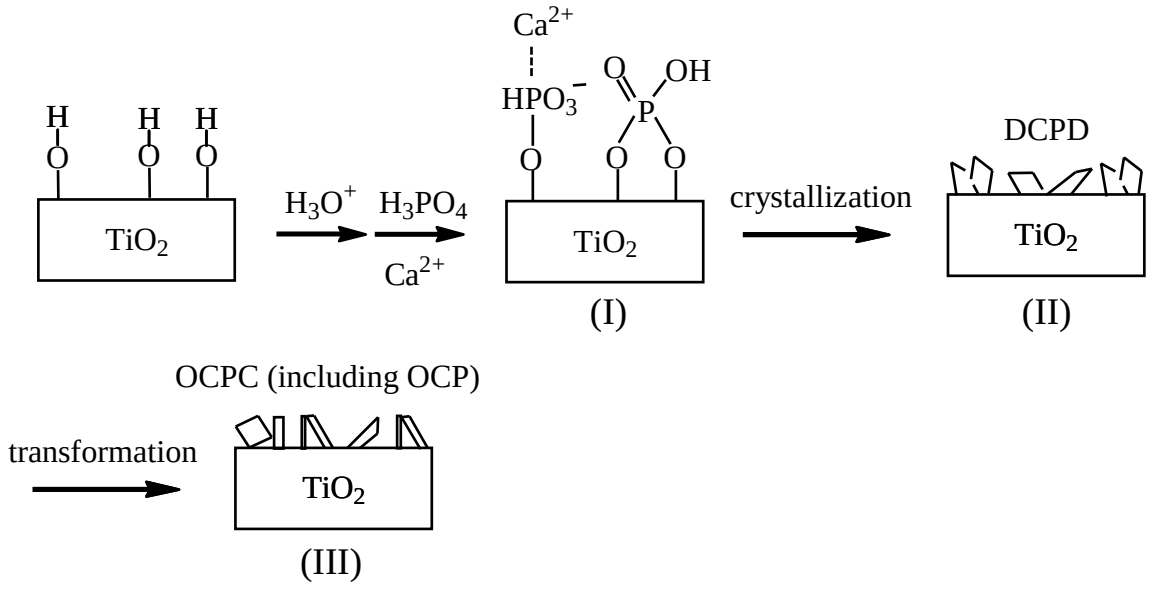

Figure 5-3 Schematic representation of the DCPD crystallization [13] and its transformation to the OCPC (including OCP) crystal on the TiO_2 surface.

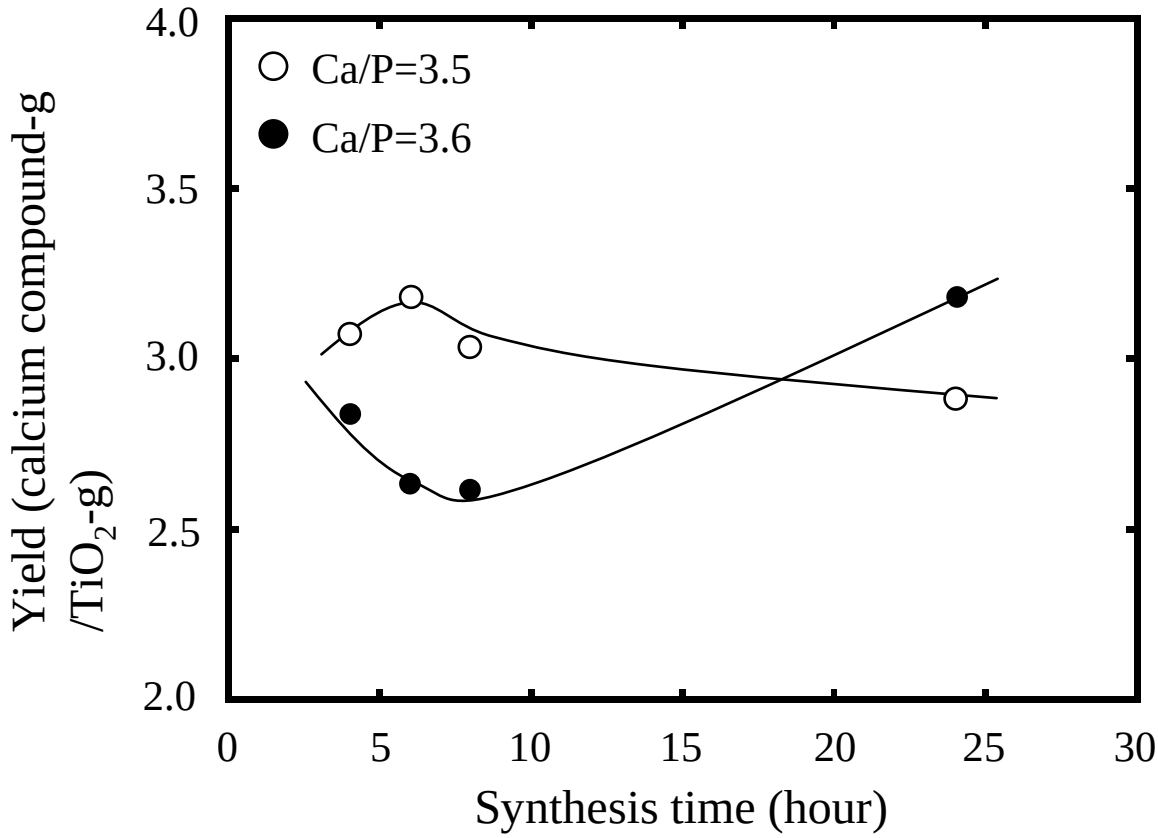

Figure 5-4 Change the specified yield (the calcium compound (g) per the TiO_2 of 1g) against the synthesis time.

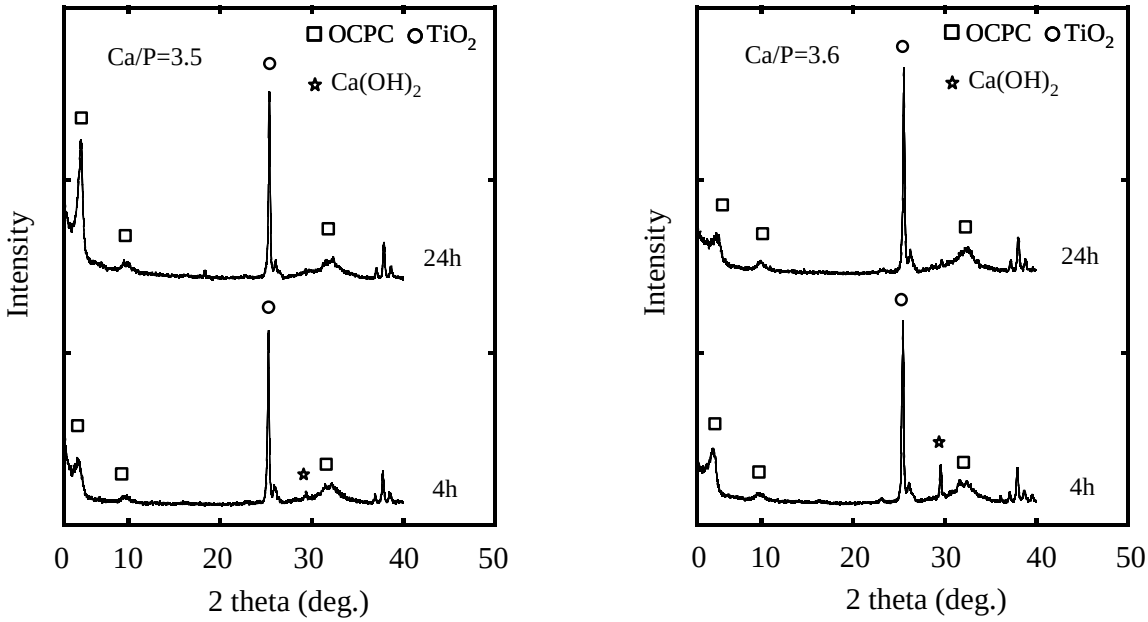

Figure 5-5 Survey XRD patterns of the products for 4h and 24 h of the synthesis time.

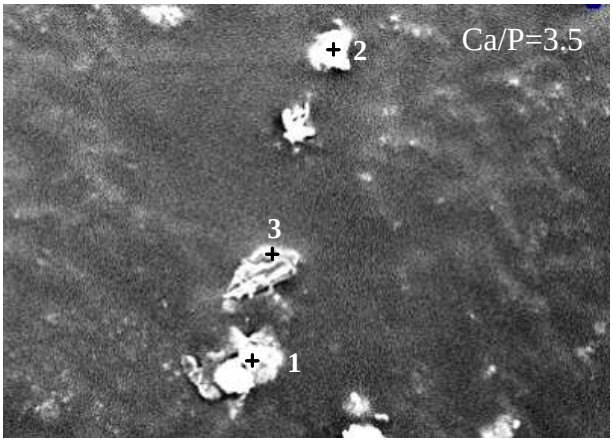

Spot	P [%]	Ca [%]	Ti [%]
1	10.00	5.53	84.47
2	22.58	7.77	69.65
3	45.06	48.44	6.50

Atomic percent. (mol%)

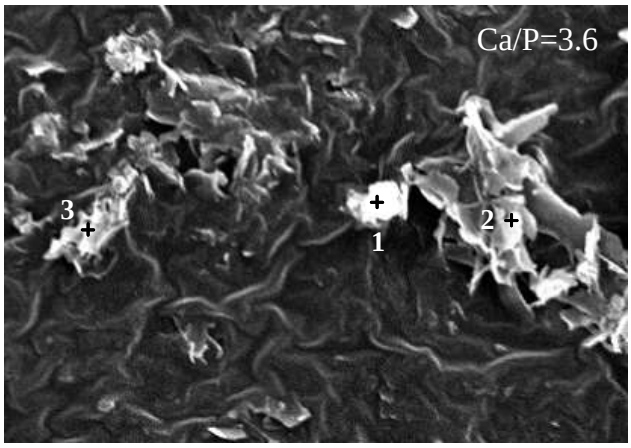

Spot	P [%]	Ca [%]	Ti [%]
1	12.74	4.15	83.11
2	38.98	38.05	22.98
3	40.08	57.06	2.86

Atomic percent. (mol%)

Figure 5-6 SEM microphotographs of the surfaces of the modified TiO_2 (Ca/P=3.5 and 3.6) and each sampling spot compositions measured by EDS analysis: The synthesis condition is at 60 ºC for 4 h.

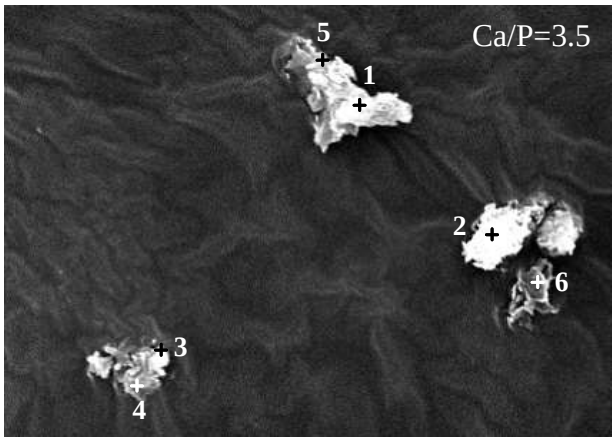

Spot	P [%]	Ca [%]	Ti [%]
1	43.17	46.44	10.18
2	16.14	15.86	68.00
3	40.76	57.06	2.18
4	61.35	34.28	4.37
5	51.03	34.10	14.87
6	53.86	35.27	10.87

Atomic percent. (mol%)

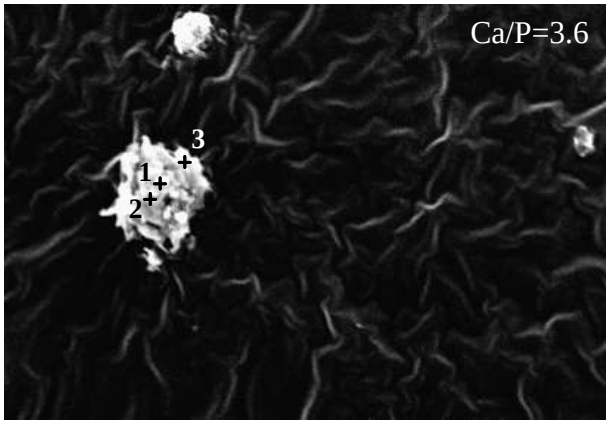

Spot	P [%]	Ca [%]	Ti [%]
1	34.84	42.63	22.53
2	39.66	48.08	12.26
3	30.49	28.28	41.23

Atomic percent. (mol%)

6 μm

Figure 5-7 SEM microphotograph of the surface of the modified TiO_2 (Ca/P=3.5 and 3.6) and each sampling spot compositions measured by EDS analysis: The synthesis condition is at 60 ℃ for 6 h.

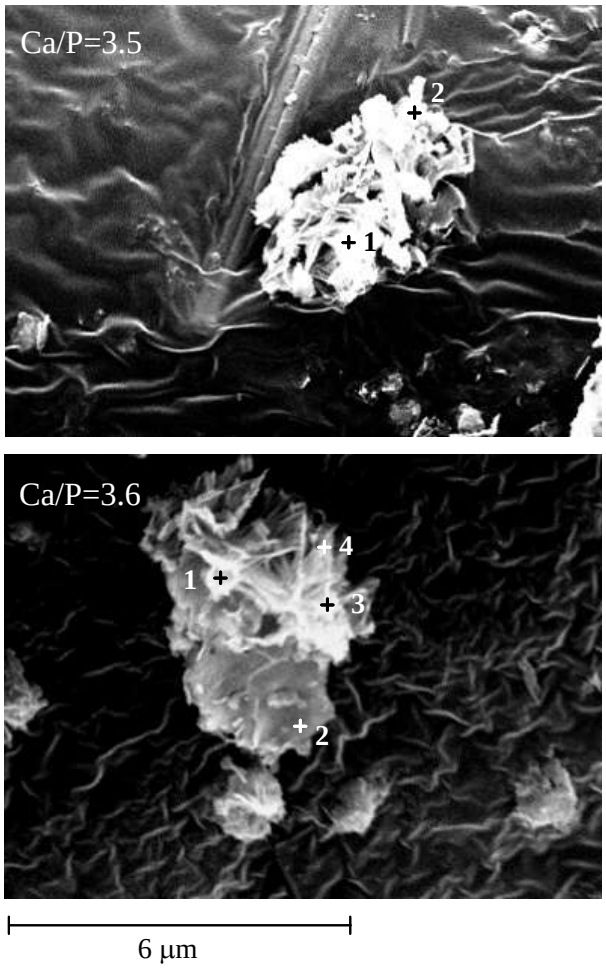

Spot	P [%]	Ca [%]	Ti [%]
1	18.03	16.97	65.00
2	43.91	44.51	11.58

Atomic percent. (mol%)

Spot	P [%]	Ca [%]	Ti [%]
1	31.51	35.80	32.69
2	41.02	37.59	21.38
3	22.16	24.60	53.24
4	38.75	44.95	16.31

Atomic percent. (mol%)

Figure 5-8 SEM microphotograph of the surface of the modified TiO_2 (Ca/P=3.5 and 3.6) and each sampling spot compositions measured by EDS analysis: The synthesis condition is at 60 ºC for 8 h.

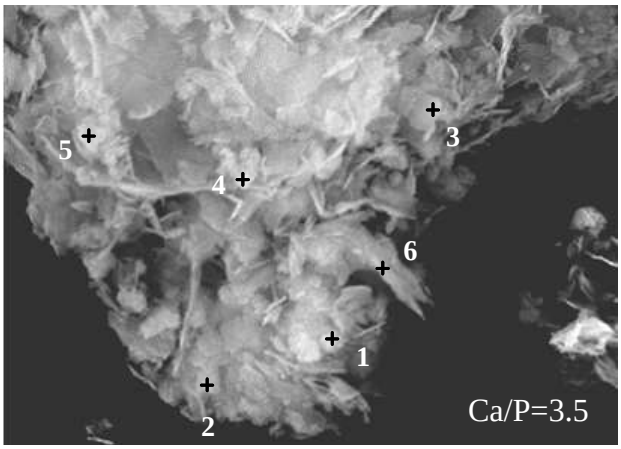

Spot	P [%]	Ca [%]	Ti [%]
1	23.77	30.40	45.83
2	17.57	21.79	60.64
3	23.46	34.68	41.87
4	22.05	31.40	46.55
5	20.89	26.87	52.24
6	31.00	45.14	23.86

Atomic percent. (mol%)

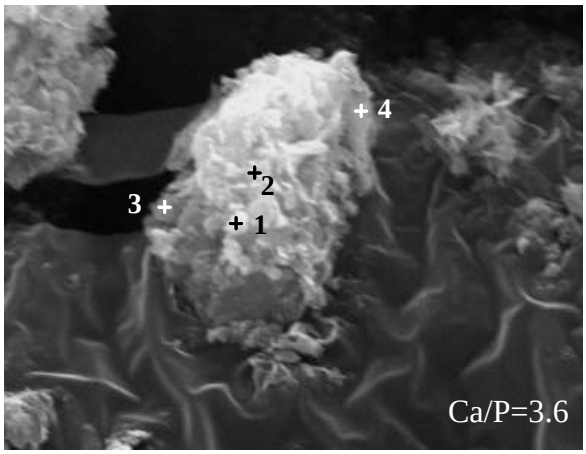

Spot	P [%]	Ca [%]	Ti [%]
1	28.54	37.84	33.62
2	31.82	47.50	20.67
3	31.40	33.80	34.80
4	37.89	47.65	14.47

Atomic percent. (mol%)

Figure 5-9 SEM microphotograph of the surface of the modified TiO_2 (Ca/P=3.5 and 3.6) and each sampling spot compositions measured by EDS analysis: The synthesis condition is at 60 ºC for 24 h.

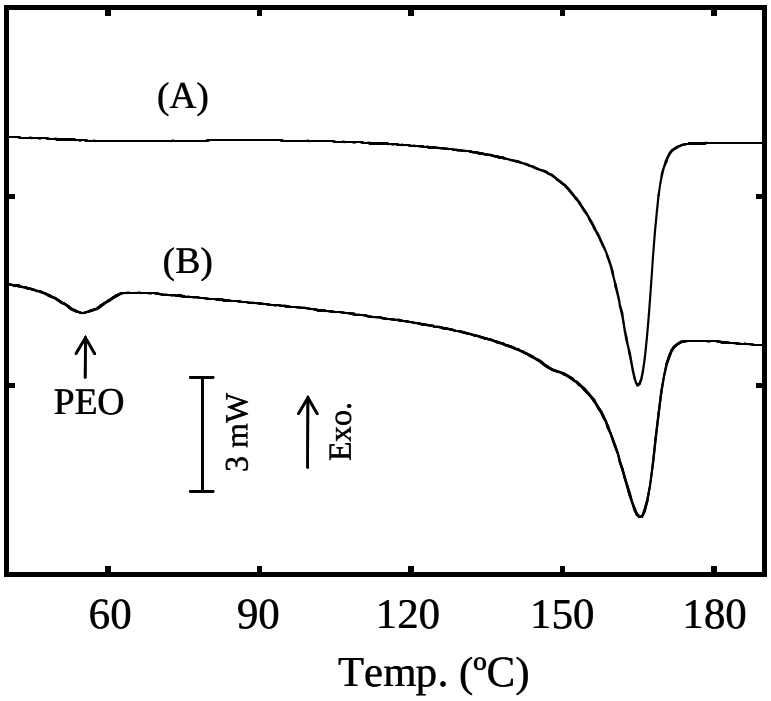

Figure 5-10 DSC curves of PP and PP/PEO/modified TiO_2 composite. A: PP. B: PP(90.0 wt%)/PEO(8.0 wt%)/modified TiO_2(TiO_2 =0.5 wt%, calcium compounds =1.5 wt%, the synthesis condition of Ca/P=3.6 at the 4 h synthesis time). The PP part crystallinity obtained from the fusion enthalpy: A, B ≈ 43 %.

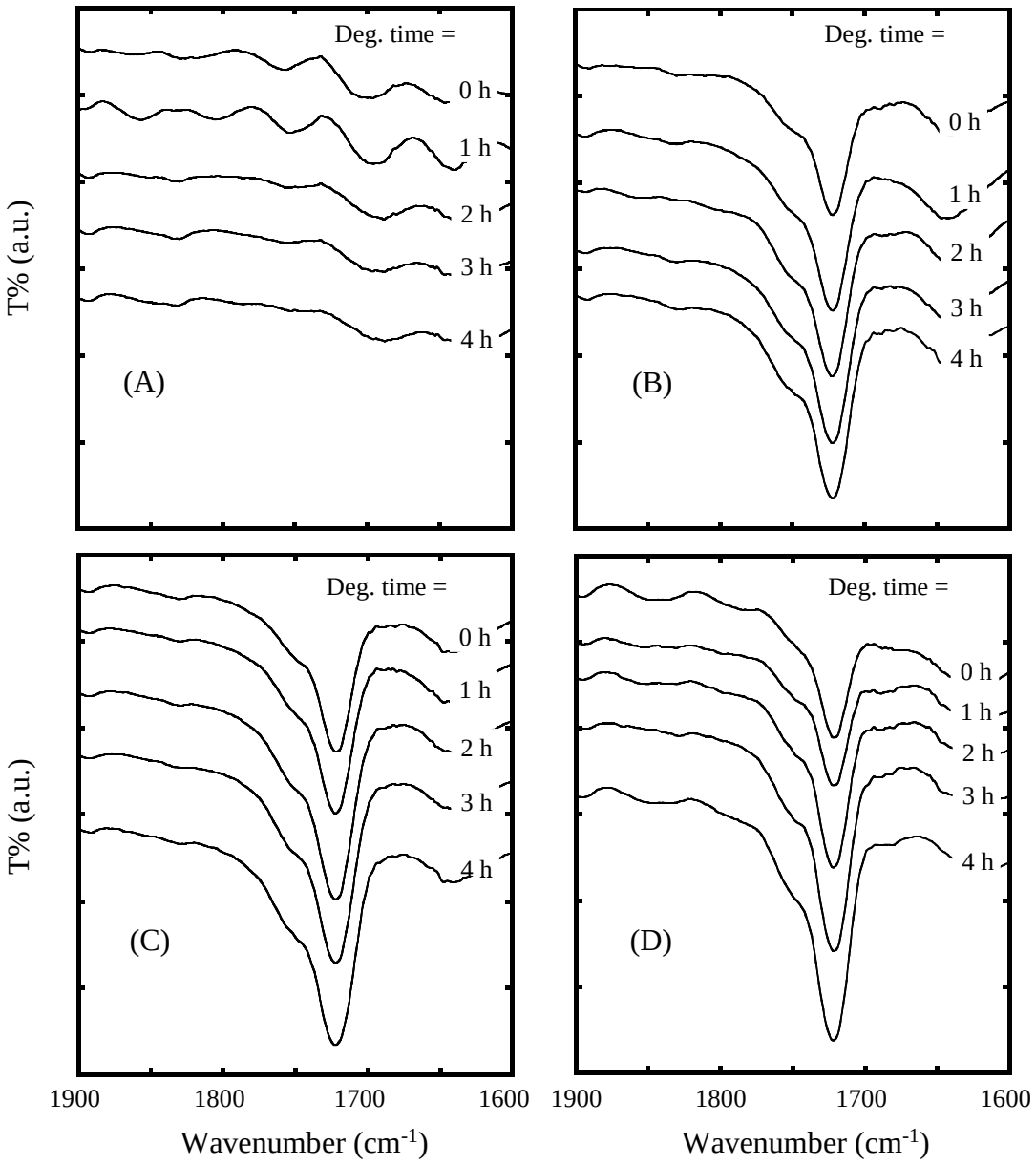

Figure 5-11 FT-IR spectra in various samples during photo-degradation. A: PP(99.5 wt%) /TiO_2(0.5 wt%). B: PP(91.5 wt%)/PEO(8.0 wt%)/TiO_2(0.5 wt%). C: PP(90.0 wt%)/PEO(8.0 wt%)/modified TiO_2(TiO_2 =0.5 wt%, calcium compounds =1.5 wt%) . The synthesis condition (Ca/P=3.5) and time (4h). D: PP(90.0 wt%)/PEO(8.0 wt%)/modified TiO_2(TiO_2 =0.5 wt%, calcium compounds =1.5 wt%) . The synthesis condition (Ca/P=3.6) and time (4h).

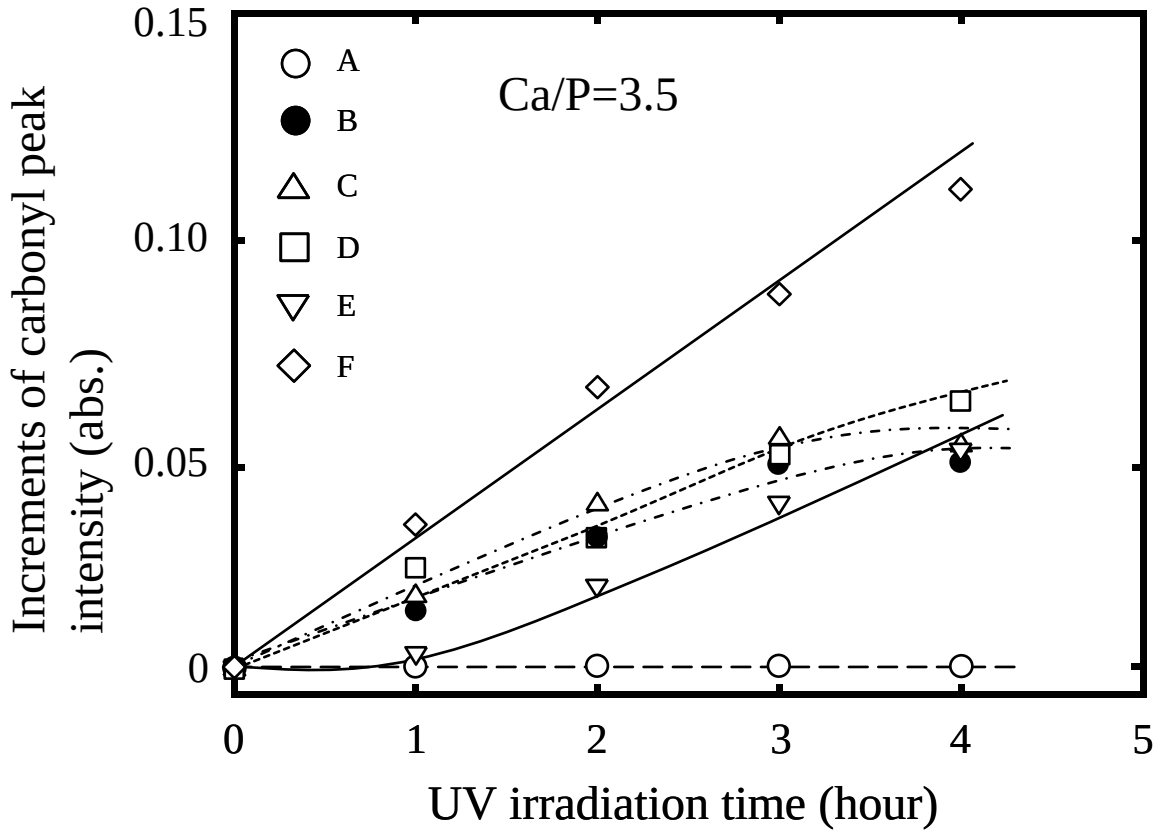

Figure 5-12 Increments of carbonyl peak intensity in various samples during photo degradation. A: PP(99.5 wt%) /TiO_2(0.5 wt%). B: PP(91.5 wt%)/PEO(8.0 wt%)/TiO_2(0.5 wt%). C - F : PP(90.0 wt%)/PEO(8.0 wt%)/modified TiO_2(TiO_2 =0.5 wt%, calcium compounds =1.5 wt%) . The synthesis time: C=4h, D=6 h, E=8h, F=24h. Initial absorbance value: A=0.005, B=0.124, C=0.125, D=0.109, E=0.114, F=0.0984.

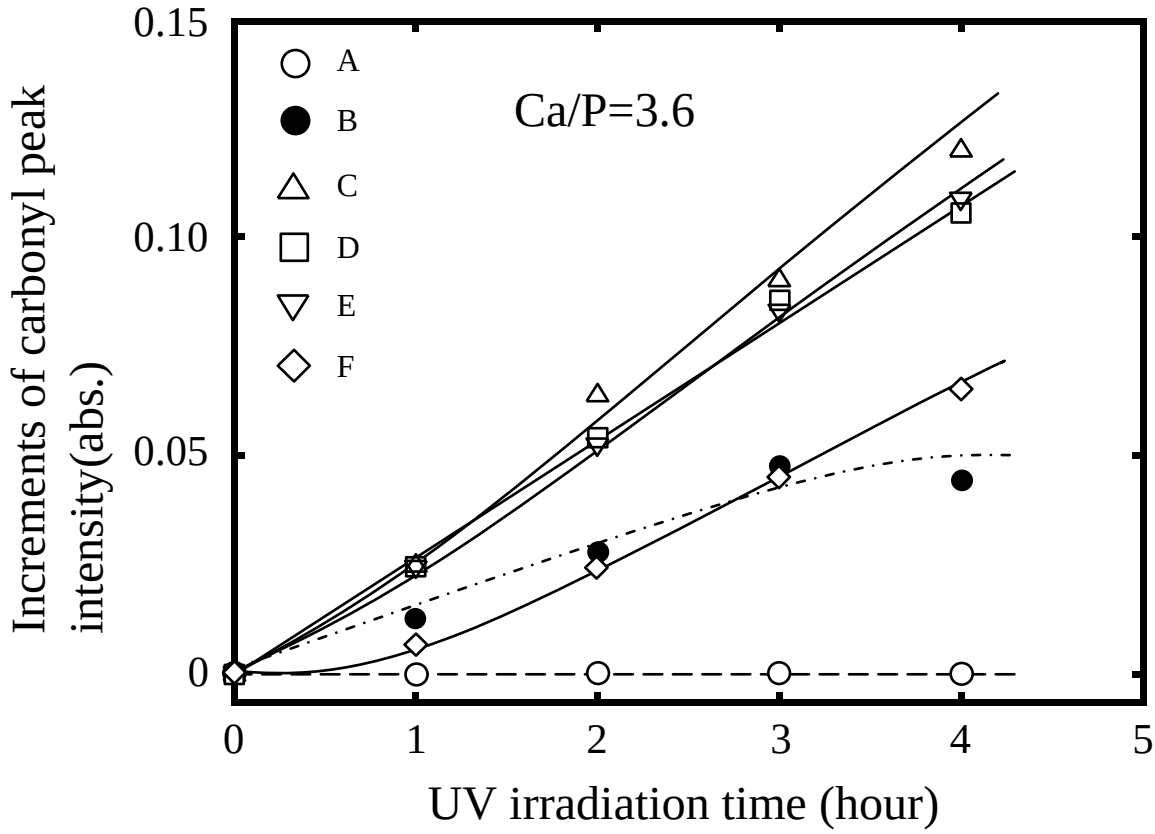

Figure 5-13 Increments of carbonyl peak intensity in various samples during photo degradation. A: PP(99.5 wt%) /TiO_2(0.5 wt%). B: PP(91.5 wt%)/PEO(8.0 wt%)/TiO_2(0.5 wt%). C - F : PP(90.0 wt%)/PEO(8.0 wt%)/modified TiO_2(TiO_2 =0.5 wt%, calcium compounds =1.5 wt%) . The synthesis time: C=4h, D=6 h, E=8h, F=24h. Initial absorbance value: A=0.005, B=0.124, C=0.102, D=0.076, E=0.082, F=0.116.

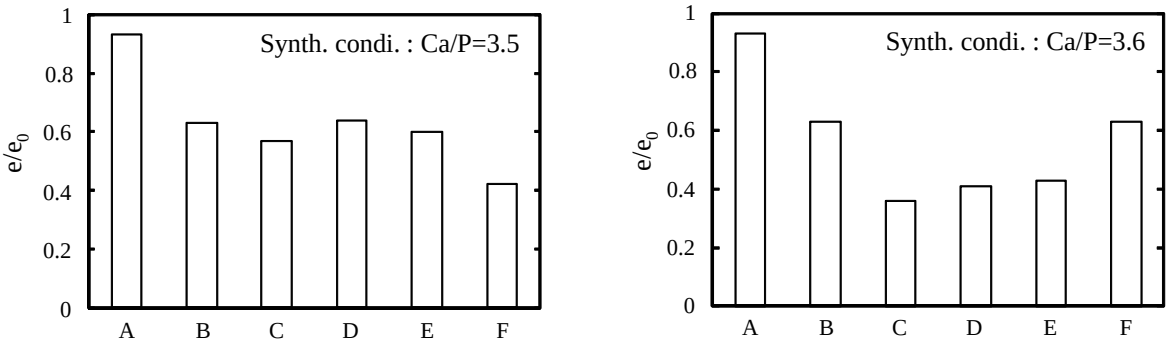

Figure 5-14 Comparison of the elongation at break ratio (e/e0) of the composites before and after the photo-degradation. A: PP(99.5 wt%) /TiO_2(0.5 wt%). B: PP(91.5 wt%)/PEO(8.0 wt%)/TiO_2(0.5 wt%). C - F : PP(90.0 wt%)/PEO(8.0 wt%) /modified TiO_2(TiO_2 =0.5 wt%, calcium compounds =1.5 wt%) . The synthesis time: C=4h, D=6 h, E=8h, F=24h.

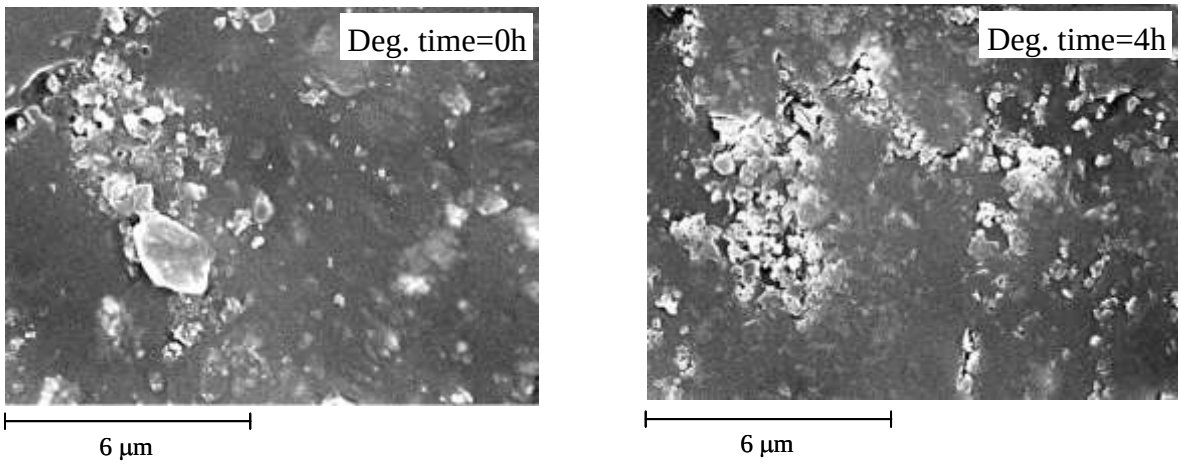

Figure 5-15 SEM microphotographs of the surfaces of the PP(90.0 wt%)/PEO(8.0 wt%) /modified TiO_2(TiO_2 =0.5 wt%, calcium compounds =1.5 wt%) before and after the photo-degradation. The synthesis condition : Ca/P=3.6, synthesis time=4h.

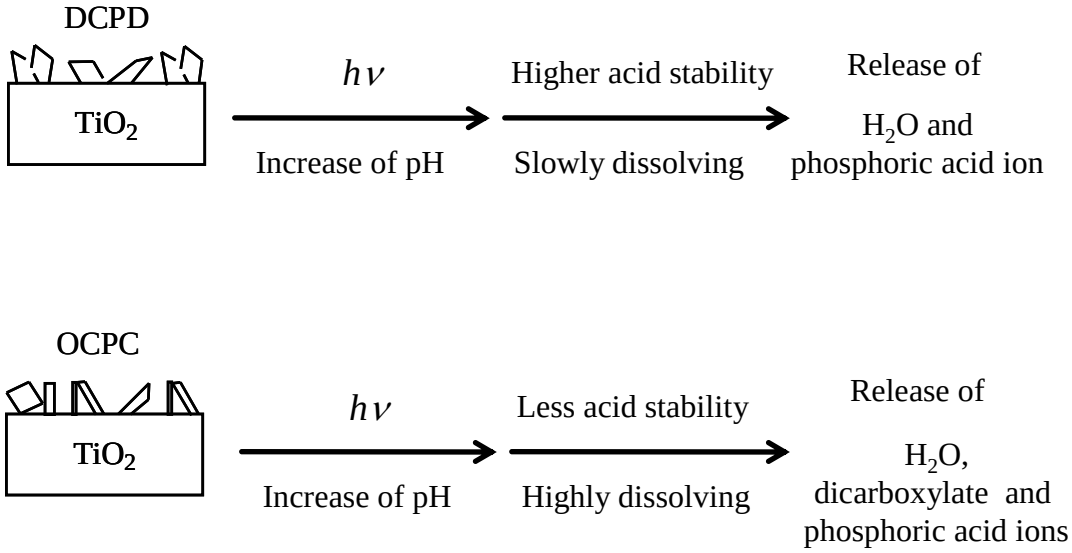

Figure 5-16 The photo-catalytic dissolution process of the covering materials in the PP/PEO/modified TiO2 under the UV irradiation.

Table 5-1 Changes of Ca/P molar ratio in the product obtained from the synthesis with the Ca/P = 3.5 and 3.6 ratios suspension against the synthesis time.

Synthesis time (h)	4	8	6	24
Ca/P = 3.5	1.5	1.46	1.43	1.44
Ca/P = 3.6	1.61	1.54	1.53	1.53

Determined by XRF.

Table 5-2 Tensile properties of PP/TiO_2, $PP/PEO/TiO_2$ and PP/PEO/modified TiO_2 (Ca/P=3.5 and 3.6) with the various synthesis time composites

Samples	Young's modulus (MPa)	Tensile strength (MPa)	Elongation at break (%)
PP/TiO_2	503 ± 37	25.1 ± 1.2	102 ± 14
$PP/PEO/TiO_2$	338 ± 27	16.4 ± 0.4	190 ± 3
PP/PEO/modified TiO_2 (Ca/P = 3.5) for			
4h (synthesis time)	468 ± 30	18.8 ± 0.4	198 ± 32
6h (synthesis time)	495 ± 8	20.3 ± 0.0	182 ± 18
8h (synthesis time)	479 ± 26	19.5 ± 1.0	192 ± 17
24h (synthesis time)	493 ± 35	19.1 ± 0.3	217 ± 18
PP/PEO/modified TiO_2 (Ca/P = 3.6) for			
4h (synthesis time)	512 ± 30	19.2 ± 0.3	112 ± 15
6h (synthesis time)	537 ± 12	20.8 ± 0.2	116 ± 17
8h (synthesis time)	500 ± 12	20.6 ± 0.6	115 ± 12
24h (synthesis time)	534 ± 18	20.0 ± 0.6	91 ± 15

PP/TiO_2=99.5 wt%/0.5 wt%. $PP/PEO/TiO_2$ =91.5 wt%/8.0 wt%/0.5 wt%. PP/PEO/modified TiO_2=90.0 wt%/8.0 wt%/Ti=0.5 wt%, calcium compounds =1.5 wt%.

Table 5-3 Tensile properties of PP/TiO_2, PP/PEO/TiO_2 and PP/PEO/modified TiO_2 (Ca/P=3.6) with the various synthesis time composites before after the photo-degradation for 6 h

Samples	Young's modulus (MPa)	Tensile strength (MPa)	Elongation at break (%)
PP/TiO_2	503 ± 37	25.1 ± 1.2	102 ± 14
PP/PEO/TiO_2	338 ± 27	16.4 ± 0.4	190 ± 3
PP/PEO/modified TiO_2 for			
Before the photo-degradation			
4h (synthesis time)	466 ± 29	20.1 ± 0.6	166 ± 32
6h (synthesis time)	477 ± 81	21.0 ± 0.5	215 ± 21
8h (synthesis time)	478 ± 32	20.1 ± 0.6	175 ± 46
24h (synthesis time)	468 ± 34	19.3 ± 0.3	199 ± 25
After the photo-degradation			
4h (synthesis time)	515 ± 57	21.6 ± 1.9	59 ± 8
6h (synthesis time)	566 ± 10	22.7 ± 0.4	89 ± 2
8h (synthesis time)	521 ± 24	20.4 ± 1.0	75 ± 5
24h (synthesis time)	503 ± 20	19.8 ± 1.8	127 ± 8

PP/TiO_2=99.5 wt%/0.5 wt%. PP/PEO/TiO_2 =91.5 wt%/8.0 wt%/0.5 wt%. PP/PEO/modified TiO_2=90.0 wt%/8.0 wt%/Ti=0.5 wt%, calcium compounds =1.5 wt%.

Chapter 6: Effect of existence of calcium phosphate on biodegradation behavior of degradable polypropylene by an addition of poly(ethylene oxide) microcapsule containing TiO_2.

6-1: Introduction

Synthetic polymeric materials easily accumulate in environment because their biodegradability is considerably less. PP is one of such materials and is known as a non-biodegradable polymer. Generally large molecule such as PP cannot easily enter into cells of microorganisms. Therefore, PP is hard to be metabolized in microorganisms. If PP is spontaneously degraded to low molecular weight compounds, the biodegradability would appear. In fact, it has been known that polyethylene (PE), which is similar to PP chemical structure, is given biodegradability by pro-oxidant [1-5]. This method is called as "oxo-biodegradation". The mechanism involves two stages which are abiotic and microbial oxidations. The rate of the biodegradation process strongly depends on the abiotic oxidation stage initiated by pro-oxidant. Microorganisms favor hydrophilic surface. Therefore, the abiotic oxidation stage is also important to make the surface hydrophilic. It is noted here that metabolism of microorganism requires inorganic phosphate as well as carbon source. In order to continuously advance the oxo-biodegradation, the supplement of inorganic phosphate is certainly required. In fact, in the cases of many studies on the oxo-biodegradation [6-10], the inorganic phosphates (HPO_4^{2-} and $H_2PO_4^-$ ions) have been used as the supplement in the microorganism cultivation and the respirometric biodegradation test.

In our previous work [11], an addition of PEO microcapsule containing TiO_2 to PP

(PP/PEO/TiO_2) was performed. The PEO was photocatalytically degraded by the TiO_2, and then acid and aldehyde compounds were produced. Since these products had an ability to facilitate PP photodegradation [12] and [13], the addition of the microcapsule caused the PP photodegradation rate to increase dramatically. In addition, the modification of the TiO_2 was performed by the synthesis of octacalcium phosphate ($Ca_8(HPO_4)_2(PO_4)_4 \cdot 5H_2O$) intercalated with succinic acid ion (OCPC), leading to much higher rate of the photodegradation [14]. The facilitation behavior was due to the photocatalytic dissolution process of the covering OCPC in the PP/PEO/modified TiO_2 under irradiation. In this composite system, acids were produced by the catalytic photolysis of the PEO component with the TiO_2 [11], and the covering OCPC was dissolved by them. The dissolution of the OCPC led to the additional production of acid species such as succinic acid and inorganic phosphates (see OCPC composition). It is noted here that the facilitation behavior is due to not inorganic phosphates but succinic acid [14]. However, the productions of the inorganic phosphates are believed to lead to the facilitation of the biodegradation.

In this study, with the aim of revealing the biodegradation behavior of the PP/PEO/TiO_2 modified by OCPC, the soil burial test was performed as compared with some kinds of PP composite. The biodegradation behavior was evaluated by scanning electron microscope (SEM)/energy dispersive X-ray spectrometer (EDS), optical microscope (OM), Fourier transform infrared (FT-IR) and differential scanning calorimetry (DSC) measurements.

6-2: Experimental

6-2-1: Materials

PP (meso pentad fraction=98%) was supplied by Japan Polypropylene Co. The number-average molecular weight (M_n) and the polydispersity (M_w/M_n) of the PP were 4.6×10^4 and 5.7, respectively.

PEO was purchased from Wako Pure Chemical Industries, Ltd. The average molecular weight was 5.0×10^5.

TiO_2 was purchased from Wako Pure Chemical Industries, Ltd. The crystal structure was anatase (over 98.5 %), and the surface area was about 6 m^2/g. The TiO_2 was used without pretreatment.

Phosphoric acid (H_3PO_4, 85%), succinic acid and calcium carbonate ($CaCO_3$) were purchased from Kanto Chemical Co., Inc., respectively.

Glutaraldehyde, 0.1 M phosphate buffer, osmic acid and ethanol were purchased from Wako Pure Chemical Industries, Ltd. , respectively.

6-2-2: Synthesis of OCPC on TiO_2 surface and its characterization.

On the basis of Kamitakahara's report [15], the synthesis of OCP intercalated with carbonyl (succinic acid) ion (OCPC) was performed. In this work, a TiO_2 surface has to be saturated with precursor ions of the nucleating crystal before the OCPC crystallization on the surface starts [16]. In particular, a more excess amount of the calcium ion must be required as the counter ion against the phosphate and the carbonyl (succinic acid) ions to smoothly form the crystal nucleus on the TiO_2 surface. In order to prepare a solution containing a more amount of the dissolved calcium ion, the solubility enhancement was provided by adding 10 times amount of an acid compound (succinic acid) as compared with that of the reference's report. The synthesis condition was as

follows: H_3PO_4 (0.01 mol) and 0.02 mol of succinic acid were added to 100 cm^3 of pure water, and then the mixture was vigorously stirred. The solution obtained was kept at 60 °C, and then 0.01 mol of TiO_2 and a predetermined amount (0.036 mol) of $CaCO_3$ were under stirring for a determined time to adjust a degree of OCPC modification for the TiO_2. The pH was monitored by a pH meter (D-51S, HORIBA. Ltd.) with a combined glass electrode. The suspension obtained was filtrated by suction filtration and washed with pure water and then dried at 60°C. The specified yield (calcium compound-g/TiO_2-g) was approximately three, suggesting that the OCPC also existed in other places besides the TiO_2 surface [14]. The production was pounded in a mortar, and the powder sample obtained was employed in this study.

6-2-3: Preparation of PEO/modified TiO_2 blend

PEO/modified TiO_2 blend was prepared by an Imoto Seisakusyo IMC-1884 melting mixer. The mixing was performed with and without the HALS and the phenolic antioxidant at 180 °C at 60 rpm for 5 min.

6-2-4: Preparation of PP/PEO/modified TiO_2 composite

Addition of PEO microcapsule containing TiO_2 (PEO/TiO_2) or modified TiO_2 (PEO/modified TiO_2) to PP was prepared by the Imoto Seisakusyo IMC-1884 melting mixer. After a small amount of the phosphite antioxidant (ADK STAB PEP-36, ca. 0.1 wt%) was added, the mixing was performed at 180 °C at 60 rpm for 5 min. The two kinds of photo-degradable composite obtained were denoted as “PP/PEO/TiO_2” and “PP/PEO/ modified TiO_2”, respectively The PP/TiO_2 was prepared by the similar method.

6-2-5: Photo-degradation test

The samples were molded into a thin film (0.06 mm) by compression molding at 190°C under 5 MPa for 5 min. The Film was cut into the 20×20 mm, and put into a vial (Pyrex reactor). The photo-degradation test was performed with a Riko rotary photochemical reactor (RH400-10W, Riko-Kagaku Sangyo Co., Ltd.) equipped with a high-pressure mercury vapor lamp of 400 W (UVL-400HA ultrahigh-pressure mercury lamp with an intensity of 5 mW/cm^2; Riko-Kagaku Sangyo Co., Ltd.,). The test was carried out at 30 °C in air.

6-2-6: Biodegradation test

A soil burial test was performed as the biodegradation test. The film samples (20×20×0.06 mm) put into containers with the soil of the flowerbed in our institute (Kitami Institute of Technology). In order to avoid the soil dryness, the containers were treated with water spray every day. The biodegradation test had been performed for 45 days at 20 °C.

6-2-7: Scanning electron microscope (SEM) and SEM/Energy dispersive X-ray spectrometer (EDS) analyses

SEM and SEM/EDS analyses were carried out with a JEOL JSM-5800 at 20 kV. Atoms were measured with an EDS (Oxford Instruments INCA Microanalysis). The samples were prefixed in 3% glutaraldehyde in 0.1 M phosphate buffer (pH 7.4) for 1-2 h at 4 °C, rinsed three times with 0.1 M phosphate buffer [6, 17]. The samples obtained were fixed in 1% osmic acid in 0.1 M phosphate buffer (pH 7.4) for 1 h [17] and then were dehydrated using a graded ethanol series (50, 70, 95, and 100% three times for 15 min each). These samples placed in dried oven maintained at 27 °C for 30 min and were sputter-coated with gold before SEM imaging.

6-2-8: Optical microscope (OM) observation

OM observation was carried out with a Nikon ECLIPSE 50/POL optical microscope (Nikon Corp. Tokyo, Japan).

6-2-9: Fourier Transform Infrared (FT-IR) analysis

The IR spectra of 16 scans were measured with an FT-IR spectrometer (Perkin-Elmer Spectrum One) at a resolution of 2 cm^{-1} over the full mid-IR range (400-4000 cm^{-1}).

6-2-10: Differential scanning calorimetry (DSC) measurement

DSC measurements were made with a Shimadzu DSC-60. The samples of about 5 mg weight were sealed in aluminum pans. The measurement of the samples was carried out at a heating rate of 10 °C /min under a nitrogen atmosphere.

6-3: Results and Discussion

Figure 6-1 shows the SEM microphotographs of the surfaces of the no photodegradation treated samples retrieved from soil burial test for 45 days of incubation at 20 °C. In the case of the PP/PEO/TiO_2, a rod-shaped bacteria can be observed on the surface. In the case of the PP/PEO/TiO_2 modified by OCPC, a fungus as well as the bacteria can be seen on the surface. Whereas, microorganism cannot be observed on the PP and the PP/TiO_2 surfaces. Figure 6-2 shows the FT-IR spectra of the samples before and after the soil burial test. It is noted here that the photodegradation treatment is not performed to these samples. In fact, there are no peaks (at 1718 cm^{-1}) assigned to the carbonyl group (−$CH(CH_3)CH_2C(=O)$−$CH_2CH(CH_3)$−) [18] in both of the PP and the PP/TiO_2 samples, suggesting that these surface are hydrophobic. Whereas, in the cases of the PP/PEO/TiO_2 and the PP/PEO/modified TiO_2 by OCPC, the corresponding carbonyl peak can be observed at 1720 cm^{-1}. The existence of the peak suggests that the photodegradation already advances (It is very likely that the degradation is already initiated by the preparation process, sun and interior lamp irradiation) without the irradiation of the high-pressure mercury vapor lamp. After the soil burial test, the carbonyl peak has completely been lost. This is typical biodegradation behavior provided by metabolism of microorganism [8], [10] and [19]. The degradation of the PEO and/or PP parts produces the carbonyl compounds with considerably lower molecular weights. The compounds are diffused on the surfaces, resulting that the microorganisms are able to adhere to the surfaces. In addition, on the PP/PEO/modified TiO_2 by OCPC, the attachment of the fungus is due to the inorganic phosphates produced by the OCPC dissolution because it is not observed on the PP/PEO/TiO_2 surface.

Figure 6-3 shows the SEM microphotographs of the surfaces of the samples, which are photodegraded and retrieved from soil burial test for 45 days of incubation at 20 °C. In the case of the photodegraded PP/TiO_2, microorganisms cannot be observed as well as the unphotodegraded sample. In contrast, in the cases of the photodegraded PP/PEO/TiO_2 and the photodegraded PP/PEO/modified TiO_2 by OCPC, more kinds of microorganism and the developing of the colonies can be observed. In particular, on the photodegraded PP/PEO/modified TiO_2 by OCPC, the microorganisms are more active. As shown in Figure 6-3(III), a fungus forms very dense filamentous mycelium on the surface, suggesting that the more dissolved inorganic phosphates support the fungal growth. Figure 6-4 shows the FT-IR spectra of the photo-irradiated (photodegradation treated) samples before and after the soil burial test. In the case of the photo-irradiated PP/TiO_2, there are no peaks, indicating that the photodegradation does not occur under the photodegradation condition. Whereas, in the cases of the photo-irradiated PP/PEO/TiO_2 and the photo-irradiated PP/PEO/modified TiO_2 by OCPC samples before the soil burial test, the increase of the corresponding carbonyl peak can be observed, suggesting that the photodegradation advances. The behavior suggests that the photodegradation of the PP matrix certainly occurs in both the samples under the photodegradation condition. In addition, interestingly, a new peak with considerably high intensity appears at 1642 cm^{-1} in both the samples. The location is the frequency corresponding to ethylenic unsaturated group in PP [18]. In this photodegradation using the PEO/TiO_2 microcapsule, the PEO plays the role as a H_2O supply source as well as the acid and the aldehyde ones. When the PEO is photodegraded, the H_2O is spontaneously produced [12] and [20]. As shown in Figure 6-5, the H_2O is continuously supplied until the PEO is consumed completely, and the OH• is continuously produced

by the photocatalytic reaction with the TiO_2. The continuous OH• supply leads to an increase of the amount of the alkyl radical species, which is produced by the reaction with the PP matrix. The alkyl radical species reacts with oxygen preferentially and leads to the autooxidation. However, small amounts of the alkyl radical species produce the ethylenic unsaturated group by the abstraction of the proton radical species (H•). The ethylenic unsaturated group is believed to accumulate by repetition of these reactions. As shown in Figure 6-4, after the soil burial test, the peak disappears as well as the carbonyl peak in both of the samples. The behavior suggests that the ethylenic unsaturation part as well as the carbonyl one is metabolized by the microorganisms.

Figure 6-6 shows the OM and the SEM microphotographs of the surfaces of the PP/PEO/TiO_2 modified by OCPC sample, which is photodegraded and retrieved from soil burial test. As the shown in the OM microphotograph, there exist many black domains all over the surface. The domain is composed of the colony of other bacteria (see SEM microphotograph in Figure 6-6). As mentioned above, the fungus forms very dense filamentous mycelium on the surface. Since these behaviors can be observed in only the photodegradation treated PP/PEO/TiO_2 modified by OCPC sample, it appears that the inorganic phosphates are very useful as the supplement in the growths of some microorganisms.

Although the fungus and the bacteria grow well, the location where some kinds of the microorganism closely exist can be also observed (see Figure 6-7(a)). The growth rate among these microorganisms is considerably different. However, it seems that these microorganisms do not grow exclusively. In this study, the facilitation effect of the PP photodegradation is due to the compounds, which are produced by the photodegradation of the PEO microcapsule with the TiO_2. Thus, the PP matrix around the PEO

microcapsule must be severely degraded and is expected to be most vulnerable to the biocorrosion.

However, as shown in Figure 6-7(b), there are no microorganisms around the trace of the PEO microcapsule. It is found from the EDX analysis that there exist only the modified TiO_2 particles in the trace. The fungus is about 5 μm away from the trace, and its growing seems to avoid the location at which the TiO_2 exists (see Figure 6-7(b)). It is known that microorganisms are inactivated by TiO_2 photocatalytic oxidation [21], [22] and [23]. However, the photocatalytic oxidation never occurs in the soil burial test. Instead, the existence of hydrogen peroxide (H_2O_2) should be considered as the factor accounting for the inhibitory behavior of the microorganisms since H_2O_2 having inhibitory effect against microorganism is certainly obtained as a by-product in the TiO_2 photocatalytic reaction (see Figure 6-5). The H_2O_2 concentration must be considerably higher around the modified TiO_2 particle acting as the active site. Therefore, the microorganisms would be hardly bred around the TiO_2 particle. In addition, N. Allen et al. reported that PE was photocatalytically decomposed by TiO_2, and the formation of holes or pits formed at the TiO_2 particle surface [24]. It seems that such polymer loss also leads to nonexistence of the microorganisms around the TiO_2 particles.

Figure 6-8 shows the DSC curves of the tree kinds of the PP/PEO/TiO_2 modified by OCPC sample. The melting point (T_m) of the photodegradation treatment and the no soil burial test sample decreases up to 162.6 °C as compared with the Tm (=165.6 °C) of the pristine sample. The T_m decrease suggests that the photodegradation certainly progresses into the PP crystalline phase [25]. In addition, another T_m (=ca. 55 °C) ascribed to the PEO disappears after the photodegradation treatment. This behavior implies that the PEO is completely consumed by the photodegradation. Whereas, in the

case of the photodegradation treatment and the soil burial test sample, the DSC curve completely coincides with that of the photodegradation and the no soil burial test one. This behavior indicates that the biodegradation does not progress into the PP crystalline phase. There are no cracks on the surfaces of all the samples retrieved from the soil burial test. In addition, the appearances of the PP/PEO/TiO_2 and the PP/PEO/TiO_2 modified by OCPC samples with and without the photodegradation treatment are almost changeless although there are considerably differences of the breeding densities of the microorganisms. These results suggest that these microorganisms have the ability to metabolize only the photodegraded parts.

6-4: Conclusion

In this study, the biodegradations of the PP and the PP/TiO_2 composite systems were carried out with the soil burial test. As the PP/TiO_2 composite systems, the PP/TiO_2, PP/PEO/TiO_2 and the PP/PEO/TiO_2 modified by OCPC samples were used, respectively. In the cases of the no photodegradation treated samples, although microorganisms were not observed on the PP and the PP/TiO_2 surfaces, the rod-shaped bacteria and/or the fungus were done on the PP/PEO/TiO_2 and the PP/PEO/TiO_2 modified by OCPC ones. In the cases of the photodegradation treated PP/PEO/TiO_2 and the PP/PEO/TiO_2 modified by OCPC samples, more kinds of microorganism and the developing of their colonies were observed. In particular, these microorganisms were more active on the photodegraded PP/PEO/modified TiO_2 by OCPC. The active behavior was due to the inorganic phosphates, which were supplied by the dissolution of the OCPC during the photodegradation. The photodegraded parts were completely metabolized by the microorganisms. In addition, the microorganisms had the inability to metabolize other parts such as the PP crystalline phase.

References

[1] A. C. Albertsson, S.O. Andresson, S. Karlsson, *Polym. Degrad. Stab.* 1987, 18(1), 73

[2] A. C. Albertsson, C. Barenstedt, S. Karlsson, *Polym. Degrad. Stab.* 1992, 37(2), 163

[3] M. Weiland, A. Daro, C. Dacid, *Polym. Degrad. Stab.* 1995, 48(2), 275

[4] I. Jakubowicz, *Polym. Degrad. Stab.* 2003, 80(1), 39

[5] M.M. Reddy, R. K. Gupta, R. K. Gupta, S. N. Bhattacharya, R. Parthasarathy *J. Polym. Environ.* 2008, 16(1), 27

[6] S. Fontanella, S. Bonhomme, M. Koutny, L. Husarova, J. M. Brusson, J. P. Courdavault, S. Pitteri, G. Samuel, G. Pichon, J. Lemaire, A. M. Delort, *Polym. Degrad. Stab*. 2010, 95(6), 1011

[7] S. Bonhomme, A. Cuer, A. M. Delort, J. Lemaire, M. Sancelme, G. Scott, *Polym. Degrad. Stab.* 2003, 81(3), 441

[8] M. Koutny, M. Sancelme, C. Dabin, N. Pichon, A. M. Delort, J. Lemaire, *Polym. Degrad. Stab*. 2006, 91(7), 1495

[9] T. Ojeda, A. Freitas, E. Dalmolin, M. D. Pizzol, L. Vignol, J. Melnik et al. *Polym. Degrad. Stab.* 2009, 94(2), 2128

[10] E. Chiellini, A. Corti, S. D'Antone, *Polym. Degrad. Stab.* 2007, 92(7), 1378

[11] K. Miyazaki, H. Nakatani, *Polym. Degrad. Stab.* 2009, 94, 2114

[12] S. P. Vijayalakshmi, G. Madras, *J. Appl. Polym. Sci.* 2006, 100(5), 3997

[13] T. Kagiya, N. Yokoyama, K. Takemoto, *Bull. Inst. Chem. Res. Kyoto Univ.* 1976, 54(1), 15

[14] K. Miyazaki, H. Nakatani, *Polym. Degrad. Stab.* 2010, 95(9), 1557

[15] M. Kamitakahara, H. Okano, M. Tanihara, C. Ohtsuki, *J. Ceram. Soc. Japan.* 2008,

116(3), 481

[16] M. Szekeres, G. Fodor, A. Fazekas, M. Radnai, K. Turzó, I. Dékány, *Colloid. Polym. Sci.* 2005, 283, 587

[17] P. Chavant, B. Martinie, T. Meylheuc, M. N. Bellon-Fontaine, M. Hebraud, *Appl. Environ. Microbiol.* 2002, 68(2), 728

[18] D. J. Carlsson, D. M. Wiles. *Macromolecules* 1969, 2(6), 597

[19] D. Hadad, S. Geresh, A. Sivan, *J. Appl. Microbiol.* 2005, 98(5), 1093

[20] S. Morlat, J. L. Gardette, *Polymer* 2001, 42(14), 6071

[21] J. C. Ireland, P. Klostermann, E. W. Rice, R. M. Clark, *Appl. Environ. Microbiol.* 1993, 59(5), 1668

[22] C. Wei, W. Y. Lin, Z. Zainal, N. Williams, K. Zhu, A. P. Kruzic, R. L. Smith, K. Rajeshwar, *Environ. Sci. Technol.* 1994, 28(5), 934

[23] K. Sunada, Y. Kikuchi, K. Hashimoto, A. Fujishima. *Environ. Sci. Technol.* 1998, 32(5), 726

[24] N.S. Allen, M. Edge, G. Sandoval, A. Ortega, C.M. Liauw and J. Stratton et al., *Polym. Deg. Stab*. 2002, 76 (2), 305

[25] M. Elvira, P. Tiemblo, J. M. Gómez-Elvira, *Polym. Deg. Stab.* 2004, 83(3), 509

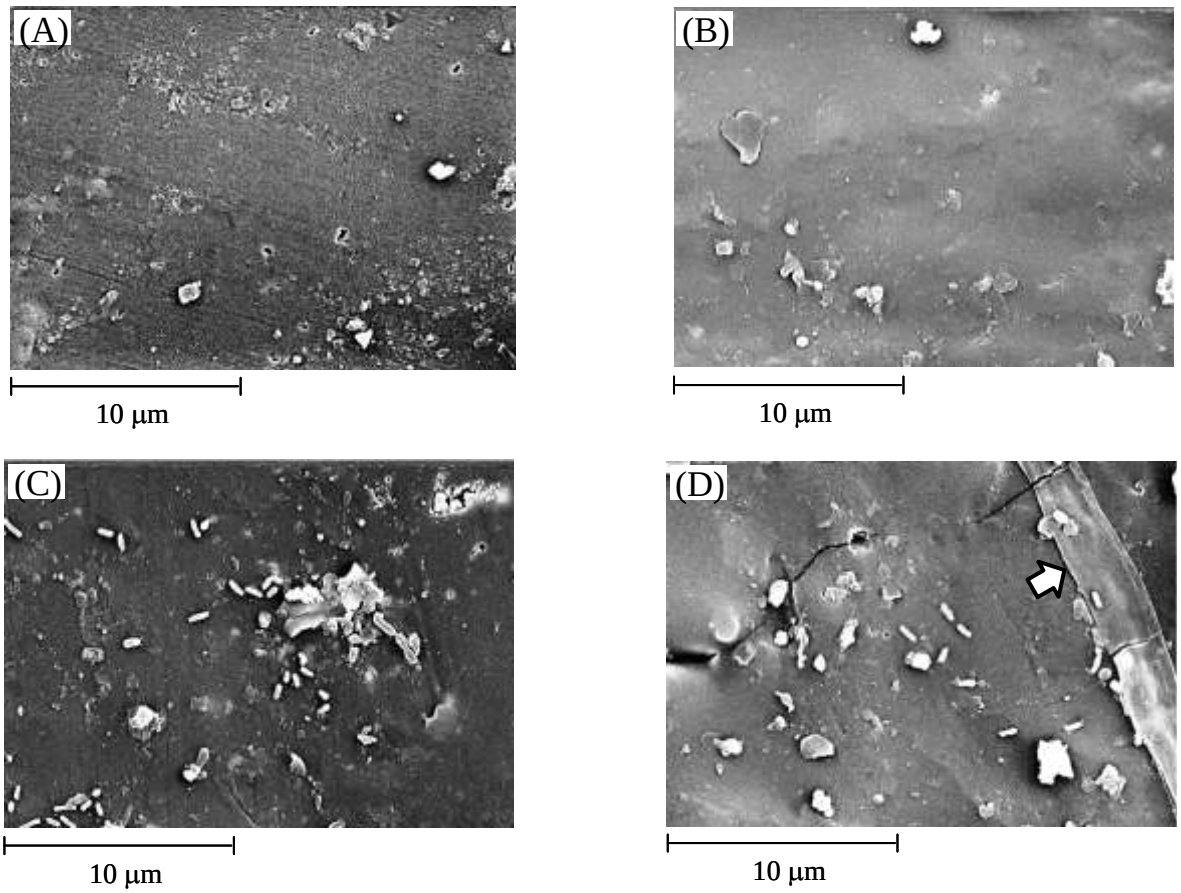

Figure 6-1 SEM microphotographs of the surfaces of samples retrieved from soil burial test for 45 days of incubation at 20 ºC: (A) PP, (B) PP(99.5 wt%)/TiO_2 (0.5 wt%), (C) PP(91.5 wt%)/PEO(8.0 wt%)/TiO_2(0.5 wt%), (D) PP(90.0 wt%)/PEO(8.0 wt%)/ TiO_2(0.5 wt%) modified by OCPC(1.5 wt%). No photodegradation treatment. The arrow indicates a fungus.

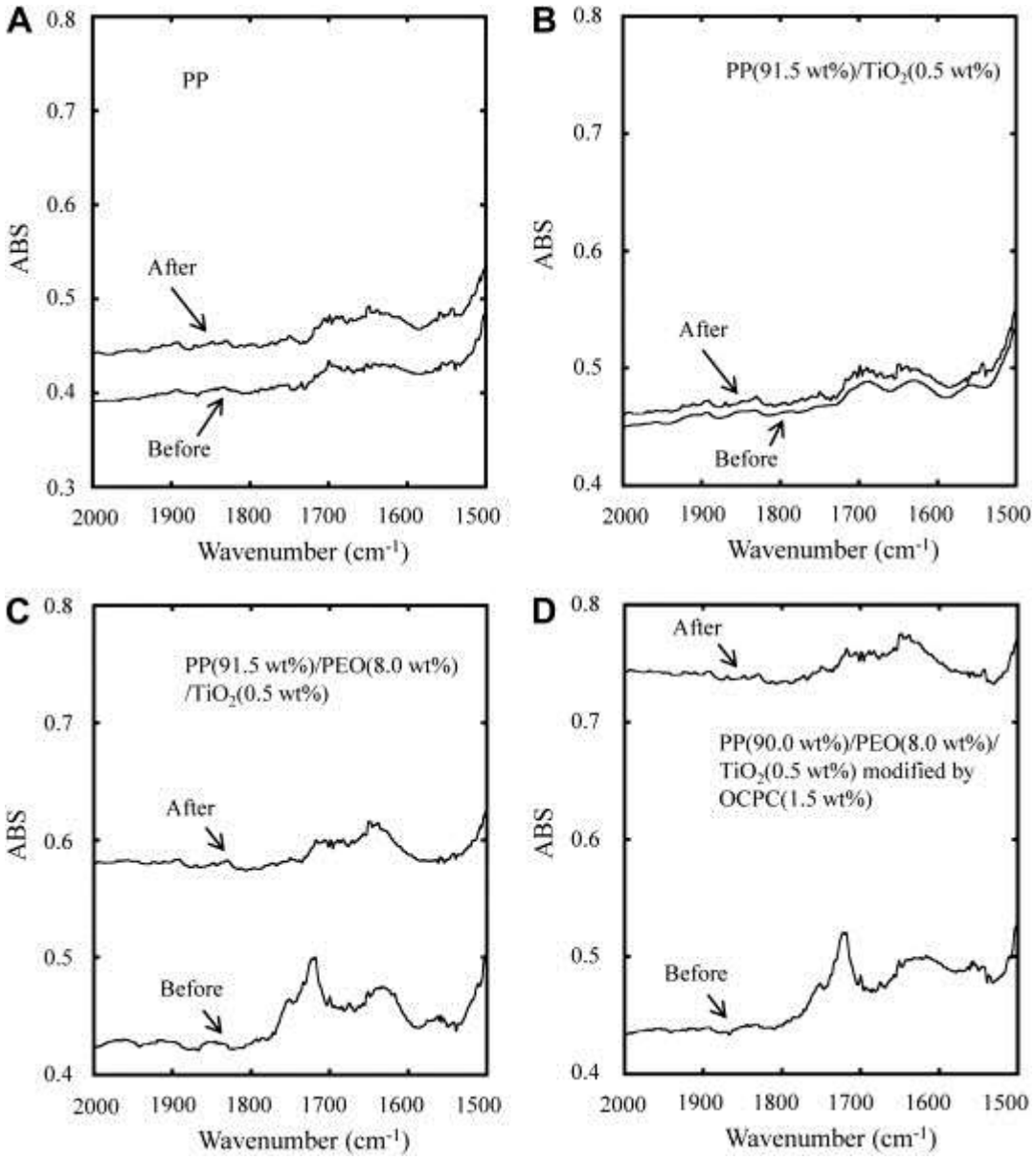

Figure 6-2 FT-IR spectra of various samples before and after soil burial test for 45 days of incubation at 20 °C. No photodegradation treatment.

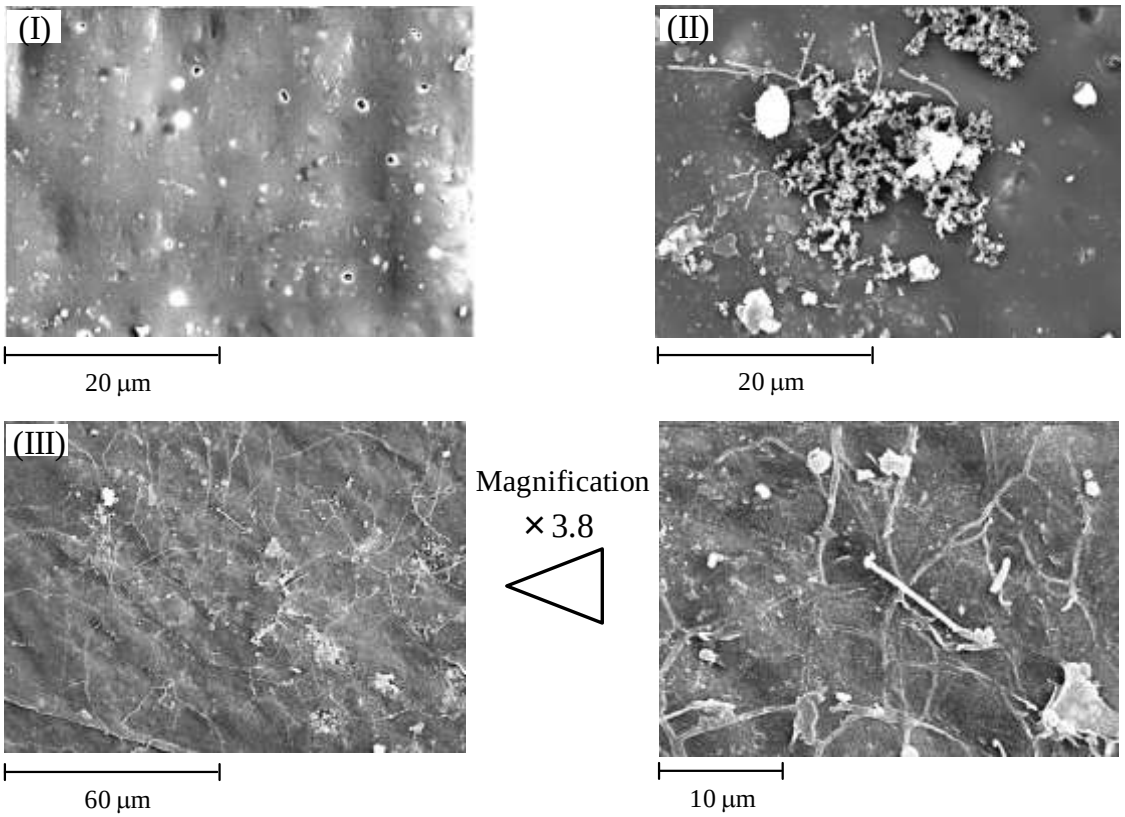

Figure 6-3 SEM microphotographs of the surfaces of photodegradation samples retrieved from soil burial test for 45 days of incubation at 20 ºC: (I) PP(99.5 wt%)/TiO_2 (0.5 wt%), (II) PP(91.5 wt%)/PEO(8.0 wt%)/TiO_2(0.5 wt%), (III) PP(90.0 wt%)/PEO(8.0 wt%)/ TiO_2(0.5 wt%) modified by OCPC(1.5 wt%). Photodegradation treatment for 24 h at 30 ºC.

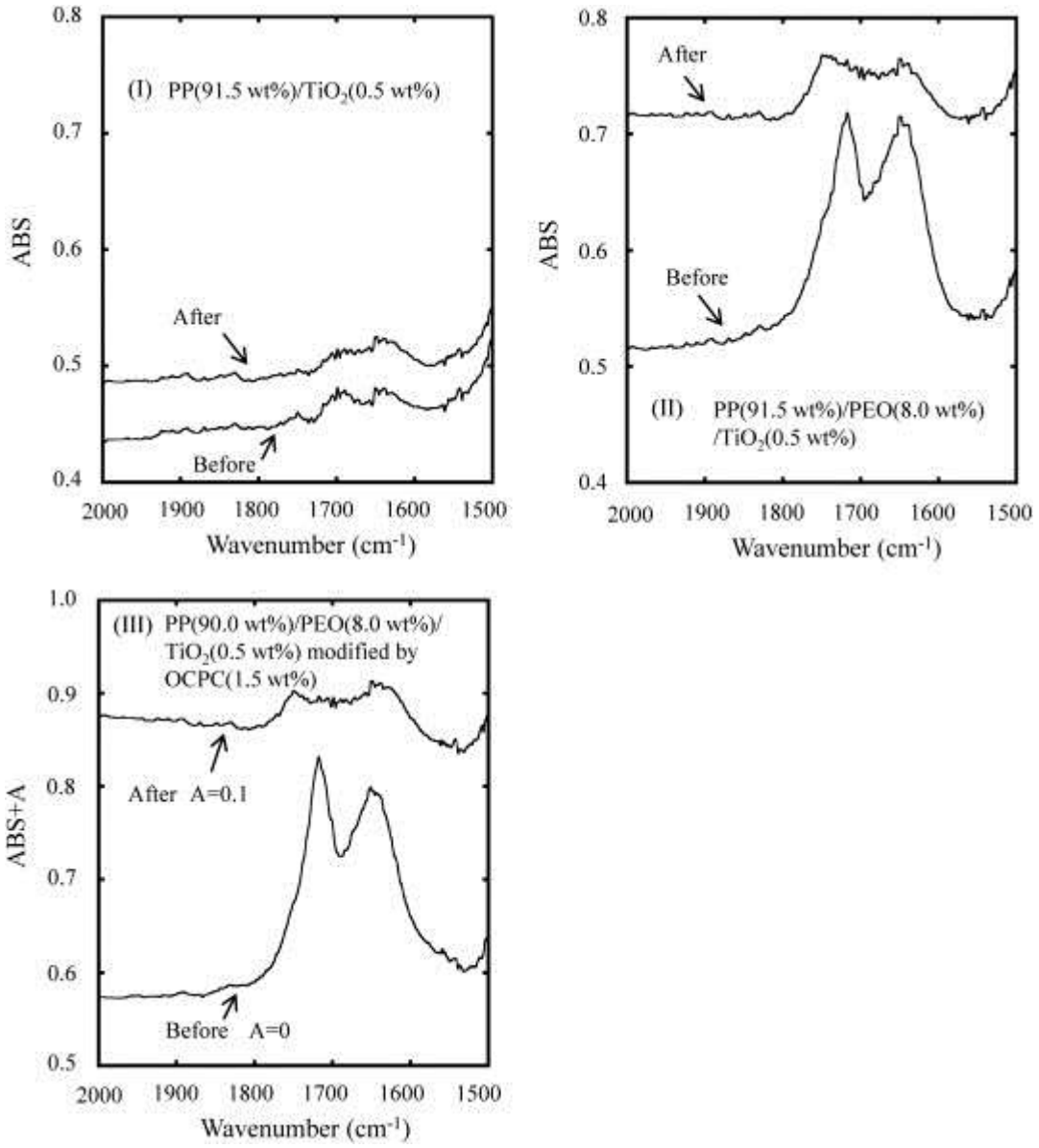

Figure 6-4 FT-IR spectra of various photodegradation samples before and after soil burial test for 45 days of incubation at 20 °C. Photodegradation treatment for 24 h at 30 °C.

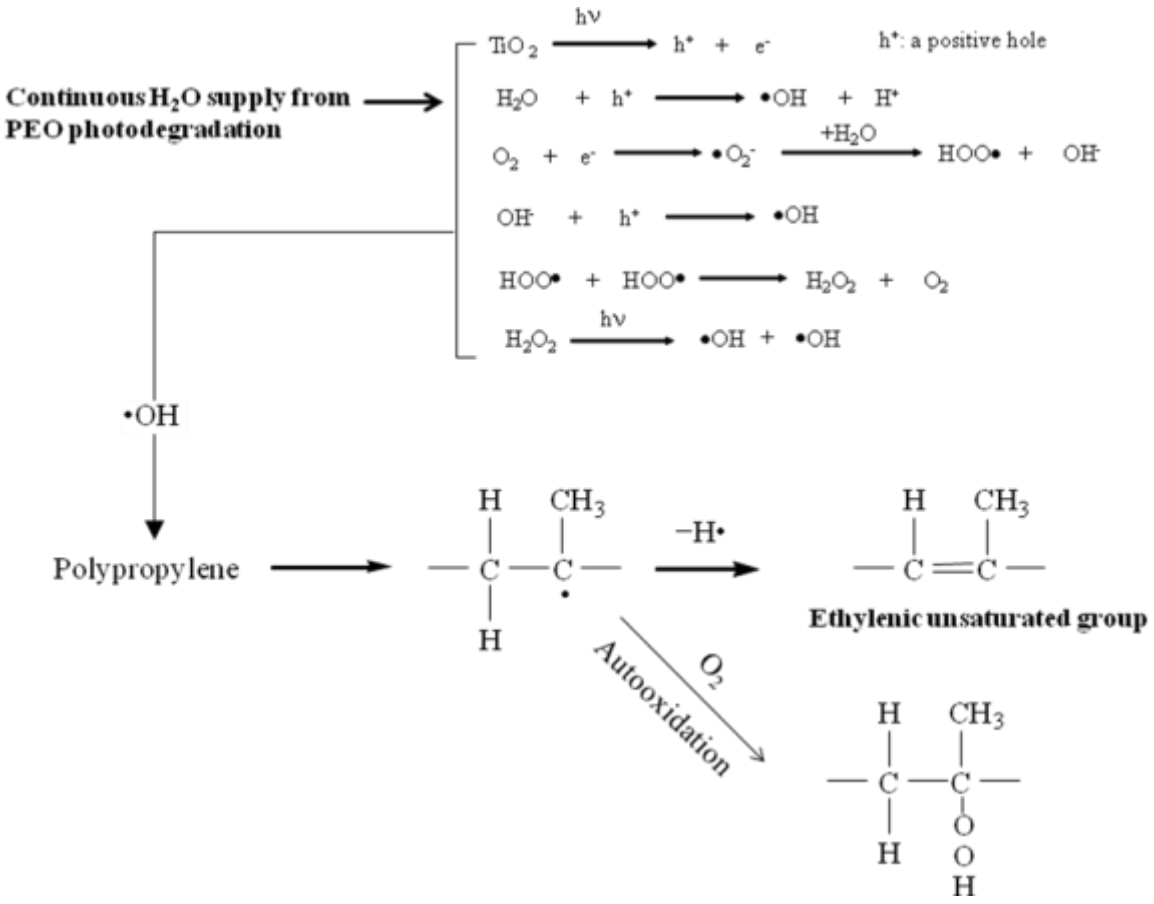

Figure 6-5 Plausible production mechanism of ethylenic unsaturated group.

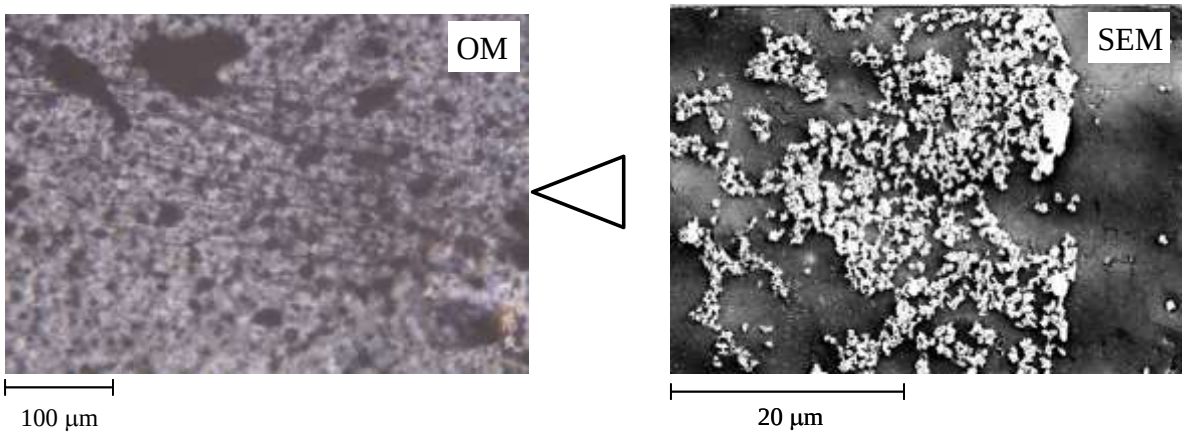

Figure 6-6 OM and SEM microphotographs of the surfaces of the PP(90.0 wt%)/PEO(8.0 wt%)/TiO_2(0.5 wt%) modified by OCPC(1.5 wt%) sample, which is photodegraded and retrieved from soil burial test for 45 days of incubation at 20 °C: Photodegradation treatment for 24 h at 30 °C.

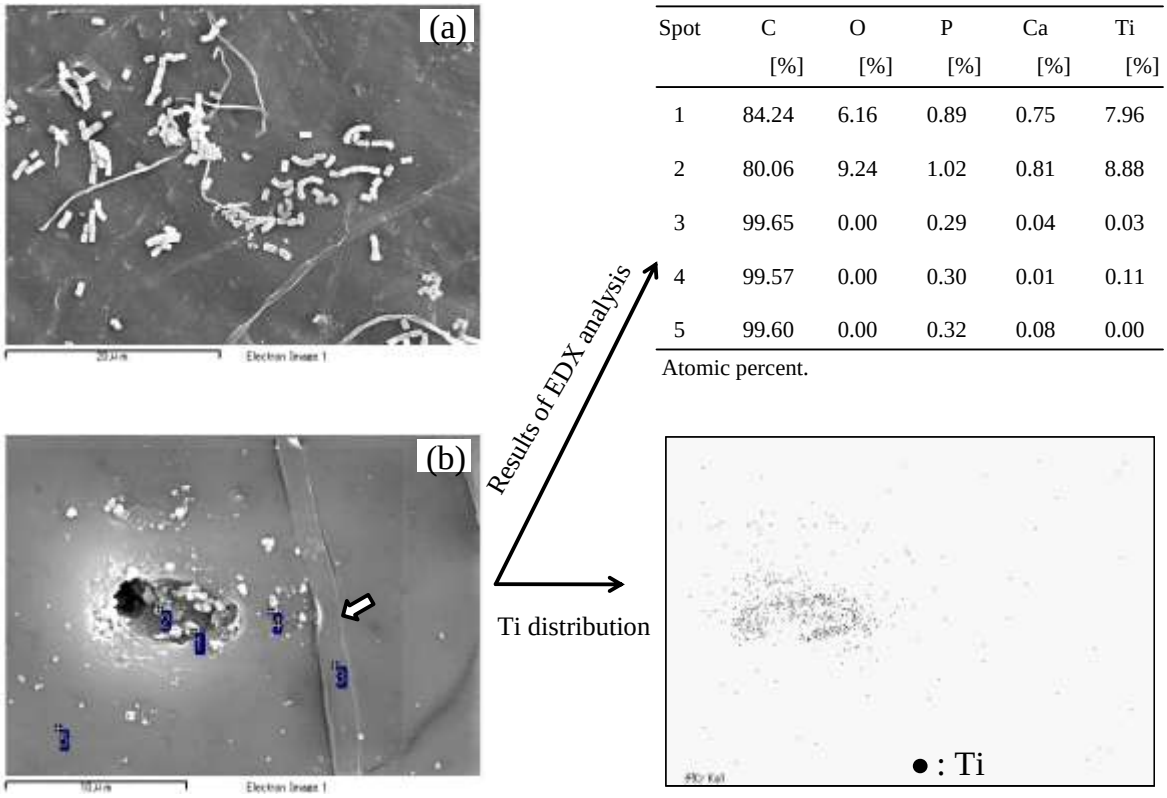

Spot	C [%]	O [%]	P [%]	Ca [%]	Ti [%]
1	84.24	6.16	0.89	0.75	7.96
2	80.06	9.24	1.02	0.81	8.88
3	99.65	0.00	0.29	0.04	0.03
4	99.57	0.00	0.30	0.01	0.11
5	99.60	0.00	0.32	0.08	0.00

Atomic percent.

Figure 6-7 SEM microphotographs and results of EDS analysis of the surfaces of photodegradation PP(90.0 wt%)/PEO(8.0 wt%)/ TiO_2(0.5 wt%) modified by OCPC(1.5 wt%) sample retrieved from soil burial test for 45 days of incubation at 20 ºC: Photodegradation treatment for 24 h at 30 ºC. (a): Location bioeroded by some kinds of microorganism. (b): Location around PEO microcapsule imprint. The arrow indicates a fungus.

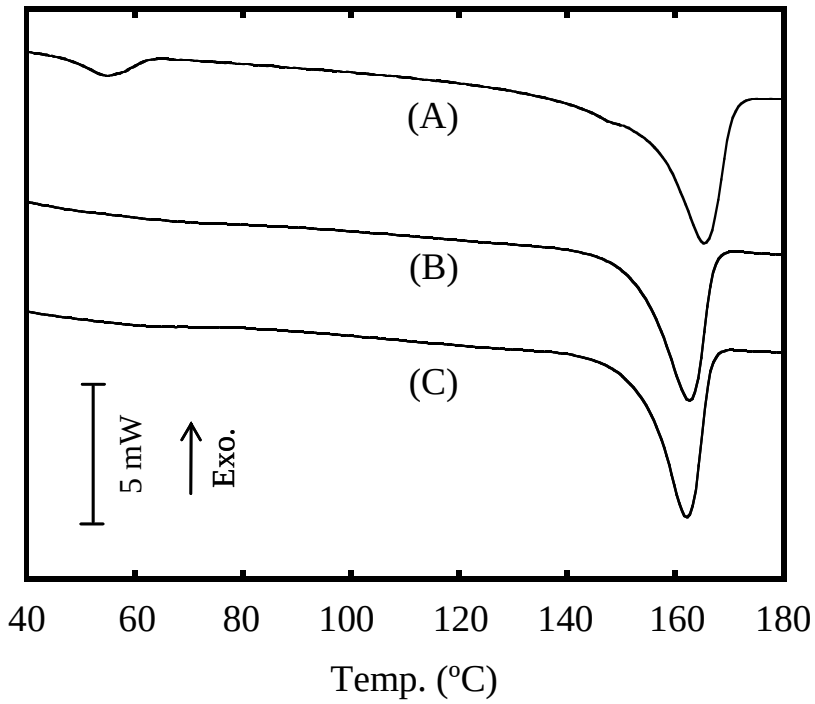

Figure 6-8 DSC curves of PP(90.0 wt%)/PEO(8.0 wt%)/ TiO_2(0.5 wt%) modified by OCPC(1.5 wt%) samples. (A): No photodegradation and no soil burial test sample. (B) Photodegradation and no soil burial test sample. (C): Photodegradation and soil burial test sample. Photodegradation treatment for 24 h at 30 ºC, soil burial test for 45 days of incubation at 20 ºC.

Chapter 7: Effect of polypropylene/cellulose composite oxo-biodegradation induced by poly(ethylene oxide)/TiO_2 initiator and accelerator system.

7-1: Introduction

Cellulose has been one of the most popular polymeric materials in the world and has been used as raw materials of building materials and paper for a long time ago. Cellulose is low cost, high modulus, renewable and biodegradable material. Recently cellulose has attracted much attention as a filler material for PP [1-6] since it has great potential for the preparation of composite materials having high-modulus and biodegradability. In fact, however, the biodegradability of PP/cellulose composite is considerably less due to non-biodegradable PP component.

PP is a typical non-biodegradable polymer since large molecule such as PP cannot enter into cells of microorganisms. Therefore, PP is hard to be metabolized in microorganisms. However, PP is able to be degraded to low molecular weight compounds by pro-oxidant and spontaneously converts to a biodegradable polymer. This method is called as "oxo-biodegradation" [7-11], and the mechanism involves two stages which are abiotic and microbial oxidations. The application would bring about biodegradability for PP/cellulose composite. However, there exists a big problem for the application to the composite. That is opacity of PP/cellulose composite. The opacity disturbs the photo-abiotic oxidation (autooxidation) stage in the inside of the composite, leading to an extreme decrease in microbial oxidation rate. Commercial application of PP/cellulose composite requires biodegradability under sunshine irradiation as well as high-modulus. It is necessary to design a novel pro-oxidant system by which the autooxidation proceeds even in the composite. As shown in the Chapter 5-7, we succeeded in preparation of an oxo-biodegradable PP by using a novel pro-oxidant

system [12-14]. The pro-oxidant system was composed of TiO_2 and PEO compounds. In this system, the TiO_2 worked as the radical initiators for both of the PP autooxidation and the PEO degradation [12]. Whereas, the PEO was photo-catalytically degraded by the TiO_2, and then acid and aldehyde compounds were produced. These products had an ability to accelerate the hydroperoxide decomposition, which is the rate-determining step in PP autooxidation [15, 16]. Namely, it was found that the PEO played the role of the accelerator of the PP autooxidation [12]. It is noted here that the PEO has a potential to accelerate the hydroperoxide decomposition even in the inside of PP/cellulose composite. Since the acid and aldehyde compounds produced by the PEO photodegradation is spontaneously spread into the inside of PP/cellulose composite, it seems that the inside hydroperoxide becomes decomposable even by irradiation with a common light source such as sunlight and mercury lamp.

In this study, the PP/PEO/TiO_2/FC composite was prepared, and its oxo-biodegradation behavior was studied with FT-IR and scanning electron microscope (SEM)/energy dispersive X-ray spectrometer (EDS). The effects of the FC loading on the tensile properties of the PP/PEO/TiO_2 composite were studied with tensile testing. In addition, the PP/PEO/TiO_2/FC composite film retrieved from the soil burial test was stained with lactophenol cotton blue, and then attached fungus morphology was observed by optical microscope to confirm its species.

Figure 7-11 shows the comparisons of the Young‘s moduli, the tensile strengths and the elongations at break of the pristine PP and the PP/PEO/TiO_2/FC films. In our previous works [22, 23], the effects of the FC and the PEO loadings on the PP tensile properties were studied. The results revealed as follows: (1) The FC loading brought about the increases of the Young‘s modulus and the tensile strength and the rapid decrease of the elongation at break, respectively; (2) The PEO loading brought about the decreases of the Young‘s modulus and the tensile strength and hardly affect the elongation at break; (3) When the PEO/FC blend was loaded into PP, the interface strength between the PEO/FC and the PP became weaker with the increase of the PEO content. In the PP/PEO/TiO_2/FC composite, the tendencies of the tensile properties are

the same. It is noted here that all the composites show the ca. 180 % higher Young‘s moduli than that of the pristine PP. The result insists that the PP/PEO/TiO_2/FC composite has the good photodegradability with the higher Young‘s modulus.

Figure 7-12 shows the SEM microphotographs, their EDX point and surface analysis images of Ti atom on PP(93.5 wt%)/PEO(5.0 wt%)/TiO_2(0.5 wt%)/FC(1.0 wt%) sample surfaces. The EDX point and surface analyses reveal that the TiO_2 particles are preferentially located on the FC, indicating that the particles are retained in the FC even after the melt-mixing process. In addition, as shown in Figure 7-13, in the sample etched by THF for 24 h, the TiO_2 particles are retained in the FC as well. It seems that there is an interaction between the TiO_2 and the FC. The retention characteristic is preferable for practical use of the PP/PEO/TiO_2/FC composite. In the case of the outdoor usage, the composite is certainly exposed to rain. The PEO component is certainly lost due to its water solubility, and the accelerator effect disappears at the same time. However, the accelerator effect must be recoverable by a readdition of the PEO component because of the TiO_2 retention characteristic.

7-2: Experimental

7-2-1: Materials

PP (meso pentad fraction=98%) was supplied by Japan Polypropylene Co. The number-average molecular weight (M_n) and the polydispersity (M_w/M_n) of the PP were 4.6×10^4 and 5.7, respectively.

PEO was purchased from Wako Pure Chemical Industries, Ltd. The average molecular weight was 5.0×10^5.

TiO_2 was purchased from Wako Pure Chemical Industries, Ltd. The crystal structure was anatase (over 98.5 %), and the surface area was about 6 m^2/g. The TiO_2 was used without pretreatment.

Fibrous cellulose (FC: W-100GK) was donated by Nippon Paper Chemicals Co. Ltd. The FC was dried in desiccator for 7 days before preparation. The moisture of the FC was below 0.7wt%. The FC dimensions are over 90wt% pass 100mesh (below 150 μm), and the average length was ca. 37 μm.

7-2-2: Preparation of PEO/TiO_2 /FC blend

Mixing of pure water (40ml/g-PEO) solution of the PEO/TiO_2/FC was performed using a 0.1-L glass equipped with a stirrer at 23°C for 24h. The water solvent was evaporated using a rotary evaporator. The sample obtained was dried at 50°C for 24h at in a vacuum oven and was used as the PEO/TiO_2/FC blend.

7-2-3: Preparation of PP/PEO/TiO_2 /FC composite

Loading of the PEO/TiO_2/FC blend into PP was prepared by an Imoto Seisakusyo IMC-1884 melting mixer. After a small amount of the phosphite antioxidant (ADK STAB PEP-36, ca. 0.1 wt%) was added, the mixing was performed at 180 °C at 100 rpm for 5 min.

7-2-4: Photodegradation test

The sample was molded into a thin film (50 or 100 μm) by compression molding at 190°C under 5 MPa for 5 min. The film was cut into the 20×20×0.05 mm or 20×20×0.1 mm, and put into a vial (Pyrex reactor). The photo-degradation test was performed with a Riko rotary photochemical reactor (RH400-10W, Riko-Kagaku Sangyo Co., Ltd.) equipped with a high-pressure mercury vapor lamp of 400 W (UVL-400HA ultrahigh-pressure mercury lamp with an intensity of 5 mW/cm^2; Riko-Kagaku Sangyo Co., Ltd.,). The test was carried out at 30 °C in air.

7-2-5: Fourier Transform Infrared (FT-IR) analysis and estimation of carbonyl group concentration

The IR spectra of 16 scans were measured with an FT-IR spectrometer (Perkin-Elmer Spectrum One) at a resolution of 2 cm^{-1} over the full mid-IR range (400-4000 cm^{-1}).

Carbonyl group (methylketone) is a main product of autooxidation of PP [17]. The corresponded IR peak appears at around 1720 cm^{-1}, and its average molar absorptivity is 330 mol $l^{-1}cm^{-1}$ [17]. The carbonyl group concentration of the photodegraded PP was estimated by Lambert-Beer law using the average molar absorptivity and the pristine PP density (0.900 g/ml).

7-2-6: Tensile testing

Stress-strain behavior was observed using a SHIMADZU EZ-S at a cross-head speed of 3 mm/min. The sample specimens were cut with dimensions 30×5×0.05 mm shape in which the gauge length was 10 mm. We chose the specialized specimen (like ISO reed-shape) to adapt to the size of our tensile testing machine. All of tensile testing were performed at 20 °C. The values of Young's modulus were obtained from the slope of the stress-strain curve (until about 1% of the strain value). All results obtained were

the average values of ten measurements.

7-2-7: Scanning electron microscope (SEM) and SEM/Energy dispersive X-ray spectrometer (EDS) analyses

SEM and SEM/EDS analyses were carried out with a JEOL JSM-5800 at 20 kV. Ti atom distribution was measured with an EDS (Oxford Instruments INCA Microanalysis). The sample placed in dried oven maintained at 27 °C for 30 min and was sputter-coated with gold before SEM imaging.

In the cases of biodegraded samples, they were prefixed in 3% glutaraldehyde in 0.1 M phosphate buffer (pH 7.4) for 1-2 h at 4 °C, rinsed three times with 0.1 M phosphate buffer [18, 19]. The samples obtained were fixed in 1% osmic acid in 0.1 M phosphate buffer (pH 7.4) for 1 h [19] and then were dehydrated using a graded ethanol series (50, 70, 95, and 100% three times for 15 min each). These samples placed in dried oven maintained at 27 °C for 30 min and were sputter-coated with gold before SEM imaging.

7-2-8: Biodegradation test

A soil burial test was performed as the biodegradation test. The film samples (20×20×0.05 mm) put into containers with the soil of the flowerbed in our institute (Kitami Institute of Technology). In order to avoid the soil dryness, the containers were treated with water spray every day. The biodegradation test had been performed at 20°C.

7-2-9: Optical microscope observation

Optical microscope observation was carried out with a Nikon ECLIPSE 50/POL optical microscope (Nikon Corp. Tokyo, Japan). The samples were stained with lactophenol cotton blue (purchased from KANTO CHEMICAL CO., INC.) before optical microscope imaging.

7-3 Results and Discussion

FC is hydrophilic and tends to aggregate, causing poor incompatibility with hydrophobic PP. In addition, the loading of opaque FC certainly makes PP a lot less transparent, resulting that the PP photodegradation interferes. Figure 7-1 shows the photographs of the PP(98.2 wt%)/PEO(0.3 wt%)/TiO_2(0.5 wt%)/FC(1.0 wt%) and the PP(95.2 wt%)/PEO(0.3 wt%)/TiO_2(0.5 wt%)/FC(5.0 wt%) films. Although the FC loading of 5 wt% brings about the considerably opaque film, the 1wt% loading film is relatively good transparence. It seems that a small loading of the FC keeps the PP transparent at some level.

Figure 7-2 (a) shows the FT-IR spectra around ethylenic unsaturated and carbonyl group peaks before the photodegradation. The broad peaks (at 1642 cm^{-1}) assigned to ethylenic unsaturated group can be observed in all the samples. The amount of the ethylenic unsaturated group hardly depends on the FC content and the PEO existence, respectively. It seems that a small amount of the ethylenic unsaturated group is spontaneously produced during the melt-mixing process. In addition, the carbonyl peak is unseen in all the samples. These results suggest that the PP autooxidation hardly occur under the melt-mixing condition. In the cases of the composition samples having the same PEO(0.3 wt%) and TiO_2(0.5 wt%) contents, as shown in Figure 7-2(b) and (c), the higher FC (5.0 wt%) content sample shows that the increase in the rate of ethylenic unsaturated group amount is higher after 6h photodegradation treatment as compared with the lower content one. This behavior suggests that the FC acts as photodegradation initiator [20].

Figure 7-3 shows the FT-IR spectra around 2000-4000 cm^{-1} of the pristine PP, PP/FC and PP/PEO/TiO_2/FC samples, respectively. In the cases of the PP/FC samples, the OH group (around ca. 3350 cm^{-1}) peak intensity of the PP(90.0 wt%)/FC(10.0 wt%) is considerably higher than that of the PP(95.0 wt%)/FC(5.0 wt%). In addition, the change of the peak intensity is not observed in both of the photodegraded PP/FC samples. This

behavior suggests that the OH group originated from hydroperoxide is not contained in these peaks. It is found that the autooxidation does not occur in these PP/FC samples under the photodegradation condition. Interestingly, the OH group peak intensity of the PP(98.2 wt%)/PEO(0.3 wt%)/TiO_2(0.5 wt%)/FC(1.0 wt%) is considerably higher than that of the PP(95.0 wt%)/FC(5.0 wt%) although the FC content is lower. The OH group peak shape is sharper than those of other samples, and the intensity is hardly changed before and after the photodegradation. The behavior suggests that the OH group originated from hydroperoxide is considerably contained in the PP(98.2 wt%)/PEO(0.3 wt%)/TiO_2(0.5 wt%)/FC(1.0 wt%). In addition, the change of the peak intensity is not observed before and after the photodegradation. Considering the good transparency in the PP(98.2 wt%)/PEO(0.3 wt%)/TiO_2(0.5 wt%)/FC(1.0 wt%) film (see Figure 7-1), it is likely that the autooxidation easily occurs in these PP/FC samples under a low-intensity light source such as interior light. Whereas, in the case of the PP(95.2 wt%)/PEO(0.3 wt%)/TiO_2(0.5 wt%)/FC(5.0 wt%) film, the OH group peak intensity is weaker as well as that of the PP(95.0 wt%)/FC(5.0 wt%) one. However, the PP(95.2 wt%)/PEO(0.3 wt%)/TiO_2(0.5 wt%)/FC(5.0 wt%) sample shows that the OH group peak intensity becomes higher after 6h photodegradation treatment as well as that of the ethylenic unsaturated group. This behavior suggests that the autooxidation occurs by the irradiation of the high-pressure mercury vapor lamp. As shown in Figure 7-1, since the film is considerably opaque, the autooxidation process would require the much stronger light source as compared with the PP(98.2 wt%)/PEO(0.3 wt%)/TiO_2(0.5 wt%)/FC(1.0 wt%) film. These results reveal that the existences of PEO and TiO_2 allow the autooxidation to proceed in the PP/FC composite.

Figure 7-4 shows that the FT-IR spectra of PP(95.5-x wt%)/PEO(x wt%)/TiO_2(0.5 wt%)/FC(1.0 wt%) film samples with various PEO content around ethylenic unsaturated and carbonyl group peaks before and after the photodegradation. It appears that the increase of the PEO content brings about the increases of both the group peak intensities.

In particular, the increments of these peak intensities between before and after the photodegradation are larger as the PEO content increases. Figure 7-5 shows FT-IR spectra of these samples around OH group peak. In the cases of the samples having the 1.0 and 2.0 wt% PEO contents, the OH group peak intensities are almost zero, and their increments are hardly seen between before and after the photodegradation although the ethylenic unsaturated and carbonyl group peak intensities increase (see Figure 7-4). Whereas, in the cases of the samples having the higher PEO (3 and 5 wt%) contents, their increments of the OH group peak intensities can be observed between before and after the photodegradation. Figure 7-6 shows the increments of the ethylenic unsaturated and carbonyl group peak intensities in the pristine PP and the PP(95.5-x wt%)/PEO(x wt%)/TiO_2(0.5 wt%)/FC(1.0 wt%) films during the photodegradation. Both of the peak intensities increase with the increase of the PEO content although those of the pristine PP are zero (no degradation) until the 6 h. However, these photodegradation time dependencies are considerably different. In the case of the ethylenic unsaturated group peak intensities, even at every PEO content, the maximum reach at around 1h photodegradation. Whereas, the carbonyl group peak intensities logarithmically increase with the increase of the photodegradation time regardless of the PEO content.

As shown in Figure 7-7, the TiO_2 has an activity to initiate the PP autooxidation [12, 13, 21]. Whereas, the PEO has an activity to produce an acid and an aldehyde, which are able to accelerate the autooxidation. In other words, the TiO_2 and the PEO work as the “initiator“ and the “accelerator”, respectively. In the autooxidation of the PP/PEO/TiO_2/FC composite, in particular, it appears that the PEO existence is important for the autooxidation process. As mentioned above, it is likely the FC acts as the autooxidation initiator as well as TiO_2. Therefore the autooxidation initiation readily occurs in the composite. Some of the generated alkyl radicals offer the ethylenic unsaturated group (terminal reaction), and others do the hydroperoxide one. The radical

species (OH•) generated by the TiO_2 photocatalysis can be spread and can initiate the autooxidation in the inside of the composite films. However, the hydroperoxide decomposition requires light and cannot occur easily in the inside of the composite films. In fact, as shown in Figure 7-3, the hydroperoxide accumulates, and the autooxidation hardly proceed in the composite films with the small amount (0.3 wt%) of the PEO. Whereas, in the cases of the composite films with much amount (>1 wt%) of the PEO, the hydroperoxide hardly accumulates, and the autooxidation considerably proceeds. The PEO is photocatalytically decomposed in presence of TiO_2 and generates acid and aldehyde compounds, which are able to accelerate the hydroperoxide decomposition [12, 13]. This PEO accelerator effect certainly supports the autooxidation process in the inside of the composite films. The generated acid and aldehyde compounds make the films degradable for lower light intensity. Therefore, the degree of the autooxidation process certainly depends on the PEO amount.

Figure 7-8 shows the carbonyl peak intensity increments of the PP/PEO/TiO_2/FC composite films having the more film thickness (100 μm) during the photodegradation. The intensity increment of the sample having the 1 wt% PEO content is distinguished and surpasses that of the sample having the 5 wt% content over the 3h. The dependence of the PEO content is different from that of the 50 μm films. Figure 7-9 shows the increments of the carbonyl group concentration (estimation as methylketone) between before and after the photodegradation in the PP(97.5 wt%)/PEO(1.0 wt%)/TiO_2(0.5 wt%)/FC(1.0 wt%) and the PP(93.5 wt%)/PEO(5.0 wt%) /TiO_2(0.5 wt%)/FC(1.0 wt%) having 50 and 100 μm film thickness, respectively. Interestingly, in the cases of the PP(97.5 wt%)/PEO(1.0 wt%)/TiO_2(0.5 wt%)/FC(1.0 wt%) films, the carbonyl group concentration increment of the 100 μm film is approximately four times higher than that of the 50 μm one. Whereas, in the cases of the PP(93.5 wt%)/PEO(5.0 wt%)/TiO_2(0.5 wt%)/FC(1.0 wt%), there is no difference between the concentration increments of the 50 μm and the 100 μm films. The difference between the incremental behavior is due to

the PEO content. As mentioned above, the acid and aldehyde compounds, which are generated by the PEO photodegradation, accelerate the hydroperoxide decomposition. The generated compounds would have a certain degree of molecular mobility. The generated accelerator (acid and aldehyde compounds) is wholly spread in the composite film. As shown in Figure 7-10, at some point distant from each of the PEO/TiO_2/FC domains, the accelerator, which is spread from other PEO/TiO_2/FC domains, fills in for the insufficient amount. The complementary effect would be amplified to a suitable level by the enhancement of the film thickness, resulting that the acceleration of the hydroperoxide decomposition occurs even with a low PEO content such as 1 wt%. In fact, as shown in Figure 7-8, the of carbonyl peak intensity of the sample having the 1 wt% PEO content shows the exponential increase between the photodegradation time of 2 h and 3h, suggesting that the accelerator reaches the requisite amount for accelerating the hydroperoxide decomposition by the spreading. It is found that the composite film having the low PEO content shows the complementary effect induced by the enhancement of the film thickness.

Figure 7-14 shows the SEM microphotographs of the surfaces of PP(97.5 wt%)/PEO(1.0 wt%)/TiO_2(0.5 wt%)/FC(1.0 wt%) samples retrieved from soil burial test for 28 days of incubation at 20 ºC. In the case of the unphotodegraded sample, microorganism cannot be observed. Whereas, in the case of the photodegraded sample, the microorganisms (fungi) can be observed. Figure 7-15 shows the FT-IR spectra of the samples before and after the soil burial test. In the case of the unphotodegraded sample, the carbonyl peak intensity is considerably low and hardly changes between before and after the soil burial test, supporting that metabolism of microorganism does not occur. In contrast, the photodegraded sample shows that the carbonyl peak intensity is much higher than that of the unphotodegraded one. The higher carbonyl peak almost disappears after the soil burial test. This is typical biodegradation behavior provided by metabolism of microorganism [14, 24-26].

In order to investigate the fungi morphology, the film retrieved from the soil burial test was stained with lactophenol cotton blue and then was measured by optical microscope. Figure 7-16 shows the optical microscope photographs. The long and short filamentous fungi can are observed, respectively. It is noted here that the septate structure can be seen in the short filamentous fungi. The fungi have the septate hypha. Motta et. al. reported that colonization and adhesion of Curvularia sp. was observed on an oxidized polystyrene surface and, the phenomenon implied its biodegradation (metabolism) by the fungus [27]. The observed filamentous fungi would be identical species, that is, Curvularia sp. since they exhibit its characteristic appearance such as ribbon-like shape and septate structure. Although the check of the fungus gene is indispensable to identification of them, it reveals that the photodegraded PP/PEO/TiO_2/FC composite shows biodegradability by them.

7-4: Conclusion

In this study, the PP/PEO/TiO_2/FC composite was prepared, and its oxo-biodegradation behavior was studied. Although the FC loading of 5 wt% brought about the considerably opaque film, the 1wt% loading film was good transparence. The FT-IR spectra of the unphotodegraded composite samples indicated that the PP autooxidation hardly occurred under the melt-mixing condition. After the ultraviolet irradiation, the autooxidation smoothly advanced in the composite. The FT-IR analyses of the composite revealed that the TiO_2 and the PEO played the roles of the initiator and the accelerator of PP autooxidation, respectively. In addition, even at a lower PEO content, the accelerator effect was found to be supplemented with the spreading of the degraded PEO component from other place by the enhancement of the film thickness. The PP/PEO/TiO_2/FC composite showed the higher Young‘s modulus. The biodegradability of the photodegraded composite was confirmed by the soil burial test, and the adherence of the filamentous fungus was observed on the surface.

Reference

[1] S. Takase, N.Shiraishi, *J. App.l Polym. Sc.i* 1989, 37(3), 645

[2] J.M. Felix, P. Gatenholm, *J. Appl. Polym. Sci.* 1991, 42(3), 609

[3] W. Qiu, F. Zhang, T. Endo, T. Hirotsu, *J. Appl. Polym. Sci.* 2003, 87(2), 337

[4] W. Qiu, F. Zhang, T. Endo, T. Hirotsu, *J. Appl. Polym. Sci.* 2004, 91(3), 1703

[5] W. Qiu, F. Zhang, T. Endo, T. Hirotsu, *J. Appl. Polym. Sci.* 2004, 94(3), 1326

[6] V. N. Hristov, S. T. Vasileva, M. Krumova, R. Lach, G. H. Michler, *Polym. Compos.* 2004, 25(5), 521

[7] A. C. Albertsson, S.O. Andresson, S. Karlsson, *Polym. Degrad. Stab.* 1987, 18(1), 73

[8] A. C. Albertsson, C. Barenstedt, S. Karlsson, *Polym. Degrad. Stab.* 1992, 37(2), 163

[9] M. Weiland , A. Daro, C. Dacid, *Polym. Degrad. Stab.* 1995, 48(2), 275

[10] I. Jakubowicz, *Polym. Degrad. Stab.* 2003, 80(1), 39

[11] M.M. Reddy, R. K. Gupta, R. K. Gupta, S. N. Bhattacharya, R. Parthasarathy *J. Polym. Environ.* 2008, 16(1), 27

[12] K. Miyazaki, H. Nakatani, *Polym. Degrad. Stab.* 2009, 94, 2114

[13] K. Miyazaki, H. Nakatani, *Polym. Degrad. Stab.* 2010, 95(9), 1557

[14] K. Miyazaki, K. Shibata, H. Nakatani, *Polym. Degrad. Stab.* 2011, 96(5), 1039

[15] R. Broska, J. Rychlý, K. Csomorová, *Polym. Degrad. Stab.* 1999, 63(2), 231

[16] P. Eriksson, T. Reiberger, B. Stanberg, *Polym. Degrad. Stab.* 2002, 78(1), 183

[17] J. Adams, *J. Polym. Sci. A-1* 1970, 8, 1077

[18] S. Fontanella, S. Bonhomme, M. Koutny, L. Husarova, J. M. Brusson, J. P. Courdavault, S. Pitteri, G. Samuel, G. Pichon, J. Lemaire, A. M. Delort, *Polym. Degrad. Stab.* 2010, 95(6), 1011

[19] P. Chavant, B. Martinie, T. Meylheuc, M. N. Bellon-Fontaine, M. Hebraud, *Appl.*

Environ. Microbiol. 2002, 68(2), 728

[20] R. Seldén, B. Nyström, R. Långström, *Polym. Comp.* 2004, 25(5), 543

[21] I. Blakey, G. A. George, *Polym. Degrad. Stab.* 2000, 70(2), 269

[22] H. Nakatani, K. Miyazaki, *J. Appl. Polym. Sci.* 2009, 112(6), 3362

[23] K. Miyazaki, H. Nakatani, *J. Appl. Polym. Sci.*2009, 114(3), 1656

[24] M. Koutny, M. Sancelme, C. Dabin, N. Pichon, A. M. Delort, J. Lemaire, *Polym. Degrad. Stab.* 2006, 91(7), 1495

[25] E. Chiellini, A. Corti, S. D'Antone, *Polym. Degrad. Stab.* 2007, 92(7), 1378

[26] D. Hadad, S. Geresh, A. Sivan, *J. Appl. Microbiol.* 2005, 98(5), 1093

[27] O. Mottaa, A. Protob, F. D. Carlob, F. D. Caroa, E. Santoroa, L. Brunettia, M. Capunzo, *Int. Hyg. Environ. Health.* 2009, 212, 61

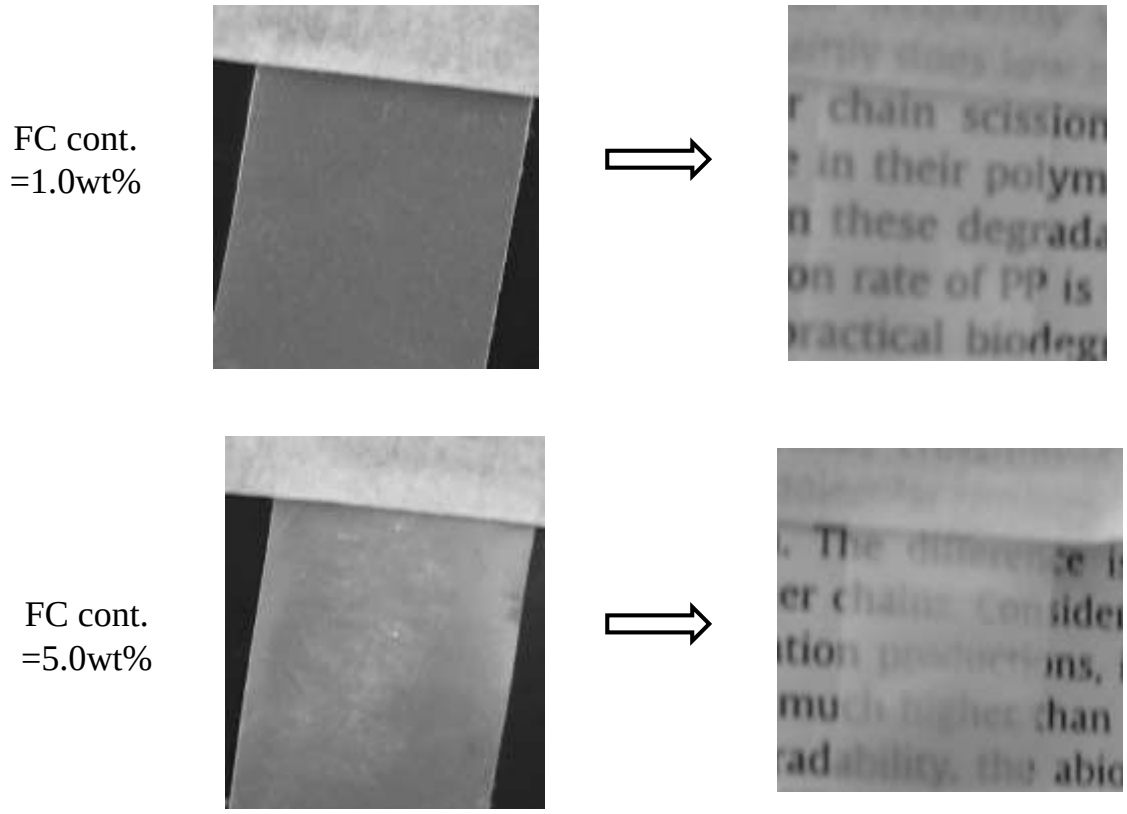

Figure 7-1 Photographs of the PP((99.2-x) wt%)/PEO(0.3 wt%)/ TiO_2(0.5 wt%)/FC(x wt%) films: Film thickness = 50 μm.

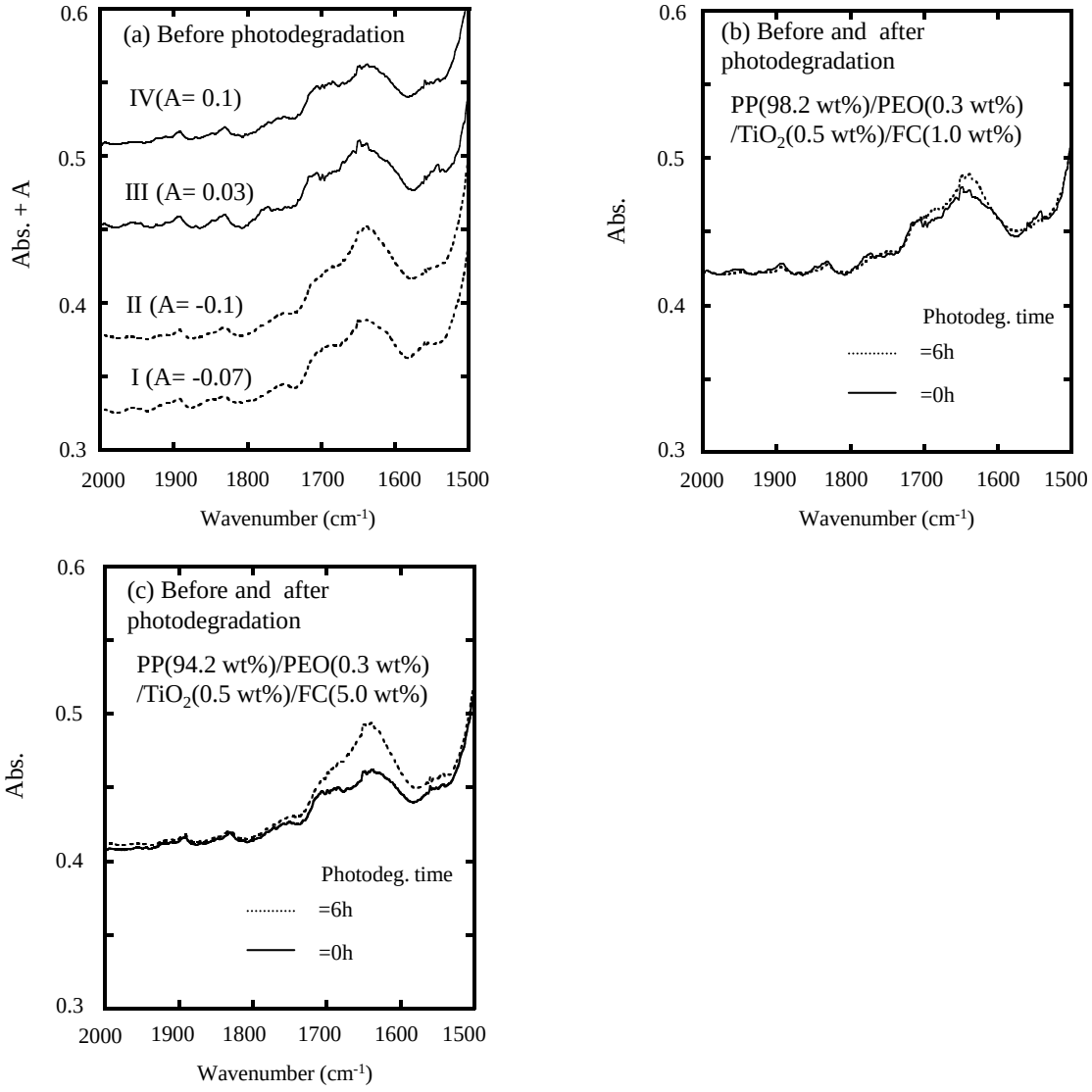

Figure 7-2 FT-IR spectra of various samples around ethylenic unsaturated and carbonyl group peaks. Film thickness = 50mm.

I= PP(95.0 wt%) /FC(5.0 wt%), II= PP(90.0 wt%) /FC(10.0 wt%), III = PP(98.2 wt%)/PEO(0.3 wt%) /TiO_2(0.5 wt%)/FC(1.0 wt%), IV= PP(94.2 wt%)/PEO(0.3 wt%) /TiO_2(0.5 wt%)/FC(5.0 wt%).

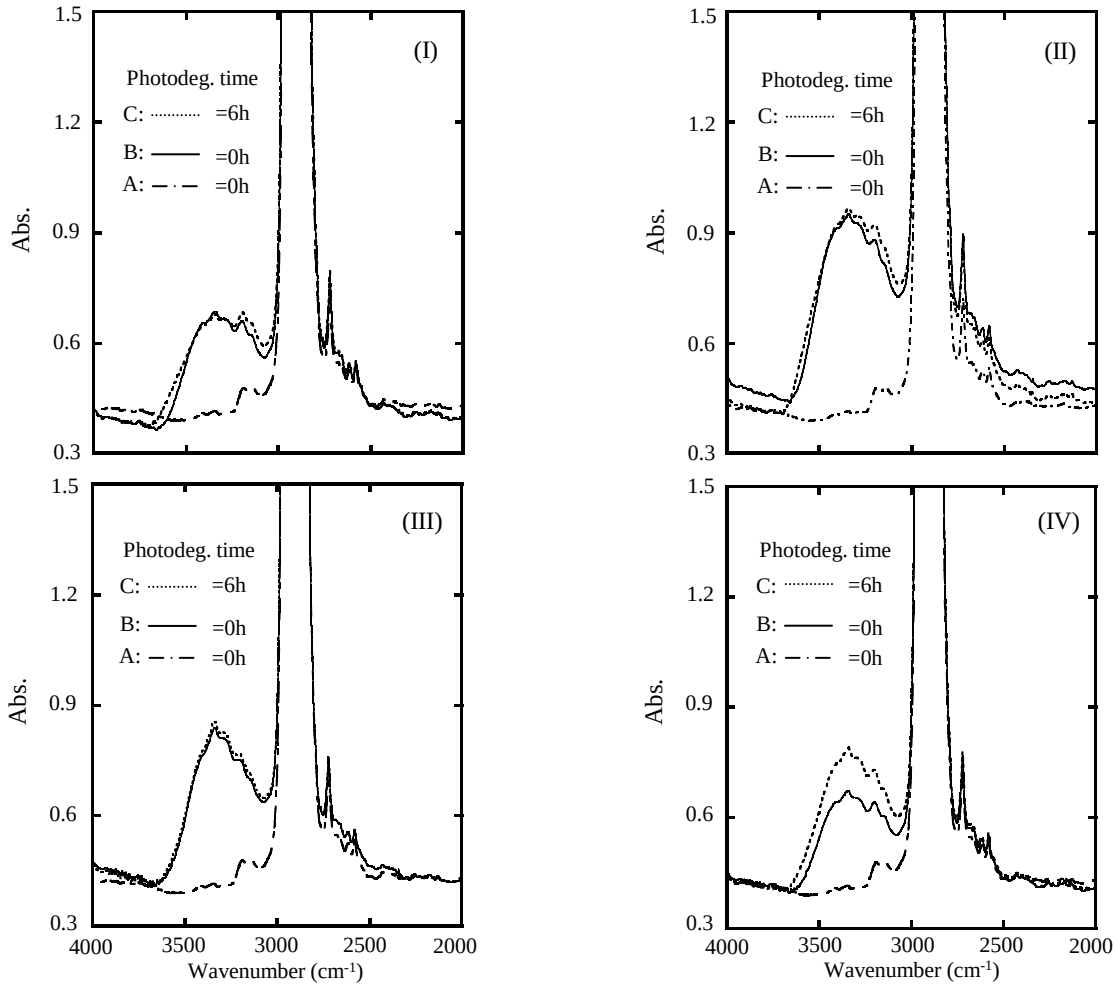

Figure 7-3 FT-IR spectra of various samples around OH group peak. Film thickness = 50mm. (I): A= pristine PP, B & C= PP(95.0 wt%)/FC(5.0 wt%). (II): A= pristine PP, B & C= PP(90.0 wt%)/FC(10.0 wt%). (III): A= pristine PP, B & C= PP(98.2 wt%)/PEO(0.3 wt%) /TiO_2(0.5 wt%)/FC(1.0 wt%). (IV): A= pristine PP, B & C= PP(94.2 wt%)/PEO(0.3 wt%) /TiO_2(0.5 wt%)/FC(5.0 wt%).

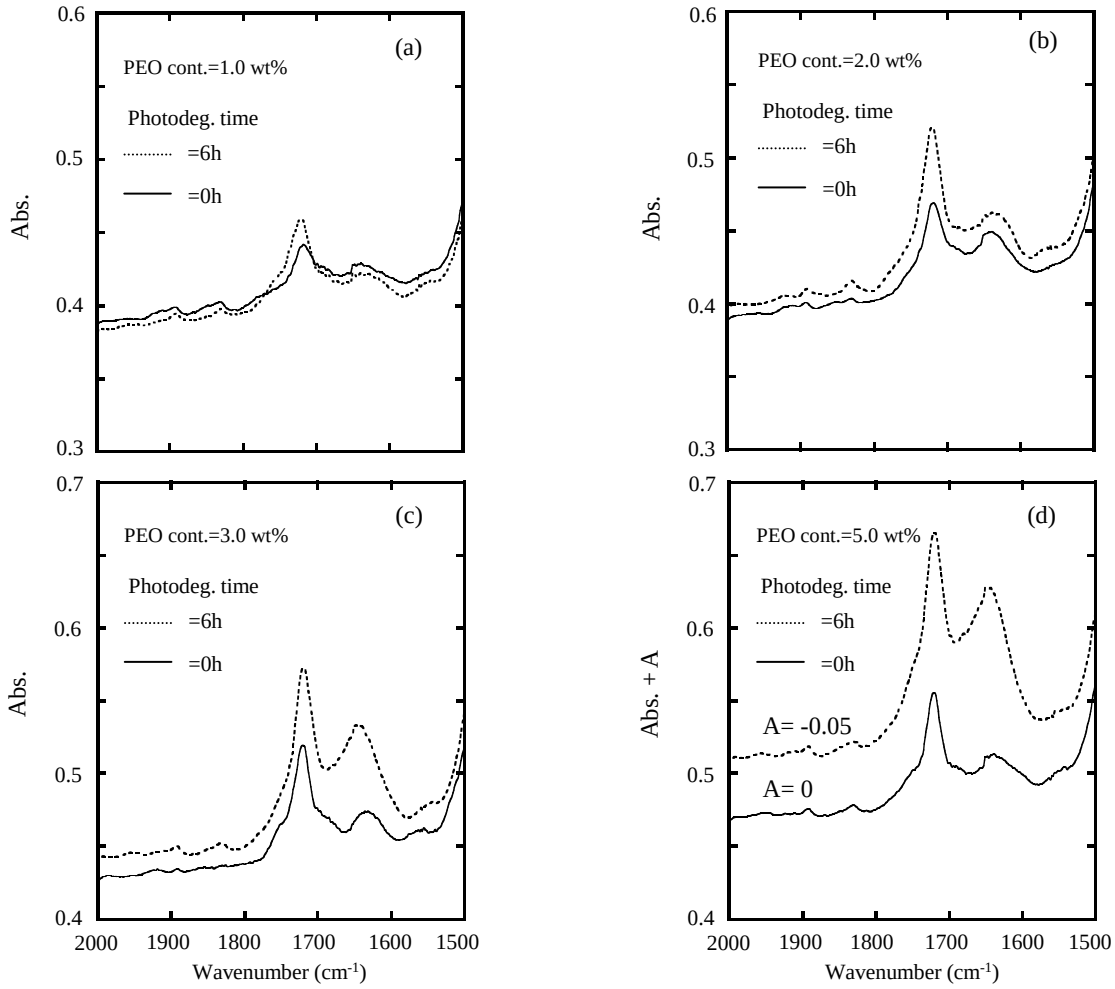

Figure 7-4 FT-IR spectra of various samples around ethylenic unsaturated and carbonyl peaks. Film thickness = 50mm. (a)=PP(97.5 wt%)/PEO(1.0 wt%) /TiO_2(0.5 wt%)/ FC(1.0 wt%). (b)= PP(96.5 wt%)/PEO(2.0 wt%) /TiO_2(0.5 wt%)/FC(1.0 wt%). (c)= PP(95.5 wt%)/PEO(3.0 wt%) /TiO_2(0.5 wt%)/FC(1.0 wt%).(d)= PP(93.5 wt%)/PEO(5.0 wt%) /TiO_2(0.5 wt%)/FC(1.0 wt%).

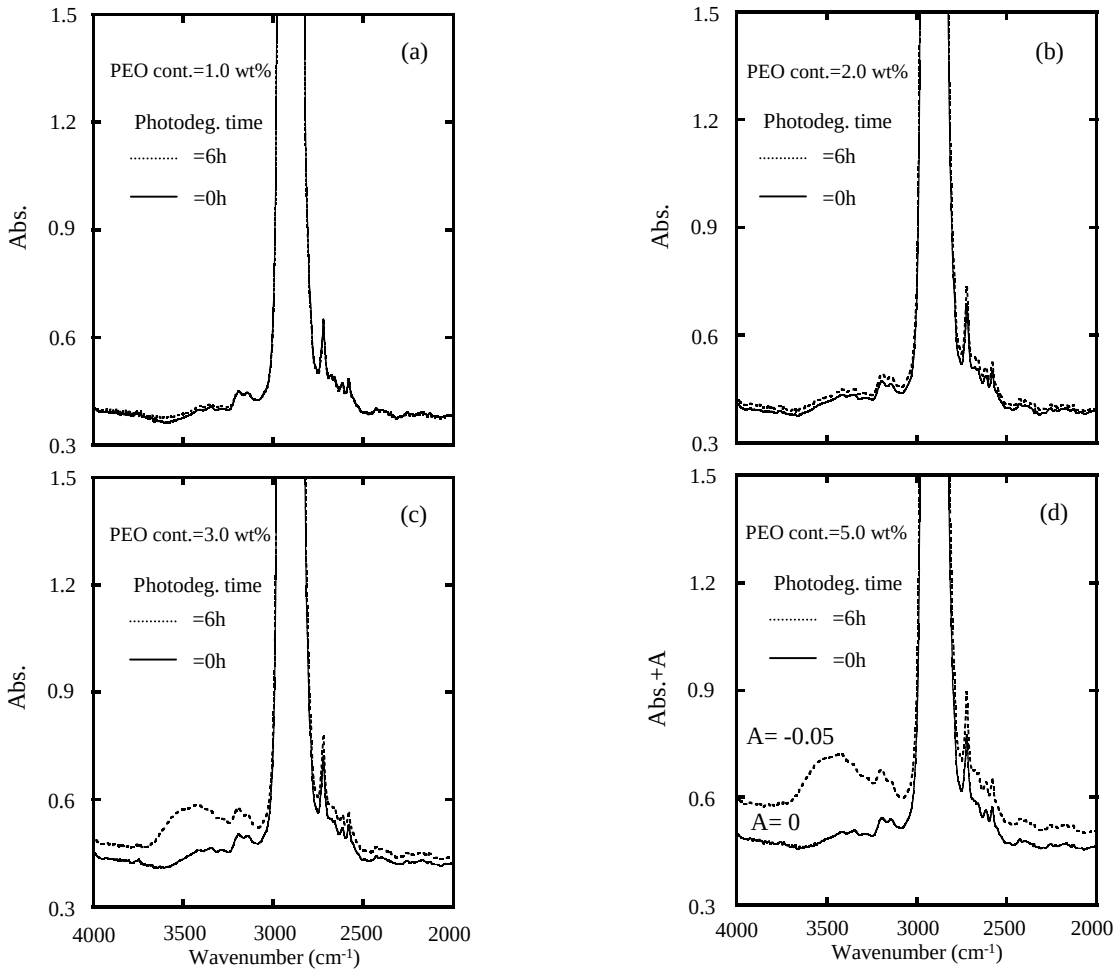

Figure 7-5 FT-IR spectra of various samples around OH group peak. Film thickness = 50mm. (a)=PP(97.5 wt%)/PEO(1.0 wt%) /TiO_2(0.5 wt%)/ FC(1.0 wt%). (b)= PP(96.5 wt%)/PEO(2.0 wt%) /TiO_2(0.5 wt%)/FC(1.0 wt%). (c)= PP(95.5 wt%)/PEO(3.0 wt%) /TiO_2(0.5 wt%)/FC(1.0 wt%).(d)= PP(93.5 wt%)/PEO(5.0 wt%) /TiO_2(0.5 wt%)/FC(1.0 wt%).

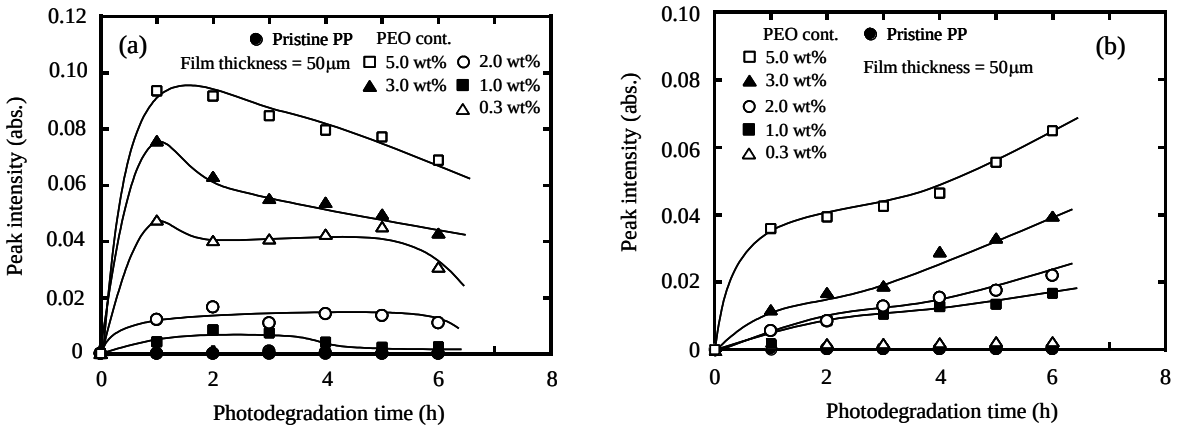

Figure 7-6 Increments of peak intensities in pristine PP and PP((98.5-x)wt%)/PEO(x wt%)/TiO_2(0.5 wt%) /FC(1.0 wt%) during photodegradation. (a): Ethylenic unsaturated group. (b): Carbonyl group.

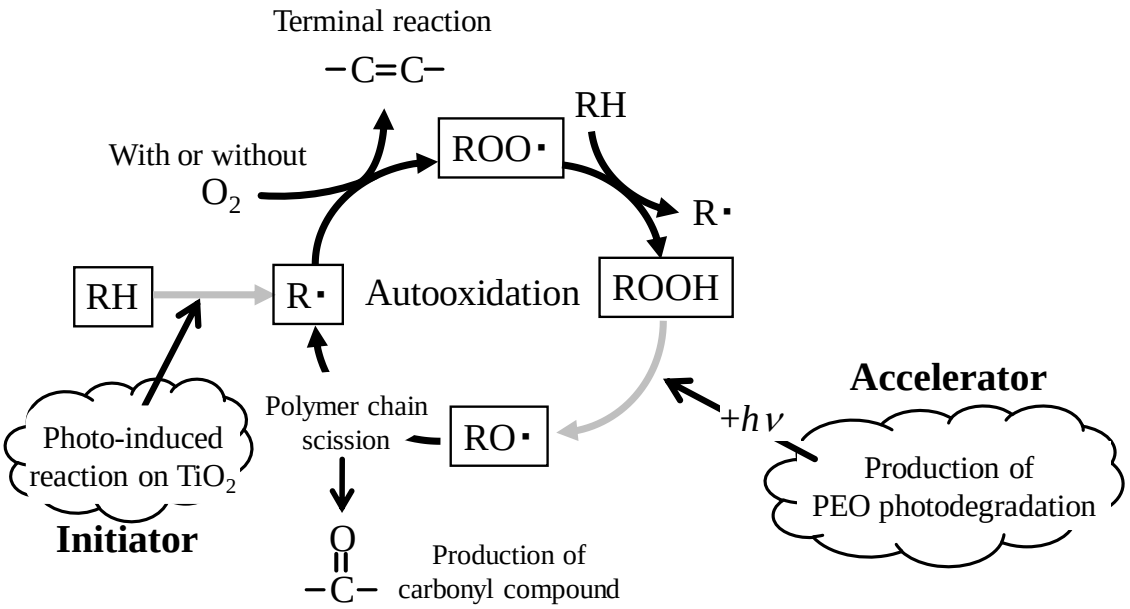

Figure 7-7 Degradation induced by PEO/TiO_2 initiator and accelerator system.

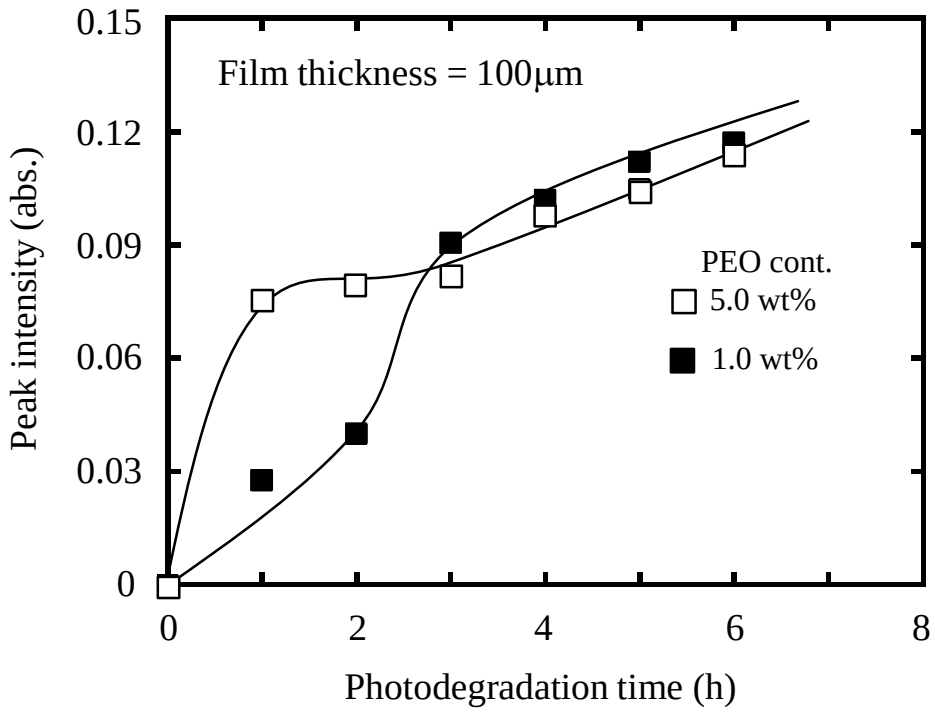

Figure 7-8 Increments of carbonyl peak intensity in PP(97.5 wt%)/PEO(1.0 wt%) /TiO_2(0.5 wt%)/ FC(1.0 wt%) and PP(93.5 wt%)/PEO(5.0 wt%) /TiO_2(0.5 wt%)/ FC(1.0 wt%) during photodegradation.

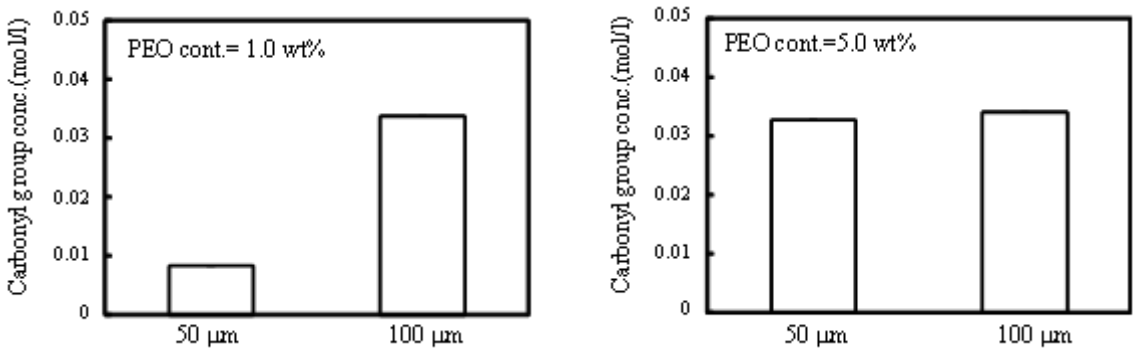

Figure 7-9 Increments of carbonyl group concentration between before and after photodegradation in PP(97.5 wt%)/PEO(1.0 wt%) /TiO_2(0.5 wt%)/ FC(1.0 wt%) and PP(93.5 wt%)/PEO(5.0 wt%) /TiO_2(0.5 wt%)/ FC(1.0 wt%) having 50 and 100 mm film thickness, respectively. photodegradation time = 5h.

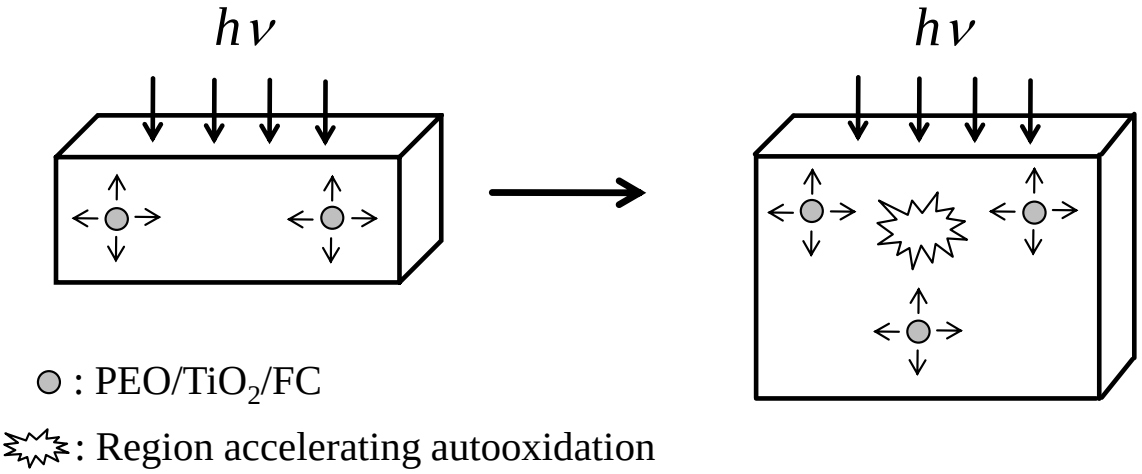

Figure 7-10 A schematical image of complementary autooxidation induced by enhancement of film thickness.

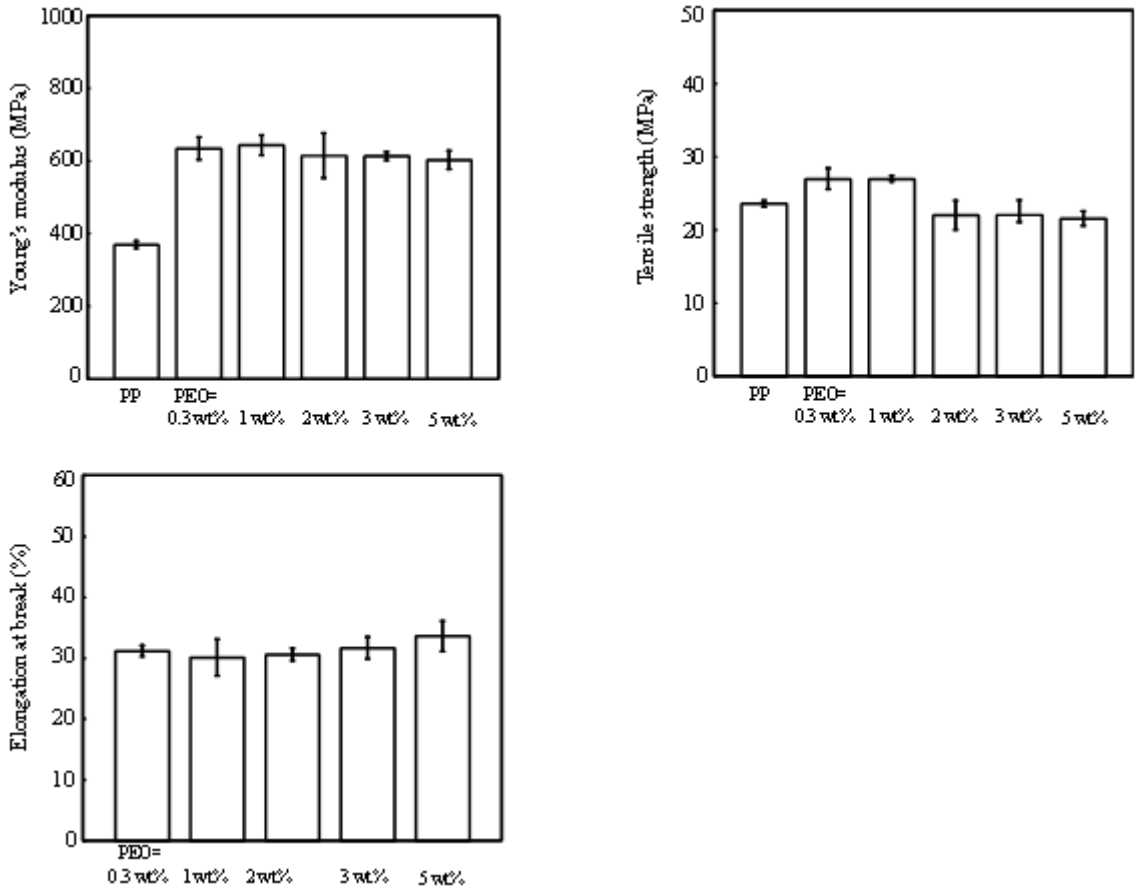

Figure 7-11 Comparisons of Young's moduli, tensile strengths and elongations at break of pristine PP and PP((98.5-x)wt%)/PEO(x wt%)/TiO_2(0.5 wt%) /FC(1.0 wt%) films: Pristine PP elongation at break = 200% over.

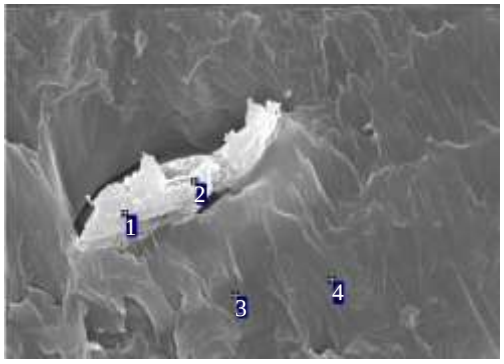

20 μm

Spot	C [%]	Ti [%]
1	97.83	2.17
2	99.08	0.92
3	99.84	0.16
4	100.00	0.00

Atomic percent.

20 μm

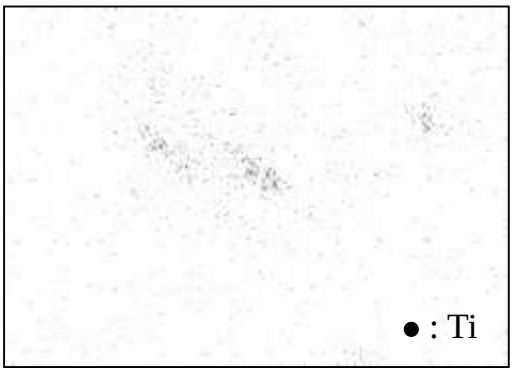

Figure 7-12　SEM microphotographs and their EDX point , surface analysis images of Ti atom on PP(93.5 wt%)/PEO(5.0 wt%) /TiO_2(0.5 wt%)/ FC(1.0 wt%) sample surfaces : No THF etching treatment.

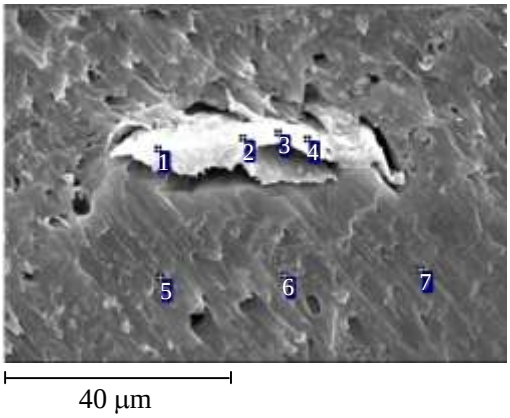

Spot	C [%]	Ti [%]
1	98.33	1.67
2	98.23	1.77
3	97.81	2.19
4	97.75	2.25
5	99.76	0.31
6	99.76	0.24
7	99.52	0.48

Atomic percent.

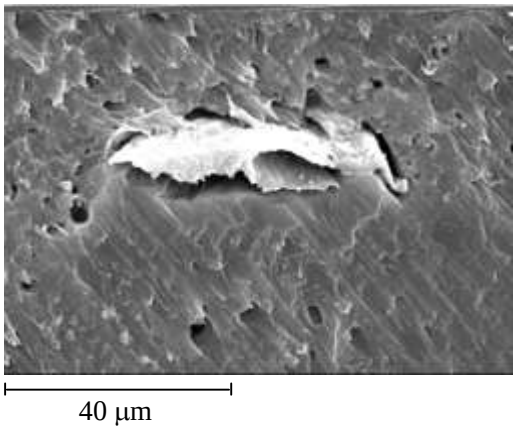

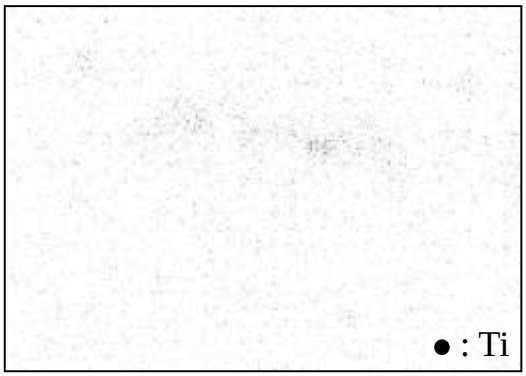

Figure 7-13　SEM microphotographs, their EDX point and surface analysis images of Ti atom on PP(93.5 wt%)/PEO(5.0 wt%) /TiO_2(0.5 wt%)/ FC(1.0 wt%) sample surfaces : THF etching treatment for 24 h at r.t.

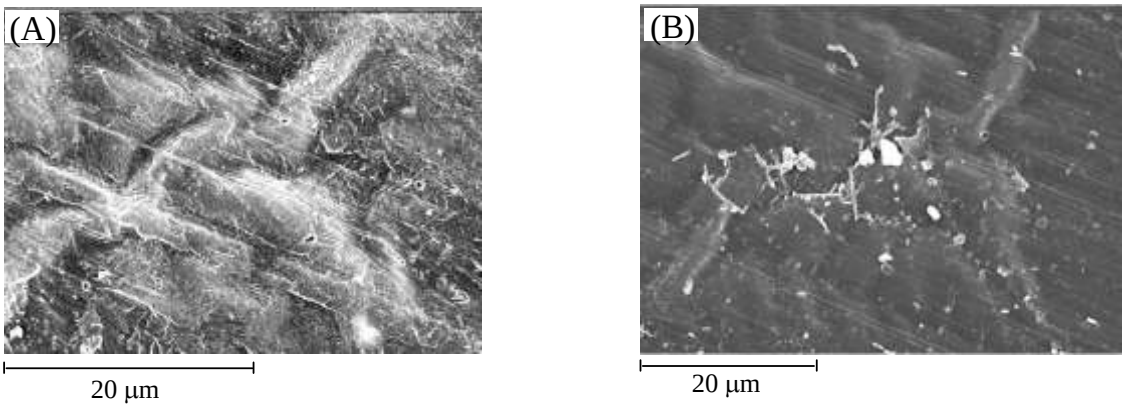

Figure 7-14 SEM microphotographs of the surfaces of PP(97.5 wt%)/PEO(1.0 wt%) /TiO_2(0.5 wt%)/ FC(1.0 wt%) samples retrieved from soil burial test for 28 days of incubation at 20 ºC: (A) No photodegradation treatment, (B) Photodegradation treatment for 24 h at 30 ºC.

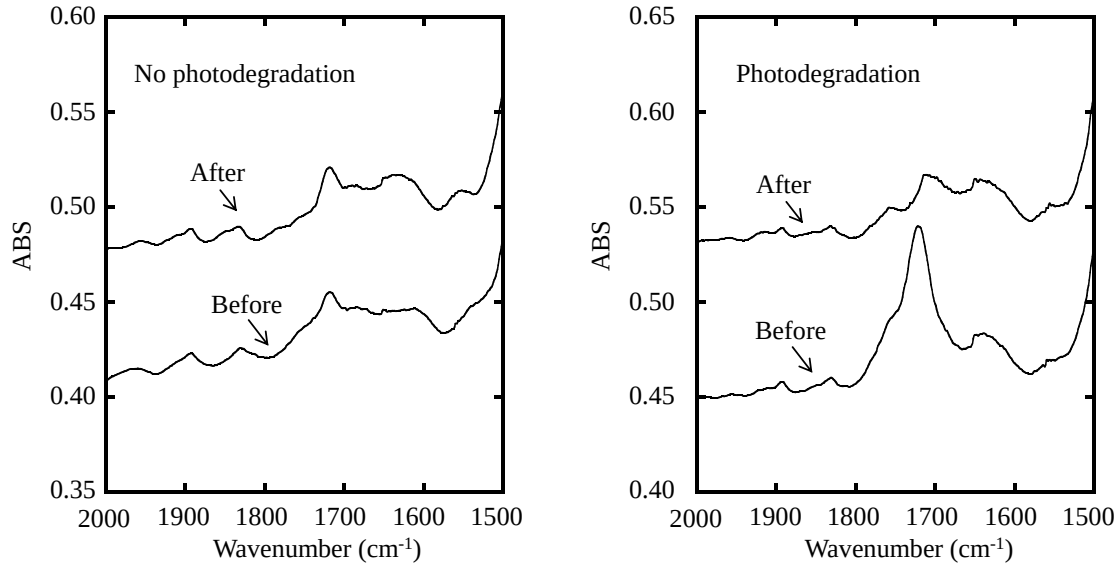

Figure 7-15 FT-IR spectra of un- and photodegraded PP(97.5 wt%)/PEO(1.0 wt%) /TiO_2(0.5 wt%)/ FC(1.0 wt%) samples before and after soil burial test for 28 days of incubation at 20 ºC. Film thickness =50 mm. Photodegradation treatment for 24 h at 30 ºC.

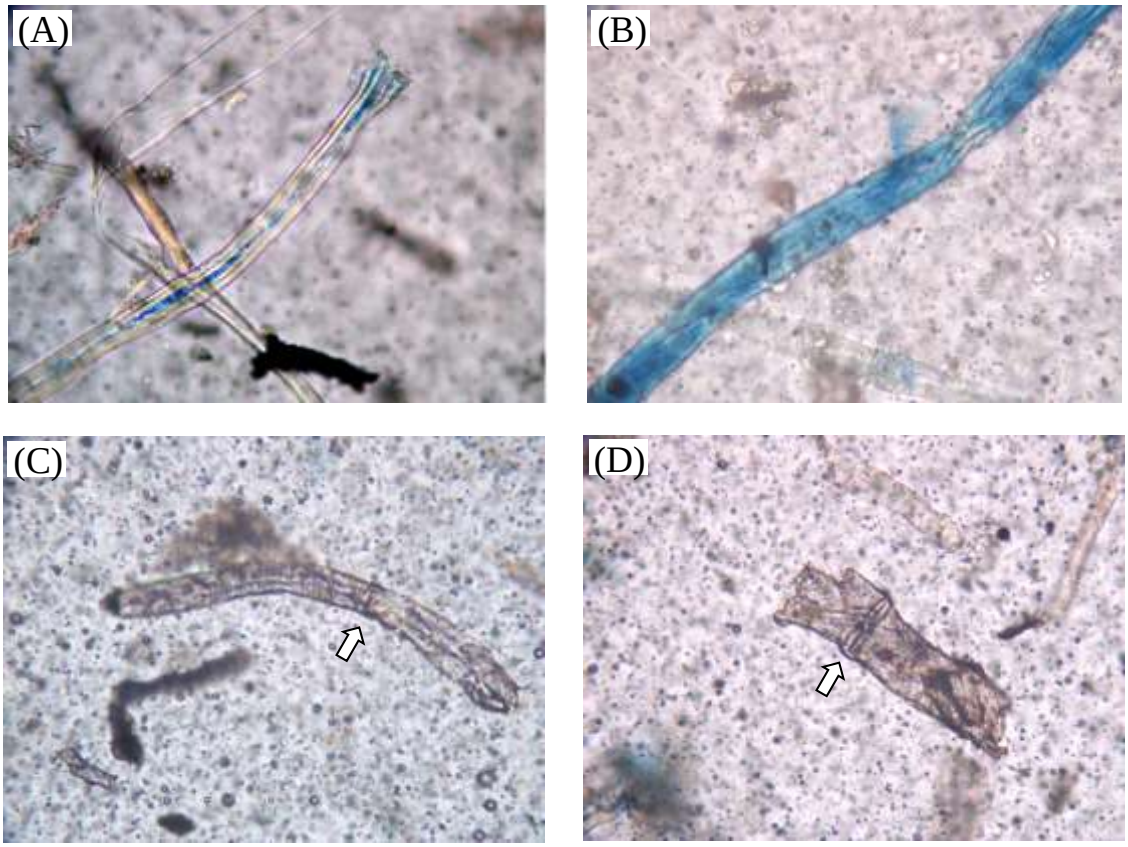

Figure 7-16 Optical microscope photographs (400 ×) of the surfaces of PP(97.5 wt%)/PEO(1.0 wt%) /TiO_2(0.5 wt%)/ FC(1.0 wt%) sample photodegraded for 24 h at 30 ºC and then retrieved from soil burial test for 28 days of incubation at 20 ºC: The film was stained by lactophenol cotton blue. (A) &(B) Long filamentous fungi , (C) & (D) short filamentous fungi showing septate. The arrows indicate septate .

Chapter 8: General Conclusion

This dissertation consists of study of reinforcement and oxo-biodegradability of polypropylene materials by Fibrous Cellulose and quasi-enzyme system.

In chapter 2, as a novel type of coupling agent for FC/PP composite, DgPP was studied. The DgPP contained acid and γ-lactone compounds which can react with the hydroxyl groups of FC. The addition of the DgPP improved the dispersibility of FC and mechanical properties of FC/PP composite. Therefore, the DgPP acted as the coupling agent. The MAPP compatibilizer was also studied. Both the DgPP and the MAPP compatibilizers had the same mechanism, using esterification between the OH group in FC and the reactive (γ-lactone, acid, and maleic anhydride) groups in the compatibilizers. However, the adhesion style with the ester bond was considerably different because of the arrangements of the reactive groups. DgPP had reactive groups at the polymer chain end, and the tensile behavior of the FC/PP/DgPP composite exhibited comparatively ductile behavior. However, MAPP had inner reactive groups, and the tensile behavior of the FC/PP/MAPP composite was quite brittle. Observation of these fracture surfaces suggested that the adhesion performance of the interface between FC and PP was strongly influenced by the arrangements of the reactive group. In addition, the performance was influenced by the molecular weight of DgPP and by the content of maleic anhydride groups in MAPP.

In chapter 3, effects of the addition of poly(ethylene oxide) (PEO) on the tensile properties of a polypropylene (PP)/fibrous cellulose (FC) composite were studied. PEO was incompatible with the PP matrix, and a PP/PEO blend showed a sea-island morphology. However, the existence of the PEO phase hardly impaired the

ductility of PP, leading to a strain constraint relaxation resulting from void formation in the phase. The tensile behavior of PP/PEO was little affected by the content (until 10 wt %) or molecular weight of PEO. The results suggested that the PEO phase was able to be deformed in a slit-like shape and had no interaction with the PP matrix. Effects of PEO on the morphology and tensile and fracture behavior of the PP/FC composite with maleated polypropylene (MAPP) as a compatibilizer critically depended on the preparation method. In the case of the addition of PEO to PP/FC/MAPP, increases in the strain and fracture energy were observed in comparison with PP/FC. In the case of the addition of FC/PEO to PP/MAPP, although the obtained composite showed a lower Young's modulus and tensile strength in comparison with PP/FC, the strain and fracture energy were considerably increased by the existence of the PEO layer coating the FC. The effects of the PEO content on the Young's moduli of the two kinds of PP/FC composite were also studied using the Kerner–Nielsen equation. In the case of the PP/maleated PP (MAPP)/FC + PEO composite, all the values of the moduli with the various PEO contents were in good agreement with the theoretical values obtained from the Kerner–Nielsen equation. Whereas the moduli of the PEO/FC + PP/MAPP composite followed the Kerner–Nielsen equation about 6 vol % of the PEO content and then unexpectedly deviated. In the scanning electron microscopy (SEM) observation, the PP/MAPP/FC + PEO composite was found to have a sea-island morphology corresponding to the PP/MAPP/FC matrix and the PEO phase. This morphology had been unchanged against the increase of the PEO content. Whereas in the case of the PEO/FC + PP/MAPP composite, the SEM micrographs showed that that the interface between the FC and the PP became worse with the increase of the PEO content, indicating that the formation of the PP/MAPP/FC matrix was blocked by the excess

PEO. The deviation of the Young's moduli from the Kerner–Nielsen equation was due to the blocking of the PEO. It was found that the adequate combination of the PEO and the MAPP was able to supply the increase of the toughness of the PP/FC composite by investigating the dependence of the PEO/FC + PP/MAPP composite on the MAPP content.

In chapter 4, in order to prepare a novel photo-degradable polypropylene (PP), an addition of poly(ethylene oxide) (PEO) microcapsule containing TiO_2 to PP was performed. Adsorbed H_2O in the PEO phase and the TiO_2 photo-catalytically reacted, and a hydroxyl radical (OH•), which initiated the PEO degradation, was produced. The degraded PEO produced an acid and an aldehyde, which were able to facilitate PP degradation. The addition of the PEO/TiO_2 microcapsule brought about the facilitative effect of the PP degradation. In addition, an addition of a hindered amine light stabilizer (HALS) had a potential to suppress the PP degradation initiated by the microcapsule. The suppression effect was rising by the simultaneous addition of a phenolic antioxidant in the early phase of the PP degradation. However, the simultaneous addition showed an antagonism after 4 h degradation. This behavior suggested that the HALS also worked as a neutralizer of the produced acid.

In chaper 5, to prepare a higher photo-degradation rare polypropylene (PP), a PP composite containing a poly(ethylene oxide) (PEO)/ modified TiO_2 microcapsule was prepared. The modification of the TiO_2 was performed by the synthesis of octacalcium phosphate intercalated with succinic acid ion (OCPC) under various Ca/P molar ratio conditions. It was found that the synthesis conditions of the Ca/P=3.5 and 3.6 molar ratios were suitable to prepare the OCPC. However, the microscopic composition on the TiO_2 surface was different between these Ca/P conditions and affected the PP

photo-degradation rate in the PP/PEO/modified TiO_2 composite. It was found from the Fourier Transform Infrared (IR) and the tensile testing measurements that the existence of the OCPC covering material on the TiO_2 surface brought about the higher PP photo-degradation rate. The facilitation behavior of the degradation was due to the release of the acid species (succinic acid ion) from the OCPC in the degradation process. In addition, the higher coverage of the OCPC on the TiO_2 surface brought about an induction period for the degradation.

In chapter 6, the biodegradation behavior of a novel polypropylene (PP) composite containing a poly(ethylene oxide) (PEO)/ modified TiO_2 microcapsule was studied with an oxo-biodegradation test combined with a photodegradation treatment (using a high-pressure mercury vapor lamp for 24 h of the irradiation at 30 °C in air) and a soil burial test (for 45 days of incubation at 20 °C). The modification of the TiO_2 was performed by the synthesis of octacalcium phosphate intercalated with succinic acid ion (OCPC). The existence of the microcapsule brought about higher PP photo- and bio-degradation rates. In the photodegraded PP composite, active colonies of some microorganisms were observed. By comparing with the PP composite without the OCPC modification, it was found that the active behavior of the microorganisms was due to the inorganic phosphates, which were supplied by the dissolution of the OCPC during the photodegradation. In addition, the photodegraded pars in the composite were completely metabolized by the microorganisms. However, the microorganisms had the inability to metabolize other parts such as the PP crystalline phase.

In chapter 7, the novel polypropylene (PP)/fibrous cellulose (FC) composite containing a poly(ethylene oxide) (PEO)/TiO_2 was prepared, and its oxo-biodegradation behavior was studied. Although the FC loading of 5 wt% brought about the

considerably opaque film, the 1wt% loading film was relatively good transparence. The Fourier transform infrared (FT-IR) spectra of the unphotodegraded composite samples revealed that the PP autooxidation hardly occurred under the melt-mixing condition. After the ultraviolet irradiation, the autooxidation smoothly advanced in the composite. The FT-IR analyses of the composite revealed that the TiO_2 and the PEO played the roles of the initiator and the accelerator of PP autooxidation, respectively. In addition, even at 1 wt% PEO content, the accelerator effect was found to be supplemented with the spreading of the degraded PEO component from other place by the enhancement of the film thickness. All the PP/PEO/TiO_2/FC composites having the various PEO contents from 0.3 to 5 wt% showed about 180% higher Young‘s moduli than that of the pristine PP. The biodegradability of the photodegraded composite was confirmed by a soil burial test, and the adherence of a filamentous fungus like *Curvularia* sp. was observed on the surface.

Achievement

Publication List

[1] Kensuke Miyazaki, Noriyasu Okazaki, Minoru Terano, Hisayuki Nakatani, "Preparation and characterization of cellulose/polypropylene composite using an oxidatively degraded polypropylene", *J. Polym. Environ.,* 2008, 16, 267–275 I.F. 1.507(2010)

[2] Kensuke Miyazaki, Kyosuke Moriya, Noriyasu Okazaki, Minoru Terano, Hisayuki Nakatani, "Cellulose/polypropylene composites: Influence of molecular weight and concentration of oxidatively degraded and maleated polypropylenes compatibilizers on tensile behavior", *J. Appl. Polym. Sci.* , 2009, 111, 1835-1841, I.F. 1.187(2008)

[3] Kensuke Miyazaki, Kyosuke Moriya, Noriyasu Okazaki, Minoru Terano, Hisayuki Nakatani, "Improvement of cellulose/polypropylene composite by an oxidatively degraded polypropylene as a dispersing agent" *J. Mater. Life Soc., Japan* 2009, 21, 40-47

[4] Kensuke Miyazaki, Hisayuki Nakatani, "Additive effect of poly(ethylene oxide) on polypropylene/fibrous cellulose composite: Effects of additive amount of poly(ethylene oxide) on Young's modulus and morphology", *J. Appl. Polym. Sci.* 2009, 114, 1656–1663, I.F. 1.187(2008)

[5] Kensuke Miyazaki, Hisayuki Nakatani, "Preparation of degradable polypropylene by an addition of poly(ethylene oxide) microcapsule containing TiO_2" *Polym. Degrade. Stab.* 2009, 94, 2114–2120, I.F. 2.594(2010)

[6] Kensuke Miyazaki, Hisayuki Nakatani, "Preparation of degradable polypropylene by an addition of poly(ethylene oxide) microcapsule containing TiO_2 part II. Modification of calcium phosphate on the TiO_2 surface and its effect" *Polym. Degrade. Stab.* 2010, 95, 1557–1567, I.F. 2.594(2010)

[7] Kensuke Miyazaki, Hisayuki Nakatani, "Preparation of degradable polypropylene by an addition of poly(ethylene oxide) microcapsule containing TiO_2 Part III. Effect of existence of calcium phosphate on biodegradation behavior." *Polym. Degrade. Stab.* 2011, 96, 1039-1046, I.F. 2.594(2010)

[8] Kensuke Miyazaki, Kazuto Shibata, Hisayuki Nakatani, “Study on polypropylene/cellulose composite oxo-biodegradation induced by poly(ethylene oxide)/TiO_2 initiator and accelerator system.” *J. Appl. Polym. Sci.* To be revised., I.F. 1.187(2008)

[9] Hisayuki Nakatani, Kensuke Miyazaki, “Modification of polypropylene and polypropylene/fibrous cellulose composite by addition of poly(ethylene oxide)”, *J. Appl. Polym. Sci.* 2009, 112, 3362-3370, I.F. 1.187(2008)

[10] Hisayuki Nakatani, Kazuya Hashimoto, Kensuke Miyazaki, Minoru Terano, ” Cellulose/ syndiotactic polypropylene composites: Effects of maleated polypropylene compatibilizer and silanized cellulose on morphology and tensile properties” *J. Appl. Polym. Sci.* 2009, 113, 2022-2029, I.F. 1.187(2008)

[11] Hisayuki Nakatani, Hiroshi Shibata, Kensuke Miyazaki, Tetsu Yonezawa, Hidetoshi Takeda, Yutaka Azuma, and Shin Watanabe, “Studies on heterogeneous degradation of polypropylene/talc composite: Effect of iron impurity on the degradation behavior” *J. Appl. Polym. Sci.* 2010, 115, 167-173, I.F. 1.187(2008)

[12] Hisayuki Nakatani, Keisuke Iwakura, Kensuke Miyazaki, Noriyasu Okazaki, Minoru Terano, "Effect of chemical structure of silane coupling agent on interface adhesion properties of syndiotactic polypropylene/cellulose composite" *J. Appl. Polym. Sci.* (2011), 119, 1732–1741, I.F. 1.187(2008)

[13] Hisayuki Nakatani, Masashi Ogura, Takanori Yoshikawa, Kensuke Miyazaki, Noriyasu Okazaki , Minoru Terano, "Preparation of polybutene-1/multiwall carbon nanotube composite by oxidation and limonene radical grafting and its characterization" *Polym. Int.* (2010), 60, 1614-1623, I.F. 2.056(2010)

International Canference

[1] Kensuke Miyazaki, Kyousuke Moriya, Minoru Terano, Hisayuki Nakatani, "Preparation and characterization of wood-plastic composite using thermal oxidative degradation of polypropylene" 1st International symposium on Ultimate stability of

nano-structured Polymers and Composites ishikawa, Japan, October, 2007

[2] Kensuke Miyazaki, Hisayuki Nakatani, "Preparation of degradalble polypropylene by an addition of poly(ethylene oxide) microcapsule containing TiO_2" 11th Pacific Polymer Conference 2009, Cairns, Australia, December, 2009

Domestic comference

[1] Kensuke Miyazaki, Minoru Terano, Hisayuki Nakatani, "Development of polypropylene /cellulose composite using degraded polypropylene" The 2007 winter meeting of The Chemical Society of Japan./ Hokkaido Branch, Sapporo, February, 2007

[2] Kensuke Miyazaki, Minoru Terano, Hisayuki Nakatani, "Development of wood plastics composite using degraded polypropylene" 56th Annual Meeting: the Society of Polymer Sceince, Japan, Kyoto, May, 2007

[3] Kensuke Miyazaki, Minoru Terano, Hisayuki Nakatani, "Development of polypropylene /cellulose composite using thermal thermal oxidative degraded polypropylene" The 2007 summer meeting of The Chemical Society of Japan./ Hokkaido Branch, Asahikawa, July, 2007

[4] Kensuke Miyazaki, Kyosuke Moriya, Minoru Terano, Hisayuki Nakatani, "Modification of interface and improvement of mechanical properties of polypropylene /cellulose composite using thermal degraded and maleated polypropylene compatibilizers." 57th Annual Meeting: the Society of Polymer Sceince, Japan, Kyoto, May, 2008

[5] Kensuke Miyazaki, Hisayuki Nakatani, "Effect of Mechanical properties of Polypropylene and Polypropylene/ Fibrous Cellulose Composites by the Addition of Poly(ethylene oxide)" The 2008 summer meeting of The Chemical Society of Japan./ Hokkaido Branch, Kitami, July, 2008

[6] Kensuke Miyazaki, Kyosuke Moriya, Minoru Terano, "Effects of addition of polyethylene oxide on mechanical properties of polypropylene/cellulose composite" 57th Symposium on Macromolecules: the Society of Polymer Sceince, Japan, Osaka, September, 2008

[7] Kensuke Miyazaki, Hisayuki Nakatani, “Preparation of degradable polypropylene by an addition of poly(ethylene oxide) microcapsule containing TiO_2” 59th Annual Meeting: the Society of Polymer Sceince, Japan, Yokohama, May, 2010

[8] Kensuke Miyazaki, Kazuto Shibata, Hisayuki Nakatani, “Preparation of degradable polypropylene by an addition of poly(ethylene oxide) microcapsule containing surface modified TiO_2” 59th Symposium on Macromolecules: the Society of Polymer Sceince, Japan, Sapporo, September, 2010

[9] Kensuke Miyazaki, Kazuto Shibata, Hisayuki Nakatani, “Preparation of oxo-biodegradable polypropylene by an addition of poly(ethylene oxide) containing TiO_2” 60th Annual Meeting: the Society of Polymer Sceince, Japan, Osaka, May, 2010

[10] Kensuke Miyazaki, Kazuto Shibata, Hisayuki Nakatani, “Preparation of oxo-biodegradable of polypropylene/cellulose composites by simulated enzyme system” 60th Symposium on Macromolecules: the Society of Polymer Sceince, Japan, Okayama, September, 2010

Prize

[1] Material Life Soc., “Material Life Soc. Paper Award” July, 2010

[2] Japan Society for the Promotion of Science (JSPS): JSPS Fellows No. 22·6529, 2010-2011

Acknowledgement

The investigations would never have been performed without the great help of Professor Dr. Hisayuki Nakatani. I really appreciate their excellent guidance and encouragement.

I am grateful to Professor Dr. Minoru Terano, Japan Advanced Institute of Science and Technology, for the great help in the studies.

I express my appreciation for Professor Dr. Takashi Yoshida, Associate Professor Dr. Noriyasu Okazaki, and Associate Professor Dr. Kazuyuki Hattori for their great advice and encouragement.

I am grateful to Japan Polypropylene Corporation and Nippon Paper Chemicals Corporation for their kind supply of sample.

Sincere thanks are due to Kyosuke Moriya, Kazuya Hashimoto, Yuta Yamada, Keisuke Iwakura, Masashi Ogura, Kazuto Shibata, Masato Hamadate, Yuta Takahashi, Masaaki Nakatani, Yuki Miyata, Takayuki Arai, Daisuke Inomata, Emu Ikarigawa, Minoru Sawada and Yasuhiro Hatanaka for their assistance and encouragement.

This work was supported by Grant-in-Aid for Japan Society for the Promotion of Science (JSPS) Fellows No. 22･6529. I am also very grateful to the JSPS for making this study possible by the financial support.

Finally I am grateful to my parents, my family for their understanding, support and encouragement during this study.

March, 2012

Kensuke Miyazaki